

UCSF

UC San Francisco Electronic Theses and Dissertations

Title

Regulation of cell contact and tissue organization by Eph/ephrin signaling

Permalink

<https://escholarship.org/uc/item/5j4395qm>

Author

Kindberg, Abigail Alexandra

Publication Date

2021

Peer reviewed|Thesis/dissertation

Regulation of cell contact and tissue organization by Eph/ephrin signaling

by
Abigail Kindberg

DISSERTATION
Submitted in partial satisfaction of the requirements for degree of
DOCTOR OF PHILOSOPHY

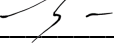
in

Biomedical Sciences

in the

GRADUATE DIVISION
of the
UNIVERSITY OF CALIFORNIA, SAN FRANCISCO

Approved:

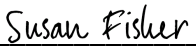
DocuSigned by:

6E99B613A5754DD... Zev Gartner
Chair

DocuSigned by:

Jeffrey Bush

DocuSigned by:

Diane Barber

DocuSigned by:

3D7FD5EAA89E411... Susan Fisher

Committee Members

Copyright 2021

By

Abigail Alexandra Kindberg

This work is dedicated to my grandparents; Shirley Ann Kindberg, my paternal grandmother, an independent, outspoken woman who always believed in me and in the power and possibilities of science, and James Biggerstaff Alcroft, my maternal grandfather, the most supportive, loving, and encouraging grandpa. Thank you for laying the foundations for the wonderful and supportive family that I am lucky to be a part of.

ACKNOWLEDGEMENTS

This dissertation is a collaboration of many people and would not exist without the assistance, knowledge and support of the people I am fortunate to have worked with while at UCSF. I would first like to thank my advisor, Dr. Jeffrey Bush. Thank you for your insightful mentorship during my time in your lab. From my rotation, and my decision switch from neuroscience to developmental biology, to deciding on what path to pursue after my time in your lab I have always appreciated your willingness to be a sounding board and provide guidance and advice while empowering me to make my own decisions. I appreciate the support, insight, and advice you provided for my research as well as my career. Thank you for teaching me so much about experimental science, writing, grantsmanship, and presenting. And thank you for always advocating for me as your trainee. I feel privileged to have received such wonderful mentorship throughout my time at UCSF.

I would also like to thank the entirety of the Bush lab, past and present, with whom I have had the pleasure and privilege of working. The lab is a wonderful environment full of hard-working and enthusiastic scientists and it has made my graduate school experience a pleasure. Thank you to Dr. Audrey O'Neill and Dr. Terren Niethamer for helping me get my project off the ground when I joined the lab, providing tissue culture, cell segregation, and EPH/EPHRIN expertise. Thank you to Ace Lewis and Dr. Akela Kuwahara for being excellent bay mates and providing support, coffee, and friendship throughout my time in the lab. A particular thanks to Ace Lewis for his endless experimental advice and expertise, and for his patience spending so many hours troubleshooting Definite Focus with me, making all of my live imaging possible.

I would also like to thank the other UCSF faculty that have been instrumental during my graduate school career and have given me the benefit of their knowledge and expertise throughout the years. My thesis committee, comprised of Dr. Zev Gartner, Dr. Diane Barber, and Dr. Susan Fisher, have given me the benefit of their time and feedback, have served as collaborators, and have given me reagents and tools to facilitate my project. I would also like to

thank all of my collaborators; Dr. Zev Gartner and Dr. Vasudha Srivastava, Dr. Valerie Weaver and Dr. Jonathan Muncie, and Dr. Ophir Klein and Dr. David Castillo Azofoeifa, all of whom gave me their time and expertise, making my work possible. I would also like to thank the PCB and HSE15, which has been a wonderful community to be a part of. This group has provided me with experimental input, support, career advice, reagents, scientific discussions, as well as a short lived soccer career. Thank you also to the additional UCSF faculty members who have given me time and feedback through research in progress seminars, joint lab meetings, and informal talks.

Thank you to the BMS program and my classmates. Thanks also to the BMS program staff, especially Demian Sainz, who have always been there to help with any administrative tasks that arose. Thank you also to the administrators of the PCB and the Department of Cell and Tissue Biology for helping me with all sorts of logistical matters.

Finally, I am so grateful for my family and friends, without whom none of this would be possible. My parents, Linda Alcroft and Kevin Kindberg, who always support me and my decisions whole-heartedly. Thank you for always being around to talk to me on my walks to and from lab, for wanting to hear about my work, my life, my frustrations, and my successes. Thank you to my sisters, Morgan and Madison Kindberg, who have been there through it all. Thank you for always being there for me, providing constant friendship, and for putting up with my excessive planning. This would not be possible without my family's love, encouragement, and belief in me and what I could achieve. To my in-laws, the Allison family, who have welcomed me into their family with open arms: Thank you for your support, many visits, and laughs. My childhood friends from New Jersey, and my college friends from Northeastern University, who despite the distance have always stuck by me as I pursued this endeavor. Thank you for your visits to San Francisco and allowing me to crash on your couches when I made it East. Thank you for the phone calls, text messages, and many years of friendship. My friends in San Francisco, who have made this city feel like home. Thank you for all of the explorations, adventures, good times, laughs, and always understanding when I need to get home early to split my cells at the lab. And last but certainly not

least, my husband, James Allison, who has been by my side throughout this entire endeavor. Thank you for following me to California, and to the Inner Sunset to shorten my commute. Thank you for your endless positivity, for being my balance when I am overwhelmed or stressed, for making me laugh, and for encouraging and supporting me daily. I could not have done this without you, nor would I have wanted to.

CONTRIBUTIONS TO THE PRESENTED WORK

The work presented in this dissertation was performed under the direct supervision and guidance of Dr. Jeffrey O. Bush, PhD. Additional guidance and insight was provided by collaborators and thesis committee members Dr. Zev J. Gartner, PhD, Dr. Diane L. Barber, PhD, Dr. Susan J. Fisher, PhD, and Dr. Valerie M. Weaver, PhD.

Chapter 1. The text and figures in Chapter 1 are modified and reproduced from the following review article: Kindberg, A.A. and Bush, J.O. (2018). Cellular organization and boundary formation in craniofacial development. *Genesis*, e23271. <https://doi.org/10.1002/dvg.23271>

I created the figures and initially drafted all sections of the manuscript. Jeffrey Bush added additional writing and edited all sections of the manuscript.

Chapter 2. The text and figures in Chapter 2 are modified and reproduced from the following review article: Kindberg, A., Hu, J.K., and Bush, J.O. (2020). Forced to communicate: Integration of mechanical and biochemical signaling in morphogenesis. *Current Opinion in Cell Biology*, 66: 59-68. doi: 10.1016/j.ceb.2020.05.004.

This manuscript is reproduced in accordance with the policies of Elsevier. I, along with Jimmy Hu and Jeffrey Bush created the figures and drafted the manuscript.

Chapter 3. The text and figures in Chapter 3 are modified and reproduced from the following publication: Kindberg, A.A., Srivastava, V., Muncie, J.M., Weaver, V.M., Gartner, Z.J., Bush, J.O. (2021). EPH/EPHRIN regulates cellular organization by actomyosin contractility effects on cell contacts. *Journal of Cell Biology*. doi: 10.1083/jcb.202005216

This manuscript is reproduced in accordance with the policies of Rockefeller University Press. I created the figures and initially drafted all sections of the manuscript. Jeffrey Bush added

additional writing and edited all sections of the manuscript. Microwell experiments in Figure 7 were performed in collaboration with Vasudha Srivastava. Atomic force microscopy experiments in Figures 9 and S3 were performed by Jonathan M. Muncie. Zev J. Gartner and Valerie M. Weaver provided valuable intellectual input and resources. All authors contributed to the editing process.

Chapter 4. This chapter is a work in progress based on data I collected to find additional models of EPH/EPHRIN driven cell segregation. I found a number of systems with potential as an invitro model, however all of these possible models need further investigation prior to their use. This data is important for the field as these systems have not been previously used to investigate the mechanisms of cell segregation.

I performed all cell and tissue culture and associated experimentation, including microwell, hanging drop, immunohistochemistry, and cell segregation experiments. I also performed NCC differentiations and cell contact angle analysis. Jeffrey Bush performed mouse rhombomere dissections. Katherine Woronowicz and Richard Schneider assisted with chick rhombomere dissections, including teaching me how to work with chick embryos and provided reagents and advice for these dissections. David Castillo Azofeifa assisted with establishing and maintaining intestinal organoid cultures and provided protocols for immunohistochemistry in intestinal organoids. Ryan Samuel and Faranak Fatahi assisted with hNCC differentiations and provided reagents as well as advice on protocols and cell culture. Akela Kuwahara performed FLOW sorting and analysis. Terren Niethamer performed western blot analysis of U251 and U87 cell lines.

Appendix 1. This appendix contains additional data I collected relevant to chapter 3. I generated the data, created the figures, and drafted the associated text. Vasudha Srivastava provided

assistance and protocol for cell:ECM measurements. Plasmids and protocols for dCas9-KRAB cell lines and sgRNA transfection were provided by Malin Akerblom and Michael McManus.

I would like to acknowledge the following sources of support and funding:

UCSF Department of Cell and Tissue Biology

UCSF Program in Craniofacial Biology

UCSF Biomedical Sciences Graduate Program

NIH/NIDCR F31DE028175 (Ruth L. Kirschstein Predoctoral National Research Service Award)

NIH/NIDCR R01DE025877 (to Jeffrey Bush)

NIH/NIDCR R21DE025923 (to Jeffrey Bush)

“Not everything that can be counted counts and not everything that counts can be counted.”

-Attributed to Albert Einstein

Abstract

Regulation of cell contact and tissue organization by Eph/ephrin signaling

Abigail Alexandra Kindberg

During development, cellular self-organization by cell segregation leads to boundary formation and is critical for the organization of morphogenetic movement and tissue patterning. Signaling between membrane-bound EPHRINS and EPH receptor tyrosine kinases is essential in boundary formation, driving segregation between EPHRIN-expressing and EPH-expressing cells. Here I examine the basic cellular mechanistic drivers of EPH/EPHRIN cellular self-organization and boundary formation. Using a cell culture system to model EPH/EPHRIN cell segregation I analyzed the contact angle of cells to estimate the interfacial tension between EPHB2- and EPHRIN-B1-expressing cells. Heterotypic cell pairs exhibited increased interfacial tension relative to homotypic cell pairs. Inhibitors of actomyosin contractility significantly diminished this increase, suggesting that actomyosin contractility drives heterotypic interfacial tension. Cell segregation assays revealed that EPH/EPHRIN driven segregation is actomyosin contractility dependent. Further, atomic force microscopy showed that EPH/EPHRIN signaling results in increased cortical tension during cell segregation. Actomyosin contractility also drives increased EPHB2:EPHB2 homotypic contacts through an increase in tension away from the cell contact. Using a mouse model I demonstrated that actomyosin contractility is critical for EPH/EPHRIN cell segregation *in vivo* as well. Finally, I demonstrated that tissue-wide changes in cellular organization and tissue shape are driven by minimization of heterotypic contact. These data suggest a model for cell segregation and tissue organization in which Eph/ephrin signaling results in a cortical actin differential that prevents cells from making stable contacts and drives cell segregation to affect tissue morphology by modulating interfacial tension.

TABLE OF CONTENTS

Chapter 1. Introduction to EPH/EPHRIN signaling and cellular organization in craniofacial development.....	1
Chapter 2. Introduction to mechanical forces in development.....	39
Chapter 3. EPH/EPHRIN regulates cellular organization by actomyosin contractility effects on cell contacts.....	55
Summary.....	56
Introduction.....	57
Results.....	62
Discussion.....	70
Materials and Methods.....	75
Chapter 4. Additional potential models of EPH/EPHRIN driven cell segregation.....	106
Summary.....	107
Introduction.....	108
Results.....	111
Discussion.....	116
Materials and Methods.....	118
Chapter 5. Conclusions and future directions.....	131
Appendix 1. Additional Data.....	135
References.....	157

LIST OF FIGURES

Figure 1.1. Cellular mechanisms underlying cell segregation and boundary formation based on differences in cell:cell adhesion or cortical actomyosin contractility.....	35
Figure 1.2. Boundaries relevant to craniofacial morphogenesis in the embryo.....	37
Figure 1.3. Migratory guidance mechanisms resulting in segregation or maintenance or segregated cell populations.....	38
Figure 2.1. Mechanisms of mechanosensation.....	52
Figure 2.2. Integregation of mechanical and biochemical signaling during morphogenesis.....	53
Figure 2.3. Mechanical modulation of chemical signaling.....	54
Figure 3.1. EPH/EPHRIN signaling increases heterotypic interfacial tension.....	83
Figure 3.2. Cell segregation is abolished by dual inhibition of ROCK and MLCK.....	84
Figure 3.3. Actomyosin contractility drives increased cellular interfacial tension.....	86
Figure 3.4. Myosin light chain localization increases at heterotypic contacts.....	87
Figure 3.5. EPHB2 cells increase homotypic contacts due to high cell:media cortical tension...	89
Figure 3.6. Cell segregation <i>in vivo</i> is disrupted by lack of actomyosin contractility.....	90
Figure 3.7. EPH/EPHRIN signaling affects tissue morphology.....	91
Figure 3.8. EPH/EPHRIN signaling modulates both cell:cell and cell:media tension, driven by actomyosin contractility to drive cellular organization.....	92
Figure 4.1. Neural progenitor cell dissection and culture.....	124
Figure 4.2. Intestinal organoid culture.....	126
Figure 4.3. Neural crest cell differentiations from patient derived iPSCs.....	127
Figure 4.4. Cell segregation in U251 or U87 cells mixed with HEK293 cells.....	129

LIST OF SUPPLEMENTAL FIGURES AND APPENDIX FIGURES

Figure S3.1. HEK293 cells lacking EPH/EPHRIN signaling do not have high interfacial tension.....	93
Figure S3.2. Cells under dual ROCK and MLCK inhibition remain migratory.....	95
Figure S3.3. Actomyosin contractility increases cortical tension during cell segregation at early timepoints.....	96
Figure S3.4. Myosin light chain localization increases at heterotypic contacts.....	97
Figure S3.5. EPHB2 cells increase homotypic contacts in response to EPH/EPHRIN signaling.....	99
Figure S3.6. EPH/EPHRIN signaling effects on cortical tension impact tissue morphology...	101
Figure A1.1. Cellular collapse upon addition of EPHRIN-B1-Fc.....	146
Figure A1.2. Additional cell:cell contact angle conditions.....	147
Figure A1.3. Additional cell segregation assay conditions.....	149
Figure A1.4. Segregation hierarchy in microwells in low Ca ²⁺ media.....	151
Figure A1.5. CRISPRi in HEK293 cells.....	153
Figure A1.6. sgRNA cloning protocol.....	155

LIST OF TABLES

Table 3.1. Crosses used to generate experimental and control embryos.....	103
Table 3.2. Numbers of embryos analyzed.....	104
Table 3.3. Sample size and replicates.....	105
Table A1.1. SgRNA sequences.....	156

CHAPTER 1.

Introduction to EPH/EPHRIN signaling and cellular organization in craniofacial development

Introduction to EPH/ EPRHIN signaling

EPH receptors, which partner with membrane bound EPHRIN ligands, constitute the largest family of receptor tyrosine kinases in the vertebrate genome (Gale et al., 1996; Henkemeyer et al., 1994; Kullander and Klein, 2002). EPHs were first identified from their over expression in human carcinoma (Hirai et al., 1987) and have since been found to be expressed widely, including broadly throughout the embryo.

EPH receptors and EPHRINs are membrane-bound and thus EPH/EPHRIN signaling primarily occurs between adjacent cells (Davis et al., 1994; Henkemeyer et al., 1994). However, EPH/EPHRIN signaling may also be mediated between non-adjacent cells through cellular protrusions or through release of EPHs and EPHRINs by exosomes (Cayuso et al., 2016; Gong et al., 2016). EPHs and EPHRINs are divided into two subclasses based on structure and binding affinity; EPHRIN-As are membrane-bound by a GPI anchor, while EPHRIN-Bs are transmembrane and contain an intracellular cytoplasmic domain (Gale et al., 1996). EPHAs have a binding affinity for EPHRIN-As and EPHBs for the EPHRIN-B family although there are some exceptions (Gale et al., 1996), EPH/EPHRIN signaling can be bidirectional with signaling transduced into the EPH receptor expressing cell defined as “forward signaling” and signaling into the EPHRIN expressing cell defined as “reverse signaling”. EPH receptor oligomerization is needed for forward signaling, and size of the EPH receptor cluster determines signaling strength (Himanen et al., 2010; Schaupp et al., 2014; Seiradake et al., 2010).

EPH/ EPHRIN signaling is critical in a wide variety of developmental contexts. Among other developmental abnormalities, mutations in EPHs and EPHRINs effect morphogenesis of the craniofacial complex, result in early embryonic lethality due to defective angiogenesis (Gerety et al., 1999; Salvucci and Tosato, 2012), disrupt neural crest-derived structures (Smith et al., 1997), and cause inappropriate axon guidance and axon crossing of the midline (Wilkinson, 2001), which is essential for proper central nervous system development. EPHs and EPHRINs have also been implicated in human diseases, such as craniofrontonasal syndrome (CFNS),

caused by X-linked mutations in *EFNB1* (Twigg et al., 2004), as well as in cancer, both as tumor suppressors, restricting tumor growth and cancer metastasis by preventing intermingling of EPH and EPHRIN cells, and as tumor promoters (Battle and Wilkinson, 2012). EPHs and EPHRINs which are frequently expressed in complementary domains and play a critical role in mediating tissue organization, including boundary formation, by driving segregation between EPHRIN-expressing and EPH-expressing cells. While the role of EPHs and EPHRINs in mediating boundary formation is well established, the mechanisms by which EPH/EPHRIN signaling drive cell segregation and boundary formation remain unclear.

Introduction to cell segregation

From early studies of developmental biology, it has been recognized that embryonic development requires the self-organization of cells into discrete regions, leading to the formation and maintenance of embryonic boundaries, preventing the intermixing of distinct cell populations. Boundary formation, a critical organizing process for embryonic cell populations, commences from the earliest stages of development and often occurs through cell segregation, in which cells with distinct identities or properties segregate, or sort, from each other. Embryonic boundaries are critical for patterning, organization, and tissue separation. Various hypotheses of the cellular mechanisms that drive cell segregation and boundary formation in different organisms and tissues have been proposed. The main cell behaviors hypothesized to underlie cell organization and boundary formation includes changes to cell adhesion, repulsion, migration and cytoskeletal dynamics such as actomyosin contractility. The first predominant hypothesis for how cell segregation and boundary formation occurs arose from seminal work by Townes and Holtfreter in which different embryonic tissues from *Xenopus* were dissociated and subsequently mixed. These studies revealed that the cells did not remain intermixed but instead segregated into aggregates of their tissue of origin (Townes and Holtfreter, 1955). Townes and Holtfretter also observed a hierarchy of cell contact strength between cell types, where some cell types were

consistently surrounded by others that sorted to the periphery (Townes and Holtfreter, 1955). These experiments gave rise to the idea of tissue affinity, describing the property of cells to recognize the identity of neighboring cells and preferentially contact “like” cells in order to re-aggregate (Townes and Holtfreter, 1955). Following the discovery of cell adhesion molecules, this idea gave way to the differential adhesion hypothesis (DAH), which proposes that cell segregation is driven by differences in adhesion between populations, achieved through the types of cadherin expressed, termed selective adhesion, or through differing levels of cadherin expression, termed differential adhesion (Fig. 1.1A) (Duguay et al., 2003; Steinberg and Takeichi, 1994). This hypothesis predicts that cells will maximize their adhesive contacts to cluster hierarchically based on adhesion differences; the most adhesive cell population will cluster internally and be surrounded by less adhesive populations (Fig. 1.1A). Support for the differential adhesion hypothesis comes from studies demonstrating that differential cadherin expression is able to predict cell aggregation *in vitro*. L-cells, which lack endogenous cadherins, can be engineered to express different types and levels of cadherins and mixed, resulting in the aggregation of the cells expressing higher levels of cadherin in the center, while the cells with lower cadherin expression segregate to the outside of these clusters (Duguay et al., 2003; Foty and Steinberg, 2005; Steinberg and Takeichi, 1994). Indeed, differences in cadherin expression occur across embryonic boundaries relevant to craniofacial morphogenesis, such as the inter-rhombomeric boundaries (Ganzler and Redies, 1995; Inoue et al., 1997; Matsunami and Takeichi, 1995; Nakagawa and Takeichi, 1995). However, there are very few *in vivo* examples of cell segregation and boundary formation that can be clearly attributed to differential adhesion, partly because manipulations of cadherin expression often cause catastrophic loss of tissue cohesion (Kintner, 1992; Lee and Gumbiner, 1995; Levine et al., 1994). Interestingly, in several studies of *in vitro* cell segregation in which cadherin expression is disrupted, primarily through shRNA knockdown of cadherins or their regulators, segregation is either unaffected or only partially abolished (Cortina et al., 2007; Taylor et al., 2017). This suggests that while cell adhesion is capable of

regulating segregation and boundary formation, it is likely not the sole driver of segregation in all systems.

Cell-cell repulsion, the collapse of cellular processes followed by migration away from the repulsive source, has also been hypothesized to drive cell segregation and boundary formation (Fig 1B) (Mellitzer et al., 1999; Poliakov et al., 2008). In this model, segregation is driven by local repulsive cues, which trigger retraction and repulsive migration (Fig. 1.1B). Several different signaling pathways important for craniofacial development, including EPH/EPHRIN and neuropilin/semaphorin signaling, can mediate cellular repulsion. EPHs and their EPHRIN signaling partners are expressed throughout the development of the vertebrate craniofacial complex and often act to restrict intermingling between EPH-expressing and EPHRIN-expressing cells (Bush and Soriano, 2010; O'Neill et al., 2016; Risley et al., 2009; Smith et al., 1997). EPH/EPHRIN mediated repulsive migration is observed in cells in culture, where upon contact with an EPHRIN-expressing cell, the EPH-expressing cell will collapse and move away from the EPHRIN-expressing cell source (Astin et al., 2010; O'Neill et al., 2016; Poliakov et al., 2008). EPHs and EPHRINs can signal bidirectionally, with forward signaling occurring through the EPH receptor and reverse signaling occurring through the EPHRIN, suggesting the possibility of simultaneous bidirectional guidance (Mellitzer et al., 1999; Xu et al., 1999). To give rise to boundary formation by this mechanism repeated repulsion and migration of cells away from heterotypic contacts would ultimately result in the segregation of these two cell types (Fig. 1.1B). Semaphorin guidance molecules can be membrane-bound or tethered, providing the ability to regulate cellular guidance locally, or at a distance. Semaphorin signaling through plexin receptors and neuropilin co-receptors mediates cellular guidance through both repulsive and attractive functions mediated by changes in the cytoskeleton and cell adhesion (Tran et al., 2007).

A third and more recently proposed mechanism for cell segregation is the differential interfacial tension hypothesis (DITH) (Fig 1C). In addition to differential adhesion, this hypothesis incorporates differential cortical tension generated by cytoskeletal contractility, stating that both

factors contribute to differences in the ability of cells to make stable contacts (Brodland, 2002; Krieg et al., 2008). Interfacial tension, or the balance of forces acting at a given interface, is frequently thought of in the context of a cell:cell interface or a cell:media interface. Whereas *in vitro* cell:media interactions involve all of the cell-non-cell interactions (e.g. substrate and liquid medium), *in vivo*, cell:medium interactions are constituted by whatever surrounds the cells that are organizing (this can be extracellular matrix (ECM), fluid, yolk, or other cells) (Cerchiari et al., 2015; Krieg et al., 2008; Maître et al., 2012). Cell:cell interfacial tension, the force with which cells contact each other, arises through the contractile cell cortex, which is coupled to cell adhesion molecules, linking neighboring cells and resulting in modulation of cell contact at the cellular interface (Lecuit and Lenne, 2007). Thus, if a population of cells has a high cortical tension, it will minimize high-tension interactions by aggregating together, resulting in segregation of populations (Fig 1C). There is increasing evidence to support a critical role of actomyosin contractility in cellular organization by driving boundary formation. For example, differential cortical tension has been shown to drive cell segregation in zebrafish germ layer separation and mammary epithelium organization (Cerchiari et al., 2015; Krieg et al., 2008; Maître et al., 2012). In both of these systems, adhesion alone was not predictive of cell sorting patterns, but rather the cells with the highest cell-medium interfacial tension aggregated at the center, thereby minimizing unfavorable, or high interfacial tension, interactions of cells with their surrounding media (Fig. 1.1C) (Cerchiari et al., 2015; Krieg et al., 2008). Additionally, in various organisms and boundary systems, including at rhombomere boundaries and aberrant boundaries in the craniofacial mesenchyme, actomyosin enrichment is observed, suggesting actomyosin contractility and differential interfacial tension may be playing a role at many boundaries in the developing embryo (Calzolari et al., 2014; Cooke et al., 2001; O'Neill et al., 2016). Given the complexity of actomyosin cytoskeletal regulation, many of these studies have employed overexpression, pharmacological inhibition, or dominant-negative disruption of pleiotropic factors, and many questions remain as

to how these mechanisms may contribute to cellular organization *in vivo* and in what contexts these cell behaviors are contributing to cellular organization and boundary formation.

Cell segregation and boundary formation in craniofacial development

Craniofacial morphogenesis is a highly dynamic and complex physical process. It requires the establishment of transcriptional identity and differentiation of cells, but also precise signaling control that organizes cells into distinct populations with boundaries between them, ultimately forming distinct craniofacial structures. A critical component of craniofacial development is the specification and migration of the cranial neural crest cells (CNCCs). These cells are multipotent progenitors that originate at the border between the neural ectoderm and non-neural ectoderm. In the embryonic hindbrain, inter-rhombomeric boundaries partition the neural ectoderm into a series of segments that act as organizing centers along the rostrocaudal axis of the embryo neuroectoderm, organizing hindbrain development, as well as impacting NCC organization and development. CNCCs undergo epithelial to mesenchymal transition (EMT), enabling delamination and migration from the rhombomeres of the hindbrain to populate the branchial arches and extensively contribute to structures of the head and face. While attractive guidance directs NCCs toward the craniofacial primordia, repulsive migratory guidance maintains the stereotyped segmentation of discrete NCC streams throughout migration. The cellular mechanisms of repulsive NCC guidance and boundary formation by cell sorting have many similarities, particularly in cell behavioral mechanisms. Segmental NCC migration from the developing forebrain and midbrain to populate the frontonasal region and first pharyngeal arch (PA) also contribute to formation of the head and face. The PAs are composed of an internal core of mesoderm surrounded by NCC-derived mesenchyme and bound externally by ectoderm and internally by endoderm. Between the PAs are the ectodermally-derived pharyngeal grooves externally, and endodermally-derived pharyngeal pouches; which also exhibit segmental organization (Frisdal and Trainor, 2014). Upon arrival of the NCCs in the PAs, continued

regulation of movement or flow of NCC-derived mesenchyme culminates in distinct populations that will give rise to neuronal and glial cell types of the peripheral nervous system, muscle, pigment cells, and undergo condensation to give rise to cartilage and bone. As differentiation of NCCs to mesenchymal derivatives begins to occur, the proper organization of cells must still be maintained; for example, suture boundaries in the skull are required to prevent ectopic bone formation.

The facial prominences undergo complex morphogenetic changes that require continual, tightly regulated rearrangement of cells to ensure appropriate development of the craniofacial complex. The mechanisms by which cellular organization is achieved during craniofacial development are varied and complicated and we are just beginning to understand them. Ultimately, elucidating the fundamental cellular principles that give rise to craniofacial structure is critical to understanding the vertebrate craniofacial form and how common defects of craniofacial structure arise.

Rhombomere organization and mechanisms of segregation

One of the best-studied examples of boundary formation, the separation between rhombomeres of the hindbrain, is particularly relevant to craniofacial development. The vertebrate hindbrain is organized into a series of 7 morphologically distinct segments, the rhombomeres, with compartment boundaries between them; this process is critical for establishing the regional identity of the hindbrain that will eventually form distinct adult brain structures (Lumsden and Krumlauf, 1996). Rhombomere boundaries also establish the NCC-segmentation patterns that will ultimately determine craniofacial organization by giving rise to skeletal elements with correct position and identity, as well as the periodic organization of neurons that innervate different facial and pharyngeal regions. The patterned induction of hindbrain positional identity by retinoic acid and Fgf signaling results in the expression of transcription factors including *Egr2/Krox20*, *Mafb*, and *Hox* genes with overlapping and initially imprecisely delimited domains that presage

rhombomere formation (Fig. 1.2A) (Tümpel et al., 2009). Two major mechanisms contribute to rhombomere compartmentalization and boundary formation; the first involves changes in gene expression to match positional identity; the second is based on the spatial segregation of cells with distinct identities (Addison and Wilkinson, 2016). Initially, upon the generation of patterned stripes, cell intermixing persists and changes in rhombomere identity can occur through regulation of gene expression (Fraser et al., 1990). For example, in the mouse hindbrain, the rhombomere 3 (r3) *Egr2* expression domain normally expands anteriorly and posteriorly at the expense of neighboring territories. In the absence of *Egr2*, r3 cells acquire the identity of neighboring r2 and r4 rhombomeres instead (Voiculescu et al., 2001). Interestingly, whereas individual cells change their identity when they move between rhombomere domains, groups of cells do not, despite the change in anterior-posterior (A-P) positional information (Addison et al., 2018; Trainor and Krumlauf, 2000). *Egr2* is a critical regulator of local cell identity switching, as mosaic expression of *Egr2* within even-numbered rhombomeres causes a non-cell-autonomous increase in *Egr2* expression in neighboring cells in chick and zebrafish (Addison et al., 2018; Giudicelli et al., 2001). A recent study has shown that this effect depends on *Egr2* repression of *Cyp26b1* and *Cyp26c1*, enzymes that degrade retinoic acid, within r3 and r5, presumably leading to a local increase in local retinoic acid levels (Fig. 1.2A) (Addison et al., 2018). This suggests that the gradient generated by the posterior retinoic acid source may be somewhat discontinuous across even-odd rhombomere boundaries, though such discontinuities have not yet been observed with existing reporters (Shimozono et al., 2013; White et al., 2007). Nevertheless, these findings provide important insights into a mechanism of early boundary establishment and sharpening.

In addition to the establishment of rhombomere cell identity by transcriptional regulation, cell sorting is critical for rhombomere boundary straightening and the formation of a physical barrier to cell crossing (Fig. 1.2A). Using clonal analysis in chick, zebrafish, and mouse embryos, it has been shown that clones of cells do not cross rhombomere boundaries after developmental time points when regional identity has been established (Fraser et al., 1990; Jimenez-Guri et al.,

2010; Xu et al., 1999). The cellular mechanisms by which rhombomere boundary segregation occurs are still under active investigation. Differential adhesion was the first mechanism proposed to drive rhombomere organization, based on studies in which cells from quail rhombomeres were transplanted into the rhombomeres of a chick host (Guthrie and Lumsden, 1991; Guthrie et al., 1993). In these experiments, it was observed that no cell mixing occurred when cells were transplanted into an adjacent rhombomere segment, while cells from the same segment did mix (Guthrie et al., 1993). These transplant experiments demonstrated that adjacent rhombomeres are immiscible, raising the possibility that these affinities were based on a fundamental property of cells specific to each individual rhombomere such as the strength or specificity of adhesion (Guthrie et al., 1993). The degree of cell mixing varied between cells derived from rhombomeres from different A-P positions, suggesting that an adhesive code may parallel the Hox code of the hindbrain (Fig. 1.2A) (Redies and Takeichi, 1996). This hypothesis was consistent with studies of cadherin expression in the hindbrain showing that different rhombomere segments expressed different cadherins throughout development (Inoue et al., 1997; Nakagawa and Takeichi, 1995). R-cadherin (Cdh4) was shown to be expressed in a subset of rhombomeres in both chick and mouse embryos (Fig. 1.2A) (Ganzler and Redies, 1995; Matsunami and Takeichi, 1995). Similarly, cadherin-6 is expressed in restricted rhombomere domains and segmentally-migrating NCCs (Fig. 1.2A) (Inoue et al., 1997; Nakagawa and Takeichi, 1995). Further, when cells from different rhombomeres were mixed *in vitro*, they preferentially re-aggregated with cells from the same rhombomere, and upon depletion of cadherin mediated adhesion, this region-specific cell segregation was no longer observed (Wizenmann and Lumsden, 1997). Despite this evidence suggesting a role of cadherin-mediated differential cell adhesion in rhombomere segmentation, phenotypic support for this mechanism as a major driver of hindbrain segmentation is lacking.

In contrast, several studies, primarily in zebrafish, have revealed that the EPH/EPHRIN signaling pathway is a key regulator of rhombomere segregation. Several EPH receptor tyrosine kinases and EPHRIN binding partners exhibit a reciprocal pattern of expression in odd-numbered

and even-numbered rhombomeres respectively (Fig. 1.2A) (Becker et al., 1994; Bergemann et al., 1995; Cooke et al., 2001; Xu et al., 1995). EPHA4 expression in r3 and r5 is directly promoted by Egr2, and EPHB4a expression in r5 and r6 is driven by the transcription factor Val/Mafba (Fig. 1.2A) (Cooke et al., 2001; Theil et al., 1998). Complementary to this expression, EPHRIN-B3 is expressed in even-numbered rhombomeres (r2/r4/r6), EPHRIN-B2a (Efnb2a) is expressed in r2/r4/r7, and EPHRIN-B2b is expressed in r1 and r4 (Fig. 1.2A) (Addison and Wilkinson, 2016; Cooke and Moens, 2002; Cooke et al., 2001; Xu et al., 1999, 1995). Disruption of EPHA4 signaling by expression of a truncated dominant-negative receptor resulted in cells with r3/r5 identity mislocalized within neighboring even-numbered rhombomeres. Mosaic overexpression of a cytoplasmic truncated EPHRIN-B2 lacking reverse signaling function resulted in exclusion of these cells from r3 and r5, and mosaic expression of truncated EPHA4 lacking intracellular forward signaling function resulted in exclusion of those cells from r2/r4/r6, suggesting that bidirectional signaling is involved in their segregation (Xu et al., 1995, 1999). In mouse, though EPHRIN-B1 does not exhibit restricted rhombomere localization, mosaic disruption of EPHRIN-B1 expression in the headfold at these stages resulted in cell segregation in the hindbrain, a process for which forward signaling, and not reverse, is required (O'Neill et al., 2016). In zebrafish, morpholino knockdown of EPHA4 or EPHRIN-B2a resulted in increased intermixing of r3 and r5 cells into their neighboring rhombomeres (Cooke et al., 2005). Interestingly, simultaneous knockdown of EPHA4 and EPHRIN-B2a resulted in a disruption of rhombomere boundaries far greater in severity than in either EPHA4 or EPHRIN-B2a knockdowns alone, consistent with the existence of additional signaling partners for both in these rhombomere boundaries, or with the existence of receptor-ligand interaction-independent roles for these molecules (Cooke et al., 2005; Kemp et al., 2009). As it has been demonstrated that EPH receptors can hetero-oligomerize (Janes et al., 2011), it will be interesting to determine whether the formation of distinct receptor/ligand complexes in different rhombomeres and at rhombomere boundaries further increases the complexity of the EPH/EPHRIN code.

Based on the role of EPH/EPHRIN signaling in repulsive axon guidance as well as time-lapse imaging of cell movement in zebrafish rhombomeres, it was hypothesized EPH/EPHRIN signaling drives repulsive interactions between adjacent EPH-expressing and EPHRIN-expressing cells, leading to formation and maintenance of the rhombomere compartments (Fig. 1.1B) (Xu et al., 1999). However, when EPHA4 knockdown cells were transplanted into wild-type zebrafish embryos, or when wild-type cells were transplanted into EPHA4 knockdown embryos, EPHA4 expressing and non-expressing cells segregated within r3 and r5, suggesting that EPHA4 expression may confer a selective adhesive property that drives boundary formation (Cooke et al., 2005). Similarly, the transplantation of Efnb2a knockdown cells into wild-type embryos, or vice versa, resulted in segregation of Efnb2a expressing and non-expressing cells (Kemp et al., 2009). EPHA4- and Efnb2a-mediated selective adhesion functioned independent of each other (Kemp et al., 2009). This intrarhombomeric segregation would not be predicted by mechanisms of repulsion alone, leading to the conclusion that EPHA4 and Efnb2a promote adhesion in addition to repulsion during rhombomere boundary formation (Cooke et al., 2005; Kemp et al., 2009).

Most recently, actomyosin contractility has also been proposed to play an important role at inter-rhombomeric boundaries. Actomyosin contractility has specifically been shown to be important in inter-rhombomeric boundary straightening and maintenance rather than in initial organization and boundary formation. Following rhombomere patterning, actin and myosin II begin to accumulate at inter-rhombomeric boundaries forming actomyosin cables (Calzolari et al., 2014). Disruption of actin or myosin II using ROCK inhibitors or blebbistatin treatment caused actomyosin cables to be dismantled, which led to jagged boundaries between rhombomeres (Calzolari et al., 2014). Conversely, calyculin A treatment, which maintains phosphorylated myosin and therefore enhances actomyosin contractility, resulted in stabilization of these rhombomere boundaries (Calzolari et al., 2014). These data suggest a critical role for actomyosin contractility in the maintenance of rhombomere compartment boundaries. It will be important to test these hypotheses using specific genetic perturbations of actomyosin contractility as this study

employed only pharmacologic inhibition of actomyosin, which could lead to indirect effects. If and how actomyosin contractility plays a role in the establishment of these boundaries remains unclear. Additionally, the relative contributions of differential adhesion, cellular repulsion, and/or actomyosin contractility to cell segregation in the establishment of the rhombomere boundaries remain unknown.

In addition to serving as physical boundaries, in many cases developmental boundaries also act as signaling centers that couple cell behaviors with patterning and cell fate specification. Specialized boundary cells at inter-rhombomere borders are critical for patterning of the hindbrain (Guthrie and Lumsden, 1991; Heyman et al., 1995; Xu et al., 1995). In chick, it has been demonstrated that border cells include a population of Sox2- expressing neural progenitor cells that give rise to neurons of both adjacent rhombomeres (Peretz et al., 2016). In zebrafish, these boundary cells express the chemorepellants Sema3fb and Sema3gb, which are critical for maintaining the positioning of Nrp2a-expressing neuronal populations within the rhombomere (Terriente et al., 2012). Boundary cells may help to determine cell affinity properties that drive the proper segregation of more differentiated rhombomere cells. The delta ligand is expressed in cells neighboring the boundary cells and activates Notch signaling within the boundary cells. Hyperactivation of Notch signaling resulted in aberrant segregation of cells to boundaries, whereas mosaic loss of Notch signaling resulted in cells segregating away from boundaries. Notch signaling is also required to prevent premature neuronal differentiation of boundary cells, thereby coupling the regulation of differentiation with the affinity properties that define rhombomeric organization (Cheng et al., 2004).

Cellular organization of NCCs

Neural crest cells arise at the border of the non-neural ectoderm and the neural plate, with induction of neural crest beginning at early gastrula stages and continuing through closure of the neural tube. Induction of NCCs at the neural plate boarder involves a host of signaling and tissue

interactions, including BMP signaling as well as Wnt, FGF, and retinoic signaling (Simões-Costa and Bronner, 2015). Following induction, NCCs undergo EMT and depart from the neural tube. Directional migration of cranial NCCs to the branchial arches occurs in segmental migratory streams, followed by their entry into the branchial arches, termination of migration and differentiation. Each of these steps requires dynamic changes in cellular organization properties in order for NCCs to arrive in their appropriate destination and give rise to properly organized craniofacial elements.

Delamination

Induction of NCCs at the neural plate border initiates a series of molecular and physical cellular changes through EMT to allow delamination and separation of NCCs from the neural tube and the adoption of a migratory phenotype. Changes in adhesion, cellular polarity and motility are tightly regulated in time and space. The changes in cadherin expression as NCCs undergo EMT are somewhat different between organisms, but have been well studied in the chick. Though initial studies posed a classical EMT view of cadherin “switching” in which E-cadherin expression is lost and N-cadherin expression is gained, more recent detailed temporal studies have demonstrated that the situation is much more complicated and nuanced (Dady and Duband, 2017; Nakagawa and Takeichi, 1995, 1998). The early neural plate expresses E-cadherin and N-cadherin, whereas the non-neural ectoderm expresses E-cadherin but not N-cadherin (Dady and Duband, 2017). As NCC induction occurs, cadherin-6B is expressed within NC progenitor cells, which still express E-cadherin but do not express significant levels of N-cadherin. Cadherin-6B expression is initially dispersed, in a salt-and-pepper pattern, among other cells of the neural tube, but this expression resolves, presumably by partitioning from non-neural ectoderm expressing Ecadherin, but not cadherin-6B, and from N-cadherin-expressing neural plate cells (Dady and Duband, 2017). In NCC cells beginning to emigrate, E-cadherin is still expressed, though at somewhat reduced levels, and N-cadherin is still not expressed (Dady et al., 2012; Dady and Duband, 2017).The

most striking change in cadherin expression through NCC delamination is in cadherin-6B, which is dramatically down regulated in migrating NCCs. As NCCs complete delamination, E-cadherin is finally lost, and the expression of cadherin 7 is dramatically up-regulated (Dady et al., 2012; Dady and Duband, 2017; Nakagawa and Takeichi, 1995, 1998). These patterns of expression suggest a tempting model in which combinatorial patterns of cadherin expression drive the segregation of the NCC from neural and non-neural ectoderm by differential affinity (Dady et al., 2012; Dady and Duband, 2017; Nakagawa and Takeichi, 1995, 1998). Unfortunately, it is not possible to discern dynamic changes in expression from cellular reorganization using static expression analysis, but future approaches utilizing live imaging or genetic lineage tracing of different cadherin-expressing populations will be of great value to answering this question. Nevertheless, it is clear that changes in cadherin expression through NCC EMT and delamination are critical, with cellular roles beyond regulation of differential affinity. Knockdown of cadherin-6B (Cad6B) in chick NCCs resulted in their premature delamination from the neural tube, while overexpression disrupted delamination with NCCs remaining clustered near the neural tube (Coles et al., 2007).

As might be expected, such dynamic regulation of cadherin-6B is complex and involves transcriptional and post-translational mechanisms. Tetraspanin18 (Tspan18) is critical to maintenance of cadherin-6B protein in premigratory NCCs (Fairchild and Gammill, 2013). When Tspan18 is lost this results in destabilization and early loss of cadherin-6B protein. Tspan18 is repressed by FoxD3, to alleviate stabilization of cadherin-6B during EMT enabling subsequent NCC migration (Fairchild and Gammill, 2013). In premigratory NCCs clatherin-mediated endocytosis and macropinocytosis also remove cadherin-6B from the cell surface (Padmanabhan and Taneyhill, 2015). Cadherin-6B down regulation is directly transcriptionally controlled both by direct suppression by the Snail2 transcription factor, and post-translationally by proteolytic cleavage by ADAM metalloproteases ADAM 10 and 19; depletion of these metalloproteases leads to the extended maintenance of cadherin-6B in the premigratory NCCs (Schiffmacher et al., 2014,

2016; Strobl-Mazzulla and Bronner, 2012; Taneyhill et al., 2007). In addition to dismantling adherens junctions to promote delamination and migration, the cleavage of cadherin-6B results in a proteolytic product, CTF2, that functions as a transcriptional regulator to feedback and reinforce the EMT gene regulatory program (Schiffmacher et al., 2016). In addition to cadherin-6B, levels of Ncadherin must be regulated for chick NCC emigration as its overexpression prevents NCC delamination (Nakagawa and Takeichi, 1998; Shoal et al., 2007). During NCC migration in *Xenopus*, E-cadherin expression levels are reduced, though it is still required for proper NCC migration (Huang et al., 2016). Meanwhile, in *Xenopus*, N-Cadherin expression increases upon the initiation of migration, promoting their collective migration (Huang et al., 2016; Scarpa et al., 2015). In *Xenopus* embryos, delamination of NCCs from the neural tube is therefore often referred to as partial EMT as NCCs initiate migration as a sheet rather than as individual mesenchymal cells (Sadaghiani and Thiébaud, 1987; Theveneau et al., 2010). Either overexpression or knockdown of Ncadherin blocks NCC migration, demonstrating the need for tight regulation of this cell adhesion molecule (Theveneau et al., 2010). *Xenopus* NCCs transition from collective migration to single cell migration between the neural tube and the branchial arches. A recent study sought to investigate the adhesive and mechanical changes associated with the dissociation of cells at early stages of *Xenopus* NCC migration using atomic force microscopy (AFM) (Blaue et al., 2018). These studies showed a uniform distribution of cell adhesion in NCC explants including semi-detached leader cells at the explant edge, suggesting that dissociation may not require weakening of cell-cell adhesions by changes in cadherin expression as previously hypothesized. Instead, NCC delamination requires a local decrease in tension mediated by increased expression of cadherin-11 to maximize cell-substrate contact and promote cell spreading and high substrate traction. Together these data provide a possible mechanism by which NCC cells transition from collective organization to a single-cell migratory phenotype (Blaue et al., 2018). While informative, all of these experiments were performed in *in vitro* explant culture; it will be necessary to test this role of cadherin-11 and cell- substrate traction in the dissociation

of *Xenopus* NCCs in the embryo. Additionally, analyzing the mechanical changes associated with EMT and delamination of NCCs in other species will be informative to the mechanisms of NCC migration across species.

Along with changes in cadherin expression, concurrent changes in cell polarization and actomyosin contractility must also occur in the cell during NCC EMT. Interestingly, in zebrafish hindbrain, cadherin-6 has been shown to be specifically required for accumulation of F-actin in NCCs to promote their detachment, further demonstrating that in certain circumstances, cadherin expression may promote cell motility over cell aggregation (Clay and Halloran, 2014). Notably, cadherin-6 is not expressed at this stage in the midbrain, consistent with the requirement of down regulation of cadherin-6B to allow NCC delamination in the chick and emphasizing regional specific differences in regulation of NCC delamination (Coles et al., 2007). *In vivo* timelapse imaging in the zebrafish hindbrain was used to reveal a number of cell behaviors during EMT including cell rounding, membrane blebbing, and filopodial extension upon the onset of migration. Disruption of myosin or Rho-kinase (ROCK), both critical for actomyosin contractility, prevented blebbing and reduced NCC EMT and migration, demonstrating a critical role for regulation of actomyosin dynamics in NCC delamination and migration (Berndt et al., 2008). Further studies in zebrafish have demonstrated that Rho/ROCK activation is restricted to the apical region of NCCs by Arhgap1 and that this Rho/ROCK activation and localization is essential for detachment from the neuroepithelium (Clay and Halloran, 2013). These studies suggest that ROCK-mediated changes in actomyosin contractility drive stereotypical cell behaviors including cell rounding and membrane blebbing that are critical for the initiation of NCC migration.

Neural Crest Segregation

Rhombomeres compartmentalize cell lineages along the A-P axis of the hindbrain, resulting in segmentation of different NCC populations during emigration from the neural border (Minoux and Rijli, 2010). Though NCCs are not generated in a segmental pattern (Sechrist et al.,

1993), their positionally segmented migration reflects rhombomeric boundary organization (Osumi-Yamashita et al., 1996). NCCs from rhombomeres r2, r4, and r6 migrate through the cranial mesenchyme in three sharp, highly stereotyped streams, avoiding the mesenchyme adjacent to r3 and r5 (Fig. 1.2B) (Lumsden et al., 1991). Some NCCs from r3 and r5 undergo apoptosis, the rest migrate to join with NCCs generated in more rostral and caudal rhombomeres (Farlie et al., 1999; Graham et al., 1993; Kulesa and Fraser, 1998).

The receptor tyrosine kinase gene *ErbB4* is expressed in rhombomeres r3 and r5, initially within the neuroectoderm, and shifting to the pial surface at these rhombomere boundaries. Its loss non-autonomously allowed invasion of transplanted wild-type r4 NCCs destined for branchial arch 2 (BA2) into the mesenchyme adjacent to r3, leading ultimately to inappropriate r4-derived NCC contribution to BA1 (Gassmann et al., 1995; Golding et al., 2000). In contrast, the neural crest-free boundary adjacent to r5 does not require *ErbB4* expression for its maintenance, and instead is regulated by unknown factors from the surface ectoderm overlying r5 (Golding et al., 2004). The *Xenopus* hindbrain is more compressed along the anterior-posterior axis and NCC-free zones are not observed. However, hindbrain origin position is maintained between streams, which may indicate that NCC-free zones are not a general requirement for segmentation of the migratory neural crest (Farlie et al., 1999).

Though rhombomere segmentation is necessary for normal initial NCC segmental migration, rhombomeres do not provide the only segmental cues as surgical removal of r3 resulted in invasion of NCCs into r3-adjacent mesenchyme, but maintenance of NCC segmental migration more ventrally (Golding et al., 2002, 2004). As in rhombomere boundary segregation, the EPH/EPHRIN signaling family has been implicated in maintaining segmented NCC streams (Fig. 1.2B). In *Xenopus*, the rhombomeric patterns of EPH/EPHRIN expression are extended into the migratory NCC streams such that *EPHA4* expression in r3 and r5 is maintained in r5-derived NCCs migrating toward the third arch, and *EPHB1* is expressed in NCCs migrating toward the third and fourth branchial arches (Fig. 1.2B) (Smith et al., 1997). *EPHRIN-B2*, in contrast, is

expressed in mesoderm along the migration pathway in a complementary pattern during NCC migration, consistent with the known roles of EPH/EPHRIN signaling in repulsive migration. Inhibition of EPHA4 or EPHB1 by overexpression of a dominant-negative mutant receptor resulted in expansion of the r5 NCC stream both rostrally and caudally from the outset of NCC emigration, with misguidance into second and fourth arch territories. Overexpression of EPHRIN-B2 to ectopically activate signaling resulted in the invasion of NCCs into ectopic sites (Smith et al., 1997). The fact that EPHA4 and EPHRIN-B2-expressing cells come into contact in the hindbrain and during early NCC migration, but are separated during migration into the arches, suggests that the NCC segmentation function of EPH/EPHRIN signaling occurs early; to what extent these functions may be related to even earlier disruption of rhombomere boundaries is not clear, but the fact that overexpression of EPHRIN-B2 can lead to a variety of redirections of the NCCs indicates that EPH/EPHRIN signaling is capable of redirecting NCCs relatively late in their migration. Though loss of function of EPHRIN-B2 in mice also results in disruption of NCC development and a hypoplastic second branchial arch, this phenotype is attributable to a role for EPHRIN-B2 within the vascular endothelium for NCC survival rather than migratory guidance (Davy and Soriano, 2007; Lewis et al., 2015). It is possible that redundancy in function may explain the lack of an obvious guidance phenotype in EPHRIN-B2 loss of function models. Defects in migration of NCCs have been documented upon loss of the related EPHRIN-B1 in mice, as NCCs destined for BA3 and 4 inappropriately intermix upon complete loss of EPHRIN-B1 or its loss specifically from NCCs (Davy et al., 2004). Several EPH receptors are also expressed in NCCs in mouse, though they are generally not as strikingly segmentally restricted to migratory NCC populations as in *Xenopus* (Adams et al., 2001; Agrawal et al., 2014; Gale et al., 1996).

Both embryological and genetic support exists for the role of Semaphorin/ Neuropilin/ Plexin signaling in cranial NCC segmentation from the earliest stages. Sema3A and Sema3F exhibit restricted expression of variable levels within r1, r3 and r5 (Fig. 1.2B). The Npn1 and Npn2 co-receptor genes are expressed in NCC streams in the periocular region and streams derived

from r2, r4 and r6; the Plexin-A1 receptor is expressed within NCCs migrating from r4 (Fig. 1.2B) (Eickholt et al., 1999; Gammill et al., 2007; Meléndez-Herrera and Varela-Echavarría, 2006; Osborne et al., 2005). In chick, implantation of *Sema3A* soaked beads in the hindbrain prevented NCC emigration, whereas expression of a Neuropilin-Fc signaling competitor resulted in invasion of NCCs into areas normally inhibitory to their migration (Osborne et al., 2005). Likewise, loss of *Npn2* or *Sema3F* in mouse and zebrafish resulted in loss of sharp NCC boundaries, with bridges of cells crossing over between NCC streams 1 and 2 (Gammill et al., 2007; Yu and Moens, 2005). Whereas no skeletal defects were observed in mouse mutants lacking *Sema3F* or *Npn2*, consistent with the ability of NCCs to adopt the identity of their new position, the trigeminal ganglia was less condensed, and defects in the fasciculation of trigeminal nerve branches occur at later stages in *Npn2* null mice (Gammill et al., 2007; Giger et al., 2000). Interestingly, in the basal vertebrate, the lamprey, *Sema3F/Npn* signaling does not work to regulate segmental migratory guidance; instead, *Sema3F* functions in the positioning of NCC derivatives including pigment, cranial sensory neurons, and elements of the head and pharyngeal skeleton (York et al., 2018). This suggests that during evolution, the roles for this pathway in the segmental organization of the head have changed, allowing rearrangement of the vertebrate head skeleton (York et al., 2018).

The transcriptional control of NCC guidance factors is beginning to be understood as well. In mutant embryos, lacking T-box transcription factor, *Tbx1*, migratory streams are maintained until entry of NCCs into the branchial arches, at which time r4-derived NCCs inappropriately invade the first branchial arch, which may explain the cranial nerve fusions and skeletal anomalies that arise in these mutants (Moraes et al., 2005; Vitelli et al., 2002). *Tbx1*, which is expressed in the branchial arch mesoderm, endoderm, and ectoderm but not neuroectoderm or NCCs, is required for normal levels of *Fgf8* expression within the branchial arch ectoderm, providing one mechanism by which *Tbx1* may non-autonomously regulate NCC development (Chapman et al., 1996; Garg et al., 2001; Vitelli et al., 2002). However, though *Fgf8* is important for NCC survival

and branchial arch formation, it does not appear to directly regulate NCC segmentation, as hypomorphic loss of *Fgf8* did not result in defects in the segmentation of NCC cells (Abu-Issa et al., 2002).

More recently, it has been demonstrated that in *Tbx1* $-/-$ mutant mouse embryos, expression of the chemoattractant *Sdf1* is reduced in the pharyngeal endoderm, and expression of *Cxcr4*, its receptor, is reduced within NCCs, suggesting that *Tbx1* may regulate *Sdf1* to properly guide NCCs into the arches (Escot et al., 2016). Indeed, disruption of *Sdf1/Cxcr4* signaling results in NCC guidance defects in chick, *Xenopus* and zebrafish (Escot et al., 2016; Olesnicky Killian et al., 2009). Rather than acting as a repulsive cue to maintain NCC segmentation, *Sdf1* promotes directional polarization of neural crest cells expressing *Cxcr4* by directionally stabilizing protrusions following NCC contacts (Theveneau et al., 2010). In *Xenopus* and zebrafish, *Sdf1* is expressed in the pre-placodal region at the border of the neural plate before NCC migration begins and is later restricted to discrete domains corresponding to individual placodes. The expression of *Sdf1* attracts NCCs, while in turn the physical NC-placode contact directionally displaces the placode, which remains segregated from the NCCs in a “chase and run” mechanism (Theveneau et al., 2013).

NCC Migration

The directed segmental migration of NCCs to the PAs involves multiple signaling pathways that coordinate complex cell behaviors. A well-established mechanism for how directed migration occurs is commonly referred to as contact inhibition of locomotion (CIL), which is also a mechanism for boundary formation and maintenance (Fig. 1.3B, C). CIL encompasses a number of constituent cell behaviors in which two cells come into contact and either cease movement or undergo active directional migration away from each other (Fig. 1.3B, C). The specific cellular details of CIL events can vary significantly, leading to the description of a variety of CIL subtypes (Martz and Steinberg, 1973; Stramer and Mayor, 2017). Whereas type I CIL

describes the situation in which the leading edge of a cell undergoes contraction upon contact with another cell, type II CIL is essentially a case of differential adhesion, wherein another cell's surface is less adhesive than the substrate, causing the cell to prefer not to migrate over the other cell (reviewed in Stramer & Mayor, 2017). It is notable, however, that neither CIL type specifies what happens following the contact, though type I CIL has been associated with active movement away from a collision partner and type II CIL has been considered as a passive response that stops cell movement (Fig. 1.3B) (Stramer and Mayor, 2017).

CIL behavior was first described in fibroblasts (Abercrombie and Heaysman, 1953) and has since been observed in other cell types, including *Xenopus* NCCs in culture and *in vivo* (Carmona-Fontaine et al., 2008). Time-lapse imaging revealed *Xenopus* NCCs making contact, collapsing protrusions and changing the direction of their migration, while NCCs encountering another cell type did not demonstrate these behaviors and invaded the neighboring tissue (Carmona-Fontaine et al., 2008). The cumulative effect of CIL interactions within a NCC stream is the coordinated directional polarization and migration of the cells within that stream. Cell contact and intercellular communication is required during CIL prior to detachment, repolarization and movement away (Fig. 1.3B, C). Both N-cadherin and cadherin-11 are essential for proper CIL behavior in *Xenopus* NCCs, with disruption of either cadherin leading to loss of CIL and non-directional migration (Becker et al., 2013; Theveneau et al., 2010). At cell-cell contacts, N-cadherin signaling function inhibits Rac1 activity and thus inhibits protrusions while promoting Rac1 activation and protrusions at the cellular free edge (Theveneau et al., 2010). Recently, it was shown that N-cadherin expression is dependent on PDGFR α /PDGF-A signaling (Bahm et al., 2017). The PDGFR α receptor tyrosine kinase and its ligand PDGFA are co-expressed in CNCCs, and their inhibition prevents N-cadherin expression, thus resulting in a loss of CIL and inhibiting NCC migration (Bahm et al., 2017). This pathway therefore achieves cell autonomous regulation of CIL by upregulating N-cadherin during EMT. A role for PDGF signaling in NCC migration has been demonstrated in zebrafish, mice and *Xenopus*, suggesting this may be a

conserved mechanism for driving the directional migration of NCCs (Bahm et al., 2017; Eberhart et al., 2008; He and Soriano, 2013; Tallquist and Soriano, 2003).

Unlike N-cadherin, cadherin-11 localizes to cellular protrusions such as lamellipodia and filopodia, and is necessary for their protrusion formation and normal NCC migration (Kashef et al., 2009). While the cytoplasmic tail of cadherin-11 has been shown to drive this protrusive phenotype, specifically reducing cadherin-11s adhesive function results in loss of CIL behavior and increased invasiveness (Becker et al., 2013; Kashef et al., 2009). As in NCC delamination, post-translational regulation of cadherin expression and function is critical for regulation of CIL. Cadherin-11 is regulated through cleavage by ADAM13, and this cleavage, which creates the extracellular fragment EC1–3, is essential for NCC migration (Abbruzzese et al., 2016; Cousin et al., 2012). In cells expressing a non-cleavable variant of cadherin-11, migration is inhibited, and migratory defects can be rescued by expression of the EC1–3 cleavage product (Abbruzzese et al., 2016). It was recently shown that the EC1–3 cleavage product stimulates phosphorylation of AKT through interactions with ErbB2, which is necessary for NCC migration (Mathavan et al., 2017). These studies indicate that cadherin-11 cleavage products have a signaling function in regulating NCC migration, further demonstrating the diverse and complex ways in which cadherins regulate NCC migration.

The repolarization of cells after contact is a critical component of NCC directional migration. In addition to N-cadherin signaling inhibiting Rac, an increase in RhoA activity at the site of cell-cell contact, regulated by the planar cell polarity (PCP) pathway is required for CIL (Matthews et al., 2008). RhoA and the proteoglycan Syn4, a proposed regulator of cell migration, inhibit Rac at the site of contact (Carmona-Fontaine et al., 2008; Matthews et al., 2008; Theveneau et al., 2010). This activation of RhoA at the site of contact, along with strong inhibition of Rac, ultimately promotes the formation of directional protrusions away from the site of contact. Further, in both *Xenopus* and chick, this pathway was shown to act through the actin binding protein calponin2 (Cnn2), which localizes to the leading edge of NCCs (Ulmer et al., 2013). Cnn2

knockdown results in random protrusion formation and migratory defects, suggesting an important role for Cnn2 in polarizing the actin cytoskeleton, promoting protrusion formation, and the formation of directional protrusions for directional migration (Ulmer et al., 2013). Knockdown of Cnn2 rescued migratory defects observed as a result of loss of Wnt signaling and ROCK, suggesting Cnn2 is acting downstream of these pathways in NCC migration (Ulmer et al., 2013). Along with inhibition of Rac1 at the contact edge, an increase in Rac1 activity is required away from the contact to drive cellular repolarization and lamellipodia formation (Scarpa et al., 2015). In cells expressing E-cadherin, which do not separate upon contact, stimulation of protrusion formation through Rac1 was sufficient to induce the separation of these cells, suggesting that this repolarization and protrusion formation at the new leading edge is sufficient to tear the adhesions at the edge of contact and lead to separation of these two cells after collision (Scarpa et al., 2015).

It has been suggested that CIL behavior alone would result in the spreading of migrating neural crest cells rather than maintenance of migratory streams. However, a mechanism of mutual cell-cell coattraction could counterbalance the tendency of cells to disperse through mechanisms such as CIL. In *Xenopus*, it has been shown that NCCs are attracted to one another through the complement fragment C3a and its receptor C3aR (Carmona-Fontaine et al., 2011). Loss of coattraction through antibodies blocking C3a/C3aR signaling disrupted coordinated movements of the NCCs. This disruption of movement, however, occurred in a variable fashion ranging from slight disruption of migratory streams to complete disorganization and lack of migration. These findings led the authors to propose a migratory mechanism in which coattraction and CIL form a balance to allow cells to self-organize and migrate (Carmona-Fontaine et al., 2011). Mathematical modeling of these two parameters of coattraction and CIL demonstrated how this balance could result in maintenance of the directionality of migration and recapitulated many properties of NCC migration *in vitro* and *in vivo* (Woods et al., 2014).

While CIL behavior and coattraction occur in the migration of NCCs in both amphibians and zebrafish (Carmona-Fontaine et al., 2011), there is some question as to whether this CIL

mechanism occurs in all species or even if collective migration occurs in NCCs of all species. In chick, detailed imaging analysis has shown that chick NCCs maintain cell-cell contacts through dynamic long- and short- range filopodial protrusions while migrating (Teddy and Kulesa, 2004). Cell-cell contact through these protrusions was shown to result in a cell changing direction to favor the neighboring cell's path suggesting that protrusions may mediate cell communication to refine directionality within the migratory stream (Teddy and Kulesa, 2004). Further, it was noted that cell morphology and protrusion dynamics differ between regions within the neural crest migratory streams, with cells at the leading edge being non-polar, containing many protrusions, and cells away from the leading edge displaying a bipolar morphology (Teddy and Kulesa, 2004). A recent study from Genuth et al. also using detailed live imaging of NCCs *in vivo* in the avian embryo to analyze protrusion dynamics made somewhat different conclusions, though differences in stages of analysis, and methods of imaging and quantification exist between the two studies (Genuth et al., 2018; Teddy and Kulesa, 2004). Notably, Genuth et al. did not observe differences in protrusion dynamics dependent on cell positioning within the migratory stream. Further, the authors of this study showed that chick NCCs have a weak spatial bias in the generation of filopodial protrusions followed by a strong spatial bias in the generation of large protrusions in the direction of movement (Genuth et al., 2018). These findings differ from those in *Xenopus*, in which NCCs undergo co-attraction and CIL, with cells migrating as a stream with only edge cells extending protrusions (Carmona-Fontaine et al., 2008). Additionally, in contrast to the CIL model of migration where cell-cell contact results in protrusion collapse, Genuth et al., observed that in the majority of migratory NCCs, protrusions continued to be extended after contact with another cell, and these cells maintained a forward trajectory following cell-cell contact. Though a thorough test of the ability of chick NCCs to undergo CIL, would require examination of cell behaviors in a lower density context, these findings nevertheless suggest a different mechanism from CIL in which chick NCCs migrate through a search and polarity refinement mechanism. Additional mechanistic studies will be necessary to determine the role of protrusion based cell-cell contacts

in NCC migration as well as the role of these protrusions in sensing the local environment, and how these inputs are coordinated to result in directional collective migration.

How this migration occurs in mouse has yet to be determined, but differences between *Xenopus* and mouse NCC migration mechanism have already been noted. Mouse NCC migration was shown to occur independently of PCP signaling, which is essential in both *Xenopus* and zebrafish (Pryor et al., 2014). Using *Vangl2* Lp/Lp mice, which lack PCP signaling, the authors showed that despite neural tube closure defects and lack of PCP signaling, normal NC specification, migration, and derivative formation occurred in these embryos, suggesting that this signaling pathway is dispensable for segmental NCC migration in mice (Pryor et al., 2014). The pathways critical for polarization in NCC migration in mice are not clear, but these discrepancies between species suggest that control of NCCs migration may be achieved by multiple mechanisms *in vivo*.

As a mechanism of developmental boundary formation, CIL behavior has parallels to cell segregation mechanisms but also has important differences. First, the cell-cell repulsion model that has been proposed to drive segregation could be considered a general subtype of CIL (Fig. 1.3A, B). Indeed, it has been demonstrated that EPH/EPHRIN signaling, a potent driver of cell segregation by cellular repulsion (Poliakov et al., 2008), does indeed also activate CIL in some cell types (Astin et al., 2010; Villar-Cerviño et al., 2013). While both CIL and repulsive cell sorting result in the migration of two cells away from one another following contact, directional Rac1 repolarization away from the site of contact has been demonstrated for CIL but has not been specifically shown for repulsive migration related to cell segregation (Fig. 1.3A, B). Second, whereas cadherins drive cell segregation by differential affinity mechanisms that promote homotypic adhesion, homotypic cadherin interactions are actually required for repulsive interactions in CIL (Fig. 1.3B). Indeed, most examples of CIL in the developing embryo involve homotypic repulsion, while cell segregation by repulsion is by definition between heterotypic cellular contacts. Finally, it has been demonstrated that actomyosin contractility is required for

EPH/EPHRIN mediated cellular collapse (Prospéri et al., 2015), whereas upon treatment with blebbistatin to inhibit myosin contractility, NCCs were still able to switch polarity, detach and migrate, suggesting that CIL behavior is not dependent upon myosin contractility (Kadir et al., 2011). Instead, RhoA activation is necessary for cellular repolarization by inhibition of Rac1 in CIL; though it has not yet been determined whether local regulation of Rac1 activity is required for cell segregation, its pharmacological inhibition did not disrupt EPH/EPHRIN mediated cell segregation, suggesting that Rac1-mediated repolarization is most likely not required (O'Neill et al., 2016). Therefore, whereas CIL, as most commonly described, is a potent regulator of cellular organization, it is distinct from other modes of cellular segregation and boundary formation, though they share some cell biological characteristics.

It is important to note that segmentation of the PAs and intervening pharyngeal pouches, outpocketings of the foregut endoderm that help to organize development of the head and neck, does not solely rely on maintenance of distinct NCC-migratory streams, but also heavily involves the endoderm. In *Tbx1*^{-/-} mice and mice lacking *Tbx1* specifically from the endoderm, pharyngeal pouches fail to evaginate from the foregut endoderm. Loss of *Fgf3* and *Fgf8* from the pharyngeal endoderm only partially disrupted pouch morphogenesis indicating that Fgf signaling is not required for pouch formation (Jackson et al., 2014). However, *Fgf8* is required, together with *Fgf3*, for segmentation of the pharyngeal endoderm into pouches in zebrafish (Crump et al., 2004). Notably, initial rhombomere organization again plays an important role, as *Fgf8* and *Fgf3* are segmentally restricted within the midbrain/hindbrain boundary and r4, and expression from the neural tube as well as the mesoderm was required for normal early pharyngeal pouch segmentation (Crump et al., 2004; Maves et al., 2002). EPH/EPHRIN signaling also has a role in pharyngeal morphogenesis beyond guidance of NCCs. In zebrafish, EPH/EPHRIN expression regulates morphogenesis of the pharyngeal pouches. Signaling between *Efnb2a/Efnb3b* and *EPHB4a* within the pouch endoderm is required to increase intercellular adhesion to regulate segmental pouch outgrowth (Choe and Crump, 2015). Finally, Wnt signaling is an important

pathway for endoderm segmentation and pouch formation (Choe et al., 2013). Wnt11r, expressed in discrete domains of the head mesoderm, along with Rac1 are important to initial outgrowth of the pouch forming cells (Choe et al., 2013). Later, Wnt4a, displaying segmental expression in the head ectoderm, and Cdc42 signaling are required to organize the developing pouch (Choe et al., 2013). Requirement for both Wnt11r and Wnt4a in pharyngeal pouch morphogenesis suggests roles for both the mesoderm and ectoderm in segmentation of the pharyngeal pouches.

Boundaries in skull vault development

Later in craniofacial development, tissue boundaries are critical for establishing normal skeletal structure. The skull vault develops from neural crest and paraxial mesoderm-derived cells that do not mix during development. Instead, they maintain a boundary that first appears in mice at E9.5 and remains a distinct interface through the neonatal stage (Fig. 1.2C) (Chai et al., 2000; Jiang et al., 2002). The transcription factor Twist1 is a key regulator of mesoderm formation and maintenance of NCC/mesoderm boundaries. In mice, homozygous loss of Twist1 results in NCC invasion into the paraxial mesoderm, and loss of Twist1 specifically within the mesoderm led to an invasion of mesenchyme into the NCC-derived ganglia (Bildsoe et al., 2013; Soo et al., 2002). Though the cellular mechanisms by which NCC/mesoderm intermixing is prevented are unknown, it is notable that in chimera experiments in mice, Twist1 $-/-$ head mesenchyme cells strikingly segregate from wild-type cells (Chen and Behringer, 1995). Interestingly, in epithelial cell lines, Twist-1 promotes EMT through repressing E-cadherin resulting in a loss of Ecadherin-mediated cell-cell adhesion, suggesting that Twist1 may regulate adhesion differences to drive cell segregation (Yang et al., 2004). Further, Twist1 loss in the coronal suture results in reduced expression of EPHRIN-A2, EPHRIN-A4, and EPHA4 suggesting another possible mode by which Twist might regulate segregation (Ting et al., 2009). It will be extremely interesting to determine the expression profiles of drivers of cell segregation such as EPH/EPHRINs and cadherins in Twist1 $-/-$ head mesenchyme cells.

In mammals, the neural crest/mesoderm boundary will ultimately coincide with the coronal suture, with NCC-derived cells forming the frontal bones and mesoderm-derived cells forming the parietal bones and coronal suture mesenchyme (Fig. 1.2C) (Jiang et al., 2002; Merrill et al., 2006; Yoshida et al., 2008). Calvarial sutures are fibrous joints that allow passage through the birth canal and accommodate the growth of the underlying brain while preventing the premature fusion of the calvarial bones of the skull (Ishii et al., 2015). The suture serves as a growth center to regulate the proliferation and differentiation of osteoprogenitors in the appositional growth of the calvaria during development and houses the mesenchymal stem cells that are the main progenitor population for craniofacial bones during postnatal growth (Zhao et al., 2015). An overabundance of NCCs, such as in mouse embryos lacking the ciliary protein Fuz, drives an expansion of the NCC-derived frontal bone at the expense of the mesoderm-derived parietal bone, but not an intermixing between these populations (Tabler et al., 2016). In contrast, mice with mutations in engrailed 1, a protein that plays a role in lineage boundaries in multiple contexts (Araki and Nakamura, 1999; Dahmann and Basler, 2000) show premature migration of neural crest-derived cells into the coronal suture territory, resulting in a shifted mesoderm/NCC boundary (Deckelbaum et al., 2012). Thus, in this context, engrailed 1 appears to be an important regulator of cell movement and therefore boundary formation at this interface.

The mesenchyme precursors that generate the coronal suture originate from the cephalic paraxial mesoderm cells that migrate to establish a lineage boundary with the neural crest derived mesenchyme (Deckelbaum et al., 2012). As at earlier stages, Twist1 is a key regulator of suture boundaries; Twist1 +/- mice exhibit coronal synostosis (a premature fusion of the frontal and parietal bones), with inappropriate invasion of NCC-derived mesenchymal cells into the mesoderm-derived coronal suture mesenchyme (Carver et al., 2002; Merrill et al., 2006). This suture boundary is apparently distinct from the earlier NCC/mesoderm boundary, as NCC invasion into mesoderm-derived tissues in Twist1 +/- embryos was not observed prior to the establishment of the suture at E14.5 (Merrill et al., 2006). Other studies have proposed that the

suture boundary may actually be unidirectional in nature, preventing NCC mixing into the suture and parietal bone, while allowing a small number of *Mesp1-cre* lineage mesoderm cells to contribute to the frontal bone (Deckelbaum et al., 2012). Nevertheless, an important function of *Twist1* at this suture boundary is to prevent aberrant cell intermixing, which is achieved in part by the regulation of EPH/EPHRIN-mediated cell segregation; expression of EPHRIN-A2, EPHRIN-A4 and EPHA4 were reduced in *Twist1* +/- sutures, and loss of signaling through EPHA4 resulted in partial suture fusion (Merrill et al., 2006; Ting et al., 2009). Though little is known about the cell behaviors involved in EPH/EPHRIN segregation at the suture boundary, it is notable that EPH/EPHRIN signaling can regulate boundary formation in contexts as distinct as the suture mesenchyme and hindbrain neuroepithelium, underlining the fact that the EPH/EPHRIN signaling pathway is a powerful regulator of cell segregation independent of cell type and developmental context. EPH/EPHRIN signaling also impacts calvarial bone formation by regulation of gap junction communication, providing a potential mechanism by which suture boundary formation and regulation of bone formation might be coupled (Davy et al., 2006).

Disruption of coronal suture boundaries was also observed in mice lacking the Notch ligand *Jagged1* from the suture mesenchyme, which exhibit invasion of mesoderm-derived cells into the frontal bone (Yen et al., 2010). The cellular mechanisms by which *Jagged* signaling regulates suture boundary formation are not yet known and it is not clear whether disruption of *Jagged1* signaling leads to loss of boundaries by aberrant cell segregation or a change in cell fate specification. *Twist1* also regulates *Jagged1* expression in the suture, and compound loss of *Twist1* and *Jagged1* resulted in a more severe craniosynostosis phenotype. *Twist1* +/- adult mice also exhibit a reduction in *Glil*-expressing MSCs in their sutures, consistent with the long-term importance of establishing developmental boundaries (Zhao et al., 2015). Together, these studies put *Twist1* at the top of a regulatory hierarchy for the establishment and maintenance of normal coronal suture boundaries. Though the concurrence of the coronal suture with the NCC/mesoderm boundary in mice provides powerful Cre-recombinase genetic tools for observing

and manipulating the coronal suture boundary, this coincidence may not be generally significant. In fact, there are species-specific differences in the location of this boundary; in chick, *Xenopus* and zebrafish, the neural crest/mesoderm boundary occurs within the frontal bone, and the coronal suture occurs between bones of mesodermal origin (Fig. 1.2C) (Kague et al., 2012; Matsuoka et al., 2005; Piekarski et al., 2014). Nevertheless, loss of *Twist1* and its partner *Tcf12* in zebrafish results specifically in coronal synostosis by a directional acceleration of bone production and exhaustion of coronal suture progenitor cells (Teng et al., 2018). These findings indicate that what is unique about the coronal suture is not related to embryonic origin, but rather that boundary maintenance can be achieved by exquisite control of directional growth dynamics. It will be exciting to determine whether other sutures also exhibit boundary characteristics, such as restriction of mesenchymal intermixing.

Cell segregation in craniofacial dysmorphology

Generally, it is difficult to determine to what extent human craniofacial conditions explicitly result from disruption of developmental boundaries, though a few examples exist. As discussed above, disruption of suture boundaries is likely to contribute to coronal synostosis upon heterozygous loss of function of *Twist1* in Saethre-Chotzen syndrome (Howard et al., 1997). Similarly, mutation of *EFNA4* has been identified in humans with coronal synostosis (Merrill et al., 2006). Craniofrontonasal syndrome (CFNS) is caused by mutations in *EFNB1*, a gene found on the X-chromosome that encodes the EPHRIN-B1 signaling protein (Twigg et al., 2004; Wieland et al., 2004). As *EFNB1* is an X-linked gene, heterozygous female CFNS patients harbor cellular mosaicism for *EFNB1* mutation due to random X-inactivation, and thus mosaic expression of EPHRIN-B1. CFNS results in coronal craniosynostosis, hypertelorism, frontonasal dysplasia and cleft lip and palate, affecting females heterozygous for *EFNB1* mutations more severely than hemizygous males with no functional *EFNB1*, suggesting that mosaicism underlies disease severity. Indeed, males with somatic mosaic *EFNB1* mutations, resulting in mosaic EPHRIN-B1

expression, also exhibit severe phenotypes similar to heterozygous females, supporting that mosaicism for EPHRIN-B1 underlies the disease phenotype (Twigg et al., 2013). *EfnB1*^{+/-} mice exhibit many of the same craniofacial phenotypes as CFNS patients, and mosaicism for EPHRIN-B1 expression results in aberrant segregation of cells in the neuroepithelium and the appearance of ectopic EPHRIN-B1 boundaries in NCC-derived mesenchyme of the craniofacial region (Fig. 1.2D) (Bush and Soriano, 2010; Compagni et al., 2003; Davy et al., 2006). Cell segregation also occurs in patient hiPSC-derived neuroepithelial cells, supporting the relevance of aberrant segregation in human CFNS (Niethamer et al., 2017). The CFNS disease model has also been instructive in studying the molecular and cellular mechanisms by which EPH/EPHRIN-mediated segregation and boundary formation may occur more generally *in vivo*. For example, whereas bidirectional signaling has previously been associated with cell segregation, mouse genetics approaches demonstrated that unidirectional forward signaling is necessary and sufficient for cell segregation in this context (O'Neill et al., 2016). Cell segregation in *EFNB1*^{+/-} embryos required ROCK function, but not the function of Cdc42 or Rac1, indicating that though actomyosin contractility is required for segregation, repolarization of cells by Rac1 or Cdc42 is not required. These data support a model in which unidirectional signaling influences cortical actomyosin contractility to drive segregation (O'Neill et al., 2016). How aberrant cell segregation and ectopic boundaries ultimately disrupt craniofacial morphogenesis remains to be determined.

Conclusion

The cellular behaviors underlying boundary formation in craniofacial morphogenesis are complex and only beginning to be uncovered. While rhombomere boundaries and neural crest migratory streams have been well-studied, much remains to be learned regarding the mechanisms of regional identity plasticity as well as the molecular and physical mechanisms driving cell segregation and how these are coupled to regulate boundary formation. Rhombomere boundaries serve as critical organizational centers, segregating the neural ectoderm into

segments and establish the initial patterning for NCC migration and pharyngeal morphogenesis. The migration of NCCs in distinct migratory streams to populate specific regions of the developing head and face are critical for proper morphogenesis. These processes begin at the earliest stages of craniofacial development, and though incompletely understood, we have a considerable amount of data on the cell behaviors underlying cell segregation and boundary formation at the early stages of craniofacial development. In contrast, we have very little information on post-migratory cellular organization of the craniofacial mesenchyme, though studies of craniofacial dysmorphology emphasize the continual importance of proper boundary formation and tissue flow. Whether and how cell segregation acts throughout later stages of craniofacial morphogenesis to enable proper cellular organization therefore remains an open question. Many commonalities exist between the mechanisms establishing different boundaries throughout craniofacial development, and each utilize an overlapping toolkit of cellular mechanisms that includes cell-cell adhesion and actomyosin cytoskeletal dynamics to regulate cell migration, cell polarization and interfacial tension to achieve craniofacial organization. Many cell behaviors discussed here have been studied *ex vivo* or in cell culture contexts; for many such cell behaviors, such as how actomyosin-mediated cortical tension influences the strength of cell contacts in NCC EMT, remains unknown. Further, it is important to consider that each of these mechanisms has broad pleiotropic roles; for example, cadherin regulation of cell behavior goes far beyond cell-adhesion function and we are just beginning to uncover the detailed molecular mechanisms regulating, and regulated by cadherins in these cellular organization processes. It is unlikely that there is a universal mechanism governing self-organization in different cell types; rather, multiple mechanisms likely influence the physical properties of cells to achieve different organization according to a few basic principles, including those described above. Indeed, the examples discussed here are likely just a few of the boundaries that contribute to craniofacial development; for example, relatively little is understood about how NCC-derived mesenchymal populations generate boundaries for the formation of distinct skeletal elements. A detailed mechanistic

understanding of the organizational principles that underlie craniofacial morphogenesis is critical to understanding how this complex process occurs.

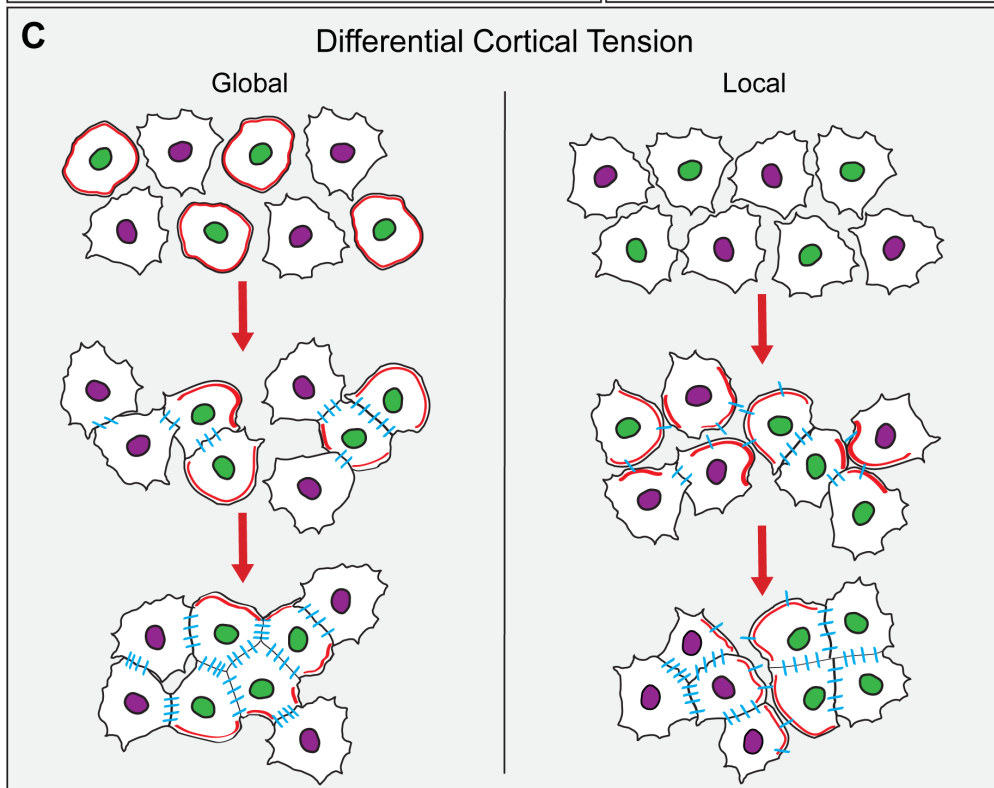
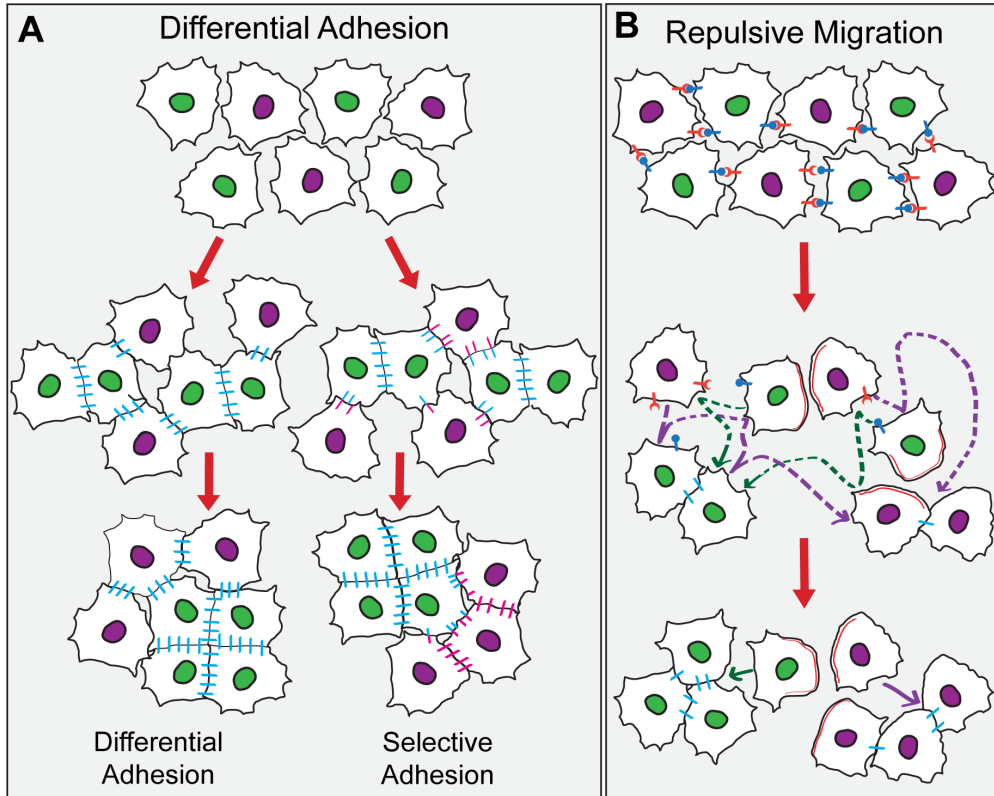


Figure 1.1. Cellular mechanisms underlying cell segregation and boundary formation based on differences in cell:cell adhesion or cortical actomyosin contractility.

(A) Differential cell adhesion can result in cell segregation either through differential adhesion resulting from different levels of cadherin expression, or selective adhesion, resulting from the types of cadherins expressed. Cells with greater adhesion will aggregate and be surrounded by the less adhesive cell population. **(B)** Cell segregation can also be achieved through cell-cell repulsion in which a local repulsive cue triggers collapse of cellular processes and repulsive migration. Over reiterative repulsive interactions cell segregation is achieved. **(C)** Differences in cortical actomyosin contractility can lead to cell segregation. Cortical contractility can be localized to a specific interface, preventing heterotypic cell pairs from making stable cell contacts, thus only forming stable contacts with like cells, giving rise to two separate populations. Contractility can also be globally high in one cell type, resulting in those cells aggregating and being surrounded by the less contractile cell type to minimize these high-tension interactions.

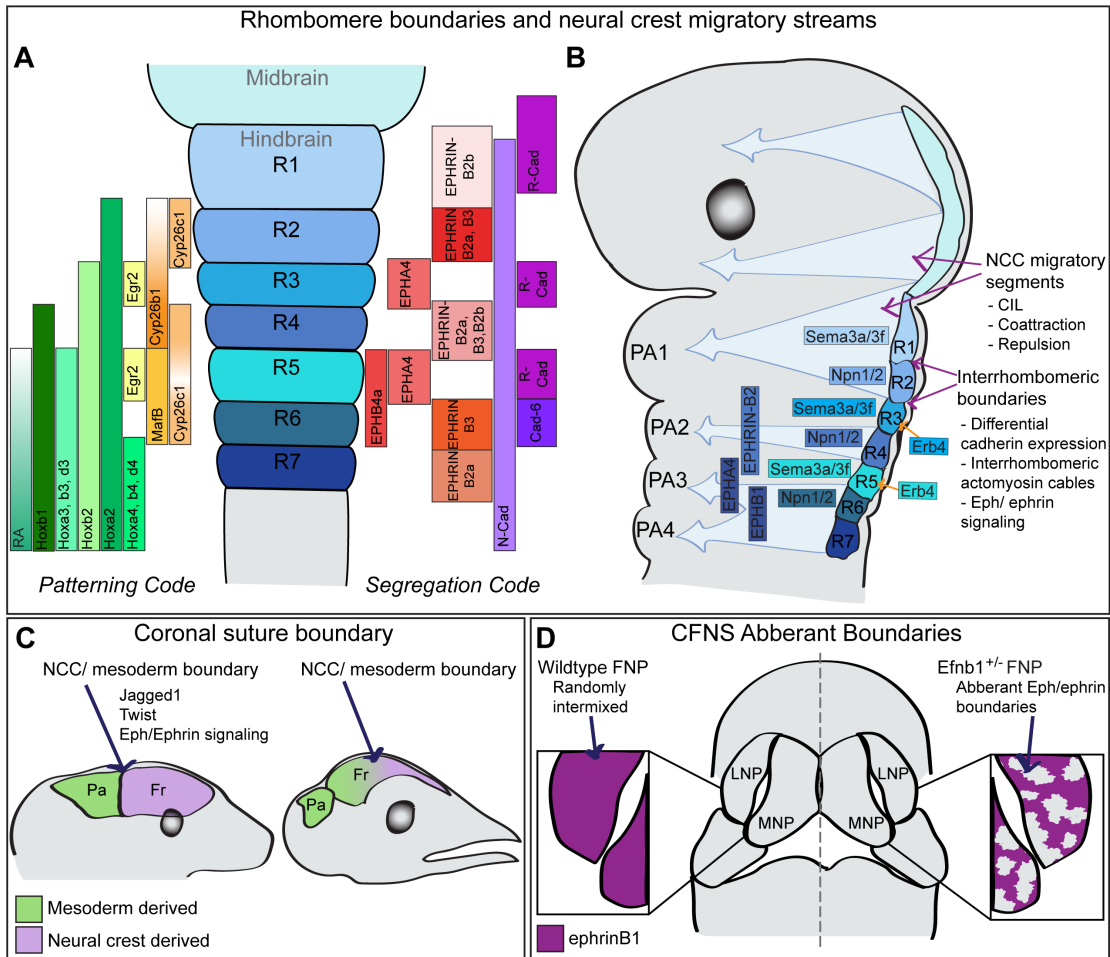


Figure 1.2. Boundaries relevant to craniofacial morphogenesis in the embryo. (A) Rhombomeres segment the neural ectoderm, acting as organizing centers along the rostrocaudal axis. Two major mechanisms contribute to rhombomere organization and boundary formation; 1) The patterning code, involving changes in gene expression to match positional identity; 2) The segregation code, giving rise to the spatial segregation of cells with distinct identities. (B) Proper migration of NCCs is required for craniofacial morphogenesis with the NCCs migrating from the rhombomeres into the branchial arches. Various repulsive cues such as Ephs/ephrins and semaphorins are required for stream maintenance. (C) In mice the NCC/mesoderm boundary occurs at the coronal suture between the frontal bone (Fr) and parietal bone (Pa). Conversely, in chick the NCC/mesoderm boundary falls within the frontal bone with the coronal suture occurring between two mesoderm derived tissues. (D) Aberrant cell segregation occurs in *EfnB1*^{+/-} embryos. Ephrin-B1 expression appears uniform in the WT frontonasal process (FNP), while patches of Ephrin-B1 expression and non-expression occur due to segregation in the FNP of *EfnB1*^{+/-} embryos. Lateral nasal process (LNP), medial nasal process (MNP).

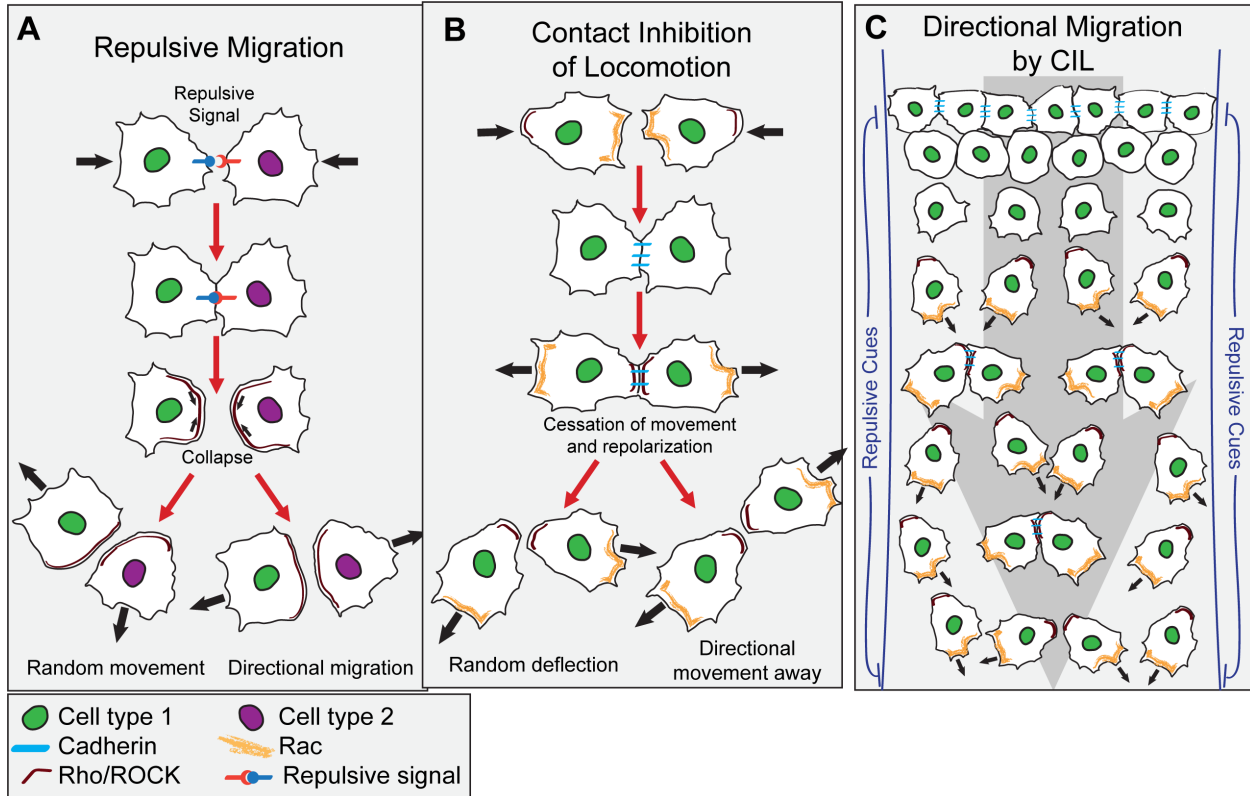


Figure 1.3. Migratory guidance mechanisms resulting in segregation or maintenance or segregated cell populations. (A) Migratory guidance and cell segregation can be achieved through a repulsive migratory mechanism by which heterotypic cell contacts, providing a repulsive signal, triggers cells to collapse, resulting in cells moving apart in either a directional or random fashion. **(B)** Contact inhibition of locomotion (CIL) is an underlying mechanism of migratory guidance and cell segregation. CIL is characterized by two cells coming into contact with one another and either ceasing movement or undergoing directional migration away with repeated interactions resulting in directional migration as has been seen in NCCs **(C)**. NCCs delaminate from the neural tube and undergo directional migration by CIL. Repulsive cues are also required for the maintenance of migratory streams.

CHAPTER 2.

Introduction to mechanical forces in development

Introduction to force generation and detection in morphogenesis

Morphogenesis is a physical process that requires the generation of mechanical forces to achieve dynamic changes in cell position, tissue shape, and size as well as biochemical signals to coordinate these events. Morphogenesis occurs across a range of time scales and physical space, requiring the coordinated interplay of a host of different cell behaviors. Although ligand-based biochemical signaling elicits cellular responses during tissue morphogenesis, the mechanical forces generated by cells downstream of this signaling ultimately mold tissues. However, these forces can also be detected by cells leading to biochemical and mechanical signal propagation within and between cells, that not only regulate cellular behavior and fate changes, but also coordinate and diversify the functional outputs of biochemical signaling to propel morphogenesis.

Cells and tissues can generate and transmit forces by several general mechanisms, but all of these begin with the cytoskeleton (Heisenberg and Bellaïche, 2013). Actin polymerization generates pushing force during the establishment of cellular protrusions, and tension is generated when non-muscle myosin II (MyoII) binds to filamentous actin (F-actin) and hydrolyzes ATP to convert chemical energy into mechanical movement (Vicente-Manzanares et al., 2009). Forces generated by actomyosin contractility are transmitted across tissues through adhesion molecules that allow individual cellular forces to be translated into global changes in tissue shape. Adherens junctions (AJs) vary in their size and composition, but are mediated by classic cadherins that connect to the actin cytoskeleton intracellularly through binding to β -catenin, which in turn binds α -catenin (Fig. 2.1A). Under contractility-generated tension, α -catenin undergoes conformational changes to recruit vinculin, which connects to F-actin (Harris and Tepass, 2010), resulting in maturation and growth of the AJ and recruitment of additional F-actin (Fig. 2.1A') (Harris and Tepass, 2010; Kale et al., 2018; Ladoux et al., 2015). This mechanosensory function allows the AJ to react dynamically to other cells and actomyosin contractility while mechanically coupling the intracellularly-generated force with surrounding cells. Whereas most of the force generation for

morphogenesis has been thought to derive from the actomyosin cytoskeleton, microtubules can also generate forces within cells, and this is coordinated by cell-signaling to regulate cell shape and epithelial morphogenesis in *Drosophila* (Takeda et al., 2018; Singh et al., 2018; Matis et al., 2014).

In addition to cell-cell adhesion, cell-extracellular matrix (ECM) adhesion is critical to convey or buffer the transmission of forces across tissues during morphogenesis (Dzamba and DeSimone, 2018; Bachir et al., 2017). Physical coupling of cells to the ECM at focal adhesions (FA) is critical for cellular reorganization and movement, but the ECM is also an instructional biochemical signal received through integrin receptors to modulate downstream signaling cascades and control a variety of cell behaviors during development (Dzamba and DeSimone, 2018). FAs are large multiprotein signaling hubs that include heterodimeric integrin receptors, which recruit intracellular adaptors including talin and vinculin, linking the FA to F-actin, and focal adhesion kinase (FAK) and SRC kinase, which can activate numerous downstream pathways (Fig. 2.1B, B'). Similar to α -catenin in AJs, physical force exerted by actomyosin contractility mechanically induces a conformational change in TALIN, allowing increased actin binding and greater FA stability (del Rio et al., 2009). The strength of cell-ECM adhesions is also modulated by the stiffness of the ECM wherein stiffer substrates allow cells to adhere more strongly and exert higher tension. Integrin/ECM binding therefore allows the detection of distinct types and compositions of ECM and organizes the formation of signaling complexes with the actomyosin cytoskeleton (Bachir et al., 2017). In this way cells effectively convert mechanical information into biochemical signals and through changes in actomyosin contractility, can reciprocally remodel ECM, resulting in a host of cellular and tissue-level changes; this form of mechanosensation has been reviewed extensively elsewhere (Dzamba and DeSimone, 2018; Muncie and Weaver, 2018), and will not be the focus of this review, which will instead focus on the ways that cells utilize force to communicate with other cells. In addition to providing a biochemical ligand for physical or chemical signaling into cells, ECM may generate forces signaling to cells; for example,

hydration of chondroitin sulfate proteoglycan in the vegetal epithelium of sea urchins results in differential expansion and bending of a bilayered cell sheet (Lane et al., 1993).

One important consequence of mechanically sensitive signaling at FAs and AJs is the biochemical activation of the Yes Associated Protein (YAP) and WW Domain Containing Transcription Regulator 1 (TAZ), leading to changes in transcription that impact cell proliferation and differentiation. YAP and TAZ, initially identified as Yorkie in *Drosophila* (Yki/YAP/TAZ), are transcriptional effectors of the Hippo (Hpo/MST1/2) kinase signaling cascade (Karaman and Halder, 2018). When this pathway is active, Hpo/MST1/2 kinases bind to the Sav/SAV1 adapter protein and phosphorylate Wts/LATS1/2 kinases to activate them. In turn, the Wts/LATS1/2 serine/threonine kinases phosphorylate Yki/YAP/TAZ and prevent them from entering the nucleus and activating transcription (Fig. 2.1C). Inactivation of the Hippo pathway results in Yki/YAP/TAZ accumulation within the nucleus, where they bind to TEAD transcription factors to drive target gene expression and promote cell proliferation and survival (Fig. 2.1C'). Mechanical change detected by FAs and AJs under actomyosin-generated contractility is a key force-sensing signaling mechanism that leads to activation of Yki/YAP/TAZ and transcriptional changes. Cell junctions serve as a site of assembly for Hippo pathway members and loss of AJ components can lead to increased YAP nuclear localization in different contexts (Karaman and Halder, 2018). In contrast, activation of YAP at FAs involves FAK and SRC activation of PI3K, leading to inhibition of LATS1/2 and nuclear accumulation of YAP (Kim and Gumbiner, 2015). Forces transmitted through FAs can also mechanically alter nuclear shapes and stretch nuclear pores to allow active nuclear YAP import (Elosegui-Artola et al., 2017). Generally, the ability of Hippo signaling to measure junctional changes depends on actomyosin contractility, and thereby provides a central pathway for translating physical information into biochemical information in the form of gene expression changes.

In addition to the described mechanisms of force detection at cell junctions, dedicated mechanosensors can detect forces within a tissue. For example, PIEZO proteins are mechanically

sensitive ion channels that are critical for mechanosensation in multiple contexts in development by sensing crowding forces to induce cell extrusion and control cell density (Eisenhoffer et al., 2012), and to regulate stem cell proliferation and differentiation (He et al., 2018; Pathak et al., 2014). Although the mechanisms by which PIEZO transduces a biochemical signal are still under active investigation, it is clear that they can function through Ca^{2+} signaling (He et al., 2018), or by impacting YAP/TAZ function (Fig. 2.1D, D') (Pathak et al., 2014; Duchemin et al., 2019).

While mechanical forces can be detected and translated into biochemical signaling, it is also the case that biochemical signaling pathways that regulate morphogenesis have outcomes that generate forces. For example, EPH/EPHRIN signaling often regulates actomyosin contractility (O'Neill et al., 2016; Cayuso et al., 2019); mitogenic signals such as WNT and SHH increase cell number, and chemoattractant pathways such as FGF increase cellular aggregation, both of which lead to increased cell density to generate compression forces. That these forces are transmitted throughout a tissue with both directional and magnitude information and detected by other cells suggests that these forces may be utilized as signal transducers downstream of biochemical signals. Here we review recent discoveries that connect biochemical signaling with mechanical signaling, focusing particularly on those cases where mechanical forces mediate biochemical signaling to regulate morphogenesis. These studies support the idea that force is not only detected during development, but that it is actively employed to transmit and convey biochemical signaling information in a manner that provides unique advantages.

Mechanical signals coordinate physical information with cellular differentiation and proliferation

Several recent papers have demonstrated that forces can signal to couple cell position within a tissue with cell fate specification, thereby coordinating physical information and cellular differentiation (Fig. 2.2A). While it is known that the stemness of epidermal progenitors can be manipulated by altering cell shape or ECM stiffness (Connelly et al., 2010; Trappmann et al., 2012), how mechanical changes are employed to enable specific cell fate decisions has remained

unclear. Totaro et al. recently demonstrated that cell shape and ECM rigidity regulates YAP/TAZ, which in turn regulate Notch signaling and downstream differentiation within the epidermis. In epidermal stem cells experiencing higher mechanical forces from either cytoskeletal or ECM rigidity, YAP nuclear localization inhibits Notch signaling, promoting epidermal stemness (Totaro et al., 2017). Conversely, low mechanical force inhibits YAP/TAZ, thus releasing Notch signaling, promoting differentiation (Totaro et al., 2017). Interestingly, YAP/TAZ increase expression of several Notch ligands, including DLL1 and DLL3, which stimulate Notch activity in neighboring cells (Lowell et al., 2000; Totaro et al., 2017). Importantly, these same ligands likely inhibit differentiation of basal cells through their cis-regulation, thus maintaining a layer of basal progenitors, and efficient differentiation of suprabasal cells (Lowell et al., 2000; Totaro et al., 2017).

Mechanical signals are integrated to coordinate boundary formation and cell differentiation during rhombomere formation in the developing hindbrain. Rhombomeres are developmentally transient blocks of neuroepithelial cells that give rise to distinct structures in the vertebrate hindbrain. Boundaries between rhombomeres are formed as a result of signaling between EPH receptor tyrosine kinases and their signaling partner, the EPHRINs; in zebrafish, alternating rhombomeres express EPHA4 and EPHRIN-B3 such that EPHA4/EPHRIN-B3 signaling only occurs at the rhombomere boundary (Becker et al., 1994; Bergemann et al., 1995; Cooke et al., 2001; Xu et al., 1999). Boundary cells express molecular markers that distinguish them from non-boundary cells, provide proliferating progenitors and organize spatially-restricted neurogenesis within segments (Gonzalez-Quevedo et al., 2010; Peretz et al., 2016; Terriente et al., 2012), and are involved in boundary straightening through the formation of actomyosin-cable like structures at rhombomeric boundaries (Calzolari et al., 2014). Disruption of either actomyosin contractility or EPH/EPHRIN signaling disrupts boundary sharpness (Calzolari et al., 2014; Cooke et al., 2005). Interestingly, increased tension from actomyosin contractility at rhombomere boundaries creates this positional information, which impacts boundary cell identity (Cayuso et al., 2019;

Voltes et al., 2019). EPHA4 loss of function results in reduced actomyosin contractility at rhombomere boundaries and a loss of boundary cells in EPHA4-expressing rhombomere segments, indicating that EPHA4 signaling generates positionally-specific tension to simultaneously specify rhombomere separation and cell identity specification (Cayuso et al., 2019). This increased tension at rhombomere boundaries promotes Taz nuclear localization and downstream activation of boundary markers (Cayuso et al., 2019; Voltes et al., 2019) in EPHA4-expressing boundary cells. When Yap/Taz pathway components are disrupted, border cell marker expression is lost (Cayuso et al., 2019). Yap also maintains the proliferative capacity and the progenitor potential in boundary cells, with neurogenesis coinciding with Yap downregulation as daughter cells exit the boundary domain (Voltes et al., 2019). Together these data elucidate a complete pathway linking boundary formation and maintenance through EPH/EPHRIN signaling to downstream cell fate decisions by a mechanical signaling intermediary. Interestingly, as Notch pathway components are also expressed in boundary cells and have been shown to regulate neurogenesis in rhombomeres, it is intriguing to postulate that integration of mechanical signals and Notch activation may similarly exist here as in the example above to preserve progenitor state in boundary cells.

In many contexts, changes in force can be interpreted as morphogenetic signals to rapidly remodel and differentiate specialized cell types that further contribute to organ development and function (Fig. 2.2B). Shear force due to blood flow is detected during outflow tract (OFT) valve development in zebrafish, coupling the positions of highest shear force due to blood flow with positional specification of smooth muscle differentiation that results in valve morphogenesis (Duchemin et al., 2019). In the regions of the OFT with the smallest diameter, where shear stress is highest, Piezo mechanosensitive channels detect this shear force, resulting in spatially-restricted expression of Klf2 and Notch signaling within the valve endothelium, and Yap1 activation and differentiation of the underlying smooth muscle. In the atrioventricular heart valve, Klf2a and Notch signaling activity are also high in regions experiencing high blood flow (Pestel et

al., 2016; Steed et al., 2016), though the structure of this valve, and the forces it experiences are somewhat different. Indeed, it is notable that Klf2 expression and Notch signaling are commonly mechanosensitive to blood flow during development (Lee et al., 2006; Groenendijk et al., 2004), supporting them as common nodes in pathways converting mechanical to biochemical signaling information in a spatially-restricted manner.

Intra-organ communication is necessary to coordinate the growth and position of discrete, but interdependent structures (Fig. 2.2C). In zebrafish heart development, Wnt8a signaling is critical for promoting cardiomyocyte formation and its overexpression results in increased atrial and decreased ventricle myocardial size (Dohn and Waxman, 2012). Interestingly, this effect is mirrored by changes in the size of the underlying atrial and ventricular endocardium (Bornhorst et al., 2019). Expansion of the myocardium places the endocardial cells under tension, which is sensed by junctional Cadherin-5 (VE-cadherin), resulting in nuclear Yap1 localization and increased proliferation of endocardial cells to compensate for myocardial overgrowth. These data reveal that tension generated by tissue growth can signal to neighboring tissues allowing the coordination of tissue-intrinsic growth rates.

Chemical signals modulate cell polarity, adhesion, and tissue deformability to signal mechanically

The emergence of coordinated collective cell behaviors requires the detection, coupling, and propagation of forces across groups of cells. Tissue rheology, or the way in which tissues mechanically react, arises from the contractility of the cells composing the tissue, the ECM, and the strength of the cell-cell contacts within a tissue. Viscoelasticity determines the deformability of the tissue and permissibility for cellular arrangement in response to inductive signals. Modulation of these properties within a tissue allows for regulated deformation and shaping of a tissue.

Chemical signals can guide morphogenesis by tuning tissue mechanics and viscoelasticity through control of adhesion, cortical contractility, and associated cell polarity. This was recently

demonstrated in the developing mouse pharyngeal arch, which is composed of a mesenchymal core surrounded by a single layer of epithelium, and undergoes extensive outgrowth and shape changes throughout development. Tao et al. demonstrated that, in the mesenchyme, WNT5a activates PIEZO1 to induce oscillations in cortical tension in the middle portion of the developing arch, resulting in reduced tissue viscoelasticity and increased cell intercalation to drive arch elongation (Tao et al., 2019). In *Wnt5a* mutant mice the shape of the mandibular arch is disrupted with diminished cortical oscillations and a decrease in oriented cell intercalation, suggesting that WNT5a coordinates mandibular cell behaviors through control of cell polarity and cytoskeleton tension (Tao et al., 2019). This study therefore demonstrates a mechanism by which chemical signals impact tissue mechanics to enable proper morphogenesis.

Signaling by WNT5a through the ROR2 receptor is also critical during angiogenesis, where it coordinates endothelial cell behavior by activating CDC42 and stabilizing vinculin at the AJ (Carvalho et al., 2019). This results in mechanocoupling between endothelial cells and their collective polarization, which is necessary for their proper migration. Therefore, non-canonical WNT signaling tunes the sensitivity of endothelial cells to junctional force to modulate their behavior. Detection and sensitivity of cells to forces is often tuned by biochemical signaling pathways, thereby allowing these pathways to influence the cellular outcomes upon experiencing a given force. As in heart development, shear force from blood flow is critical for vessel reorganization during angiogenesis, such that the direction and strength of flow dictates endothelial cell polarization and migration. Endothelial non-canonical WNT signaling is required for the detection of shear force, and modulates sensitivity to this force in order to select which vessels undergo normal pruning (Franco et al., 2016). Interestingly, VEGFR3 signaling also influences sensitivity of endothelial cells to shear stress from flow, indicating that in this context multiple biochemical pathways converge to regulate sensitivity to a force-based signal (Baeyens et al., 2015). Differences in VEGFR3 levels may be a major determinant of differences in sensitivity to shear stress by vascular endothelial cells, compared with lymphatic endothelial cells,

which have a higher sensitivity to shear stress allowing detection of lower flow rates and therefore the remodeling of these different vascular cell types at different force reception set-points (Baeyens et al., 2015).

Mechanical modulation of chemical signaling by cell density and crowding forces

As morphogenesis progresses, changes in tissue shape and cell organization can concurrently reshape the spatial distribution of signaling molecules (Fig. 2.3A). For instance, villi formation in the developing chick gut as a result of mechanical buckling of the endodermal epithelium distorts the SHH signaling gradient from the epithelium, concentrating the signal at the tip of each villus to activate high threshold response genes in the mesenchyme that ultimately determine the location of intestinal stem cells (Shyer et al., 2015). This suggests that tissue mechanical forces can actively modulate signaling pattern via emerging cellular organization. This idea is consistent with recent findings in developing chick feather buds, which arise in the midline of the dorsal skin as regularly spaced mesenchymal aggregates beneath epidermal placodes, with subsequent new buds formed laterally in a spatiotemporal manner. Feather bud development is initiated as a result of MyoII-dependent mesenchymal contraction that amplifies randomly formed small cell clusters into larger aggregates (Shyer et al., 2017). Condensed mesenchyme in turn compresses the overlying epithelium and mechanically induces nuclear accumulation of β -catenin to initiate the follicle genetic program (Shyer et al., 2017; Huelsken et al., 2001). This mesenchymal contraction also concentrates and upregulates local FGF20 signaling from the epithelium to further promote mesenchymal condensation (Ho et al., 2019; Jung et al., 1998). Simultaneously, condensed mesenchyme begins to express BMP4, which diffuses and inhibits epithelial *Fgf20* expression neighboring the condensate (Ho et al., 2019). Tissue mechanical forces thus help shape FGF20 and BMP4 expression pattern with altering peaks and troughs of FGF20 and BMP4 signaling activities, which function as the activator and inhibitor respectively in

a Turing reaction-diffusion system (Turing, 1952) to establish the formation of feather buds repetitively at a regular interval.

Formation of repetitive structures can also be achieved through molecular oscillators, such as in the vertebrate presomitic mesoderm (PSM). In this model, cyclic activation of Notch and WNT pathways and corresponding signaling responsive genes generate periodic travelling waves of signaling activation and instruct the formation of segmented structures called somites (Hubaud and Pourquié, 2014). Interestingly, when PSM cells are dissociated and scrambled in primary cell culture, they continue to oscillate and produce waves of Notch signaling (Hubaud et al., 2017). However, this phenomenon is only maintained when the cell density is above certain threshold. The system exhibits a quorum sensing behavior involving YAP, which functions as a checkpoint to only allow full Notch signaling when a certain cell crowding threshold is reached. Intriguingly, quorum sensing via YAP can be modulated by cell shapes and actin-dependent mechanical forces, raising the possibility that signaling oscillation during somite formation is regulated by mechanical inputs associated with changes in crowding-force (Hubaud et al., 2017). It will be interesting to determine if such an excitable density detection system similarly functions in other developmental contexts involving cell condensation, such as in the feather bud example above, to govern local activation of specific signaling cascades and generation of signaling waves.

Mechanical force as a long-range intermediary signal to regulate morphogenesis

While paracrine signaling is only effective over a relatively short distance of 50-100 μm (spanning 5-10 cells) due to rapid signal dilution and decay in its intensity (Lee et al., 1994; Francis and Palsson, 1997; Handly et al.), mechanical forces can be directionally transmitted over a longer distance and function as a long-range morphogenetic signal downstream of a localized biochemical stimulus (Fig. 2.3B). One example demonstrating mechanical signaling over distance is the regulation of zebrafish body elongation by the tail organizer (Das et al., 2019). Bmp signaling from the tail organizer is postulated to promote an ordered anterior-to-posterior cell flow in the tail

bud that contributes to body elongation (Lawton et al., 2013; Mongera et al., 2018). When Bmp signaling is perturbed, a cell-to-cell relay of disturbed cell motion in the tail bud results in a mechanical transmission of cellular jamming that travels posterior-anteriorly, resulting in disorganized cell motion outside the Bmp signaling range (Das et al., 2019). This hints at a mechanism whereby signaling ligands may induce directional movement of cells outside the signaling range by propagating mechanical signals through neighboring cells.

How then do cells propagate mechanical signals over distance without dampening force transmission? A recent paper addressed this question by studying *Drosophila* endoderm morphogenesis, a MyoII-dependent process involving invagination of endoderm primordium moving posterior-anteriorly (Bailles et al., 2019). Importantly, while Rho1/MyoII activation is initiated by secreted Fog/GPCR signaling, a wave of MyoII actomyosin contractility continually propagates endoderm invagination anteriorly along the dorsal epithelium without Fog signal propagation. As MyoII can be activated in response to mechanical stimuli, such as increased cellular tension (Heissler and Sellers, 2016; Fernandez-Gonzalez et al., 2009; Mitrossilis et al., 2017), cellular forces associated with epithelial buckling trigger apical spreading in unbuckled cells at the anterior edge of the furrow and activate MyoII in these cells and their subsequent buckling, thus cyclically amplifying the travelling mechanical wave. Interestingly, sequential activation of MyoII is also observed in other developmental contexts, such as the mechanical interaction between the invaginating endoderm and extending germband in *Drosophila* and the zippering process during neural tube closure in *Ciona intestinalis* (Lye et al., 2015; Hashimoto et al., 2015), all suggesting that mechanical forces can act as a long-range signal and as a second messenger to regulate morphogenesis at a distance. Future work will determine whether such mechanisms can also control other cell behaviors, such as differentiation, proliferation, and polarity in this and other developmental processes.

Conclusion

Cells may have evolved to actively utilize force as an extracellular second messenger to transduce information between cells with several advantages. The recent studies that we describe above give insight into this idea, and present explanations of the advantages that might be achieved by employing mechanical signals: these signals can coordinate growth of organs, specify cell fate with respect to tissue architecture, modulate chemical signals, and act over longer distances than biochemical signals. Importantly, mechanical force is a multiparameter signal; whereas a biochemical signal detected at a single point has only a magnitude value, mechanical force is a vector quantity, encoding both magnitude and directional information. This property makes mechanical forces particularly compelling for providing information to organize directed cell behaviors such as cell polarity and cell migration. Multiple biochemical signals may therefore converge to collate and convert information from multiple cellular inputs into a mechanical force signal that can be transmitted in a coordinated fashion. As mechanical signals have been historically challenging to observe, increasingly integrating techniques such as atomic force microscopy and laser ablation with genetic and biochemical approaches as well as the application of new techniques such as the application of oil droplets, or magnetic beads to measure and apply forces, will be transformative in further understanding the interplay between mechanical and biochemical signals during development (Campàs et al., 2014; Zhu et al., 2020).

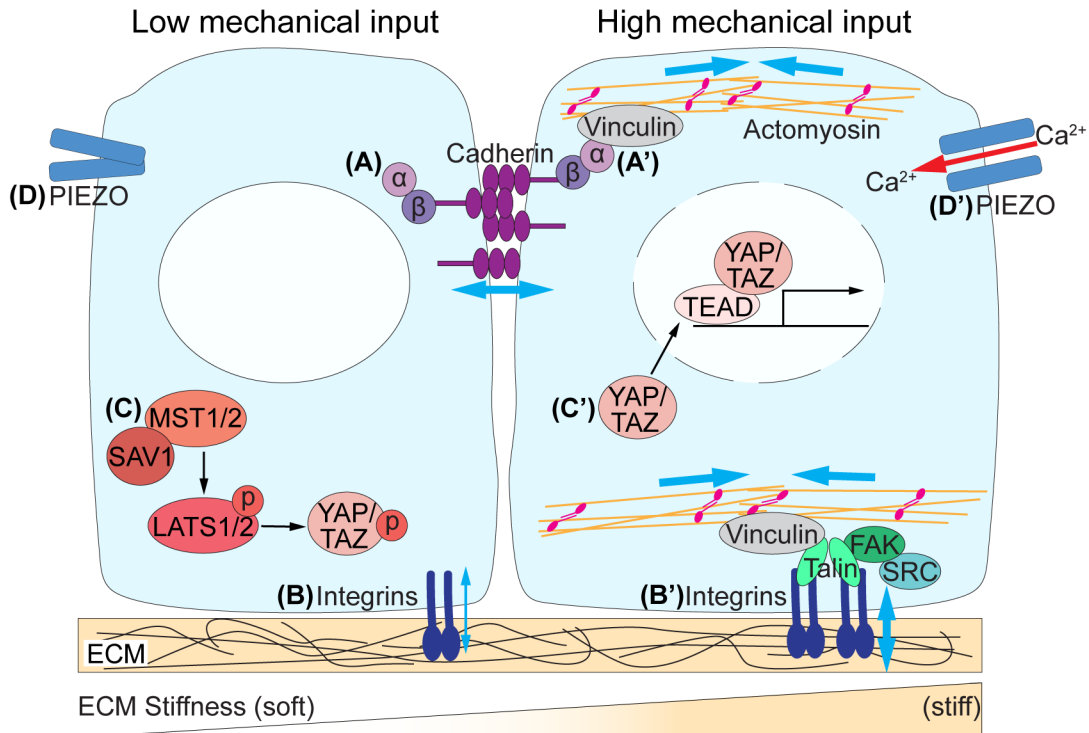


Figure 2.1. Mechanisms of mechanosensation. Mechanical forces are sensed and transmitted across cells and tissues through a variety of mechanisms. **(A)** Cadherins, bound intracellularly to β -catenin, which in turn binds α -catenin, make up adherens junctions. **(A')** Under tension, generated by actomyosin contractility, α -catenin recruits the actin-binding protein vinculin. The mechanosensory function of adherens junctions allows the mechanical coupling of adjacent cells. **(B)** Focal adhesions, composed of integrins, couple cells to the ECM, providing cells with both mechanical and biochemical information. **(b')** Under tension, a series of intracellular adaptors are recruited to focal adhesions, including FAK, SRC, talin, and vinculin, linking the focal adhesions to actomyosin. **(C)** The Hippo/YAP/TAZ pathway is a critical mechanosensitive signaling pathway. When there is low mechanical input, MST1/2 kinases bind SAV1, phosphorylating LATS1/2 kinases, which in turn phosphorylate YAP/TAZ, preventing them from entering the nucleus. **(C')** When there is high mechanical input, Hippo signaling is inactive, allowing YAP/TAZ to translocate to the nucleus, where they bind to TEAD transcription factors, driving target gene expression. **(D)** Dedicated mechanosensors, such as PIEZO proteins, can also detect forces within a tissue. **(D')** When sensing crowding forces, PIEZO channels undergo a conformational change, enabling a calcium influx into the cell to impact downstream signaling. ECM, extracellular matrix; FAK, focal adhesion kinase.

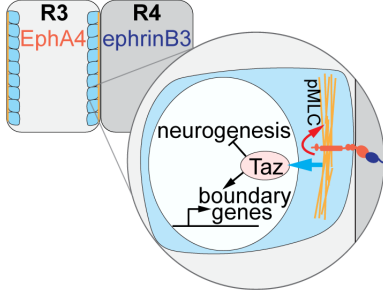
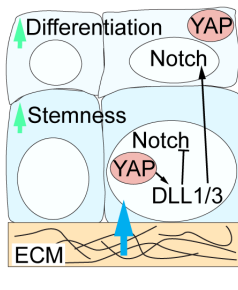
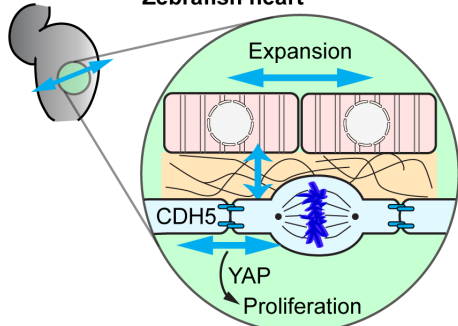
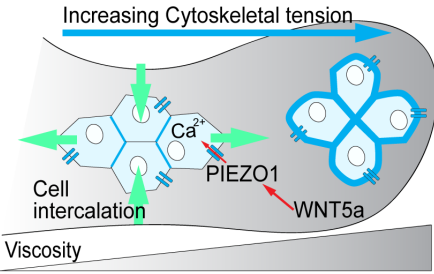
Outcome	Developmental systems and examples	Advantage
A) Coupling morphogenesis and differentiation	<div style="display: flex; justify-content: space-around;"> <div style="text-align: center;"> Zebrafish Rhombomeres  </div> <div style="text-align: center;"> Mouse Epidermis  </div> </div>	Couple cell positioning and local micro-environment to cell fate decisions
B) Coupling tissue growth	<div style="text-align: center;"> Zebrafish heart  </div>	Provide rapid responses to changing tissue functional demands
C) Controlling tissue viscoelasticity	<div style="text-align: center;"> Mouse Mandibular Arch  </div>	Fine tuning of tissue properties to enable localized deformations and shape changes

Figure 2.2. Integration of mechanical and biochemical signaling during morphogenesis. Mechanical and biochemical signaling can be integrated to affect various morphogenetic outcomes including tissue growth and cellular differentiation. **(A)** In developing zebrafish rhombomeres, morphogenesis is coupled to cellular differentiation through Eph/–ephrin signaling–generated actomyosin contractility, which in turn activates Yap/TAZ signaling in boundary cells. In addition, YAP/TAZ mechanotransduction inhibits Notch signaling in the developing mouse epidermis to maintain epidermal stemness in basal cells, while promoting differentiation of the suprabasal layer. **(B)** In the zebrafish heart, myocardial growth and endocardial growth are coupled through tension sensing via vascular endothelial cadherin (VE-cadherin) and Yap1 to regulate cell proliferation. **(C)** Mechanical and biochemical signaling can also be integrated to modulate tissue viscoelasticity as demonstrated in the developing mandibular arch, where WNT5a acts upstream of YAP and PIEZO1 to coordinate cellular polarity and force oscillations in the middle arch to diminish tissue rigidity, enabling cell intercalations. ECM, extracellular matrix.

Outcomes	Developmental systems and examples	Advantage
A) Diversifying chemical signaling	<div style="display: flex; justify-content: space-around;"> <div style="text-align: center;"> <p>Chick feather buds</p> </div> <div style="text-align: center;"> <p>Chick PSM cells</p> </div> </div>	Dynamically alter the gradient and pattern of ligand-based signaling
B) Long distance signaling	<div style="display: flex; justify-content: space-around;"> <div style="text-align: center;"> <p>Zebrafish tailbud</p> </div> <div style="text-align: center;"> <p>Drosophila endoderm</p> </div> </div>	Extend chemical signaling range

Figure 2.3. Mechanical modulation of chemical signaling. Tissue mechanical forces can modulate the gradient and pattern of biochemical signaling. **(A)** In the chick feather buds, condensing mesenchyme contracts the overlying epithelium to concentrate local FGF20 and at the same time secretes BMP4 that diffuses and inhibits the neighboring FGF20 expression, resulting in a Turing-like pattern. In the chick presomitic mesoderm (PSM), YAP integrates mechanical information from the substrate and cell density to transform signaling pulses into oscillations and waves. **(B)** Tissue forces can also function as a second messenger downstream of a biochemical source to relay its instructive signal across space. For instance, in the zebrafish tail bud, the anterior-to-posterior cell flow is modulated by mechanical signals transmitted from cell to cell and thus beyond the range of BMP signaling in the tail organizer. Similarly, during *Drosophila* endoderm invagination, although the initial MyoII activation is initiated by Fog signaling, the subsequent traveling wave of MyoII activation and apical contraction is independent from Fog signaling and is induced by cyclic forward pushing of buckling cells and apical spreading of edge cells along the vitelline membrane (VM). FGF, fibroblast growth factor; ECM, extracellular matrix; MyoII, myosin II.

CHAPTER 3.

EPH/EPHRIN regulates cellular organization by actomyosin contractility effects on cell contacts

Summary

EPH/EPHRIN signaling is essential to many aspects of tissue self-organization and morphogenesis, but little is known about how EPH/EPHRIN signaling regulates cell mechanics during these processes. Here we utilize a series of approaches to examine how EPH/EPHRIN signaling drives cellular self-organization. Contact angle measurements reveal that EPH/EPHRIN signaling decreases the stability of heterotypic cell:cell contacts through increased cortical actomyosin contractility. We find EPH/EPHRIN-driven cell-segregation is dependent on actomyosin contractility, but occurs independently of directed cell migration and without changes in cell adhesion. Atomic force microscopy and live cell imaging of myosin localization supports that EPH/EPHRIN signaling results in increased cortical tension. Interestingly, actomyosin contractility also non-autonomously drives increased EPHB2:EPHB2 homotypic contacts. Finally, we demonstrate that changes in tissue organization are driven by minimization of heterotypic contacts through actomyosin contractility in cell aggregates and by mouse genetics experiments. These data elucidate the biomechanical mechanisms driving EPH/EPHRIN based cell segregation, wherein differences in interfacial tension, regulated by actomyosin contractility, govern cellular self-organization.

Introduction

Embryo morphogenesis requires the self-organization of cells into discrete regions, leading to the formation and maintenance of embryonic boundaries–interfaces that prevent cell intermixing to support patterning, maintain organization and often, drive tissue separation (Fagotto, 2014). EPH/EPHRIN signaling plays a critical role in mediating tissue organization, and is particularly important in establishing embryonic boundaries. The molecular mechanisms by which EPH/EPHRIN signaling directs tissue self-organization and boundary formation has been extensively studied in numerous systems. However, the biomechanical mechanisms underlying these processes remain unclear.

EPH receptors, and their signaling partners, the membrane-bound EPHRINs, are expressed in most tissues of the vertebrate embryo, and are often expressed in complementary domains. EPH/EPHRIN signaling mediates boundary formation by driving segregation between EPHRIN-expressing and EPH-expressing cells in many developmental contexts, including the germ layers during gastrulation, rhombomeres, somites, limb buds, cranial sutures, and intestinal crypts (Calzolari et al., 2014; Watanabe et al., 2009; Cooke et al., 2001; Batlle et al., 2002; Merrill et al., 2006; Rohani et al., 2011; Ting et al., 2009). At least one human congenital disease, craniofrontonasal syndrome, is caused by aberrant EPH/EPHRIN-based cell segregation (Kindberg and Bush, 2019; Twigg et al., 2004; O'Neill et al., 2016; Niethamer et al., 2020, 2017), and misregulation of EPHs and EPHRINs has been implicated in cancer metastasis (Pasquale, 2010; Batlle and Wilkinson, 2012; Porazinski et al., 2016). There are two subclasses of EPHRINs: A-type, which are membrane bound by a GPI anchor, and B-type, which are transmembrane and contain an intracellular cytoplasmic tail (Gale et al., 1996; Kullander and Klein, 2002). Because both EPH receptors and EPHRIN ligands are membrane bound, cell:cell contact is required for signaling, which can be transduced bidirectionally. “Forward” signaling occurs through activation of the EPHB receptors, while “reverse” signaling is facilitated by adaptor proteins that bind to conserved phosphorylated tyrosines on the intracellular domain of B-type EPHRINs, or to a C-

terminal PDZ-binding domain. Forward signaling can occur through both kinase-dependent and kinase independent mechanisms (Kullander and Klein, 2002; Niethamer and Bush, 2019).

Several hypotheses have been proposed for how EPH/EPHRIN signaling drives segregation and boundary formation between cell populations. Cell:cell repulsion—wherein cell:cell contact between EPH and EPHRIN expressing cells triggers migration of the EPH cell away from the repulsive EPHRIN source—is a long standing hypothesis for EPH/EPHRIN mediated cell segregation (Poliakov et al., 2008; Taylor et al., 2017; Mellitzer et al., 1999; Wu et al., 2019). This phenomenon is readily observed in culture at low cell density. Upon contact with an EPHRIN-expressing cell, the interface of the EPH-expressing cell mediating contact will collapse and retract away from the EPHRIN-expressing cell (Taylor et al., 2017; O'Neill et al., 2016; Poliakov et al., 2008; Astin et al., 2010). Cell segregation of fully intermixed cells by this mechanism, would require repeated directional repulsion and migration of cells away from heterotypic contacts resulting in an increased total migratory distance. However, we have observed that at high densities, segregation occurs without an increase in the migratory distance traveled, an observation inconsistent with this repulsive migration hypothesis (O'Neill et al., 2016).

Regulation of differential adhesion is a second hypothesis for how EPH/EPHRIN signaling drives cell segregation. According to the classical differential adhesion hypothesis, cells maximize their adhesive contacts to cluster hierarchically based on adhesive differences: the most adhesive cell population will cluster internally and be surrounded by less adhesive populations (Duguay et al., 2003; Steinberg and Takeichi, 1994; Steinberg, 1963; Foty and Steinberg, 2005). Differences in adhesive strength, also known as adhesion tension, between populations can be achieved through differing levels of cell adhesion molecule expression, termed differential adhesion, or through the type of cell adhesion molecule expressed, termed selective adhesion. There is evidence that EPH/EPHRIN signaling can modulate adhesion, including the ability of EPH-activation to recruit ADAM10 metalloprotease, which cleaves E-cadherin, resulting

in cadherin shedding and a decrease in cell:cell adhesion at the cell surface engaged in active EPH/EPHRIN signaling (Solanas et al., 2011).

Regulation of actomyosin contractility (e.g. differential cortical tension) also contributes to cell segregation (Harris, 1976), and provides a unifying explanation for these processes when combined with the notion of differential adhesion (Krieg et al., 2008; Maître et al., 2012; Cerchiari et al., 2015; Winklbauer, 2015). The resulting differential interfacial tension hypothesis states that forces arising from cell adhesion and cortex tension act in opposition to modulate the ability of cells to make stable contacts (Lecuit and Lenne, 2007; Brodland, 2002; Krieg et al., 2008). In recent years, it has come to be appreciated that the cell contact forces provided by cadherin-based adhesion tension are relatively small compared with those from cortical tension, and that the role of cadherins in cell segregation is instead primarily to mechanically couple the contractile cell cortices to transduce actomyosin-generated forces (Maitre et al., 2012; Maître and Heisenberg, 2013; Stirbat et al., 2013; Winklbauer, 2015; Lecuit and Yap, 2015). It should also be noted that cadherins and actomyosin contractility modulate each other biochemically to dynamically regulate adhesion tension and cortical contractility (Maître and Heisenberg, 2013; Lecuit and Yap, 2015; Slováková et al., 2020). The balance of forces determines the mechanical potential of each interface; low-tension interfaces are favored over high-tension interfaces. According to the differential interfacial tension model, cell segregation minimizes the overall interfacial tension of the tissue. Thus, if a population of cells has a high interfacial tension at the cellular interface, it will be less able to form stable contacts with neighboring cells, resulting in the segregation of populations (Krieg et al., 2008; Brodland and Chen, 2000). However, the amount of contact at the cell:cell interface is also determined by the relative tension of the cortex away from the contact, known as the cell:medium cortical tension (Maître et al., 2012). Whereas *in vitro* cell:medium interactions involve all of the cell-non-cell interactions (e.g. substrate and liquid medium), *in vivo*, cell:medium interactions are constituted by whatever surrounds the organizing cells (this can be extracellular matrix (ECM), fluid, yolk, or other cells) (Cerchiari et al., 2015; Krieg

et al., 2008; Maître et al., 2012). Further, cells dynamically regulate these forces through the action of signaling molecules acting at each interface. Currently how upstream signaling pathways regulate cell:cell and cell:medium tension is largely unknown; specifically, how EPH/EPHRIN signaling regulates interfacial tension to achieve cell segregation is not clear.

While the role of EPH/EPHRIN signaling in differential interfacial mechanics is poorly understood, much is known about EPH/EPHRIN signaling as a regulator of actomyosin contractility. Actin accumulation and phosphorylated myosin light chain are frequently observed at the interface between EPH/EPHRIN boundaries, including rhombomere boundaries, aberrant boundaries in the craniofacial mesenchyme, and in mesenchymal and epithelial cell culture (O'Neill et al., 2016; Calzolari et al., 2014; Cayuso et al., 2019; Rodríguez-Franco et al., 2017). Further, disruption of EPH/EPHRIN signaling leads to a loss of actin accumulation and phosphorylated myosin light chain at these interfaces. However, how EPH/EPHRIN-driven actomyosin contractility contributes to initial segregation or to the maintenance of segregated cell populations is not known. Further, how EPH/EPHRIN signaling generally impacts the physical properties of cells to mediate cell segregation, has not been examined.

Here, we ask how EPH/EPHRIN signaling regulates the biophysical properties of cells to modulate their ability to maintain stable cell:cell contacts during tissue organization. We use a HEK293 cell culture system, in which EPHRIN-B1 and EPHB2 expression in two separate populations of cells drives robust segregation (O'Neill et al., 2016; Poliakov et al., 2008). We specifically examine how EPH/EPHRIN signaling impacts individual cell:cell contacts under conditions designed to minimize the role of cell migration. By examining isolated cell pairs, by performing live cell imaging of myosin light chain localization, and by utilizing atomic force microscopy (AFM), we determine that EPH/EPHRIN signaling raises interfacial tension and decreases cell contact through increasing cortical actomyosin contractility. Surprisingly, we find that EPH/EPHRIN signaling also impacts homotypic cell contact through a cell:medium effect on

cortical tension. Our findings support a view of segregation driven by minimization of overall interfacial tension both *in vitro* and *in vivo*.

Results

EPH/EPHRIN signaling increases heterotypic interfacial tension

To measure the effect of EPH/EPHRIN signaling on interfacial tension we utilized a cell:cell contact angle assay to measure isolated cellular contacts between EPHRIN-B1 and EPHB2 expressing HEK293 cells in the absence of confounding effects of cell migration and cell-matrix adhesion (Cerchiari et al., 2015). We collected cell pairs in 20 μ m by 40 μ m agarose microwells made from polydimethylsiloxane (PDMS) stamps, designed to allow two cells to adhere only to one another but not the substrate, and measured the subsequent angle of cell contact (Θ) as an estimate of interfacial tension (Fig. 3.1A). (Cerchiari et al., 2015; Maître et al., 2012) (Fig. 3.1A). We mixed HEK293 cells expressing EPHB2 and membrane localized GFP (EPHB2-GFP) with cells expressing EPHRIN-B1 and Lifeact-mCherry (EPHRIN-B1-LifeAct-mCherry) and quantified interfacial tension at 4 hours after mixing (Fig. S3.1A). This time-point was chosen based on a time course that showed stabilization of wildtype HEK293 (WT) cell-contacts at 4 hours after pairing in microwells. Our analysis revealed a significantly decreased contact angle between heterotypic EPHB2:EPHRIN-B1 cell pairs, while homotypic EPHRIN-B1:EPHRIN-B1 and EPHB2:EPHB2 cell pairs maintained close contact indicating an increase in interfacial tension only at the heterotypic, EPHB2:EPHRIN-B1 interface (Fig. 3.1B, C). When we live-imaged cell pairs over 12 hours, we observed that heterotypic EPHB2:EPHRIN-B1 cell pairs moved between extreme states of sparse and close contact throughout the time-course. (Fig. 3.1D, Fig. S3.1B) However, considered across the entire population of cells measured, high heterotypic interfacial tension was consistent at any given timepoint despite contacts being dynamic over time, indicating that heterotypic cell pairs favored sparse contact while homotypic pairs favored close contact (Fig. 3.1C, D, Fig. S3.1C). This increased interfacial tension between heterotypic cell pairs was greatly diminished when signaling was blocked using exogenous

unclustered EPHRIN-B1-Fc as a competitor of EPH/EPHRIN signaling (Fig. 3.1C). Cell contact between WT and EPHB2-GFP cells was similar to that observed in WT:WT cell pairs, indicating that changes in interfacial tension for EPHRIN-B1:EPHB2 cell pairs were a consequence of activation of EPH/EPHRIN signaling in trans (Fig. S3.1D). Together, these data indicate that in these cells, the balance of adhesion, cell:cell, cell:medium tension favors extensive cell contact in the absence of EPH/EPHRIN signaling, and that EPH/EPHRIN signaling drives increased cell:cell interfacial tension, preventing heterotypic cell pairs from maintaining close, stable, cell:cell contacts.

Hierarchy of segregation is consistent with high EPHB2:EPHRIN-B1 cellular interfacial tension

We next examined how EPH/EPHRIN-driven cell segregation occurs in 3D. Based on the premise that cells minimize high-energy contacts, hierarchy experiments in which two populations are mixed and the pattern of segregation is analyzed in 3D culture, have been used to determine whether cell:cell contacts or cell:medium contact is relatively favorable (Krieg et al., 2008; Brodland and Chen, 2000). We performed 3D segregation experiments by mixing EPHB2-GFP-LifeAct-mCherry cells and EPHRIN-B1-LifeAct-mCherry cells into 180 μ m circular agarose microwells. These cells robustly segregated, and rather than one cell type segregating to the center and being surrounded by the second cell type, as would be predicted by either differential adhesion or cell:medium tension that exceeds cell:cell tension, the two populations segregated completely and minimized contact with one another (Fig. 3.1E). This is consistent with our cell contact angle measurements that show a high interfacial tension at the EPH/EPHRIN interface, and thus this high-energy interaction at the EPH/EPHRIN cell:cell interface overcomes cellular cell:medium tension forces that would otherwise contribute to organizing the cells hierarchically.

Actomyosin contractility but not cadherin-mediated adhesion is critical to establish and maintain cellular self-organization

We previously demonstrated that EPH/EPHRIN-driven segregation can be disrupted, although not completely abolished, by inhibiting components of the actomyosin contractility pathway, such as Rho-kinase (ROCK) or Myosin light chain kinase (MLCK) (O'Neill et al., 2016). We further investigated how actomyosin contractility contributes to cell segregation by performing cell mixing experiments in the presence of multiple actomyosin contractility pathway inhibitors, and quantified cell sorting using nearest neighbor analysis, as previously described (Poliakov et al., 2008; O'Neill et al., 2016). Notably, when Y27632 (ROCK inhibitor) and ML7 (MLCK inhibitor) were added to the culture together, segregation was completely lost with EPHB2-expressing and EPHRIN-B1-expressing cells remaining randomly intermixed (Fig. 3.2A, B). This dual-inhibition condition did not affect the ability of the cells to migrate in culture, as the total path length of these cells was the same as in EPHRIN-B1:EPHB2 cells with DMSO (Fig. S3.2A) and these cells were healthy because they were still able to segregate upon removal of inhibitors after 24 hours (Fig. 3.2D). As inhibition of actomyosin contractility could affect cell division, we asked whether inhibition of cell proliferation affected EPH/EPHRIN-driven cell segregation by mitomycin C treatment. Mitomycin C treated cells still underwent robust segregation, indicating that proliferation does not play a critical role in EPH/EPHRIN driven cell segregation (Fig. S3.2C, S3.2D).

We next tested how classical cadherin-mediated adhesion might affect cell segregation. A recent study demonstrated that knockdown of N-cadherin does not abrogate cell segregation, but left open possible compensation by other classical cadherins (Taylor et al., 2017). Classical cadherins are dependent on binding of extracellular calcium to rigidify the extracellular domains that enable binding of neighboring cadherins (Brasch et al., 2012). We used cell culture medium without calcium (Ca^{2+}) to disrupt cadherin-based cell:cell adhesion, but we did not chelate intracellular calcium so as to minimize effects on intracellular Ca^{2+} -dependent functions

(Bhagavathula et al., 2007; Yi et al., 2011). Indeed, in the cell:cell contact assay, this low Ca^{2+} media drastically reduced HEK293 cell:cell contacts (Fig. S3.2B). Interestingly, we found that low Ca^{2+} did not disrupt EPH/EPHRIN driven cell sorting (Fig. 3.2A, C), suggesting sorting is independent of changes in cadherin-mediated adhesion.

In various contexts, actomyosin enrichment is observed at EPH/EPHRIN boundaries once segregation has occurred (Calzolari et al., 2014; Cooke et al., 2001; O'Neill et al., 2016; Taylor et al., 2017). To determine if actomyosin contractility is required to maintain separate EPH-expressing and EPHRIN-expressing compartments, we applied actomyosin contractility inhibitors to cultures after segregation had already occurred. When Y27632 and ML7 were added together 24 hours after mixing, significant remixing of EPHB2-expressing cells and EPHRIN-B1-expressing cells occurred by 48 hours (Fig. 3.2A, D). This result would not be expected if these inhibitors blocked actomyosin-dependent cell migration and demonstrates that actomyosin contractility is critical for maintaining EPH/EPHRIN boundaries by minimizing EPH/EPHRIN cell intermixing. These data demonstrate that actomyosin contractility is not only critical for driving increased interfacial tension at the heterotypic cell:cell interface but is also necessary for establishing and maintaining cellular organization without impacting cell migration in this system, while regulation of cadherin mediated adhesion is not essential for this process.

EPH/EPHRIN signaling increases cortical tension and requires actomyosin contractility to increase interfacial tension

To determine if increased cell:cell interfacial tension between heterotypic cell pairs is attributed to actomyosin contractility, we performed cell:cell contact angle assays in the presence of well-characterized inhibitors of the actomyosin contractility pathway. Blebbistatin, an inhibitor of myosin II ATPase activity, significantly diminished heterotypic interfacial tension (Fig. 3.3A, B), with increased contact between EPHB2:EPHRIN-B1 cell pairs, more similar to what we observed in homotypic cell pairs or when EPH/EPHRIN signaling was blocked. We confirmed this relaxation

of interfacial tension using other inhibitors of actomyosin contractility pathways including dual-inhibition by Y27632 and ML7 (Fig. 3.3A, B). These data show that actomyosin contractility is required for EPH/EPHRIN heterotypic interfacial tension and modulates the ability of these cells to generate stable contacts.

Modulating the balance between contractility and adhesion would be expected to change cell contact regardless of whether EPH/EPHRIN signaling acts directly to impact adhesion or cortical actomyosin contractility (Maître et al., 2012; Lecuit and Lenne, 2007). To determine whether EPH/EPHRIN signaling changes cortical contractility, we performed AFM to measure the mechanical stiffness of EPHB2 or EPHRIN-B1 expressing cells when cultured alone or when mixed and undergoing cell segregation for 24 hours (Fig. 3.3C). In mixed cultures we probed regions of EPHB2-GFP or EPHRIN-B1-Life-Act-mCherry and compared these with control cultures grown alone. Notably, we found an increase in stiffness of both EPHB2 cells and EPHRIN-B1 cells when undergoing cell segregation in mixed cultures compared with either population alone, suggesting that EPH/EPHRIN signaling increases actomyosin cortical tension during cell segregation (Fig. 3.3D). We observed an increase in stiffness at 4 hours following mixing EPHB2 and EPHRINB1 cells, and before any sorting was visible, indicating that this increased cortical actomyosin contractility was a consequence of EPH/EPHRIN signaling, rather than a consequence of cell segregation (Fig. S3.3A, S3.3B). As expected, inhibition of actomyosin contractility with Y27632 and ML7 resulted in a significant decrease cellular stiffness across EPHB2 and EPHRINB1-expressing cells compared to sorted controls (Fig. S3.3C). Taken together, these results indicate that increased cortical contractility at heterotypic cell:cell interfaces disrupts the ability of EPH-expressing and EPHRIN-expressing cells to maintain stable contacts, thereby dictating cellular organization during segregation based on minimization of heterotypic contacts.

Myosin localizes at heterotypic contacts

Contractile forces generated by the actomyosin cytoskeleton are driven by the activity of myosin on actin filaments. To determine if actomyosin contractility is increased at heterotypic interfaces, we visualized the localization of myosin at heterotypic and homotypic contacts in HEK293 cell lines expressing EPHB2 and EPHRIN-B1 as well as a myosin light chain (MLC)-cherry fusion protein (EPHB2-GFP-MLC-cherry and EPHRIN-B1-MLC-cherry). Upon contact between EPHB2 and EPHRIN-B1 expressing cells EPHB2 cells show an increase in MLC at the EPH:EPHRIN contact interface (Fig. 3.4C,E, S4C). This localized MLC is not observed in homotypic contacts or at heterotypic contacts in the presence of unclustered-EPHRIN-B1-Fc (Fig. 3.4A-E, S4A-D). These results indicate that EPH/EPHRIN signaling gives rise to localized increased myosin, further demonstrating high heterotypic interfacial tension is driven by actomyosin contractility.

EPHB2 cells increase homotypic contacts by a cadherin-independent mechanism

It has been reported that EPHB2 cell groups condense during EPH/EPHRIN driven cell segregation (Taylor et al., 2017). We interrogated whether EPH-EPHRIN signaling might also impact homotypic cell:cell contacts. We found that EPHB2 cells show an increased density after undergoing segregation compared with EPHRIN-B1- or EPHB2- expressing cells cultured alone, similar to a previous report (Taylor et al., 2017). Interestingly, the increase in EPHB2 cell density persisted in low Ca^{2+} media conditions (Fig. 3.5A, B, Fig. S3.5A, B), indicating that this condensation is independent of cadherin-based cell adhesion.

Based on this finding, we further investigated this adhesion-independent homotypic cell density effect by performing the cell:cell contact angle assay in the absence of calcium. As expected, in the absence of calcium-dependent adhesion, EPHRIN-B1 homotypic contacts decreased dramatically, indicating that cadherin-based adhesion likely drives homotypic contact between EPHRIN-B1 expressing cells (Fig. 3.5C, D). Also unsurprisingly, heterotypic EPHRIN-

B1:EPHB2 cell pairs retained limited contact in the absence of calcium, with additional loss of the high-contact subpopulation, suggesting a loss of dynamic oscillation between high and low contact states (Fig. 3.5C, D). However, EPHB2 homotypic pairs retained close contact, even in the absence of calcium-dependent adhesion (Fig. 3.5C, D). Given our findings indicating that calcium-mediated adhesion does not play an important role in cellular self-organization and that EPHB2 cells increase their homotypic affinity independent of calcium-dependent adhesion, we examined whether EPH/EPHRIN signaling had non-autonomous effects on cellular organization. Whereas EPHB2-expressing cells readily mix with wildtype HEK293 cells labelled only with LifeAct-BFP (WT-LifeAct-BFP) (Fig. S3.5C); mixing EPHB2 cells with both WT-LifeAct-BFP and EPHRIN-B1-expressing cells resulted in nearly complete exclusion of WT-LifeAct-BFP cells from EPHB2 cell clusters, WT-LifeAct-BFP instead intermixed with EPHRIN-B1 cells (Fig. S3.5C). These data indicate that upon receiving stimuli from EPHRIN-B1 expressing cells, EPHB2 cells preferentially organize homotypically, and prevent the invasion of signaling inert HEK293 cells.

The configuration of a cell:cell contact is not only due to the cell:cell interfacial tension but is an outcome of the relative forces acting at the cell:cell interface and cell:medium interface (Maître et al., 2012; Brodland and Chen, 2000). Whereas high actomyosin contractility at the cell:cell interface limits stable contacts, high cell:medium interfacial tension driven by actomyosin contractility is minimized by driving increased cell:cell contact. To determine if high cell:medium tension was driving increased EPHB2 homotypic cell contact we measured the cell:cell contact angle in the absence of calcium and in the presence of blebbistatin to decrease cortical actomyosin contractility at both the cell:cell and cell:medium interface (Fig. 3.5C, D). We found that blocking contractility in the absence of calcium-dependent adhesion decreased contact between EPHB2 homotypic cell pair, suggesting that EPHB2-expressing cells have a high cell:medium interfacial tension driven by cortical actomyosin contractility away from the cell:cell interface (Fig. 11C, D). Taken together, these data suggest that the EPH/EPHRIN mediated cellular organization, with robust segregation between EPHB2- and EPHRIN-B1-expressing cells

and increased density of EPHB2 cells, is a result of both increased heterotypic cell:cell interfacial tension and EPHB2-homotypic affinity driven by high cell:medium tension.

Actomyosin contractility is important for cell segregation *in vivo*

To determine if increased actomyosin contractility at heterotypic cell interfaces drives cell segregation *in vivo* we utilized a genetic mouse model which is mosaic for EPHRIN-B1. Mosaicism for mutations in X-linked EPHRIN-B1, arising from random X-inactivation around embryonic day 5.5 (E5.5) in heterozygous females, results in cell segregation between EPHRIN-B1 expressing and non-expressing cells in mice (Compagni et al., 2003; O'Neill et al., 2016; Niethamer et al., 2020; Bush and Soriano, 2010). To disrupt actomyosin contractility we utilized mice carrying floxed alleles of non-muscle myosin IIA (NMIIA) and non-muscle myosin IIB (NMIIB) and a *Shox2*^{iresCre} allele to drive recombination and robust cell segregation in the anterior palate. We also included in these experiments an X-linked GFP transgene as an independent marker of the extent of cell segregation (Hadjantonakis et al., 1998). We observed robust cell segregation in the anterior palate of *Efnb1*^{loxXGFP/+}; *Shox2*^{iresCre/+} embryos (Fig. 3.6A) whereas *Efnb1*^{loxXGFP/+}; *NMIIA*^{lox/lox}; *NMIIB*^{lox/lox}; *Shox2*^{iresCre/+} embryos exhibited disruption of cell segregation with smaller patches and more single, unsorted XGFP positive cells appearing throughout the palate (Fig. 3.6A). We quantified the extent of cell segregation by counting the number of cells per XGFP⁺ patch and measuring patch area which revealed a significant decrease in XGFP positive patch size compared to *Efnb1*^{loxXGFP/+}; *Shox2*^{iresCre/+} embryos (Fig. 3.6B, C). These data demonstrate the importance of actomyosin contractility in driving cell segregation *in vivo*.

Cell segregation by EPH/EPHRIN signaling affects tissue morphology

Boundaries between EPH and EPHRIN expressing populations are critical for tissue separation and morphogenesis in numerous contexts, including germ layer separation, somites, and rhombomeres (Calzolari et al., 2014; Watanabe et al., 2009; Cooke et al., 2001; Rohani et

al., 2011). To determine in a simple system how the properties of heterotypic and homotypic contact strength that we have uncovered here influence larger scale organization and tissue shape, we performed cell-segregation assays in 3D hanging drop culture. In control aggregates, where EPHB2-GFP cells were mixed with EPHB2-GFP-LifeAct-mCherry cells, cells intermixed and the overall morphology appeared spherical and smooth. However, when EPHB2-GFP-LifeAct-mCherry cells were mixed with EPHRIN-B1-LifeAct-mCherry cells, cells segregated, and the morphology of the aggregates was highly irregular and tortuous (Fig. 3.7A). Because it was difficult to determine how the tortuous morphology correlated with boundary formation in these large aggregates, we also generated smaller aggregates by isolating small groups of cells 24 hours after cell mixing and culturing these aggregates in isolation for an additional 24-48 hours (Fig. S3.6A). Consistent with our earlier cell sorting assays in circular microwells (Fig. 3.7E), we observed that the EPHB2- and EPHRIN-B1 cell- populations minimize their contact with one another, minimizing high tension interactions and altering aggregate morphology at the point of heterotypic contact (Fig. 3.7B). To determine if these changes in morphology were also driven by actomyosin contractility we added Y27632 and ML7 to this hanging drop assay. When these inhibitors were added to the culture medium at 24 hours, a timepoint at which segregation has occurred, the morphology of the aggregate changed dramatically. The aggregates appeared much more spherical and contact was no longer minimized at EPH/EPHRIN interfaces (Fig. 3.7B). This was also true when inhibitors were added to large tortuous aggregates at 72 hours and cultured for an additional 48 hours (Fig. S3.6B). These data show that actomyosin contractility driven by heterotypic EPH/EPHRIN cell contact not only governs cellular organization, but also likely underlies the subsequent tissue separation shape changes that are often observed at EPH/EPHRIN boundaries *in vivo*.

Discussion

While long known to regulate cells' ability to intermix and self-organize, we now discover how EPH/EPHRIN signaling regulates cell contacts to drive cellular self-organization and boundary formation. The differential interfacial tension hypothesis predicts that cells minimize contacts with high mechanical potential (Brodland and Chen, 2000). These high-tension interfaces can occur between a cell and the media, the matrix, or another cell population. The outcome of self-organization is therefore driven by the minimization of overall tension by increasing the relative surface area of low tension interfaces at the expense of high-tension interfaces (Maître et al., 2012). Overall interfacial tension is dictated by a combination of adhesion and cortical tension, wherein the balance between cell:cell and cell:medium tensions modulate cell contact (Winklbauer, 2015). When tension is highest between heterotypic cell types, cells minimize cell:cell contacts. Indeed, our data show that EPH/EPHRIN signaling results in increased relative cell:cell interfacial tension by modulating actomyosin contractility and cortical tension at heterotypic contacts, which results in cell segregation and boundary formation (Fig. 3.8A,B). Consistent with this mechanism, cell segregation is abolished *in vitro* and highly disrupted *in vivo* when actomyosin contractility is disrupted and both EPHB2 and EPHRIN-B1 cells increase their stiffness when undergoing segregation.

If tension is highest at the cell:medium interface, cells minimize contact with the medium in favor of cell:cell interactions. Differential cell:medium cortical tension has been shown to drive cell segregation in zebrafish germ layer separation and mammary epithelium organization (Cerchiari et al., 2015; Krieg et al., 2008; Maître et al., 2012). In these systems, cells with the highest cell:medium interfacial tension aggregated at the center, thereby minimizing unfavorable, high interfacial tension interactions with the surrounding medium (Cerchiari et al., 2015; Krieg et al., 2008). The relative influence of cell:cell and cell:medium tension is reflected by 3D segregation hierarchy experiments where we observe that the two populations minimize their

contact with one another rather than one population being enveloped by the other. However, whereas heterotypic EPH/EPHRIN interactions are the least energetically favorable interaction and dominate cellular organization, a secondary effect of cell:medium tension also contributes to self-organization by increasing contact between EPH expressing cells (Fig. 3.8A,B). In our experiments, the absence of cadherin based adhesion revealed EPHB2 homotypic cell contact that is driven by cell:medium tension driven by actomyosin contractility rather than cell:cell adhesion tension. This discovery is somewhat surprising, as cadherins are thought to be required to mechanically couple the cortices of cells to enable cortical tension to regulate cell contact (Maître et al., 2012). The ability of EPHB2 homotypic signaling to expand cell contacts in low Ca^{2+} conditions may therefore reflect that cadherin function is incompletely abrogated in our experiments, though we do not think this is the case as EPHRIN-B1:EPHRIN-B1 homotypic contacts and WT:WT homotypic contacts are dramatically reduced in these conditions. Alternatively, our results may suggest the existence of a cadherin-independent adhesion mechanism for coupling cell cortices or more passive spreading of cells on one another, as was previously demonstrated upon disruption of adherence junctions through removal of α -catenin (Stirbat et al., 2013).

High interfacial tension at the cell:cell interface has also been suggested to drive segregation in *Xenopus* at the mesoderm-endoderm boundary, though this effect was proposed to be independent of cortical tension (Canty et al., 2017). Our data support a model in which actomyosin contractility at the EPH/EPHRIN cell:cell interface prevents heterotypic cell pairs from maintaining stable contacts and thus segregating from one another, while homotypic contacts driven by cell:medium interfacial tension help to reinforce this interaction (Fig. 3.8A,B). The pathways employed downstream of EPH/EPHRIN signaling to differentially regulate tension at the cell:cell and cell:media interfaces will be an exciting future research question.

Because of the well-established role of EPH/EPHRIN signaling in mediating axon guidance via growth cone collapse, cellular guidance by repulsive migration has been a long-

standing hypothesis for how EPH/EPHRIN signaling drives cell segregation and boundary formation. Indeed, EPH/EPHRIN mediated repulsive migration has been observed in pairs of individual cells (Astin et al., 2010; O'Neill et al., 2016; Poliakov et al., 2008). Further, computer simulations of cell segregation using experimentally measured parameters of contact duration, frequency of cellular collapse, and migration away, do show robust cell segregation, while in these same simulations solely decreasing contact frequency between heterotypic cell pairs only drives mild cell segregation (Taylor et al., 2017). However, several observations do not support cell migration as a driver of cell segregation in our system. First, we previously showed that during cell segregation, EPHB2 cells decrease their total migratory distance, rather than traveling a greater distance as would be predicted by repetitive repulsive migration (O'Neill et al., 2016). Second, we do not see changes in migratory behaviors of cells when blocking actomyosin contractility and thus preventing segregation. Further, upon inhibition of actomyosin contractility after segregation has occurred, cells remix, indicating that inhibition of actomyosin contractility does not prevent cells from migrating. Instead, the “repulsive” effect of EPH/EPHRIN signaling in our system is one that regulates interfacial cortical tension to allow cells to minimize their heterotypic contacts, while increasing homotypic EPHB2 contacts.

Nevertheless, it is possible that cell migration is playing a role in EPH/EPHRIN driven cell segregation in other contexts *in vivo* where cells are confronted with dynamic and complex environments. The results of our mouse genetics experiments are consistent with the requirement for cellular contractility in driving EPH/EPHRIN cellular self- organization, however these experiments do not rule out the role of actomyosin in cell migration as a possible contributing mechanism as well. There is also the possibility that mechanisms of segregation may differ between cell types. Our study examines HEK293 cells and craniofacial mesenchyme cells. While HEK293 cells were thought to be epithelial in origin, HEK293 cells express a number of mesenchymal markers such as N-cadherin and vimentin, and indeed have been speculated to have a neural crest-derived adrenal medulla origin (Inada et al., 2016; Lin et al., 2014). The effects

of EPH/EPHRIN signaling on cortical tension and cell contacts will need to be examined in additional cell types that also form EPH/EPHRIN boundaries to determine the extent to which mechanisms differ between cell types.

Previous findings indicate that at the boundary between the mesoderm and ectoderm, tissue separation occurs due to EPHB forward signaling, and this separation occurs through repeated rounds of adhesion, which brings EPHs and EPHRINs into contact for active signaling which then induces repulsion and detachment of the two tissues (Rohani et al., 2011). This is similar to our findings that cell:cell contacts are not static but rather are dynamic over time. This detachment between the mesoderm and ectoderm could represent minimization of contact between germ layers driven by changing tension at the mesoderm-ectoderm interface. The analogy of EPH/EPHRIN signaling in segregation to its role in growth cone collapse, may therefore better reflect the commonality of actomyosin contractility in cellular collapse and modulation of cell:cell contact, rather than migratory guidance. Actomyosin contractility pathways are well-established to be downstream of EPH/EPHRIN signaling, and classically known to be involved in cellular collapse phenotypes induced by EPH/EPHRIN signaling (Wahl et al., 2000). The idea that EPH/EPHRIN signaling results in minimization of cell contacts by increased interfacial tension therefore may represent a broadly applicable mechanism by which EPHs and EPHRINs regulate cell behavior and boundary formation in morphogenesis.

It is notable that AFM revealed cortical stiffness increases in both EPHB2-expressing and EPHRIN-B1-expressing cells during segregation, whereas MLC fluorescence increases in EPHB2 cells at EPHB2: EPHRIN-B1 heterotypic contacts. Previous genetic experiments in the *EFNB1* mutant mouse model indicated that unidirectional forward signaling drives EPH:EPHRIN cell segregation in the developing embryo, whereas reverse signaling is dispensable (O'Neill et al., 2016). Recent findings have shown that whereas polarized forward signaling is the principal driver of cell sorting, reverse signaling also play a role in preventing cell intermingling, consistent with the increases in cortical stiffness that we observe in EPHRIN-B1 cells. This suggests a

contribution of both forward and reverse signaling to EPH:EPHRIN cell segregation in cell culture, whereas forward signaling is sufficient *in vivo*, and the contributions of reverse signaling *in vivo* may be difficult to detect.

The data presented here suggest a novel model for EPH/EPHRIN driven cell segregation, in which both cell:cell and cell:medium tension, driven by actomyosin contractility drive cellular organization and boundary formation. This expands our knowledge of boundary formation and suggests a generalizable mechanism by which EPH/EPHRIN signaling drives boundary formation.

Materials and Methods

HEK293 cell culture

Stable HEK293 cell lines expressing EPHRIN-B1 or EPHB2 plus membrane-targeted GFP were obtained from A. Poliakov and D. Wilkinson (laboratory of D. Wilkinson, Medical Research Council National Institute for Medical Research, London, England, UK; (Jørgensen et al., 2009; Poliakov et al., 2008). Stable HEK293 cell lines expressing EPHB2, membrane-targeted GFP and LifeAct-mCherry were generated as described in O'Neill et al. 2016. Stable HEK293 cell lines expressing EPHB2 or EPHRIN-B1 and MLC-cherry constructs were generated by transfecting EPHB2-GFP or EPHRIN-B1 cells with MLC-cherry plasmid DNA followed by selection with hygromycin. All cells were cultured at 37°C with 5% CO₂ in DMEM supplemented with 10% fetal bovine serum, glutamine, and antibiotics. Serum starvation medium was made using DMEM with glutamine and antibiotics, and low calcium (Ca²⁺) medium was made using SMEM supplemented with 5% dialyzed FBS, glutamine, and antibiotics.

Cell segregation assay, static analysis of sorting, cell density quantification, and live imaging

Cell segregation assays were performed as previously described (O'Neill et al., 2016; Poliakov et al., 2008). Each cell type was aliquoted into and resuspended in medium to a cell density of 150,000/mL, with various inhibitors and plated in 24-well plates coated with 10µg/mL fibronectin (Sigma-Aldrich). For mixing experiments; HEK293 cells expressing GFP, LifeAct-mCherry, and high levels of EPHB2 (EPHB2-GFP-LifeAct-mCherry) are mixed with HEK293 cells expressing GFP and high levels of EPHB2 (EPHB2-GFP) as a control, or with HEK293 cells expressing high levels of EPHRIN-B1 and LifeAct-mCherry (EPHRIN-B1-LifeAct-mCherry). Mixing of cells expressing EPHB2 with cells expressing EPHRIN-B1 results in dramatic segregation. Cells are mixed in a 1:1 ratio. For three cell type mixing experiments EPHB2-GFP-LifeAct-mCherry cells are mixed with EPHRIN-B1-LifeAct-mCherry and HEK293 cells expressing LifeAct-BFP (WT-LifeAct-BFP). Cells were then cultured for 24 or 48 hours.

Images of live cells were acquired on an Axio Observer.Z1 spinning disk confocal microscope (ZEISS) at 37° using a 10x objective lens. Zen software was used to acquire images, adjust brightness and contrast and export tiff images. For each condition 6-8 images were obtained per experimental replicate and images were manually thresholded in ImageJ (Table 3.3). Experiments were repeated 3-4 times (Table 3.3). Segregation was then quantified using the nearest-neighbor method (Mochizuki et al., 1998; O'Neill et al., 2016; Poliakov et al., 2008). This method converts each image into a lattice of squares, roughly corresponding to cells, and each square is scored as GFP positive, or GFP negative. For each GFP positive square the number of neighboring GFP positive squares among the four nearest neighbors is counted, and this information generates a sorting score, as detailed in Mochizuki et al. Sorting scores were normalized to the EPHB2-GFP + EPHB2-GFP-LifeAct-mCherry condition (negative control; set to 0.5), and raw data from images were averaged and analyzed using ANOVA and Dunnett's tests. All conditions were compared with the positive control condition (EPHB2-GFP-LifeAct-mCherry + EPHRIN-B1-LifeAct-mCherry+ DMSO).

Cell density quantification was quantified by adding Hoechst to cells at 24 or 48 hours for 30 minutes prior to imaging cells. For each condition 6-8 images were obtained per experimental replicate and images were manually thresholded in ImageJ (Table 3.3). Experiments were repeated 3-4 times (Table 3.3). In each image the number of nuclei were counted, using the cell counter in Image J. Nuclei were counted by cell type by using GFP to mark EPHB2 cells and absence of GFP for EPHRIN-B1 cells. GFP+ area was then measured in Image J along with the total image area (in μM). Nuclei number was then divided by GFP+ area for EPHB2 cells and GFP- area for EPHRIN-B1 cells to obtain final cell density. For images with only one cell type total nuclei number was divided by total image area.

For live imaging of cell segregation, EPHB2-GFP-LifeAct-mCherry and EPHRIN-B1-LifeAct-mCherry cells were mixed, at a 1:1 ratio, and plated in a glass bottomed imaging dish coated with 10µg/ml fibronectin (Sigma-Aldrich) to a final cell density of 400,000/mL. Mixing was performed in the presence of 20µM Y27632 and 25µM ML7 (EMD Millipore), or vehicle (0.25% DMSO). Live imaging began 1 hour after plating and was performed at 37°C. 15 mM HEPES buffer was added and the dish sealed to buffer CO₂. Confocal stacks (3 × 2 µm) were acquired every 10 min for 16 hours using an Axio Observer.Z1 spinning disk confocal microscope (ZEISS) at 37°C, a 40× water LD C-Apochromat objective lens (numerical aperture 1.1; ZEISS), and an AxioCam 506 camera (ZEISS). Zen software was used to acquire images, generate maximum intensity projections. Three videos were acquired and cell tracking analysis was performed using the Manual Tracking plugin in ImageJ. Cells that could not be tracked for at least 12 consecutive frames (2 hours in real time) were excluded from the analysis (Table 3.3). For statistical analysis, ANOVAs (with Dunnett's post hoc tests) were used.

For low density live imaging of cell contacts, cells were plated in a glass bottomed imaging dish coated with 10µg/ml fibronectin to a final cell density of 60,000/mL. In mixed EPHRIN-B1-MLC-cherry+ EPHB2-GFP-MLC-cherry cultures, EPHRIN-B1 cells were plated 30 minutes prior to plating EPHB2 cells. In control EPHRIN-B1-MLC-cherry conditions, half of the total EPHRIN-B1 cells were plated 30 minutes prior to plating the second half of the EPHRIN-B1 cells, and in control EPHB2 conditions EPHB2-GFP cells were plated first followed by EPHB2-GFP-MLC-cherry cells. Live imaging began 15 minutes after plating the second cell population and was performed at 37°C. 15 mM HEPES buffer was added and the dish sealed to buffer CO₂. Confocal stacks (3 × 2 µm) were acquired every 3 min for 8 hours using an Axio Observer.Z1 spinning disk confocal microscope (ZEISS) at 37°C, a 40× water LD C-Apochromat objective lens (numerical aperture 1.1; ZEISS), and an AxioCam 506 camera (ZEISS). Zen software was used to acquire images. Line scan analysis was performed on a single Z- position using ImageJ, with line scans being

drawn approximately perpendicular to the cell:cell contact. We chose cell pairs where we believed we were analyzing the first heterotypic cell:cell interaction. The change in MLC fluorescence was calculated by taking the highest value from the linescan at the membrane toward the cell:cell contact both before contact, $t = -15$ min, and after contact, $t = 30$ min. The value before contact was subtracted from the value after contact to determine the change in MLC fluorescence at the cell:cell contact. Five cell pairs were analyzed for each condition.

Fabrication of agarose microwells, cell:cell contact angle and circular microwell hierarchy assays, and cell:cell live imaging

Agarose microwells were prepared as described in Cerchiari et al, PNAS 2015. Briefly, photomasks containing the desired features (a grid of 20x40 or 30x90 μ m oblongs, or 180 μ m circles) were obtained from CAD/Art Services, Inc. (Oregon, US). Silicon wafers were spin-coated with a 50 μ m thick layer of SU-8 photoresist, and baked at 135 $^{\circ}$ C for 10 min. The photomask was positioned above the wafer, and irradiated with UV light for 2 min. The wafer was placed in SU-8 developer for 10 min after one minute post-exposure bake at 135 $^{\circ}$ C. After development, the wafer was rinsed twice with SU-8 developer and once with isopropanol, and baked at 135 $^{\circ}$ C for 5 min. SYLGARD 184 silicone elastomer was prepared as per manufacturer's instruction, and poured over the developed wafer. Any air bubbles present were removed by placing in a desiccator for 15-30 minutes. The PDMS was cured at 60 $^{\circ}$ C overnight. Stamps were made by removing the PDMS from the wafer, and cutting PDMS into 1 cm by 1cm pieces. To make the microwells, a PDMS stamp was gently placed on top of molten 2% agarose in PBS within a two-well chambered coverglass. The PDMS stamp was carefully lifted once the agarose solidified.

Cell: cell contact angle assay was performed similarly to previously described in Cerchiari et al. Unmixed or mixed populations of cells were centrifuged into agarose microwells at 200 xg for 6 minutes at a concentration of 10⁶/ mL. Excess cells were then washed away with culture medium

and the remaining cells confined in wells were incubated for 4 to 12 hours for 2- cell pairs and 24 to 48 hours for circular microwells. Cell pairs were imaged 4 hours after plating using an Axio Observer.Z1 spinning disk confocal microscope (ZEISS) at 37°C, a 40× water LD C-Apochromat objective lens (numerical aperture 1.1; ZEISS). Cell aggregates were imaged immediately after plating (0 hours), as well as at 24 and 48 hours. Zen software was used to acquire images, adjust brightness and contrast and export tiff images. Contact angles were measured manually using the ImageJ tool for angle measurement. For each cell doublet angles M_1 - M_4 were measured and subtracted from 180 to obtain Θ (Fig. 3.7A). These 4 Θ values were then averaged to generate one contact angle measurement per cell doublet and plotted as contact angles. Between 54-205 cell doublets were measured per condition across 3-10 replicates (Table 3.3). Raw data from images were analyzed using ANOVA and Dunnett's tests.

For live imaging of cell:cell contact, 2% agarose in PBS microwells were made within a glass bottomed imaging dish and incubated in cell culture media for 24 hours. EPHB2-GFP-LifeAct-mCherry and EPHRIN-B1-LifeAct-mCherry cells were mixed, or plated without being mixed, into microwells and centrifuged into agarose microwells at 200 xg for 6 minutes. Excess cells were then washed away, and 15mM HEPES buffer was added and the dish sealed. Imaging began 30 minutes after plating and was performed at 37°C. Confocal stacks ($5 \times 2 \mu\text{m}$) were acquired every 5 min for 12 hours using an Axio Observer.Z1 spinning disk confocal microscope (ZEISS) at 37°C, a 40× water LD C-Apochromat objective lens (numerical aperture 1.1; ZEISS), and an AxioCam 506 camera (ZEISS). Zen software was used to acquire images, generate maximum intensity projections.

Hangin drop assays

EPHB2-GFP-LifeAct-mCherry cells were mixed with either EPHB2-GFP (control), or EPHRIN-B1-LifeAct-mCherry (cell segregation conditions). Cells were mixed in a 1:1 ratio for a total of 10^6

cells/mL. 10 μ L drops of cell suspension were plated on the lid of a 10cm dish and inverted for culture. Media was put into the dish to maintain humidity. For large hanging drops cultures were incubated for 72 hours and imaged for controls or 96 and 120 hours with the addition of inhibitors at 72 hours. For isolated hanging drops, small aggregates that form by 24 hours of culture were manually isolated using a dissecting microscope to visualize individual aggregates. Individual aggregates were then plated in 10 μ L drops on the lid of a 10cm dish and inverted for culture. Aggregate isolation and re-plating was performed in the presence of 20 μ M Y27632 and 25 μ M ML7, or DMSO. Isolated aggregated were then cultured for an additional 48 hours. Hanging drops were imaged by transferring single drops onto a glass bottom dish for imaging. Images were acquired using an Axio Observer.Z1 spinning disk confocal microscope (ZEISS) at 37°C at 10x and an Axiocam 506 camera (ZEISS). Zen software was used to acquire images, generate maximum intensity projections.

Atomic Force Microscopy

EPHB2-GFP and EPHRIN-B1-LifeAct-mCherry cells were serum starved for 48 hours in order to synchronize cell cycle. After 48 hours of serum starvation cells were switched back into regular culture media for 24 hours prior to mixing. EPHB2-GFP and EPHRIN-B1-LifeAct-mCherry cells were either mixed and plated or plated alone onto glass cover slips coated with 10 μ g/ml fibronectin (Sigma-Aldrich) to a final cell density of 400,000/ml. For inhibitor experiments Y27632 and ML7, or DMSO for controls, were added at time of cell mixing. Atomic force microscopy (AFM) was performed 2, 4, or 24 hours after mixing. For inhibitor experiments and 2- and 4-hour analysis data was collected across EPHB2 and EPHRIN-B1 cell types and presented as pooled data, while at 24 hours EPHB2 and EPHRIN-B1 populations were measured separately in mixed conditions. Glass cover slips were placed on slides and placed on the stage of an MFP3D-BIO inverted optical AFM (Asylum Research) mounted on a Nikon TE2000-U inverted microscope. Indentations were made using silicon nitride cantilevers with spring constants ranging from .05 to .07 N/m and

modified with borosilicate glass spherical tips 5µm in diameter (Novascan Tech). The cantilevers were calibrated using the thermal oscillation method prior to each experiment. Cells were indented at rates ranging from 0.75 to 1.5µm/s and with a maximum force of 4.5 nN. The Hertz model was applied to the force curves obtained from each cell indentation to calculate the elastic modulus (Young's modulus, stiffness). Cells were assumed to be incompressible; therefore a Poisson's ratio of 0.5 was used in the calculation of the elastic modulus. Experiments were repeated 3-6 times per condition (Table 3.3). Raw data were analyzed using ANOVA and Dunnett's tests.

Inhibitors

Inhibitors used in cell segregation assays, cell-cell contact angle assays, and live imaging were 2µg/ml unclustered EPHRIN-B1-Fc (R&D Systems), 20µM Y27632 (Cayman), 25µM ML7 (EMD Millipore), 20µM blebbistatin (Sigma-Aldrich), and 5 µg/ml Mitomycin C (Sigma-Aldrich).

Mouse lines

All alleles used here have been previously described. All mice were maintained on a congenic C57BL/6J genetic background. *EFNB1*^{lox}, MGI: 3039289 (Davy et al., 2004); XGFP, MGI: 3055027 (Hadjantonakis et al., 1998), *Shox2*^{IresCre}, MGI: 5567920 (Dougherty et al., 2013), *NMIIA*^{lox/lox}, MGI: 4838521 (Jacobelli et al., 2010) and *NMIIB*^{lox/lox}, MGI: 4443039 (Ma et al., 2009) (Table 3.1). To ensure X chromosome mosaicism all embryos were female and were collected at E13.5.

Immunofluorescence

Embryos were fixed in 4% PFA in PBS, dehydrated through sucrose, embedded in OCT, and frozen in dry ice/ ethanol. 10 µm sections were cut using a CryoStar NX70 Cryostat (Thermo Scientific) cryostat. Slides were washed with PBS, blocked in 5% normal donkey serum (Jackson ImmunoResearch) and 0.1% Triton-X-100 in PBS, incubated in primary antibody overnight at 4°C,

washed with PBS, and incubated in secondary antibody at room temperature. Slides were counterstained in DAPI (Millipore) in PBS and coverslips were mounted on slides using Aquamount (Thermo Scientific) for imaging. Images were acquired on LSM900 (Zeiss), on a LD LCI Plan-Apochromat 25x/0.8 Imm Corr DIC M27 objective lens. Zen software was used to acquire images, generate maximum intensity projections.

Quantification of cell segregation *in vivo*

Quantification of cell segregation *in vivo* was performed on cryosections immunostained for EPHRIN-B1 and XGFP, and counterstained with DAPI. For quantification continuous XGFP-expressing regions were selected in FIJI/ImageJ and area was calculated as a measure of the amount of cell segregation. Additionally, the total number of nuclei in each XGFP-positive patch were counted manually, using the cell counter plug-in. XGFP-positive patches were binned into patches of size 1-5, 6-64, 65-128, >128 nuclei and the number of patches in each bin was divided by the total number of XGFP-positive patches in that section to generate the percentage of patches of different size ranges. Images from 3 different embryos of each genotype were analyzed (Table 3.2, 3.3).

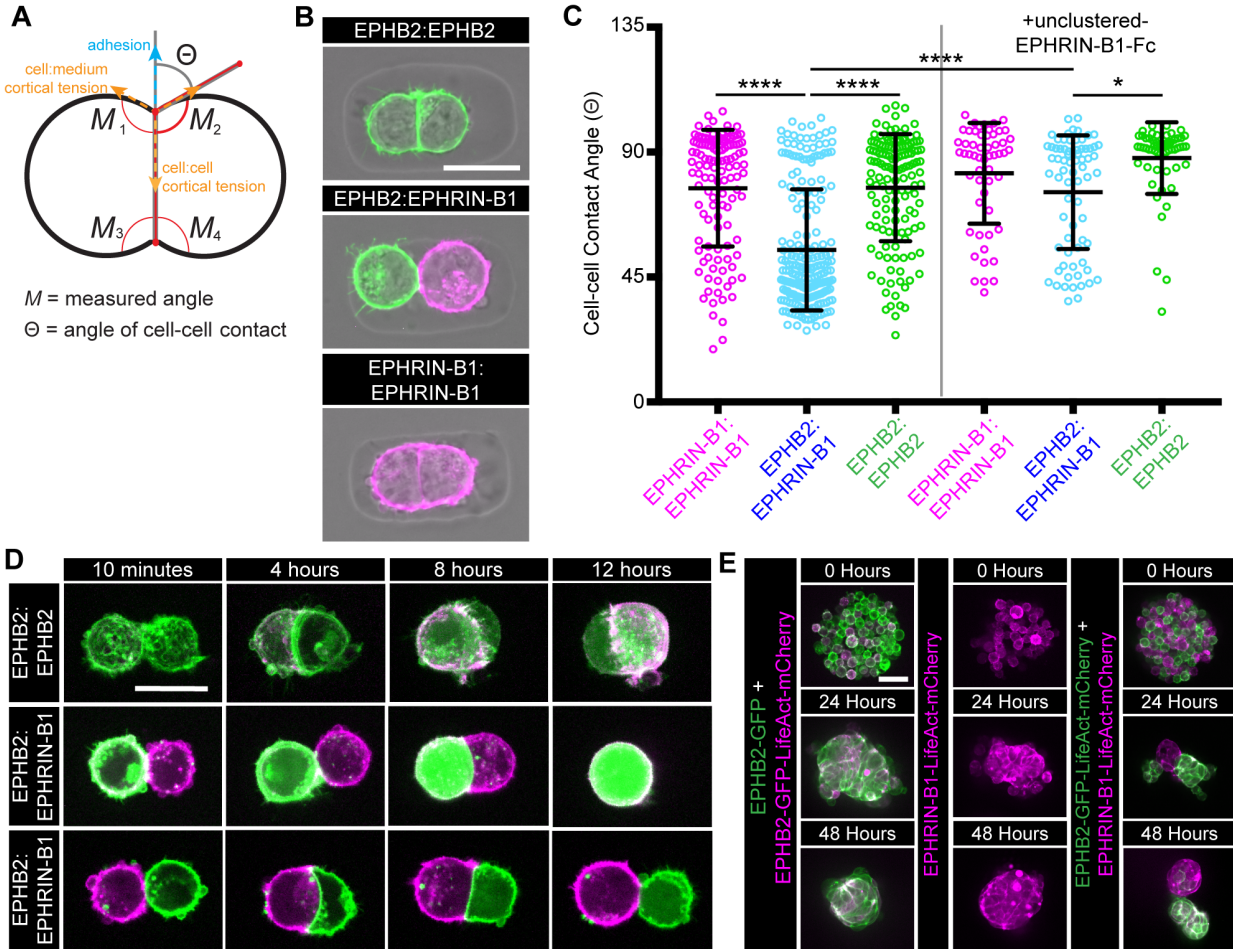


Figure 3.1. EPH/EPHRIN signaling increases heterotypic interfacial tension. (A) Schematic for cell:cell contact angle measurements. (B) Representative images of cell doublets in agarose microwells. EPHRIN-B1-mCherry (magenta) and EPHB2-GFP (green). Scale bars, 20 μ m. (C) Quantification of cell:cell contact angles 4 hours after plating. EPHB2:EPHRIN-B1 cell pairs show a decreased contact angle, or increased interfacial tension. Upon the addition of unclustered-EPHRIN-B1-Fc, to block EPH/EPHRIN signaling, this relative increase in interfacial tension between heterotypic cell pairs is diminished. (D) Individual frames from live imaging experiments at 10 minutes, 4 hours, 8 hours, and 12 hours of live imaging, showing cell:cell contacts are dynamic over time. EPHRIN-B1-mCherry (magenta) and EPHB2-GFP-LifeAct-mCherry (green). Scale bars, 20 μ m. (E) HEK293 3D cell aggregates in circular agarose microwells (180 μ m). Scale bars, 50 μ m. *, P < 0.05 ****, P < 0.0001. (ANOVA followed by Dunnett's multiple comparison test).

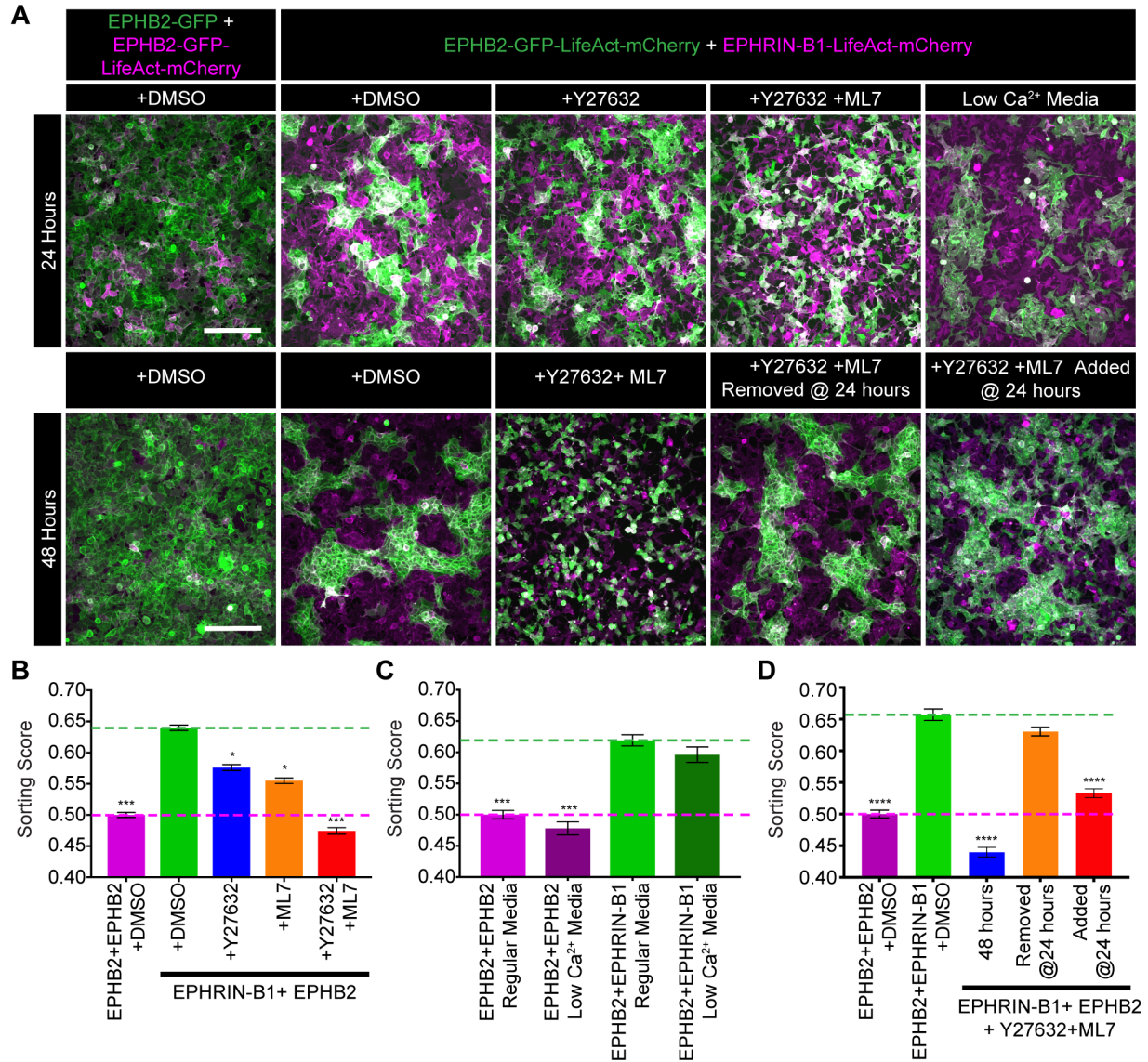


Figure 3.2. Cell segregation is abolished by dual inhibition of ROCK and MLCK. (A) Cell segregation in mixed populations of HEK293 cells. In the far-left panels EPHB2-GFP (green) cells were mixed with EPHB2-GFP-LifeAct-mCherry (magenta) cells. In the rest of the panels EPHB2-GFP-LifeAct-mCherry (green) cells were mixed with EPHRIN-B1-mCherry (magenta) cells and treated with vehicle (DMSO) or inhibitors, or cultured in low Ca²⁺ media to determine effect on cell segregation. For images at 48 hours some inhibitors were added or removed at 24 hours. Scale bars, 200µm. **(B)** Quantification of cell segregation for several of the conditions illustrated in A. Dual inhibition of ROCK and MLCK abolished cell segregation. **(C)** Quantification of cell segregation in the absence of calcium. Cell segregation was undisturbed by the lack of calcium in the media. **(D)** Quantification of cell segregation upon the addition or removal of inhibitors. Cell segregation is still able to occur upon removal of ROCK and MLCK inhibitors after 24 hours, and addition of these inhibitors to media at 24 hours after sorting disrupts cell segregation. Cell segregation was quantified using the nearest-neighbor method. Column heights represent means of the technical replicates, and error bars represent SEM. *, P < 0.05; ***, P < 0.001, ****, P < 0.0001 versus (B) EPHB2 + EPHRIN-B1 + DMSO condition (C) EPHB2 + EPHRIN-B1 regular

media condition and (D) EPHB2 + EPHRIN-B1 + DMSO condition at 48 hours. (ANOVA followed by Dunnett's multiple comparison test). Results are representative of three experiments.

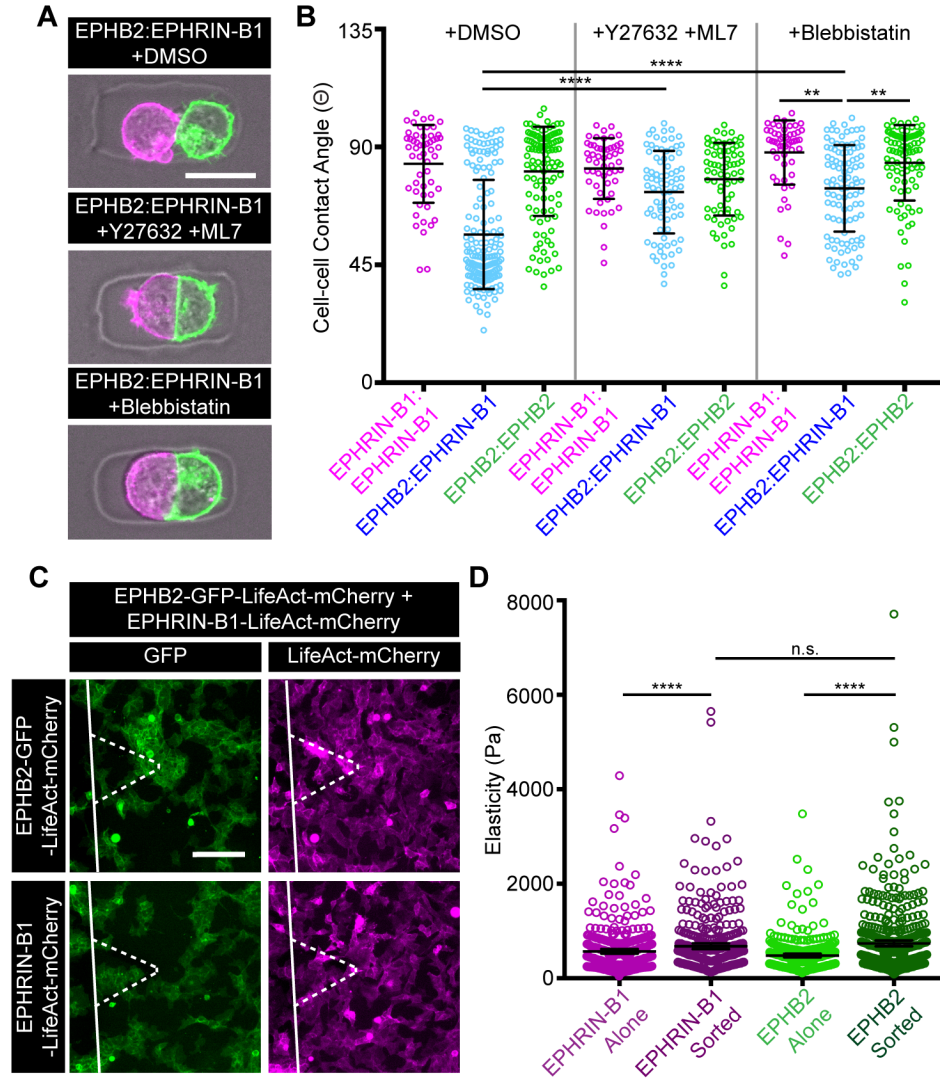


Figure 3.3. Actomyosin contractility drives increased cellular interfacial tension. (A) Representative images of cell doublets in agarose microwells. EPHRIN-B1-mCherry (magenta) and EPHB2-GFP (green), treated with vehicle (DMSO) or inhibitors. Scale bars, 20 μ m. **(B)** Quantification of cell:cell contact angles 4 hours after plating. In HEK293 media with DMSO EPHB2:EPHRIN-B1 cell pairs show a decreased contact angle compared with EPHRIN-B1:EPHRIN-B1 homotypic cell pairs or EPHB2:EPHB2 homotypic cell pairs ****, $P < 0.0001$. (ANOVA followed by Dunnett's multiple comparison test). Upon the addition of Y27632 and ML7 or the addition of blebbistatin EPHB2:EPHRIN-B1 cell pairs no longer show diminished contact compared with EPHB2:EPHRIN-B1 cell pairs in media with DMSO control. **, $P < 0.01$ ****, $P < 0.0001$. (ANOVA followed by Dunnett's multiple comparison test). **(C)** Representative images of EPHRIN-B1-mCherry (magenta) cells and EPHB2-GFP (green) cells mixed and segregated after 24 hours, when AFM was performed. White outline represents location of AFM machinery in each image. Scale bar, 200 μ m. **(D)** Quantification of cellular elasticity (Pa) determined by AFM either when EPHRIN-B1 or EPHB2 cells were cultured alone, or when these cells were mixed and allowed to segregate. Both cell types in sorted conditions show increased stiffness compared to when cultured alone. ****, $P < 0.0001$ (ANOVA followed by Dunnett's multiple comparison test).

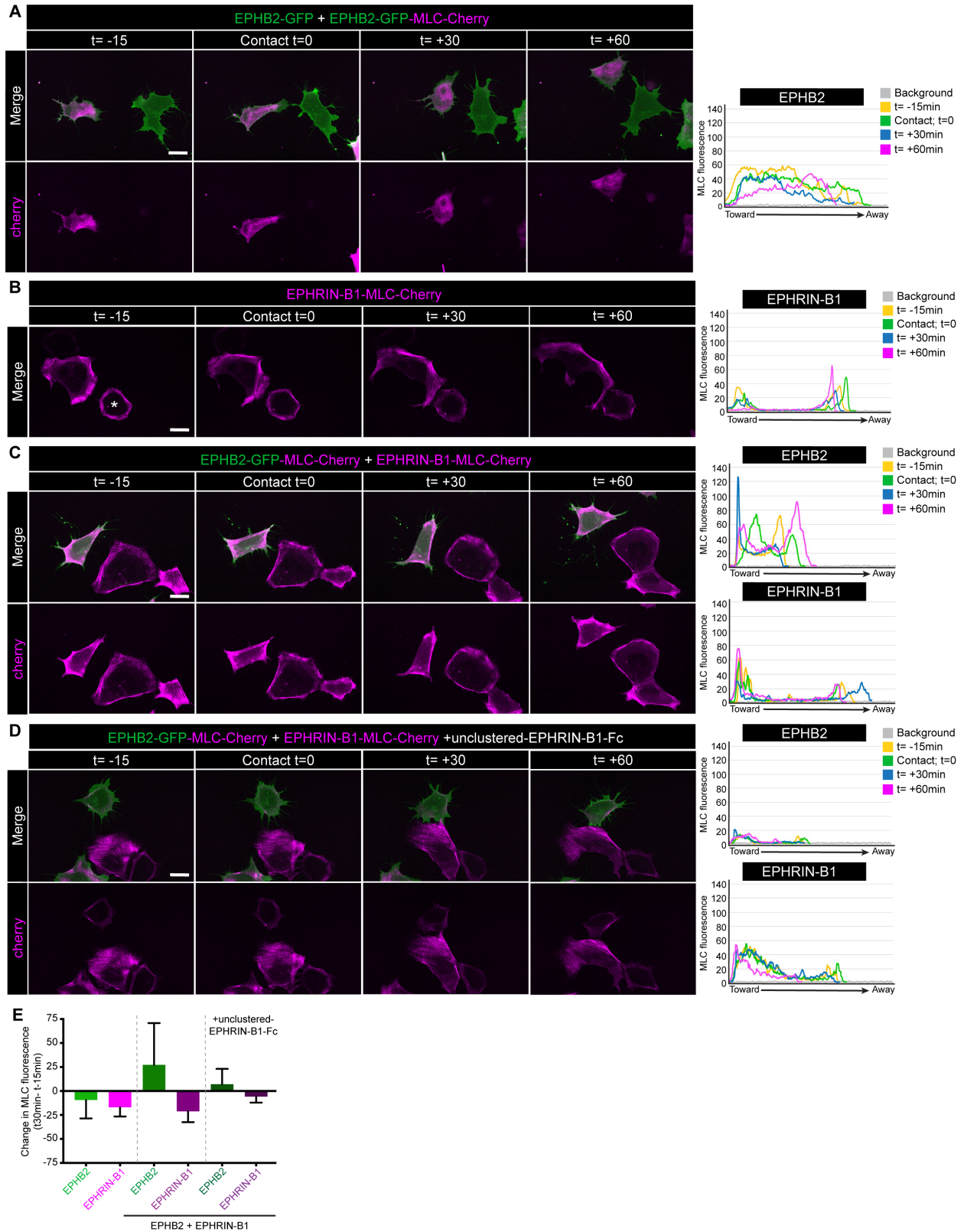


Figure 3.4. Myosin light chain localization increases at heterotypic contacts. (A) Example images from live imaging experiments of EPHB2 homotypic conditions at low density. EPHB2-

GFP (green) cells were mixed with EPHB2-GFP-MLC-Cherry (magenta). Linescan analysis of cell pair at various timepoints shows no change in MLC localization upon contact. **(B)** Example images from live imaging experiments of EPHRIN-B1 homotypic conditions at low density. EPHRIN-B1-MLC-Cherry (magenta). Asterix indicates analyzed cell. Linescan analysis of cell pair at various timepoints shows no change in MLC localization upon contact. **(C)** Example images from live imaging experiments of heterotypic conditions at low density. EphB2-GFP-MLC-Cherry (green) cells were mixed with EPHRIN-B1-MLC-Cherry (magenta) cells. Yellow arrows at $t = +30$ min indicate localized increase in MLC. Linescan analysis of cell pair at various timepoints shows MLC localized to cell contact in EPHB2 cells upon contact. **(D)** Example images from live imaging experiments of heterotypic, with unclustered-EPHRIN-B1-Fc, conditions at low density. EphB2-GFP-MLC-Cherry (green) cells were mixed with EPHRIN-B1-MLC-Cherry (magenta) cells, unclustered-EPHRIN-B1-Fc was added to prevent signaling. Linescan analysis of cell pair at various timepoints shows no change in MLC localization upon contact. **(E)** Quantification of the change in MLC fluorescence from before contact ($t = -15$ min) to after contact ($t = 30$ min). EPHB2 cells show an increase in MLC localization at heterotypic interface upon contact with EPHRIN-B1-expressing cell. This effect is blocked by the addition of unclustered-EPHRIN-B1-Fc. White arrow at $t = 0$ min indicates point of contact. Toward indicates toward contact, while away indicates away from contact. $t =$ time. Scale bars, $20\mu\text{m}$.

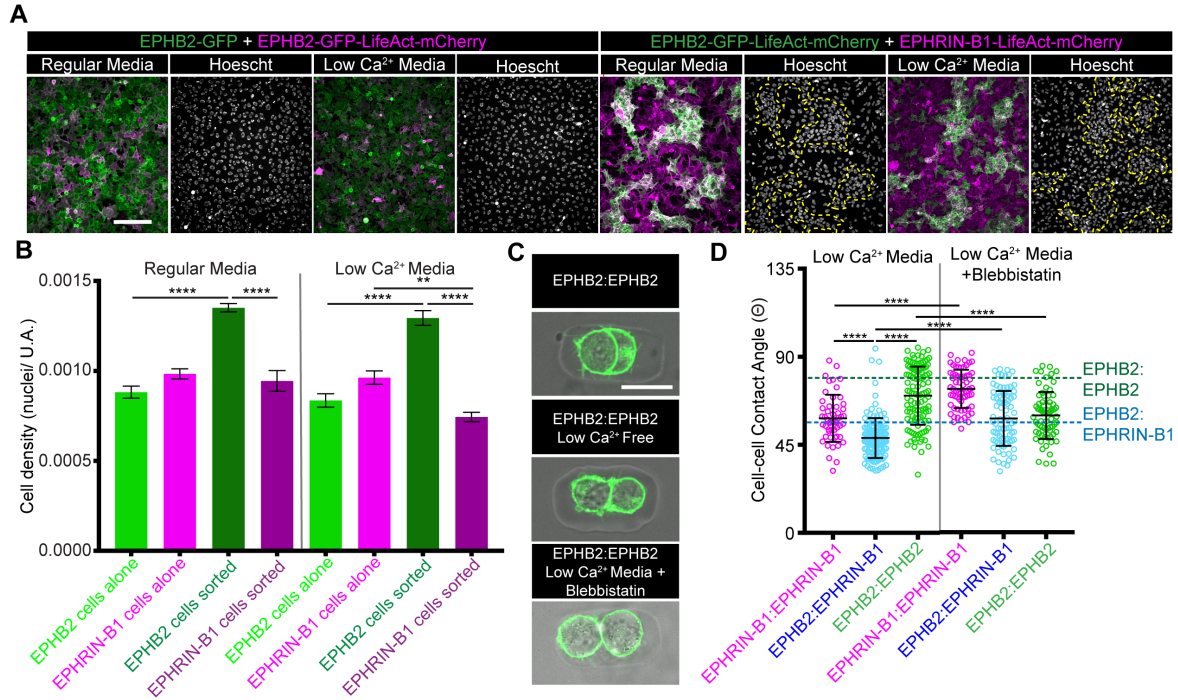


Figure 3.5. EPHB2 cells increase homotypic contacts due to high cell:media cortical tension. (A) Cell segregation in mixed populations of HEK293 cells. In the left panels EPHB2-GFP (green) cells were mixed EPHB2-GFP-LifeAct-mCherry (magenta) cells in either regular or low Ca²⁺ media. In the right panels EPHB2-GFP-LifeAct-mCherry (green) cells were mixed with Ephrin-B1-LifeAct-mCherry (magenta) cells in regular HEK293 or low Ca²⁺ media. Hoescht images shown to visualize nuclei. Yellow dashed lines outline EPHB2 cell patches. Scale bars, 200 µm. **(B)** Quantification of nuclear density for the conditions illustrated in A. In both regular and low Ca²⁺ media EPHB2 cells have a significantly increased density. **, P<0.01, ****, P < 0.0001. **(C)** Representative images of cell doublets in agarose microwells. EPHB2-GFP (green). Scale bars, 20µm. **(D)** Quantification of cell: cell contact angles in the absence of calcium. Cell:cell contacts diminish in the absence of calcium, however EPHB2:EPHB2 homotypic contacts are somewhat retained. In low Ca²⁺ media with the addition of blebbistatin EPHB2:EPHB2 contacts are diminished. Dashed lines indicate average cell:cell contact angles in regular media conditions. ****, P < 0.0001.

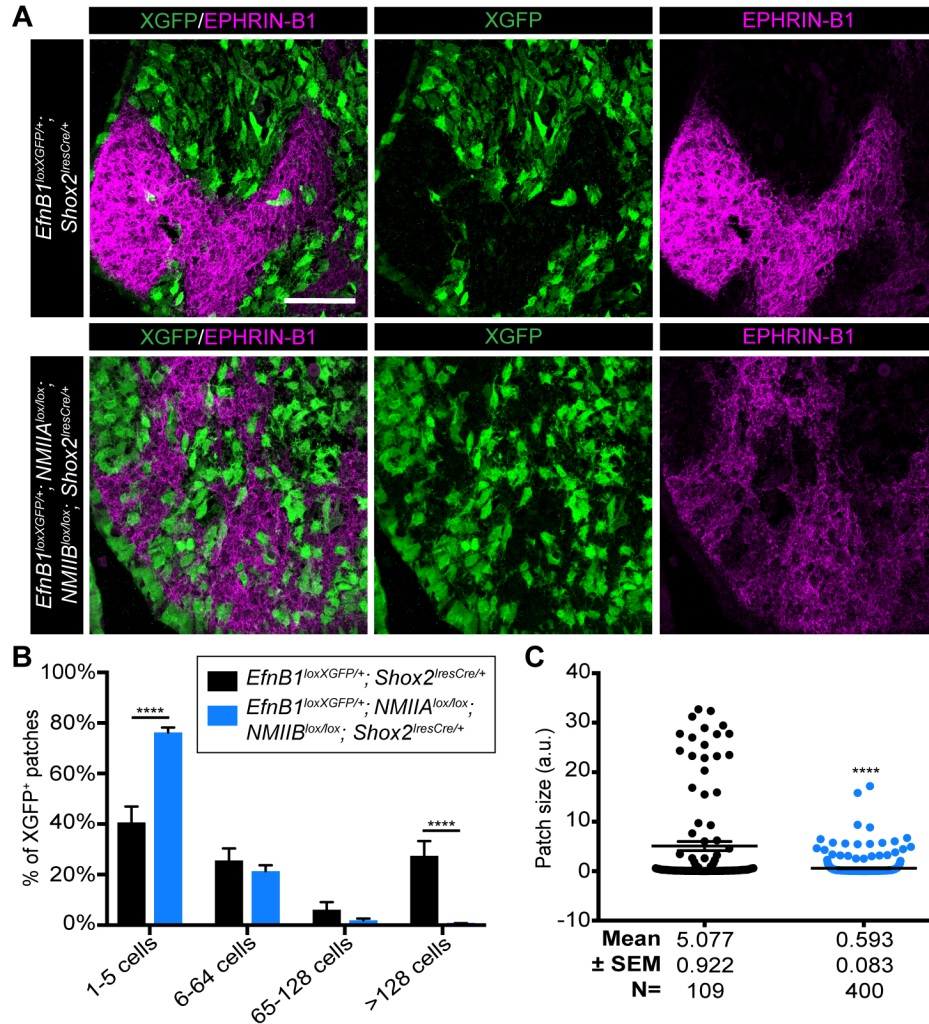


Figure 3.6. Cell segregation *in vivo* is disrupted by lack of actomyosin contractility. (A) Immunostaining of E13.5 coronal sections for EPHRIN-B1 (magenta) and GFP (green) shows segregation in *EfnB1*^{loxXGFP/+}; *Shox2*^{iresCre/+} embryos and diminished segregation when actomyosin contractility is disrupted in *EfnB1*^{loxXGFP/+}; *Shox2*^{iresCre/+}; *NMIIA*^{lox/lox}; *NMIIB*^{lox/lox} embryos. **(B)** Distribution of percentage of XGFP-positive patches of various sizes. Column height represents means of the distributions across all sections measured for a given genotype, error bars represent S.E.M. **(C)** Patch sizes represented as scatterplots. Horizontal bars represent means, and error bars represent S.E.M. ****, $P < 0.0001$.

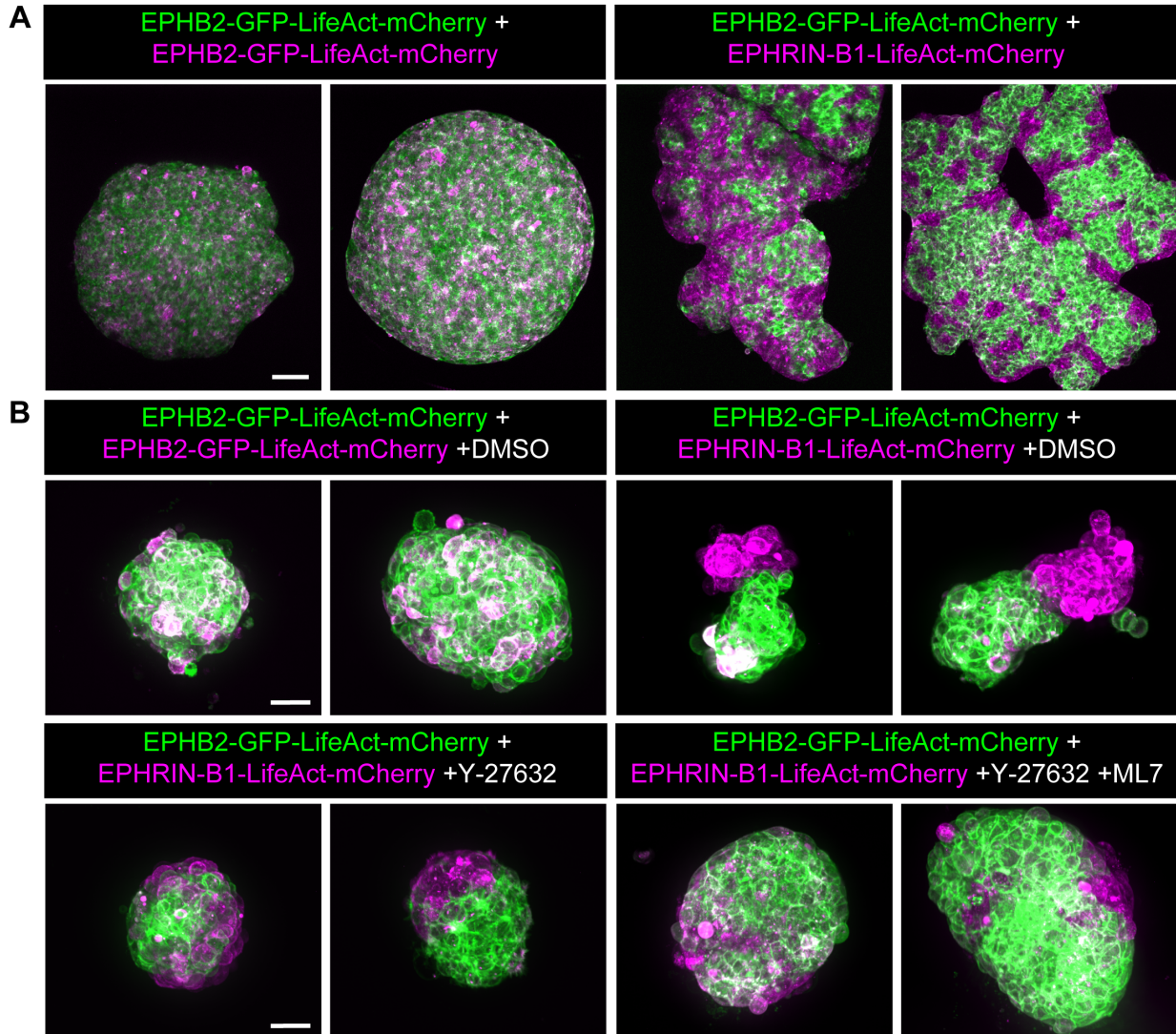


Figure 3.7. EPH/EPHRIN signaling affects tissue morphology. (A) Representative images of EPHB2-GFP (green) cells mixed with EPHB2-GFP-LifeAct-mCherry (magenta) cells in hanging drop cultures for 72 hours on left form circular aggregates. In the right panels EPHB2-GFP-LifeAct-mCherry (green) cells mixed with EPHRIN-B1-LifeAct-mCherry (magenta) cells in hanging drop cultures for 72 hours segregate and form highly tortuous aggregates. Scale bars 100 μ m. (B) HEK293-cell isolated aggregates formed in hanging drop cultures 72 hours after mixing. Morphology changes observed in segregated aggregates are disrupted by inhibition of ROCK and MLCK with Y27632 and ML7. Scale bars 50 μ m.

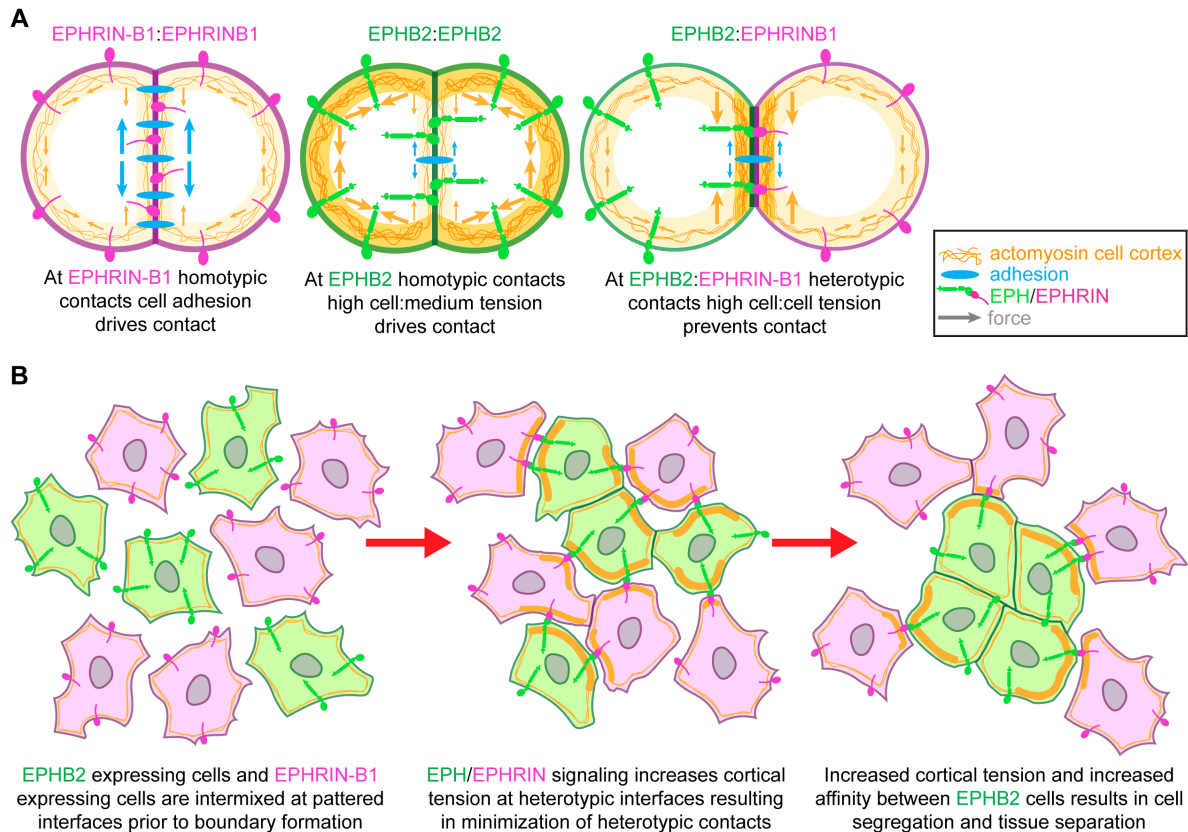


Figure 3.8. EPH/EPHRIN signaling modulates both cell:cell and cell:media tension, driven by actomyosin contractility to drive cellular organization. (A) Schematic of cell:cell contacts and the forces that modulate these contacts. EPHB2:EPHB2 homotypic contact is driven by increased cell:medium tension, while EPHRIN-B1:EPHRIN-B1 homotypic contact is driven by cell adhesion. EPHB2:EPHRIN-B1 heterotypic cell pairs show high cell:cell interfacial tension due to increased actomyosin contractility at the cell:cell interface. **(B)** High cell:cell interfacial tension between EPHB2 and EPHRIN-B1 expressing cells results in a minimization of contact between these cell populations. Together with increased EPHB2 homotypic affinity, this increased cortical tension, preventing the formation of stable heterotypic contacts drives cell segregation.

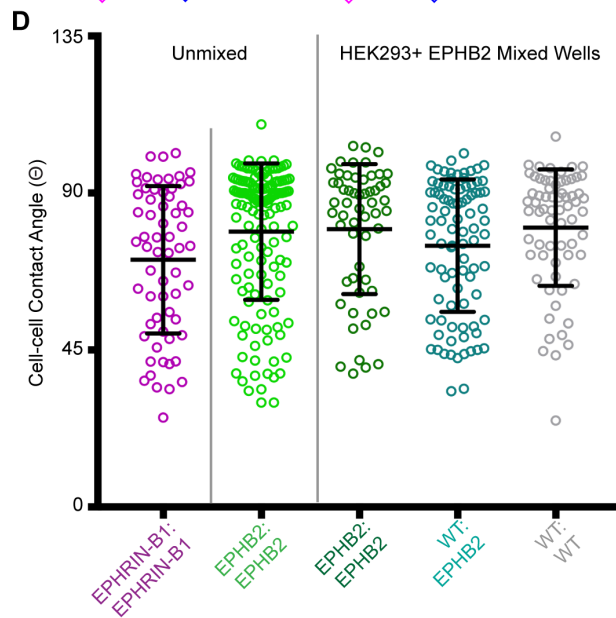
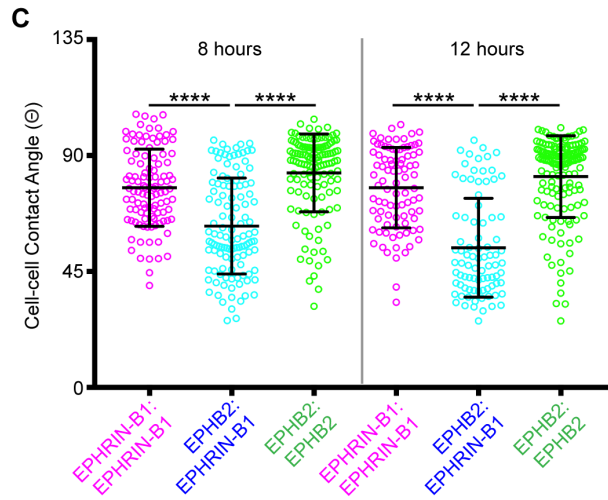
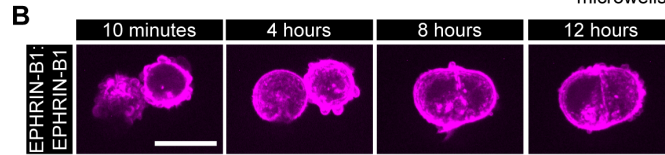
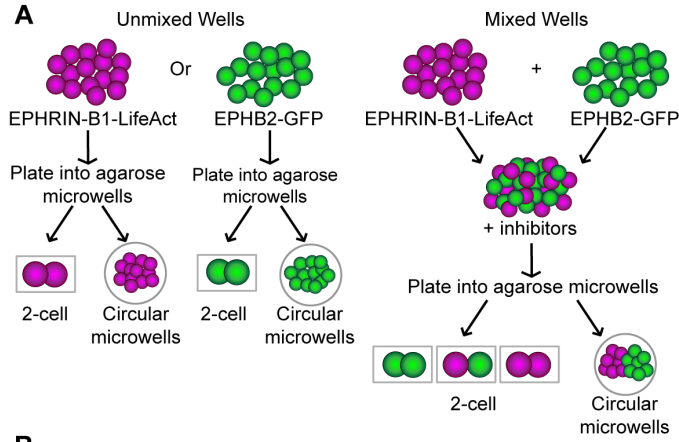


Figure S3.1. HEK293 cells lacking EPH/EPHRIN signaling do not have high interfacial tension. A) Schematic of cell:cell contact angle assay set up for both unmixed and mixed conditions. B) Individual frames from live imaging at 10 minutes, 4 hours, 8 hours, and 12 hours of EPHRIN-B1 live imaging, showing cell:cell contacts are dynamic over time. Scale bars, 20 μ m. C) Quantification of cell:cell contact angles at 8 hours and 12 hours after plating. EPHB2:EPHRIN-B1 cell pairs show a decreased contact angle, or increased interfacial tension, over time. D) Quantification of cell:cell contact angles at 4 hours after plating for unmixed EPHRIN-B1, unmixed EPHB2 cells, and mixed EPHB2 cells with wildtype HEK293 cells showing that heterotypic cell pairs where no EPH/EPHRIN signaling is occurring do not display increased interfacial tension compared to homotypic cells.

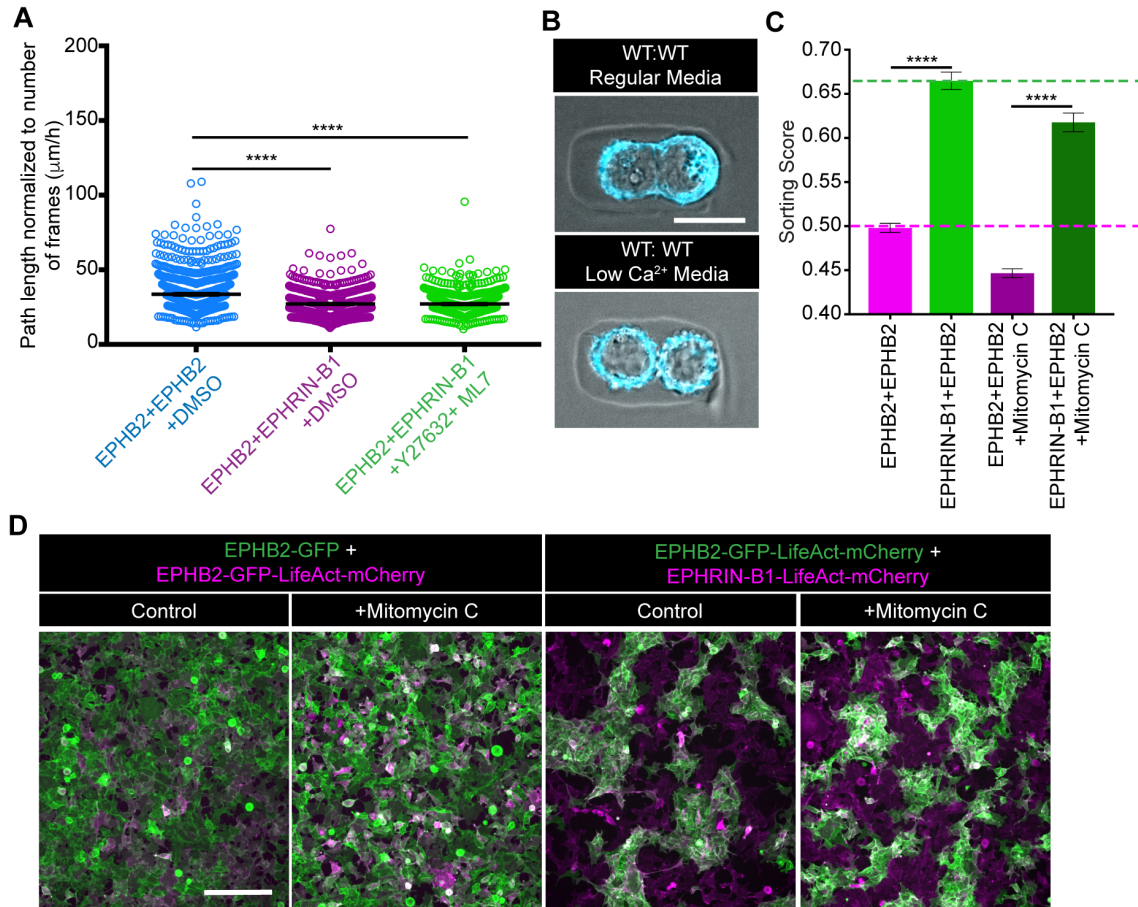


Figure S3.2. Cells under dual ROCK and MLCK inhibition remain migratory. A) Cell tracking analysis of overall EPHB2 cell movement over 16 h. EPHB2 cells in segregation conditions migrate less than when mixed with other EPHB2 expressing cells, however addition of Y27632 and ML7 do not diminish migration from what is seen in cell segregation conditions. B) Representative images of wildtype HEK293 cells in regular media and in low Ca²⁺ media. Cell contact is dramatically reduced in the absence of calcium. C) Quantification of cell segregation in the presence of Mitomycin C. Inhibition of cellular proliferation does not block cell segregation. D) Representative images of cell segregation in mixed population of HEK293 cells in the presence of Mitomycin C inhibitor. Scale bars, 200μm. ****, P < 0.0001.

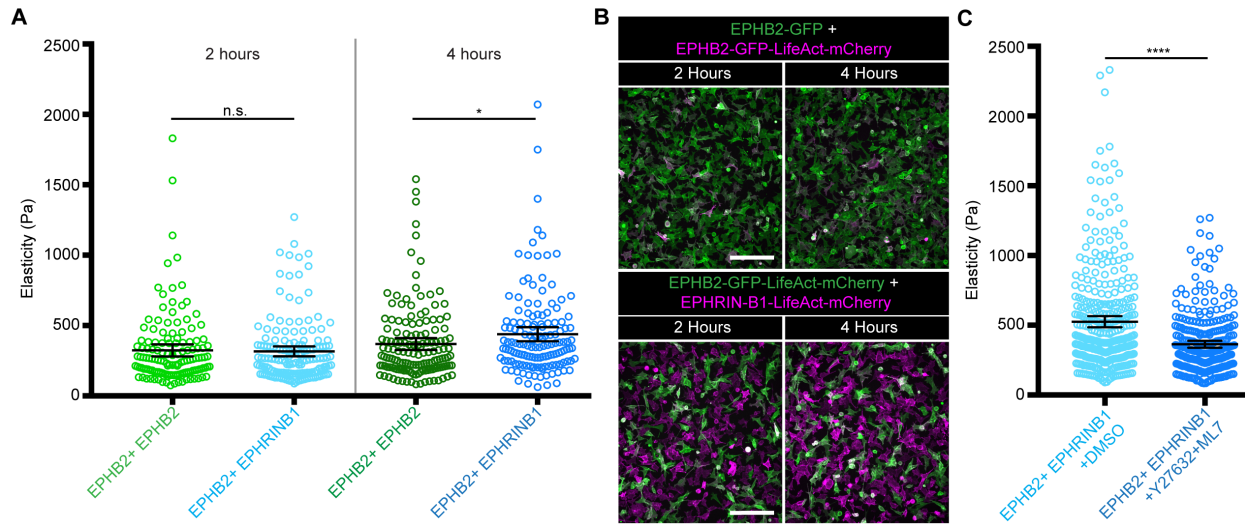


Figure S3.3. Actomyosin contractility increases cortical tension during cell segregation at early timepoints. A) Quantification of cellular elasticity (Pa) determined by AFM in mixed EPHB2 cells cultured alone and EPHRIN-B1: EPHB2 mixed cultures at 2 and 4 hours after plating. By 4 hours after plating EPHB2:EPHRIN-B1 mixed cultures show increased stiffness compared to EPHB2 cells cultured alone. *, $P < 0.05$. B) Representative images of EPHB2-GFP-LifeAct-mCherry (magenta) cells mixed with EPHB2-GFP (green) cells mixed or EPHRIN-B1- LifeAct-mCherry (magenta) cells at 2 hours and 4 hours when AFM was performed. Cells in EPH:EPHRIN mixed cultures are not yet segregated. Scale bars, $200\mu\text{m}$. C) Quantification of cellular elasticity (Pa) determined by AFM in mixed EPHRIN-B1: EPHB2 cultures in the presence of DMSO or actomyosin contractility inhibitors Y27632 and ML7 after 24 hours. In the presence of contractility inhibitors cells show a decrease in stiffness compared to DMSO controls. ****, $P < 0.0001$ (ANOVA followed by Dunnett's multiple comparison test).

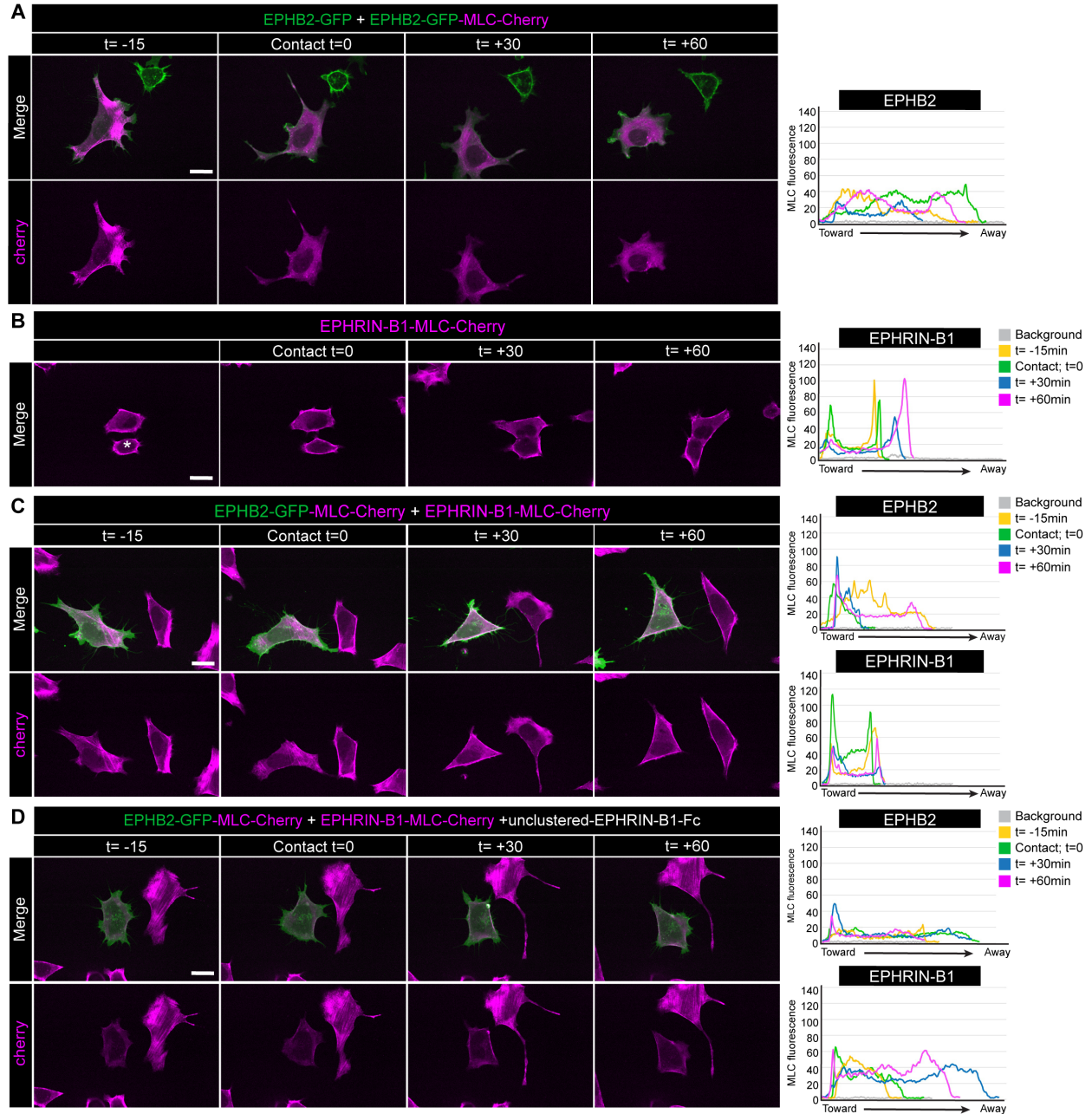


Figure S3.4. Myosin light chain localization increases at heterotypic contacts. A) Example images from live imaging experiments of EPHB2 homotypic conditions at low density. EPHB2-GFP (green) cells were mixed with EPHB2-GFP-MLC-Cherry (magenta). Linescan analysis of cell pair at various timepoints shows no change in MLC localization upon contact. B) Example images from live imaging experiments of EPHRIN-B1 homotypic conditions at low density. EPHRIN-B1-MLC-Cherry (magenta). Asterisk indicates analyzed cell. Linescan analysis of cell pair at various timepoints shows no change in MLC localization upon contact. C) Example images from live imaging experiments of heterotypic conditions at low density. EphB2-GFP-MLC-Cherry (green) cells were mixed with EPHRIN-B1-MLC-Cherry (magenta) cells. Yellow arrows at t = +30 min indicate localized increase in MLC. Linescan analysis of cell pair at various timepoints shows MLC localized to cell contact in EPHB2 cells upon contact. D) Example images from live imaging

experiments of heterotypic, with unclustered-EPHRIN-B1-Fc, conditions at low density. EphB2-GFP-MLC-Cherry (green) cells were mixed with EPHRIN-B1-MLC-Cherry (magenta) cells, unclustered-EPHRIN-B1-Fc was added to prevent signaling. Linescan analysis of cell pair at various timepoints shows no change in MLC localization upon contact. White arrow at t=0 min indicates point of contact. Toward indicates toward contact, while away indicates away from contact. t= time. Scale bars, 20 μ m.

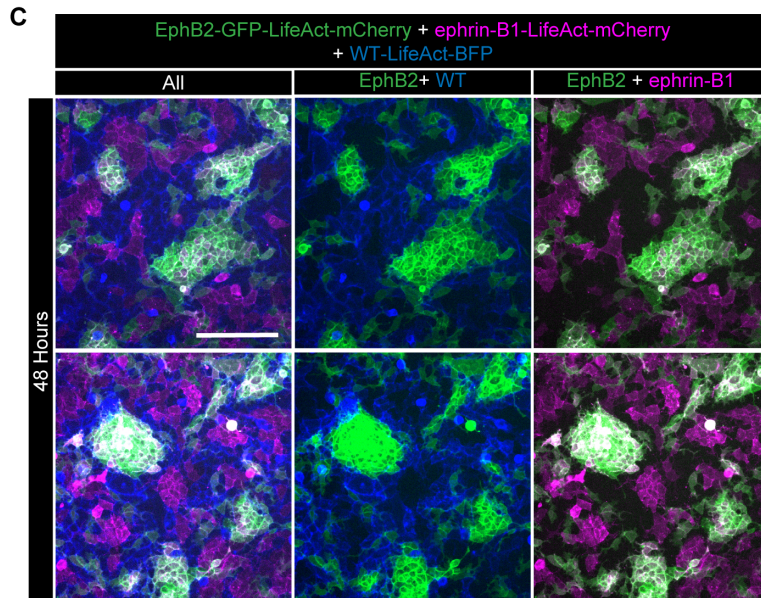
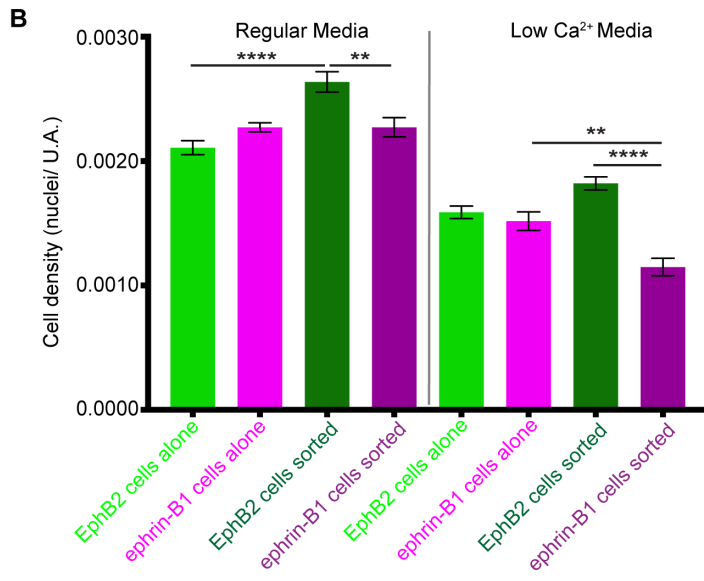
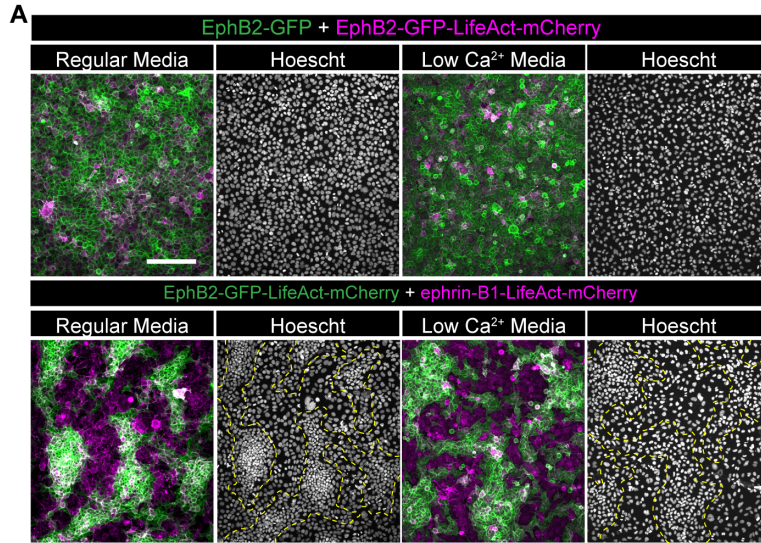


Figure S3.5. EPHB2 cells increase homotypic contacts in response to EPH/EPHRIN signaling. A) Cell segregation in mixed populations of HEK293 cells at 48 hours. In the left panels EPHB2-GFP (green) cells were mixed with EPHB2-GFP-LifeAct-mCherry (magenta) cells in either regular or low Ca^{2+} media. In the right panels cells EPHB2-GFP-LifeAct-mCherry were mixed with cells overexpressing EPHRIN-B1-LifeAct-mCherry (magenta) cells in regular HEK293 or low Ca^{2+} media. Hoescht images shown to visualize nuclei. Yellow dashed lines outline EPHB2 cell patches. Scale bars, 200 μm . B) Quantification of nuclear density for the conditions illustrated in B. In both regular and low Ca^{2+} media EPHB2 cells have a significantly increased density. **, $P < 0.01$, ****, $P < 0.0001$. C) Cell segregation in mixed populations of HEK293 cells. EPHB2-GFP (green) cells were mixed with EPHRIN-B1-LifeAct-mCherry (magenta) cells and WT-LifeAct-BFP (blue) cells. Cell segregation robustly occurs and WT-LifeAct-BFP do not intermix with EPHB2 cells.

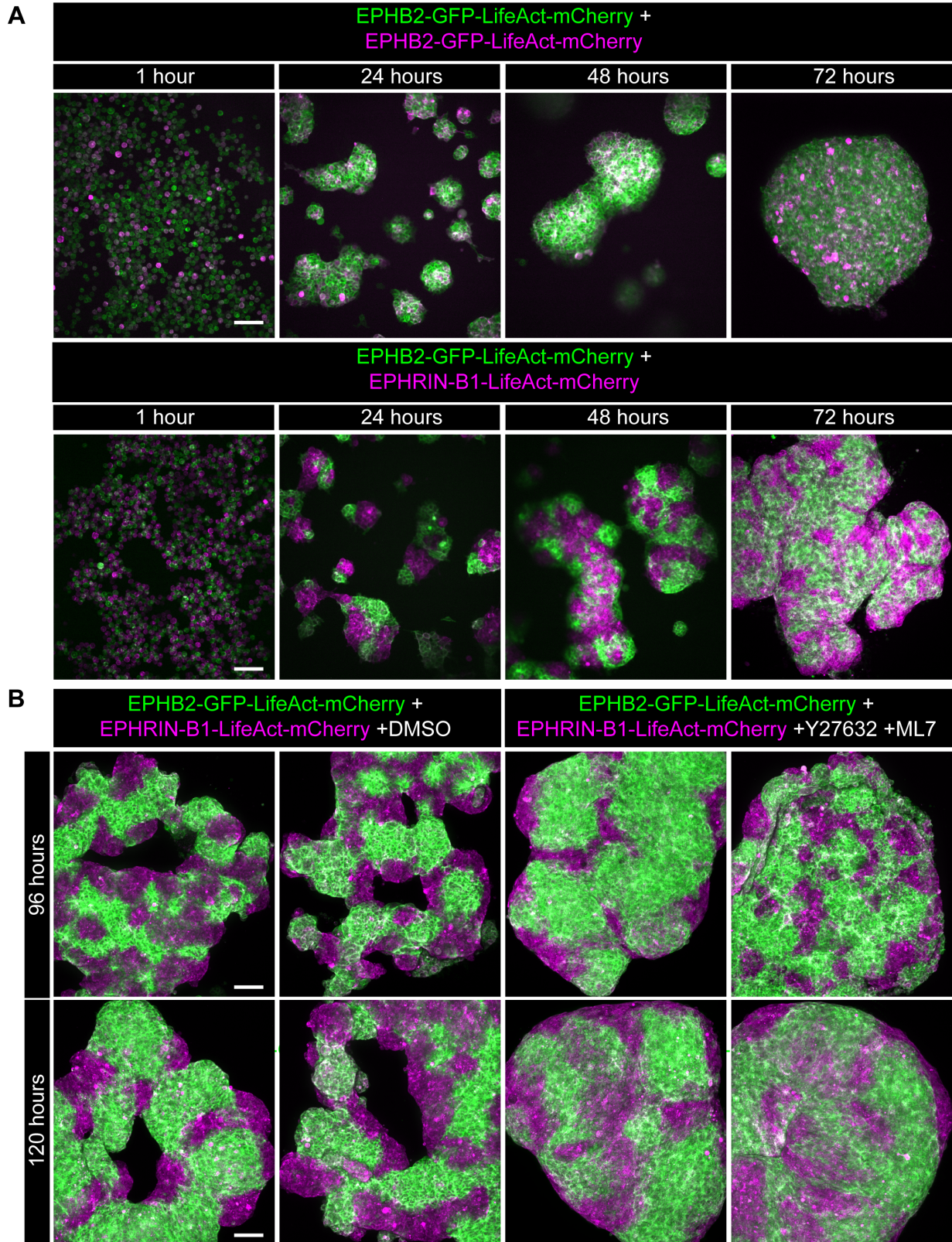


Figure S3.6. EPH/EPHRIN signaling effects on cortical tension impact tissue morphology.
 A) Top: Representative images of EPHB2-GFP (green) cells mixed with EPHB2-GFP-LifeAct-

mCherry (magenta) cells in hanging drop cultures at multiple timepoints during aggregate formation. Bottom: Representative images of EPHB2-GFP- LifeAct-mCherry (green) cells mixed with cells overexpressing EPHRIN-B1- LifeAct-mCherry (magenta) at multiple timepoints during aggregate formation. Aggregates fully formed by 72 hours. Scale bars 100 μ m. B) Hanging drop aggregates formed by EPH: EPHRIN mixed cultures at 96 and 120 hours with the addition of DMSO (controls) or Y27632 and ML7. Morphology changes observed in segregated aggregates are disrupted by inhibition of ROCK and MLCK with Y27632 and ML7.

Table 3.1. Crosses used to generate experimental and control embryos.

Figure	Sire genotype (strain)	Dam genotype (strain)	Experimental offspring	Control offspring
3.5	<i>Shox2</i> ^{iresCre/+} (C57BL/6J)	<i>Efnb1</i> ^{loxXGFP/lox} (C57BL/6J)	n/a	<i>Efnb1</i> ^{loxXGFP/+} ; <i>Shox2</i> ^{iresCre/+}
3.5	<i>Efnb1</i> ^{loxXGFP/Y} ; <i>NMIIA</i> ^{lox/lox} ; <i>NMIIB</i> ^{lox/lox} (C57BL/6J)	<i>Efnb1</i> ^{loxXGFP/lox} ; <i>NMIIA</i> ^{lox/+} ; <i>NMIIB</i> ^{lox/+} ; <i>Shox2</i> ^{iresCre/+} (C57BL/6J)	<i>Efnb1</i> ^{loxXGFP/+} ; <i>NMIIA</i> ^{lox/lox} ; <i>NMIIB</i> ^{lox/lox} ; <i>Shox2</i> ^{iresCre/+}	n/a

Table 3.2. Numbers of embryos analyzed.

Figure	Panel	Row	Condition	Number of embryos
3.5	A	1	<i>Efnb1</i> ^{loxXGFP/+} ; <i>Shox2</i> ^{iresCre/+}	3
		2	<i>Efnb1</i> ^{loxXGFP/+} ; <i>NMIIA</i> ^{lox/lox} ; <i>NMIIB</i> ^{lox/lox} ; <i>Shox2</i> ^{iresCre/+}	3

Table 3.3. Sample size and replicates.

Figure	Panel	Condition	Sample Size	Replicates
3.1	C	<i>Control</i>		10
		EPHRIN-B1; EPHRIN-B1 EPHB2; EPHRIN-B1 EPHB2; EPHB2	n= 122 cell doublets n= 204 cell doublets n= 140 cell doublets	
		<i>+ Unclustered-EPHRIN-B1-Fc</i>		5
		EPHRIN-B1; EPHRIN-B1 EPHB2; EPHRIN-B1 EPHB2; EPHB2	n= 55 cell doublets n= 72 cell doublets n= 59 cell doublets	
3.2	B	<i>All conditions</i>	n= 34 images	3
3.2	C	<i>All conditions</i>	n= 18 images	3
3.2	D	<i>All conditions</i>	n= 18 images	3
3.3	B	<i>+ DMSO</i>		9
		EPHRIN-B1; EPHRIN-B1 EPHB2; EPHRIN-B1 EPHB2; EPHB2	n= 54 cell doublets n= 162 cell doublets n= 115 cell doublets	
		<i>+ Y27632+ ML7</i>		6
		EPHRIN-B1; EPHRIN-B1 EPHB2; EPHRIN-B1 EPHB2; EPHB2	n= 54 cell doublets n= 81 cell doublets n= 72 cell doublets	
		<i>+ Blebbistatin</i>		6
		EPHRIN-B1; EPHRIN-B1 EPHB2; EPHRIN-B1 EPHB2; EPHB2	n= 54 cell doublets n= 103 cell doublets n= 96 cell doublets	
3.3	D	EPHRIN-B1 Alone	n= 380 AFM measurements	6
		EPHRIN-B1 Sorted	n= 391 AFM measurements	6
		EPHB2 Alone	n= 327 AFM measurements	6
		EPHB2 Sorted	n= 496 AFM measurements	6
3.5	B	<i>All Regular Media</i>	n= 24 images	3
		<i>All Low Ca²⁺ Media</i>	n= 24 images	3
3.5	D	<i>Low Ca²⁺ Media</i>		10
		EPHRIN-B1; EPHRIN-B1 EPHB2; EPHRIN-B1 EPHB2; EPHB2	n= 52 cell doublets n= 133 cell doublets n= 117 cell doublets	
		<i>Low Ca²⁺ Media + Blebbistatin</i>		5
		EPHRIN-B1; EPHRIN-B1 EPHB2; EPHRIN-B1 EPHB2; EPHB2	n= 67 cell doublets n= 83 cell doublets n= 71 cell doublets	
3.6	B	<i>Efnb1^{loxXGFP/+}; Shox2^{iresCre/+}</i>	n= 3 mice	3
		<i>Efnb1^{loxXGFP/+}; NMIIA^{lox/lox}; NMIIIB^{lox/lox}; Shox2^{iresCre/+}</i>	n= 3 mice	3
3.6	C	<i>Efnb1^{loxXGFP/+}; Shox2^{iresCre/+}</i>	n= 109 XGFP ⁺ patches	3
		<i>Efnb1^{loxXGFP/+}; NMIIA^{lox/lox}; NMIIIB^{lox/lox}; Shox2^{iresCre/+}</i>	n= 400 XGFP ⁺ patches	3
S3.1	C	<i>8 hours</i>		6
		EPHRIN-B1; EPHRIN-B1 EPHB2; EPHRIN-B1 EPHB2; EPHB2	n= 108 cell doublets n= 119 cell doublets n= 128 cell doublets	
		<i>12 hours</i>		3
		EPHRIN-B1; EPHRIN-B1 EPHB2; EPHRIN-B1 EPHB2; EPHB2	n= 90 cell doublets n= 86 cell doublets n= 147 cell doublets	
S3.1	D	EPHRIN-B1; EPHRIN-B1 Unmixed	n= 63 cell doublets	4
		EPHB2; EPHB2 Unmixed	n= 142 cell doublets	6
		<i>Mixed wells</i>		9
		EPHB2; EPHB2 EPHB2; HEK293 HEK293; HEK293	n= 57 cell doublets n= 89 cell doublets n= 67 cell doublets	
S3.2	A	EPHB2+ EPHB2+ DMSO	n= 870 cell tracks	3
		EPHB2+ EPHRIN-B1+ DMSO	n= 1147 cell tracks	3
		EPHB2+ EPHRIN-B1+ Y27632+ ML7	n= 733 cell tracks	3
S3.2	C	<i>All</i>	n= 24 images	4
S3.3	A	<i>2 hours</i>		4
		EPHB2+ EPHB2 EPHB2+ EPHRIN-B1	n= 137 AFM measurements n= 155 AFM measurements	
		<i>4 hours</i>		4
		EPHB2+ EPHB2 EPHB2+ EPHRIN-B1	n= 149 AFM measurements n= 144 AFM measurements	
S3.3	C	EPHB2+ EPHRIN-B1+ DMSO	n= 253 AFM measurements	4
		EPHB2+ EPHRIN-B1+ Y27632+ ML7	n= 220 AFM measurements	4
S3.5	B	<i>All Regular Media</i>	n= 24 images	3
		<i>All Low Ca²⁺ Media</i>	n= 24 images	3

CHAPTER 4.

Potential models of EPH/EPHRIN driven cell segregation

Summary

HEK293 cells, in which EPHB2 and EPHRIN-B1 are overexpressed in two separate populations of cells, are widely used as a model to examine mechanisms of cell segregation. While HEK293 cells provide an excellent culture system for studying the mechanisms of EPH/EPHRIN driven cell segregation, additional systems are needed to determine generalizable mechanisms driving cell segregation *in vivo*. There are many potential systems, including additional cell lines, iPSC derived cell types, and *ex vivo* culture systems, however none of these systems have been well established for this use. Here I show preliminary data in several potential cell segregation systems including; mouse and chick neural progenitor cells, intestinal organoids, hiPSC derived NCCs, and additional cell lines, U251 and U87 cells. All of these systems need further trouble shooting and refining to determine if cell segregation is observed and if they are a viable system for mechanistic study *in vitro*.

Introduction

Membrane-bound EPHRINs and EPH receptor tyrosine kinases mediate boundary formation during many developmental processes by driving cell segregation and boundary formation between EPHRIN-expressing and EPH-expressing cells. Among other developmental abnormalities, mutations in EPHs and EPHRINs effect morphogenesis of the craniofacial complex (Bush and Soriano, 2010; Risley et al., 2009), result in early embryonic lethality due to defective angiogenesis (Gerety et al., 1999; Salvucci and Tosato, 2012; Lewis et al., 2015), cause inappropriate neural crest migration and disrupt neural crest-derived structures (Smith et al., 1997), and cause inappropriate axon guidance and axon crossing of the midline (Wilkinson, 2001), which is essential for proper central nervous system development. EPHs and EPHRINs have also been implicated in human diseases, such as craniofrontonasal syndrome (CFNS), caused by X-linked mutations in *EFNB1* (Twigg et al., 2004), as well as in cancer, both as tumor suppressors, restricting tumor growth and cancer metastasis by preventing intermingling of EPH and EPHRIN cells, and as tumor promoters (Battle and Wilkinson, 2012). While critical in a wide range of developmental processes how EPH/EPHRIN signaling regulates cell segregation and boundary formation at mechanistic level across different contexts and cell types remains unclear.

HEK293 cells, along with other cell lines, have been widely used to study EPH/EPHRIN driven cell segregation (Poliakov et al., 2008; Taylor et al., 2017). The HEK293 system is a highly reliable system in which to study cell segregation and is amenable to mechanistic studies. In addition HEK293 cell segregation closely phenocopies the appearance of cell segregation *in vivo*. However, there are also limitations to this system. First, It relies on overexpression of EPHs and EPHRINs to drive segregation. Second, HEK293 cells are not a well-defined cell type, as their tissue-origin is debated, and are aneuploid. Both of the above present limitations to this system and to the interpretations of data collected (Inada et al., 2016; Lin et al., 2014). Segregation *in vivo* occurs in numerous different cell types and with endogenous expression levels of EPHs and EPHRINs. To determine if the mechanisms uncovered in HEK293 cells and other overexpression

systems are a generalizable mechanism by which EPH/EPHRIN signaling drives cell segregation *in vivo* additional systems of cell segregation are needed.

There are many possible systems in which mechanistic investigation of EPH/EPHRIN driven cell segregation and boundary formation could be performed, however few systems have been developed and utilized for this purpose. Rhombomeres are a well-studied example of boundary formation. EPH/EPHRIN signaling is a key regulator of rhombomere segregation with reciprocal expression patterns of EPHs in odd numbered rhombomeres and EPHRINs in even-numbered rhombomeres (Fig. 1.2A) (Becker et al., 1994; Bergemann et al., 1995; Cooke et al., 2001; Xu et al., 1995). Differential adhesion has been proposed to drive rhombomere organization as different rhombomere segments express different cadherins throughout development (Inoue et al., 1997; Nakagawa and Takeichi, 1995). However actomyosin contractility has been suggested to be important at inter-rhombomeric boundaries, with actin and myosin II accumulation occurring at boundaries (Calzolari et al., 2014). Further investigation is necessary to determine the cellular mechanisms underlying rhombomere segregation. Additionally, cells from different rhombomeres have been shown to undergo re-aggregation *in vitro*, highlighting their amenability to *ex vivo* investigation (Wizenmann and Lumsden, 1997).

The crypt-villus axis is an additional example of an EPH/EPHRIN boundary amenable to *in vitro* examination due to the prevalence of intestinal organoid culture models. In the developing intestine EPHB2 and EPHB3 have been shown to have strong expression in the crypt base while EPHRIN-B1 has been shown to be expressed more outside of the crypt base into the villus (Fig. 4.1A) (Batlle et al., 2002). This EPH/EPHRIN expression pattern generates a boundary between proliferative cells and differentiated cells in the intestine (Batlle et al., 2002). One study in Co115 cells, a colorectal cancer cell line, found that cleavage of E-cadherin by ADAM-10 metalloprotease regulates segregation downstream of EPH/EPHRIN signaling (Solanas et al., 2011). However, mechanistic investigation of how EPH/EPHRIN signaling regulates cell positioning in the intestine remains limited despite the ability to culture and manipulate intestinal organoids *in vitro*.

Other potential models of EPH/EPHRIN mediated cell segregation include iPSC derived cell types, or additional cell lines with endogenous expression of EPHs and EPHRINs. iPSC derived cell types not only may provide a good model to study cell segregation but may also provide insights into human diseases, such as CFNS. CFNS is a rare X-linked disorder characterized by craniofacial, skeletal and neurological anomalies as a result of mutations in *Efnb1*. Heterozygous females, mosaic for expression of EPHRIN-B1 are more severely affected than hemizygous males, with no expression of *EFNB1*. *EFNB1*^{+/-} mice exhibit many of the same craniofacial phenotypes as CFNS patients, and mosaicism for *Efnb1* results in aberrant segregation of cells (Bush and Soriano, 2010; Compagni et al., 2003; Davy et al., 2006; O'Neill et al., 2016; Niethamer et al., 2020). It has been demonstrated using the *EFNB1*^{+/-} mouse model that segregation occurs in the early neuroepithelium (O'Neill et al., 2016) as well as in post-migratory NCCs and also in the craniofacial mesenchyme (Niethamer et al., 2020). Cell segregation has been shown to occur in patient human iPSC (hiPSC)-derived neuroepithelial (NE) cells, presenting a potential model for mechanistic study (Niethamer et al., 2017). While promising due to the ability of hiPSC derived NE to undergo segregation, differentiations of NE are inconsistent and these cells cannot be maintained for many passages before undergoing terminal differentiation. Well-established protocols for hiPSC derived neural crest cells (NCCs) provide an additional avenue for utilizing these hiPSCs to examine the mechanisms of cell segregation in a disease relevant cell type. In mouse models, post-migratory NCC-derived mesenchymal cells readily undergo cell segregation (Niethamer, 2020). hiPSC derived NCCs do not require as lengthy of a differentiation and can be passaged as spheroids in culture, which may also enable 3D studies, however it remains unknown if these cells will undergo segregation in culture.

Unlike HEK293 cells, which have very low expression levels of endogenous EPHs and EPHRINs other cell lines have higher endogenous levels, raising the possibility of a cell line model where EPHs and EPHRINs do not have to be over expressed. U251 and U87 cells, both human malignant glioblastoma cell lines, express various EPHs and EPHRINs. U87 cells express mRNA

for EPHB1, EPHB1, and some EPHB4, as well as EFNB2 (Nakada et al., 2004). U251 cells express EPHB4 and EFNB3 mRNA (Nakada et al., 2004). Exact expression levels of these various EPHs and EPHRINs at the protein level need to be determined, as well as the ability of these cells to undergo segregation.

An alternative approach to additional *in vitro* models is to directly test potential mechanisms *in vivo*, such as our utilization of *Efnb1*^{loxXGFP/+}; *NMIIA*^{lox/lox}; *NMIIB*^{lox/lox}; *Shox2*^{IresCre/+} embryos as described in Chapter 3. While this type of approach is very useful for testing specific aspects of a mechanism it is less amenable to further mechanistic studies. Having a system in culture with endogenous expression levels of EPHs and EPHRINs but that can be manipulated *ex vivo* would enable interrogation of generalizable principals of EPH/ EPHRIN driven cell segregation and boundary formation.

Results

Mouse Neural Progenitor Cells

To determine if primary mouse neural progenitor cells would undergo cell segregation in culture we obtained *Krox20*^{cre}; *Rosa26*^{mtmg} embryos at E9.25. Because *Krox20* is expressed in rhombomeres (R) 3 and 5 these rhombomeres show robust expression of GFP upon dissection, while R4 expresses cherry, enabling us to distinguish between EPH (GFP+) and EPHRIN (cherry+) expressing cells (Fig. 4.1A). The hindbrain from R3 to R5 were collected, dissociated, and plated for culture (Fig. 4.1A). Some cells immediately following dissociation were used in our cell:cell contact angle assay. Due to the small size of the neural progenitor cells, frequently more than 2 cells were present per well (Fig. 4.1B). Additionally, due to the low number of cells plated very few 2-cell pairs were found and no measurement of cell:cell contact was performed (Fig. 4.1B). Cells cultured as hanging drops formed several small aggregates (Fig. 4.1C). These aggregates were composed of both GFP+ and cherry+ cells however no segregation was apparent (Fig. 4.1C). NPCs plated in 2D culture survived well for over a week, however, upon passage had a severely altered morphology, appearing more neuronal, when compared to the

cells prior to passage (Fig. 4.1D). Despite the change in morphology the cells continued to survive and proliferate for at least an additional week in culture (Fig. 4.1D). It did not appear as though segregation was occurring between cells of distinct rhombomeres, despite prolonged culture (Fig. 4.1D).

Chick Neural Progenitor Cells

To determine if chick neural progenitor cells may be a viable cell segregation system I isolated the rhombomeres from the hindbrain of chicken embryos at Hamburger Hamilton (HH) stages HH11 to HH13 (Fig. 4.1E). I performed several dissections to determine the best methods for dissecting and isolating R1 to R5. Once tissue was dissected it was then dissociated to single cells and cultured as hanging drops (Fig. 4.1E). These cells formed very spherical aggregates within the hanging drops, that appeared to get larger with continued culture (Fig. 4.1F). There was some cell death within these hanging drops as well (Fig. 4.1F). While the formation of hanging drop aggregates was successful the cell numbers obtained from a single embryo were small, only allowing for the plating of approximately 2 hanging drops per embryo. This could be overcome by increasing the number of dissections and pooling embryos, however at the time these experiments were performed there were issues with egg supply that prevented additional experiments.

Intestinal Organoids

To determine if intestinal organoids would be a viable system to examining EPH/ EPHRIN driven cell segregation at a mechanistic level we generated intestinal organoids using $Lgr5^{DTR-GFP}$ mice. We wanted to analyze EPH/EPHRIN expression in these wildtype organoids to determine the extent of EPH/EPHRIN expression in the organoid model. We performed immunohistochemistry for EPHRIN-B1 and lysozyme, a marker of Paneth cells in the intestinal

crypt. This enabled us to visualize the expression of EPHRIN-B1, which appears to be higher outside of the crypt base, and visualize the restriction of Paneth cells to the crypts (Fig. 4.2B). We generated intestinal organoids from *EfnB1*^{Δ/+} mice, mosaic for the expression of EPHRIN-B1. While we expected to find organoids that were mosaic in their expression of EPHRIN-B1, instead we found that entire organoids were either EPHRIN-B1 expressing or non-expressing (Fig. 4.2B). In *EfnB1*^{Δ/+} organoids expressing EPHRIN-B1, morphology of the organoids was not distinguishable from those generated from *Lgr5*^{DTR-GFP} mice and Paneth cells were restricted to crypts (Fig. 4.2B). However, in *EfnB1*^{Δ/+} organoids lacking EPHRIN-B1 expression the organoids seemed to have fewer crypt-like protrusions and lysozyme was not restricted in localization (Fig. 4.2B).

To further determine if we would be able to analyze strength of cell-cell contacts using cells from intestinal organoids we attempted to perform our cell: cell contact angle assay using dissociated organoids. When we dissociated the organoids and plated them into 20μm x 40μm agarose microwells we consistently observed far more than 2 cells per well (Fig. 4.2C). Most wells had 5 or more cells, which is not conducive to cell: cell analysis (Fig. 4.2C). In order for this assay to be successful with cells from intestinal organoids much smaller microwells would be necessary. Generating smaller microwells was attempted, however I was unable to get good resolution of the smaller wells in agarose. This could be because the features of the PDMS stamp were so small I was unable to get good resolution of these features in agarose, or because the features on the PDMS stamp itself were not well resolved. Further trouble shooting to make these smaller wells would be necessary.

iPSC derived neural crest cells

I performed Three separate hNCC differentiations. Patient derived hiPSC lines 3A14i (wildtype- WT), 1B25i (heterozygous- HET), and 2A29i (hemizygous- HEMI) were used for

differentiations. In hNCC differentiation #1, by day 12 a lot of cell death had occurred and thus differentiation was not carried forward to spheroid stage (Fig. 4.3B). In hNCC differentiation #2 when cells were transitioned to spheroid culture very few spheres were formed (Fig. 4.3C). 3A14i formed very small cell aggregates, 1B25i did not form any spheres, and 2A29i formed some spheres (Fig. 4.3C). From hNCC differentiation #2, cells were collected at day 12 for FLOW analysis using CD49d as a marker of NCC differentiation. Differentiation efficiency was extremely low (Fig. 4.3D). hNCC differentiation was performed one additional time and included the H9-Sox10-GFP cell line as a control. When these cells undergo differentiation and begin to express Sox10, a marker of NCCs, they will also express GFP, enabling a rough visualization of differentiation efficiency. 2A29i and H9-Sox10-GFP did successfully form some spheroids, however efficiency still appeared quite low (Fig. 4.3E).

Cell Lines

To examine the ability of U251 and U87 cells to undergo cell segregation we utilized our cell segregation assay. Because both U251 cells and U87 cells were initially unlabeled we were unable to mix them with one another, but were able to mix them with our existing HEK293 cell lines to determine if cell segregation could occur. U87 cells when mixed with HEK293 cells expressing EPHB2, GFP, and LifeAct-mCherry (293-EPHB2-GFP-LifeAct-mCherry), wildtype HEK293 cells labeled with cell tracker dye (293-WT), or HEK293 cells expressing EPHRIN-B1 and LifeAct-mCherry (293-EPHRIN-B1-LifeAct-mCherry) did not appear to undergo segregation (Fig. 4.4A). However, the spindle-like morphology of the U87 cells made it difficult to determine conclusively if cell segregation was occurring or if the cells were remaining intermixed (Fig. 4.4A).

U251 cells however proved to be a much better cell type than U87 cells for examining cell segregation. When mixed with 293-EPHB2-GFP-LifeAct-mCherry cells or 293-WT cells robust cell segregation occurred (Fig. 4.4B). No segregation occurred however when U251 cells were mixed with 293-EPHRIN-B1-LifeAct-mCherry cells suggesting that signaling from U251 cells to

EPHB2-expressing HEK293 cells was driving segregation (Fig. 4.4B). We next examined if we could disrupt segregation between U251 cells and 293-EPHB2-GFP-LifeAct-mCherry or 293-WT cells with either inhibitors of actomyosin contractility or unclustered-EPHRIN-B1-Fc to block signaling. For these inhibitor experiments we obtained U251-pMXI cells which express GFP enabling us to better visualize the U251 cells. We also utilized wildtype HEK293 cells labeled with LifeAct-BFP (293-WT-LifeAct-BFP). With the addition of unclustered-EPHRIN-B1-Fc sorting between U251-pMXI and either 293-EPHB2-GFP-LifeAct-mCherry or 293-WT-LifeAct-BFP sorting was partially disrupted. This was also true of the addition of Y27632 and ML7 to inhibit actomyosin contractility, however it was less clear if segregation was disrupted upon the addition of Y27632 and ML7 to U251-pMXI cells mixed with 293-EPHB2-GFP-LifeAct-mCherry cells (Fig. 4.4C). These experiments would need to be repeated and quantified to determine quantitatively the extent to which segregation was disrupted in these conditions.

We additionally performed western blots for EPHB2 and EPHRIN-B1 expression to determine if we could begin to establish the EPHs and EPHRINs driving segregation in this mixed U251: HEK293 cell system. U251 cells expressed low levels of EPHB2 (Fig. 4.4F), although these levels are above that expressed in wildtype HEK293 cells, although if segregation was driven by EPHB2 expression in U251 cells we would have expected to see robust segregation between U251 cells and HEK293 cells expressing EPHRIN-B1, a condition in which no segregation occurred (Fig. 4.4B). U251 cells do show some EPHRIN-B1 expression which could be driving segregation with HEK293 cells expressing EPHB2 (Fig. 4.4E), and why this segregation is disrupted with the addition of unclustered-EPHRIN-B1-Fc (Fig. 4.4C), however further analysis of EPH/EPHRIN expression would need to be performed to determine more conclusively what is driving segregation.

Because U251 cells and HEK293 cells are a similar size, 2- U251 cells fit well into our 20 μ m x 40 μ m microwells established for use with HEK293 cells. We performed a contact angle time course to determine at what time did U251 homotypic contacts stabilize. Interestingly,

contacts between homotypic cell pairs were not very extensive (Fig. 4.4G). Contact angles did not change dramatically after 10 to 12 hours, stabilizing at approximately 60 degrees (Fig. 4.4H).

While U251 cells show a lot of promise for a cell segregation system, this current method which is a mixed HEK293: U251 cell system, relies upon our HEK293 cells and thus does not present an entirely new model for segregation. Further, U251 cell lines stably expressing EPHs or EPHRINs could be made, but this would still rely on overexpression of an EPH or EPHRIN for segregation rather than endogenous expression levels.

Discussion

While HEK293 cells provide an excellent culture system for studying the mechanisms of EPH/EPHRIN driven cell segregation, additional systems are needed to determine generalizable mechanisms driving cell segregation *in vivo*. There are many potential systems including rhombomeres, intestinal organoids, neural crest cells, or additional cell lines. We performed some preliminary testing of several of these systems and while several show promise, further testing is necessary to determine the most viable system for further investigation.

Neural progenitor cells derived from rhombomere dissections, would be an excellent system for examining EPH/EPHRIN driven cell segregation. This system has endogenous expression of EPHs and EPHRINs and represents an endogenous boundary critical in morphogenesis. Further examinations of rhombomere boundaries *in vivo* have revealed a critical importance of EPH/ EPHRIN signaling in boundary maintenance (Cooke et al., 2001, 2005; Kemp et al., 2009; Calzolari et al., 2014). Mouse neural progenitor cells show promise as a system to examine cell segregation. The advantages of this system include the ease of *in vivo* labeling of different rhombomeres as well as the ease of dissection and culture. While no obvious segregation was observed additional dissections and mixing experiments in different conditions would be beneficial to determining if cell segregation will occur in this model *ex vivo*. Chick neural progenitor cells present a few more complications. While we were able to maintain these cells in

culture, we were unable to assess the ability of these cells to segregate since the cells were unlabeled. Because a labeling strategy would have to be performed *ex vivo*, this would require a FLOW sorting strategy, to distinguish cells from different rhombomeres, and a much larger number of cells.

Mouse derived intestinal organoids also represent an important *in vivo* boundary system. These organoids are easy to generate and propagate continually in culture which would be very beneficial for mechanistic studies. In order to examine EPH/EPHRIN segregation using this system, further analysis of EPH and EPHRIN expression would need to be performed in organoids. Additionally, to utilize many of the biophysical assays utilized in Chapter 3, troubleshooting would be necessary to adapt these assays to a smaller cell size. It is very interesting that generating organoids from *EfnB1^{Δ/+}* mice generates some organoids that express EPHRIN-B1 and others with no EPHRIN-B1 expression. Why some organoids completely lack EPHRIN-B1 expression is an interesting question for future inquiry.

iPSC derived neural crest cells would be a fascinating system in which to study EPH/EPHRIN driven cell segregation. Directional migration of NCCs in segmental migratory streams, followed by their entry into the branchial arches, termination of migration and differentiation, has been well studied providing excellent background literature for this system. Utilizing patient derived iPSC lines would also provide fascinating insights into the dynamics of NCC migration and segregation in heterozygous patients. Due to the variability in differentiations we were unable to examine the ability of these iPSC derived NCCs to undergo segregation in culture. Further troubleshooting of the differentiation protocol, or use of different iPSC lines may be necessary in order to establish this as a viable system for mechanistic investigation.

Lastly, while U251 cells undergo robust segregation when mixed with various HEK293 cell lines, thus appearing very promising as an additional system in which to study cell segregation, this system does not present the same advantages over use of HEK293 cells that either an *in vivo* or primary cell culture system would. In these segregation experiments HEK293 cells are still

overexpressing EPHB2, and while WT HEK293 cells also undergo segregation when mixed with U251 cells, we are still examining HEK293 cells in this system. It would be more ideal to create a U251 cell only system, however this would rely on determining which EPHs and EPHRINs are driving segregation in this system, and overexpressing or knockdown of at least one EPH or EPHRIN to achieve segregation between U251 cells. While it would still be beneficial to have an additional cell type in which to examine mechanisms of EPH/ EPHRIN cell segregation, endogenous EPH and EPHRIN expression would be beneficial.

While many of these systems present potential for examining EPH/EPHRIN driven cell segregation on a mechanistic level, further investigation is necessary to determine the most viable and beneficial system for this purpose.

Materials and Methods

Mouse lines

All mice were maintained on a congenic C57BL/6J genetic background. Krox20^{cre}, MGI: 1931056, Rosa26^{mTmG}, MGI: 3716464, *Efnb1lox*, MGI: 3039289 (Davy et al., 2004), Actin-cre^{Tg}, MGI: 2176050 (Lewandoski and Martin, 1997), Lgr5^{DTR-GFP/+}, MGI: 5294798 (Tian et al., 2011).

hiPSC generation and characterization Generation of hiPSC lines and characterization are described in detail in Niethamer et al. 2017.

Mouse Rhombomere dissection

Embryos were collected at E9.25. GFP Fluorescence was used to identify rhombomere 3 to rhombomere 5 (R3-R5) (Fig. 4.1A). R3 to R5 were dissected as single piece of tissue and taken to cell culture for dissociation and culture.

Chick Rhombomere dissection

Fertilized chicken eggs were incubated at 37.5°C in a humidified chamber until they reached embryonic stages HH11-13 (approximately 40 hours). Neural tubes were isolated by removing the embryo from the egg, washing in PBS and removing surrounding tissue through mechanical dissection with sharpened tungsten needles. Rhombomere 1 through rhombomere 5 (R1-R5) were isolated using the characteristic landmarks of the developing neural tube by cutting just below the midbrain- hindbrain boundary and just above the auditory vesicle (Fig. 4.1E)

Mouse neural progenitor cell culture

Once R3-R5 were dissected cells were dissociated using TrypLE Select (Life Technologies) by being incubated at 37°C and pipetting periodically to break up tissue, until all large pieces of tissue had been dissociated. Media was then added to inactivate TrypLE. Cells were spun down and resuspended in 50uL media to remove TrypLE. Cells were cultured either as plated cells or in hanging drops in N2B27 media; Neurobasal media and Advanced DMEM/F12 supplemented with Pen/Strep, GlutaMAX, N2 supplement, B27 supplement without vitamin A, BSA, and FGF2. For plated culture cells from one embryo were plated into 1 well of 24 well plate coated with fibronectin in N2B27 media. Cells were split on day 4 by dissociating cells with 0.25% Trypsin for 5 minutes at 37C and replating into fibronectin coated wells.

Chick neural progenitor cell culture

Once the rhombomeres were isolated tissue was placed in N2B27 media (described above). Cells were then incubated in TrypLE Select (Life Technologies) at 37°C and pipetting periodically to break up tissue, until all large pieces of tissue had been dissociated. Media was then added to inactivate TrypLE. Cells were resuspended and plated as hanging drops.

Mouse intestinal organoid establishment and culture

Small intestinal crypts were isolated from adult mice following Klein lab protocol. Approximately 10cm of the proximal small intestine was dissected and luminal contents flushed using cold CMF-PBS. The intestine was then opened and villi removed by scraping intestine with a glass coverslip. The intestine was then cut into 2-4cm pieces, washed with CMF-PBS. CMF-PBS was removed and intestine was then incubated at 4°C in crypt chelating buffer (CMF-PBS+ 5mM EDTA). Chelating buffer was then removed and replaced with PBS and tube was shaken by hand. Supernatant was then filtered through 100uM filter to obtain crypts. Crypts are then plated at approximately 500 crypts per 50uL drop of Matrigel. Matrigel containing crypts is then incubated for 10 minutes at 37°C before adding media. Organoids are cultured in medium supplemented with human recombinant EGF, human recombinant Noggin and R-Spondin. Organoids were grown in 24-well plastic plates, and passaged approximately every 5 days.

hiPSCs culture

hiPSCs were cultured in feeder-free conditions in E8-Flex medium (ThermoFisher Scientific) on dishes coated with hESC-qualified Matrigel (Corning). When passaged E8-Flex media was supplemented with ROCK inhibitor, Y27632, to reduce cell death, and then switched to E8-Flex media 24 hours after passaging.

hNCC cell differentiation and culture

hNCC differentiations from hiPSCs were performed using a modified protocol from Barber et al. 2019. To initiate differentiation hiPSCs were grown to 80-90% confluency, and media was changed to E6 media supplemented with 1ng/mL BMP4, 10uM SB431542, and 600nM CHIR 99021 (Fig 4.3A) (day 0). On day 2 of differentiation media was changed to E6 media supplemented with 10uM SB431542, and 1.5uM CHIR 99021 (Fig. 4.3A). Cells remain in this media from day 2 through day 12 with media changed every other day (Fig. 4.3A). On day 12

cells are passaged into spheroid culture by first rinsing wells with PBS, followed by incubation in Accutase for 30 minutes at 37°C. Spheroid media (Neurobasal media supplemented with 10uL/mL N2 supplement, 20uL/mL B27 Supplement, 10uL/mL GlutaGo, 10uL/mL non-essential amino acids (NEAA), 10ng/mL FGF2, and 3uM CHIR 99021 (Fig. 4.3A)) is added to each well and cells are pipetted vigorously to remove from plate. Cells are then centrifuged at 1200RPM for 1 minute and cell pellet is resuspended and plated into ultra low-attachment plates. hNCCs are maintained in spheroid media and passaged every four days.

U251, U87, and HEK293 cell culture

All cells were cultured at 37°C with 5% CO₂. U251, U251-pMXI, and U87 cells were cultured in H21 DME supplemented with 10% fetal bovine serum, and antibiotics. HEK293 and MDCK cells were cultured in DMEM supplemented with 10% fetal bovine serum, glutamine, and antibiotics.

Cell segregation assay

Cell segregation assays were performed as previously described (O'Neill et al., 2016; Poliakov et al., 2008). Each cell type was aliquoted into and resuspended in medium to a cell density of 150,000/mL, with various inhibitors and plated in 24-well plates coated with 10ug/mL fibronectin (Sigma-Aldrich). For mixing experiments; wildtype HEK293 cells labeled with cell tracker dye (Thermo-Fisher), HEK293 expressing LifeAct-BFP, HEK293 cells expressing GFP, LifeAct-mCherry and expressing high levels of EPHB2, or HEK293 cells expressing LifeAct-mCherry and high levels of EPHRIN-B1 were mixed with U251 cells, U251-pMXI, or U87 cells. Cells are mixed in a 1:1 ratio. Inhibitors added to cells at time of mixing. Cells were then cultured for 24 hours and imaged to assess the degree of segregation.

Hanging drop assay

Cells were resuspended in N2B27 media. Number of cells in cell suspension was not counted due to small amounts of tissue collected for trial experiments. 10uL of cell suspension was plated as drops on the lid of a 10cm tissue culture dish. Media was added to bottom of tissue culture dish to maintain humidity in culture.

Cell: cell contact angle assay

Cell: cell contact angle assay was performed similarly to previously described in Cerchiari et al. Once rhombomeres were dissociated to single cell suspension cells were centrifuged into agarose microwells at 200 xg for 6 minutes. Excess cells were then washed away with media and the remaining cells confined in wells were incubated for 4 to 28 hours and imaged.

FLOW analysis

Cells were collected at day 12 using passaging protocol described above. Once cells were collected and centrifuged cells were fixed in 4%PFA for 30 minutes at room temperature. The cell pellet was then washed with PBS three times to remove PFA. Cells were then resuspended in PBS with 2% Donkey serum and incubated at room temperature for 30 minutes. The CD49d PE-conjugated antibody (R&D systems) was diluted (1:200) in PBS with 2% Donkey serum. Cells were incubated in antibody solution overnight at 4C. Three five minute washed in PBS were performed to remove excess antibody and cell suspension was transferred into a FACs tube by pipetting through a 35 µm cell strainer. Cells were sorted using a BD FACS Aria II.

Western blot

Cells were lysed in NP-40 lysis buffer (20mM Tris-HCl, 137mM NaCl, 10% glycerol, 1%NP-40, 2mM EDTA) supplemented with 1mM dithiothreitol (Sigma) and the following protease and phosphatase inhibitors: aprotinin, 2 µg/mL; leupeptin, 5 µg/mL; pepstatin, 1 µg/mL; PMSF, 1

mM; NaF, 10 mM; and NaVO₄, 1 mM. Lysates were cleared by centrifugation at 16,000 x g for 10 minutes at 4°C prior to use. Protein quantification was performed using the Pierce BCA Protein Assay Kit (Thermo Fisher Scientific). Immunoblotting was performed according to standard procedures using Odyssey® TBS blocking buffer (LI-COR) for blocking and dilution of antibodies and TBS with 0.1% Tween-20 for washing. Imaging of immunoblots was performed using an Odyssey® Infrared Imaging System (LI-COR), and analysis and quantification was carried out using Image Studio™ software (LI-COR).

Organoid immunofluorescence

For immunofluorescence, organoids were fixed in 4% PFA in PBS for 1 hr before blocking in 10% Donkey serum and 0.1% Triton X-100. Primary antibody was incubated overnight at four degrees and secondary antibody was incubated for >2 hr at RT. Reagents used for immunofluorescence were as follows: EPHRIN-B1 antibody (R&D), EPHB2 antibody (R&D), Lysosyme antibody, E-cadherin antibody, GFP antibody (Aves Labs).

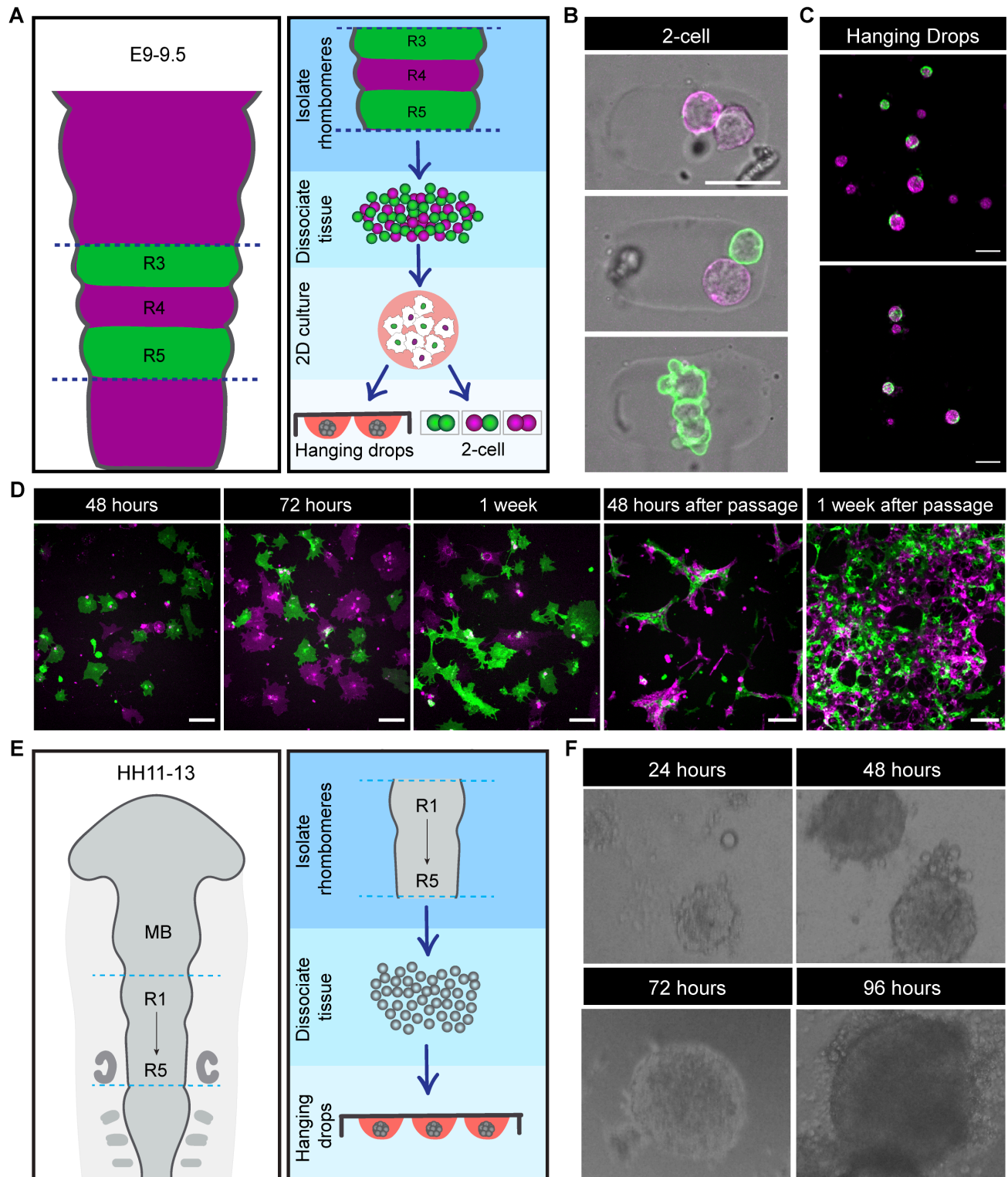


Figure 4.1. Neural progenitor cell dissection and culture. (A) Schematic of *Krox20^{cre}; Rosa26^{mtmg}* neural ectoderm at E9-9.5. Rhombomeres segment the neural ectoderm in the developing mouse embryo. *Krox20* is expressed in rhombomeres (R) 3 and 5, and therefore express GFP in *Krox20^{cre}; Rosa26^{mtmg}* embryos. Dissection of rhombomeres was performed using

GFP as a guide to isolate rhombomeres 3 through 5. These cells were then dissociated for culture and use in hanging drops or cell:cell contact angle assay. **(B)** Example images of mouse neural progenitor cells plated for 2-cell assay in agarose microwells. Scale bars, 20 μ m. **(C)** Example images of mouse neural progenitor cells in hanging drop culture. Scale bar, 100 μ m. **(D)** Example images of mouse neural progenitor cells in 2D culture over time. After passage cells adopt an altered morphology that is less spread and more neuronal in appearance. Scale bar, 100 μ m. **(E)** Schematic of chick embryo at HH11-13. Rhombomeres (R) 1 through 5 were isolated using characteristic landmarks of the developing neural tube, cutting just below the midbrain (MB)-hindbrain boundary and at the auditory vesicles. These cells were then dissociated and cultured as hanging drops. **(F)** Example images of hanging drops over time. Large hanging drops formed and were cultured for multiple days.

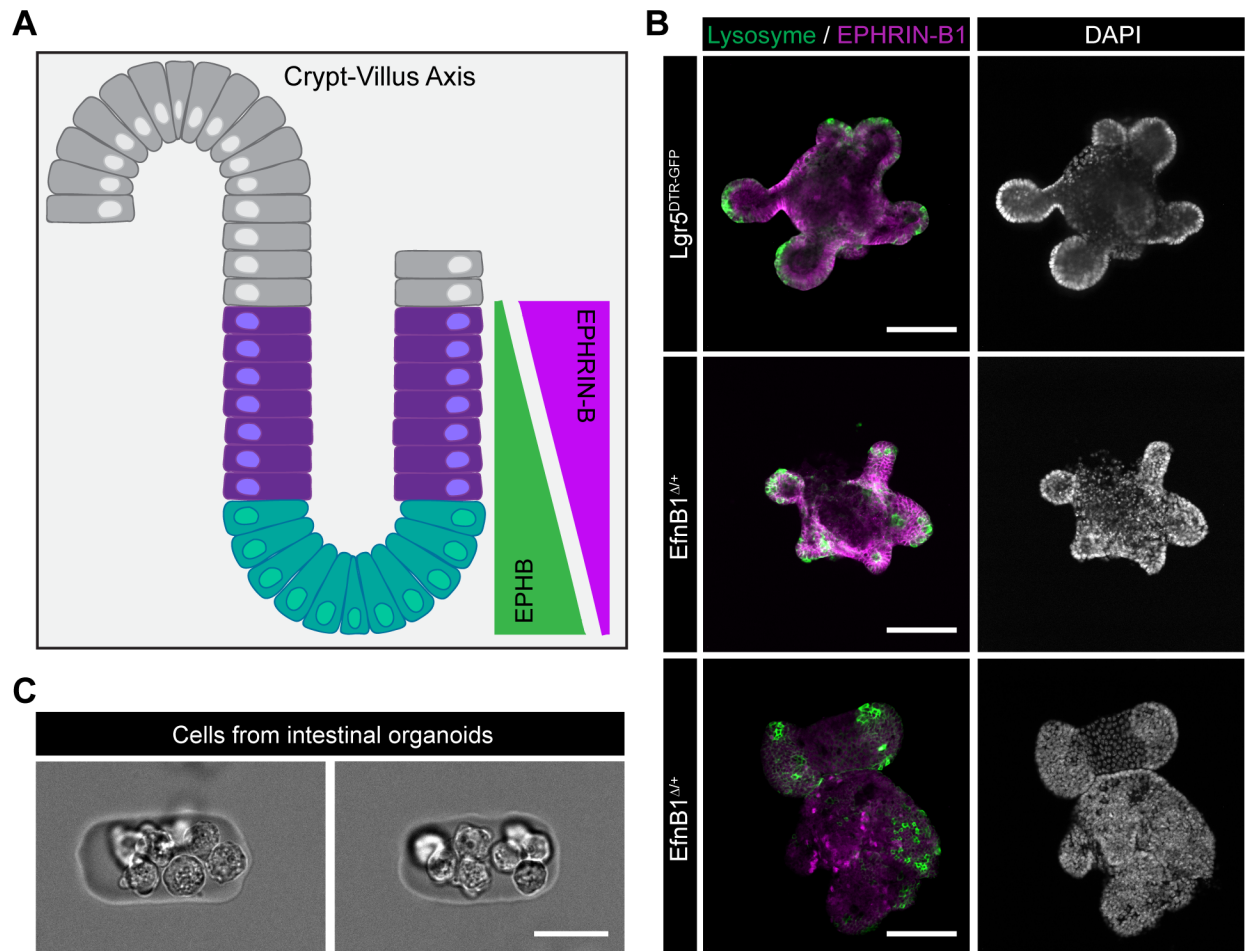
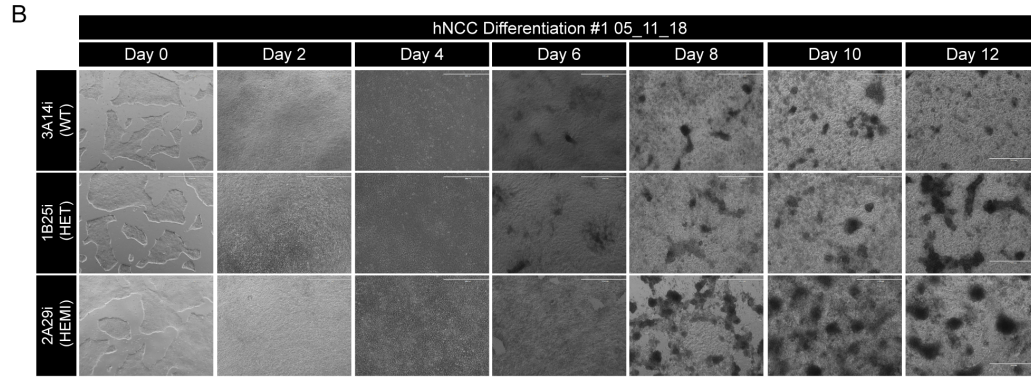
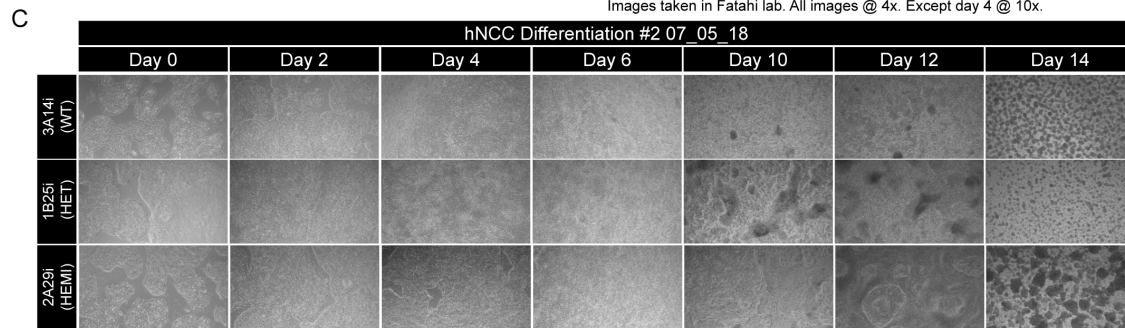


Figure 4.2. Intestinal organoid culture. (A) Schematic of EPH/EPHRIN expression along the crypt-villus axis in the intestine. EPHBs are expressed strongly at the crypt base while EPHRINs are expressed more strongly outside of the crypt base and up the villus axis, maintaining a boundary between proliferative and differentiating cells in the intestine. (B) Immunostaining of intestinal organoids for EPHRIN-B1 (magenta) and Lysosyme (green). In *Lgr5*^{DTR-GFP} wildtype organoids lysosyme is restricted to the crypt base. Some *EFNB1*^{Δ/+} express EPHRIN-B1, while others show no EPHRIN-B1 expression. In *EFNB1*^{Δ/+} organoids expressing EPHRIN-B1 lysosyme is restricted to crypts, however in *EFNB1*^{Δ/+} organoids without EPHRIN-B1 expression lysosyme is seen throughout the organoid. Scale bar, 50μm. (C) Example images of cells dissociated from intestinal organoids plated for 2-cell assay in agarose microwells. Scale bar, 20μm.

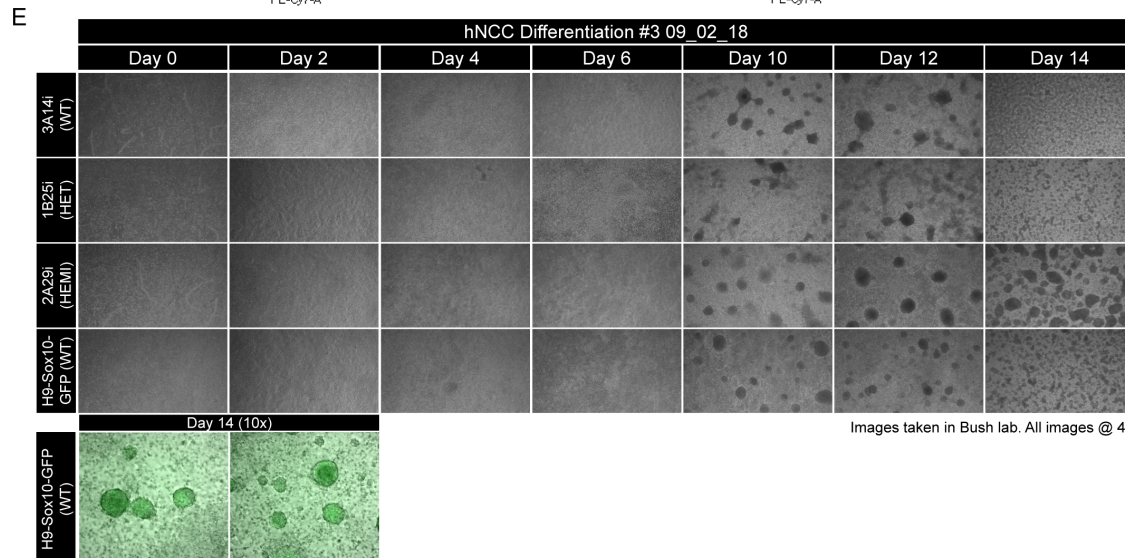
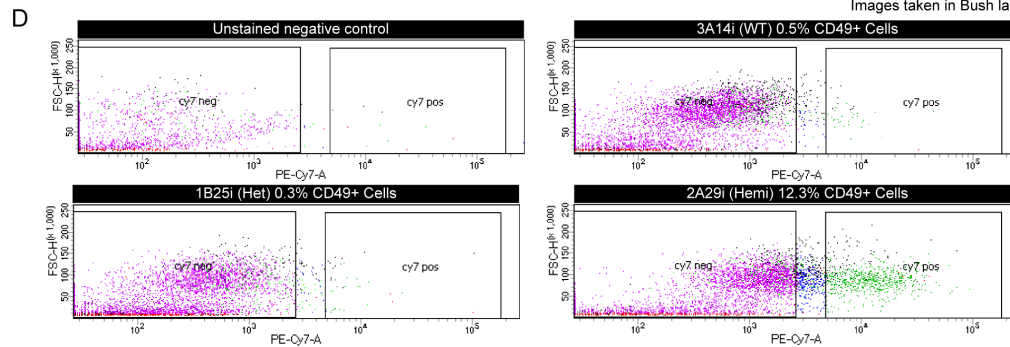
A	Day 0 80-90% confluent	Day 2	Day 4	Day 6	Day 8	Day 10	Day 12 Passage to spheres	Day 14-end Sphereoid culture
	E6 Media						Neurobasal Media	
	+BMP4+ SB431542 + CHIR99021			SB431542 + CHIR99021			+N2+ B27+ CHIR99021+ FGF2 +Glutagra+ NEAA	



Images taken in Fatahi lab. All images @ 4x. Except day 4 @ 10x.



Images taken in Bush lab. All images @ 4x.



Images taken in Bush lab. All images @ 4x.

Figure 4.3. Neural crest cell differentiations from patient derived iPSCs. (A) Schematic of differentiation protocol for human iPSC derived neural crest cells (hNCCs). (B) hNCC differentiation #1 using 3A14i (WT), 1B25i (HET), 2A25i (HEMI) iPSC lines. At day 12 of differentiation a lot of cell death was observed and differentiation was terminated. (C) hNCC differentiation #2 using 3A14i (WT), 1B25i (HET), 2A25i (HEMI) iPSC lines. When passaged to spheres very few spheres formed. (D) FLOW analysis of differentiation #2 using CD49d as a marker of NCC differentiation. Differentiation efficiency was very low. (E) hNCC differentiation #3 using 3A14i (WT), 1B25i (HET), 2A25i (HEMI) and H9-Sox10-GFP (WT) iPSC lines. When passaged to spheres very few spheres formed.

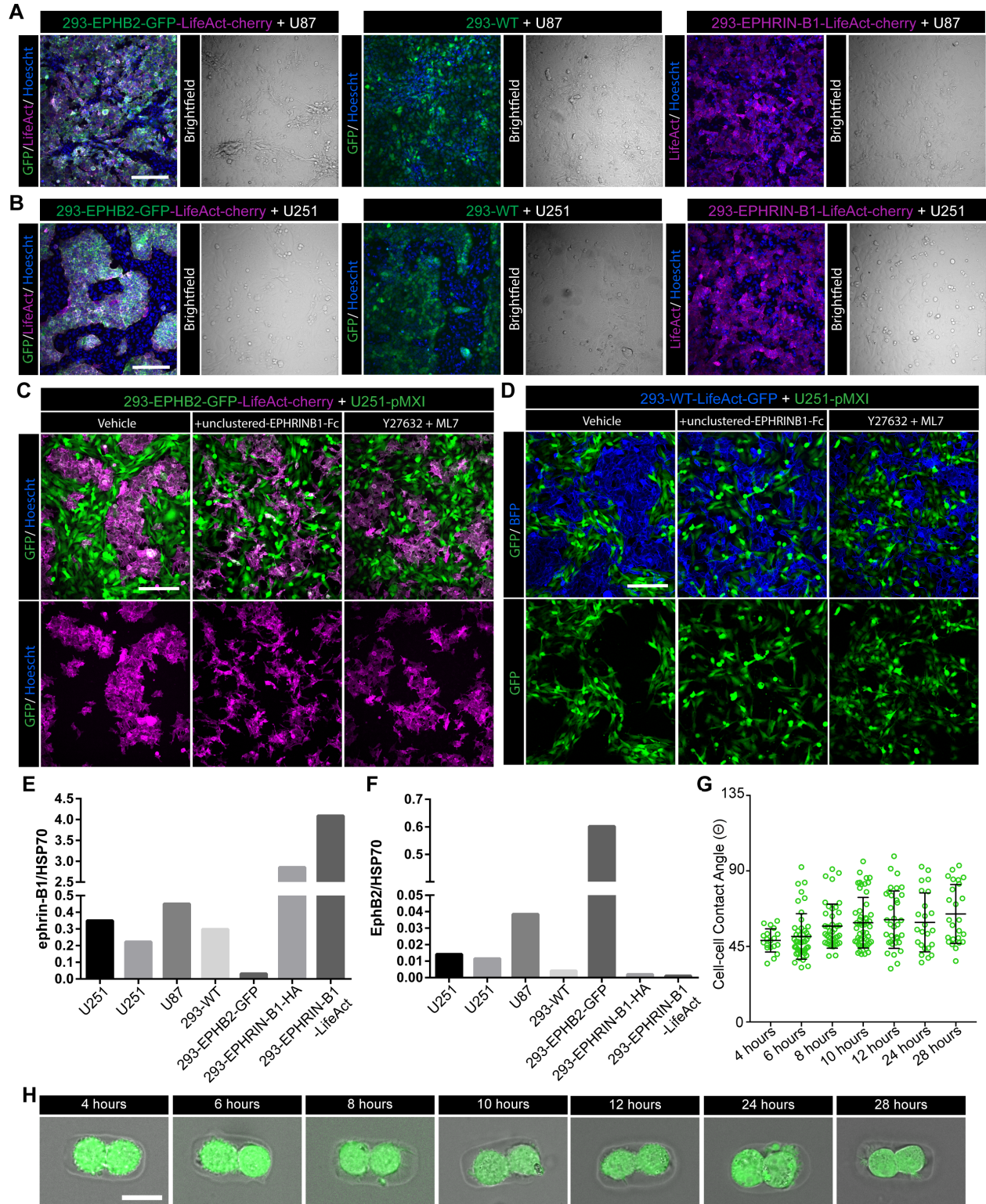


Figure 4.4. Cell segregation in U251 or U87 cells mixed with HEK293 cells. (A) Cell segregation in mixed U87 and HEK293 cell culture. Due to the morphology of U87 cells segregation is difficult to determine. Scale bars, 200 μ m. **(B)** Cell segregation in mixed U251 and HEK293 cell culture. U251 cells undergo robust segregation when mixed with 293-EPHB2-GFP-

LifeAct-cherry (green) or 293-WT (green) cells but no segregation is observed in U252 + 293-EPHRIN-B1-LifeAct-cherry cultures. Scale bars, 200 μ m. **(C)** Cell segregation between U251-pMXI (green) cells and 293-EPHB2-GFP-LifeAct-cherry (magenta) cells. Segregation is somewhat disrupted by the addition of unclustered-EPHRIN-B1-Fc, but it is difficult to determine if contractility inhibitors (Y27632+ML7) disrupt segregation. Scale bars, 200 μ m. **(D)** Cell segregation between U251-pMXI (green) cells and 293-WT (blue) cells. Segregation is somewhat disrupted by the addition of unclustered-EPHRIN-B1-Fc and contractility inhibitors (Y27632+ML7). Scale bars, 200 μ m. **(E)** Expression of EPHRIN-B1 in various cell lines used for mixing experiments. Expression levels normalized to HSP70. **(F)** Expression of EPHB2 in various cell lines used for mixing experiments. Expression levels normalized to HSP70. **(G)** Quantification of cell:cell contact angles in time course beginning 4 hours after plating. U251 cell pairs show a low contact angle overtime that stabilizes around hours 10-12. **(H)** Example images of cells U251-pMXI cells plated for 2-cell assay in agarose microwells. Scale bar, 20 μ m.

CHAPTER 5.
Conclusions and Future Directions

This work explores the cellular mechanisms by which EPH/ EPHRIN signaling directs cellular self-organization during morphogenesis. It has been understood for some time that EPH/EPHRIN signaling is an important regulator of cell segregation and boundary formation in development, including between the germ layers during gastrulation, rhombomeres, somites, cranial sutures, and intestinal crypts (Calzolari et al., 2014; Watanabe et al., 2009; Cooke et al., 2001; Battle et al., 2002; Merrill et al., 2006; Rohani et al., 2011; Ting et al., 2009). While several hypotheses have been proposed for how EPH/EPHRIN signaling drives segregation and boundary formation between cells, the cellular mechanisms by which segregation occurs remain unclear. Here we specifically investigate how EPH/EPHRIN regulates the biophysical properties of the cell and cell:cell contacts to drive cellular self-organization.

Using the well-established HEK293 EPHB2/EPHRIN-B1 model of cell segregation we have demonstrated that EPH/EPHRIN signaling regulates cell contacts by modulating interfacial tension to drive cellular self-organization. The differential interfacial tension hypothesis predicts that cell will minimize high tension contacts to minimize overall tension of the system (Brodland and Chen, 2000, Maître et al., 2012). Our data indicate that EPH/EPHRIN signaling increases tension at heterotypic cell:cell contacts by modulating actomyosin contractility. This high tension at the EPH/EPHRIN interface thus minimizes heterotypic cell contacts, and favors homotypic contacts, giving rise to cell segregation. We also demonstrate a secondary effect of cell:medium tension in contributing to self-organization by increasing EPHB2 homotypic contacts. Consistent with our discoveries *in vitro* we see that cell segregation is highly disrupted *in vivo* when actomyosin contractility is disrupted. Together this data suggests a novel model for EPH/EPHRIN driven cell segregation in which both cell:cell and cell:medium tension, driven by actomyosin contractility drive cellular organization and boundary formation. This greatly enhances our knowledge of the role of EPH/EPHRIN signaling in cellular self-organization and boundary formation.

Many outstanding questions remain regarding the role of EPH/EPHRIN signaling in boundary formation and morphogenesis. It remains unclear if EPH/EPHRIN boundary formation occurs by the same mechanisms of action in different developmental contexts. There is data to support that actomyosin contractility is an important regulator of boundary formation and maintenance in rhomeres and germ layer separation (Calzolari et al., 2014; Krieg et al., 2008; Maître et al., 2012). Along with the *in vivo* data presented here thus suggests the possibility that EPH/EPHRIN regulation of cell contacts through increased cortical tension may be a more generalizable mechanism. We began to address this question through attempting to develop additional culture models of EPH/EPHRIN cell segregation. While several of these models show promise, further trouble shooting is necessary before mechanistic studies could be performed.

Our HEK293 cell system relies on segregation between EPHB2 and EPHRIN-B1. Segregation in the craniofacial mesenchyme in the *EfnB1* mutant mouse model is driven between EPHRIN-B1 and EPHB2 and EPHB3 because segregation is lost or greatly diminished when these receptors are removed from *Efnb1*^{+/-} embryos. However, there are many different EPH/EPHRIN signaling pairs, and several of these are known to be critical at different developmental boundaries. Additional culture systems to examine the mechanisms of EPH/EPHRIN cell segregation will not only elucidate the mechanisms of segregation in different contexts, but will also aid in determining if all EPH/EPHRIN signaling pairs drive boundary formation by the same mechanisms of action.

While our work here demonstrates an important role for EPH/EPHRIN signaling in regulating actomyosin contractility to drive cell segregation the signaling downstream of the EPH/EPHRIN signaling event remains entirely unclear. First, it will be important to determine if cell segregation in the HEK293 model is dependent on forward, reverse or bi-directional signaling. While earlier studies in the mouse neuroepithelium suggest that segregation is driven by forward signaling, it has not been established if this is true in the HEK293 cell culture model, or other potential models of cell segregation (O'Neill et al., 2016). Our AFM data shows an increase in

cortical stiffness of both EPHB2 and EPHRIN-B1 cells, suggesting a contribution of both forward and reverse signaling to EPH/EPHRIN cell segregation in culture. Once the directionality of signaling is established what downstream signaling is occurring to regulate actomyosin contractility is another critical question to understand EPH/EPHRIN driven cell segregation.

EPH/EPHRIN driven cell segregation and boundary formation is critical to proper embryo morphogenesis. Understanding this process at a mechanistic level greatly enhances our knowledge of morphogenesis and understanding of how cellular organization occurs in development. Future applications of this research will further this improved understanding and will elucidate key mechanisms that regulate the intricate process of embryo development.

APPENDIX 1.

Additional data

Results

Cellular collapse upon addition of EPHRIN-B1-Fc

Exogenous EPHRIN-B1-Fc can be utilized to block signaling in the unclustered form or to inducing signaling when clustered. We applied clustered-EPHRIN-B1-Fc to our EPHB2-GFP cells and imaged the resulting cellular collapse behavior (Fig. A1.1A). When EPHB2 cells collapse the cellular processes retract and cells round up dramatically (Fig. A1.1A). They also cluster together into patches (Fig. A1.1A). Collapse occurs quickly and is maintained for some time. We wanted to know if addition of ROCK inhibitor to these cultures would prevent collapse from occurring. When clustered-EPHRIN-B1-Fc is added to EPHB2 cells in the presence of ROCK inhibitor the cells do not appear to collapse or change morphology (Fig. A1.1A).

We are able to quantify this collapse behavior by measuring the contact of a cell with the substrate or ECM on which they are plated before and after the addition of clustered-EPHRIN-B1-Fc (Fig. A1.1B). By taking high resolution z-stack images of cells we are able to visualize and thus measure the cell:ECM contact (Fig. A1.1B, C). In the presence of clustered-EPHRIN-B1-Fc EPHB2 cells round up and reduce their contact with the ECM, while EPHB2 cells alone are very spread across the ECM and have high contact with the ECM (Fig. A1.1 C, D). As a control we also performed this experiment using EPHRINB1-LifeAct-mCherry cells which maintained contact with the ECM and had no response to the addition of clustered-EPHRIN-B1-Fc (Fig. A1.1C, D).

Additional cell:cell contact angle conditions

We measured various conditions of cell:cell contact. Cell contact between WT HEK293 cells was used to determine at what time point to measure cell:cell contact angles. WT contacts stabilize at around $\theta = 70$ (Fig. A1.2A). Additionally, mixing of WT cells and EPHRIN-B1 expressing cells was performed as a control, and there are no differences between homotypic and heterotypic cell pairs in this condition (Fig. A1.2A).

We also measured contact angles with contractility inhibitors alone, rather than in combination (Fig. 3.3B). The addition of Y27632 or ML7 alone is sufficient to decrease interfacial tension between heterotypic cell pairs, and greatly diminished the difference between EPHB2:EPHRIN-B1 heterotypic and homotypic cell pairs (Fig. A1.2B).

Additional perturbations of signaling were performed by adding clustered-EPHRIN-B1-Fc to various cell:cell contact conditions. When added to EPHB2 cells alone, or mixed EPHB2:EPHRIN-B1 wells there was no differences observed from these conditions without clustered-EPHRIN-B1-Fc (Fig. A1.2C). When added to EPHB2:WT mixed wells clustered-EPHRIN-B1-Fc results in a reduction of heterotypic contact such that there is a difference between WT:WT or EPHB2:EPHB2 homotypic contacts and WT: EPHB2 heterotypic contacts. This may be due to increased cortical tension in the EPHB2 expressing cells. Unclustered-EPHRIN-B1-Fc was also added in low Ca^{2+} media conditions. Like blebbistatin the addition of unclustered-EPHRIN-B1-Fc to EPHB2: EPHRIN-B1 mixed wells greatly reduced EPHB2 homotypic contacts (Fig. A1.2E). Interestingly, close EPHB2 homotypic contacts were retained in WT and EPHB2 mixed wells as well as EPHB2 cells alone in low Ca^{2+} media (Fig. A1.2E). In EPHB2 cells alone contact was also diminished by the addition of unclustered-EPHRIN-B1-Fc (Fig. A1.2E). This suggests that the maintenance of close EPHB2 homotypic contact in low Ca^{2+} media conditions may be dependent on EPH: EPHRIN signaling, however not all data is consistent.

To further determine how interfacial tension differentials between homotypic and heterotypic contacts drive cellular organization, we designed a triplet cell contact angle assay. We fabricated larger 30 μ m by 90 μ m size microwells to fit 3 cells and mixed 293-EPHB2-GFP and 293-EPHRIN-B1-LifeAct-mCherry cells to give rise to 6 different configurations of cell contact. Interestingly when an EPHB2:EPHB2 cell pair is also in contact with an EPHRIN-B1 expressing cell (EPHB2:EPHB2:EPHRIN-B1) the EPHB2:EPHB2 homotypic contact is closer than when in contact with a third EPHB2 expressing cell, however this difference is not statistically significant

(Fig. A1.2D). No increase in cell contact was observed between two EPHRIN-B1 cells in contact with an EPHB2 cell, consistent with the increased density of EPHB2 cells but not EPHRIN-B1 cells in segregation assays. This data also suggests that the increase in cortical actomyosin tension in response to heterotypic cell contact occurs locally within the cell, while the other side has a cortical tension that relatively favors is compatible with making close, stable, contacts.

Additional cell segregation assay conditions

We performed cell segregation assays in many different conditions to inhibit actomyosin contractility. We also tried to enhance contractility in our system using calyculin A, a myosin light chain phosphatase inhibitor, to prevent the dephosphorylation, and thus inactivation, of myosin. Upon the addition of calyculin the cells rapidly rounded up and lifted off the plate (Fig. A1.3A). There was also a lot of cell death observed (Fig. A1.3A). Due to this response we were unable to analyze these results.

We also tried to disrupt cadherin mediated adhesion in a more specific manner than low Ca^{2+} media. We did this by using an N-cadherin blocking antibody (Theveneau et al., 2010) to block N-cadherin cell:cell adhesion from occurring. Because cell segregation still occurs in mixed EPHB2/ EPHRIN-B1 cultures even in the absence of cadherin mediated adhesion it was difficult to determine if the antibody treatment had any effect of cell adhesion (Fig. A1.3A). Seeing if this N-cadherin antibody treatment diminished contact between WT cells in the cell:cell contact angle assay may allow verification of the functionality of the N-cadherin antibody in blocking cell adhesion. It is worth noting that while in Low Ca^{2+} conditions the cells are more spaced out without tight contact between neighboring cells, cells in regular HEK293 media with N-cadherin AB are indistinguishable from cells in HEK293 media with no inhibitors.

To investigate if forward or reverse signaling drives cell segregation in HEK293 cells we generated signaling mutant cell lines. We first re-generated a wildtype (WT) EPHB2 cell line, labeled with LifeAct-BFP. These cells did not segregate when mixed with EPHB2-GFP cells but

did undergo segregation when mixed with EPHRIN-B1-LifeAct-mCherry cells (Fig. A1.3B). We additionally generated cells labeled with LifeAct-BFP and a kinase dead (KD) EPHB2. This kinase dead EPHB2 should not have any kinase dependent forward signaling (Taylor et al., 2017). These kinase dead cells segregate when mixed with EPHRIN-B1-LifeAct-mCherry cells (Fig. A1.3B). This indicates that either kinase dependent forward signaling is not driving cell segregation in this model or kinase dependent forward signaling has not been abolished. We performed immunoprecipitation for phosphorylated Tyrosine (pTyr), as a readout of active signaling, followed by western blot for EPHB2 (Fig. A1.3C). These westerns showed a large amount of phosphorylated EPHB2 indicating that kinase dependent signaling was still occurring (Fig. A1.3C). We also generated EPHRIN-B1-6F Δ V-LifeAct-BFP cells. EPHRIN-B1-6F Δ V cells lack reverse signaling due to mutations of the six phosphorylatable intracellular tyrosines and deletion of the C-terminal valine, which is required for binding PDZ domain proteins (Bush and Soriano, 2009). When mixed with EPHB2-GFP cells these EPHRIN-B1-6F Δ V-LifeAct-BFP still undergo segregation. While we confirmed the presence of the mutations through sequencing we did not functionally confirm that all phosphorylation was lost. Based on these cell lines we are unable to determine the requirement for forward, reverse, or bi-directional signaling in the HEK293 cell culture model of cell segregation.

Segregation hierarchy in microwells in low Ca²⁺ media

We established using circular microwells that high interfacial tension at the EPH: EPHRIN cell: cell interface results in segregation in 3D into two populations that minimize their contact with one another, rather than organizing hierarchically (Fig. 3.1E). We also wanted to know the effect of contractility inhibitors on sorting in aggregates and if aggregates were able to form in low Ca²⁺ conditions. We looked at EPHB2-GFP+ EPHB2-GFP-LifeAct-cherry, our control, and EPHB2-GFP-LifeAct-mCherry+ EPHRIN-B1-LifeAct-mCherry, out sorted condition, aggregates in regular media and low Ca²⁺ media with and without blebbistatin. In regular media EPHB2 control

aggregates form very spherical compact aggregates (Fig. A1.4A). The addition of blebbistatin to this condition did not alter the ability of the aggregate to form or the appearance of the aggregate (Fig. A1.4A). EPHB2 control aggregates in low Ca^{2+} media appeared to have more sparse cell:cell contact and did not form a spherical compact aggregate, however upon the addition of blebbistatin in low Ca^{2+} media these aggregates were indistinguishable from those in regular media (Fig. A1.4A). In regular media EPHB2:EPHRIN-B1 segregated aggregates sort into two distinct populations so as to minimize heterotypic contact (Fig. 3.1E, and A1.4B). When blebbistatin is added to this condition the aggregates formed are very spherical and cells are no longer minimizing heterotypic contacts (Fig. A1.4B). EPHB2: EPHR-B1 segregated aggregates in low Ca^{2+} media appeared to have more sparse cell:cell contact and did not form a compact aggregate, however upon the addition of blebbistatin in low Ca^{2+} media these aggregates were quite compact and spherical (Fig. A1.4B). This is somewhat surprising since in our two cell assay we see that EPHB2 cells retain close contact in low Ca^{2+} media and that this close contact is lost upon addition of blebbistatin (Fig. 3.5D). It is unclear why blebbistatin would result in more compact aggregates in the absence of cadherin mediated adhesions.

CRISPRi in HEK293 cells

We wanted to determine the signaling downstream of EPH/EPHRIN signaling driving cell segregation. To do this we decided to utilize CRISPRi in our HEK293 cell system. CRISPRi utilizes a catalytically dead Cas9 protein (dCas9) to repress transcription rather than cleave the DNA. Because HEK293 cells are aneuploid the CRISPRi approach allows gene knockdown without having to target multiple copies of every gene. The dCas9 plasmid contains the KRAB protein, a zeomycin resistance cassette, and the fluorescent protein, mKate2 (Fig. A1.5A). We generate stable dCas9 expressing HEK293 cells that expressed either EPHB2 (EPHB2-dCas9-KRAB-mKate2) or EPHRIN-B1 (EPHRIN-B1-dCas9-KRAB-mKate2) so that we could knockdown genes in either cell type during a mixing experiment. Once stable cell lines were generated

sgRNAs were introduced into cells through transfection of plasmid-783 containing the guide sequence in place of the stuffer sequence (Fig. A1.4B). We designed guides for both EPHB2 and EPHRIN-B1 to determine if we could knockdown their expression and prevent segregation (Fig. A1.5C). We did not see any disruption of segregation using these EPHB2 and EPHRIN-B1 guides in our EPHB2-dCas9-KRAB-mKate2 or EPHRIN-B1-dCas9-KRAB-mKate2 (Fig. A1.5D, E). We do see mKate2 expression in both EPHB2-dCas9-KRAB-mKate2-line2 and EPHRIN-B1-dCas9-KRAB-mKate2-line6 cell lines (Fig. A1.5D, E), indicating our dCas9 plasmid should be expressed, however we cannot be sure based on this the levels at which dCas9 is being expressed or if the protein is functional. Our guides may also not be efficiently targeting the dCas9 protein for knockdown, especially since these proteins are overexpressed in these cell lines. Additional guides for CDH2, MYH9, MYH10, and GFP were designed but not tested (Table A1.1).

Materials and Methods

HEK293 cell culture

See Chapter 3 Materials and Methods.

Cell segregation assay

See Chapter 3 Materials and Methods.

Live imaging of cellular collapse

For live imaging of cellular collapse, EPHB2-GFP cells were plated in a glass bottomed imaging dish coated with 10µg/ml fibronectin (Sigma-Aldrich) to a final cell density of 400,000/mL. Plating performed in the presence of 20µM Y27632 and or vehicle (0.25% DMSO). Live imaging began 1 hour after plating and was performed at 37°C. 15 mM HEPES buffer was added and the dish sealed to buffer CO₂. Clustered-EPHRIN-B1-Fc was added. Confocal stacks (3 × 2 µm) were acquired using an Axio Observer.Z1 spinning disk confocal microscope (ZEISS) at 37°C, a 40× water LD C-Apochromat objective lens (numerical aperture 1.1; ZEISS), and an AxioCam 506 camera (ZEISS). Zen software was used to acquire images, generate maximum intensity projections. Images were then obtained from select live imaging timepoints.

Fabrication of agarose microwells, cell:cell contact angle and circular microwell hierarchy assays.

See Chapter 3 Materials and Methods.

Cell: ECM contact angle assays.

Cells were plated in a glass bottomed imaging dish coated with 10µg/ml fibronectin (Sigma-Aldrich) to a final cell density of 400,000/mL. Fibronectin was labeled using NHS-ester tagged to Alexa-647 at 0.4% final concentration. Cells allowed to plate down for 1 hour. Clustered-EPHRIN-B1-Fc added 10 minutes prior to imaging. Imaging was performed using 63x oil objective, taking

0.24 μ m sections to obtain good z-resolution. The contact angle at the cell-substrate interface was estimated by analyzing 63X confocal Z- stacks FIJI. For all cell-substrate contact angle assays, we measure the contact angle as the angle formed between the substrate and the body of the cell (Fig. A1.1B).

Inhibitors

Inhibitors used in cell segregation assays and cell- cell contact angle assays were 2 μ g/ml unclustered EPHRIN-B1-Fc (R&D Systems), 2 μ g/ml clustered-EPHRIN-B1-Fc (R&D Systems), 100ng/mL Calyculin (Abcam), 20 μ M blebbistatin (Sigma-Aldrich), 20 μ M Y27632 (Cayman), 25 μ M ML7 (EMD Millipore), and 40 μ g/mL N-cadherin Antibody (Sigma-Aldrich).

Clustered-EPHRIN-B1-Fc was generated by combining EPHRIN-B1-Fc, donkey anti-human serum, and ddH₂O, rotating at 4°C for 90 minutes.

Generation of new cell lines.

Plasmid DNA is linearized overnight using restriction enzyme for restriction site that will not disrupt desired DNA insert. Linearized DNA run on gel and extracted using Qiagen Gel Extraction Kit, following Qiaquick Gel Extraction Kit protocol. DNA then introduced into cells through transfection using Lipofectamine 2000 (Invitrogen) following Lipofectamine 2000 protocol. Media is changed 24 hours follow transfection, and selection, using appropriate antibiotic, started 24 hours later. Cells are then maintained in selection media for one week, changing media every other day. Following one week of selection clonal dilution is performed, plating 100 μ L of 100 cells/mL cell solution into 96 well plate. Wells then screened for growth of single clonal colony.

Generation of EPHRIN-B1-6F Δ V signaling mutants.

EPHRIN-B1-6F Δ V signaling mutants were generated using site directed mutagenesis (SDM). Starting plasmid used was pcDNA3.1(+) efnb1-wt corrected. Site directed mutagenesis was performed using QuikChange Lightning Site-Directed Mutagenesis Kit. Three rounds of SDM were performed, first using efnb1_Tyr_Phe_1_2 F (ACGGACTACAGAGAACAACACTTCTGCCCC CACTTTGAGAAGGTGAG) and efnb1_Tyr_Phe_1_2 R (CTCACCTTCTCAAAGTGGGGGCAG AAGTTGTTCTCTGTAGTCCGT) primers, second using efnb1_Tyr_Phe_3_4_F (AGAAGGTGAGTGGGGACTTCGGGCATCCTGTCTTCATCGTCCAGG) and efnb1_Tyr_Phe_3_4_R (CCTGGACGATGAAGACAGGATGCCCGAAGTCCCCACTCACCTTCT) R, and the third using plasmid_efnb1_56deIV_F (GAGCCCGGCGAACATCTTCTTCAAGTGAAGGCCCAA TC) and plasmid_efnb1_56deIV_R (GATTGGGCCTTCACTTGAAGAAGATGTTCGCCGGGCT C). Mutations were confirmed by sequencing.

CRISPRi cell lines and guide RNAs.

dCas9-KRAB-mKate2 construct was obtained from McManus lab and cloned into pcDNA3.1-Zeo plasmid. This pcDNA3.1-Zeo-cag-puro-mKate2-p2a-dCas9-KRAB plasmid was then linearized and transfected into EPHB2 or EPHRIN-B1 expressing cells. Clonal cell lines were made as described above. Once clonal lines were obtained uniform mKate2 expression was screened for. sgRNAs were designed by; 1. Obtaining guide sequences from McManus lab whole genome library, and 2. Checking these sequences for predicted efficacy using IDT guide design tool. Guide sequences were obtained as oligos and then cloned into 783 vector following McManus lab sgRNA cloning protocol (Fig. A1.6). Plasmid-783 containing sgRNA sequence was then introduced into dCas9-KRAB expressing cell lines via transfection 24 hours prior to mixing.

Western blot and Immuno-precipitation.

See Chapter 4 Materials and Methods for western blot.

For immuo-precipitation (IP), cells were lysed in NP-40 lysis buffer. Lysates were cleared by centrifugation at 16,000 x g for 10 minutes at 4°C prior to use. Lysate was transferred into a clean tube and 100µL of protein A/G beads were added to each tube, this was then rotated @ 4°C for one hour. Lysate and beads were then spun down at 14,000 x g for 10 minutes at 4°C. Supernatant was then transferred to a new tube and beads discarded. Phosphotyrosine antibody (Milipore 05-321) was then added to each tube, and tubes were rotated overnight at 4°C. The following day 50µL of protein A/G beads were added to each tube and rotated at 4°C for 4 hours. Tubes were then spun down at 2500 x g for 3 minutes at 4°C. Supernatant was removed and discarded. Fresh NP-40 lysis buffer was added to each tube to wash beads and rotated for 1 hour at 4°C. This was repeated three times. After 3 washes 25µL of loading buffer was added to each tube, gently mixed, and boiled at 95°C for 5 minutes. Tubes were again spun down at 2500 x g for 3 minutes at 4°C. Supernatant can then be used for western.

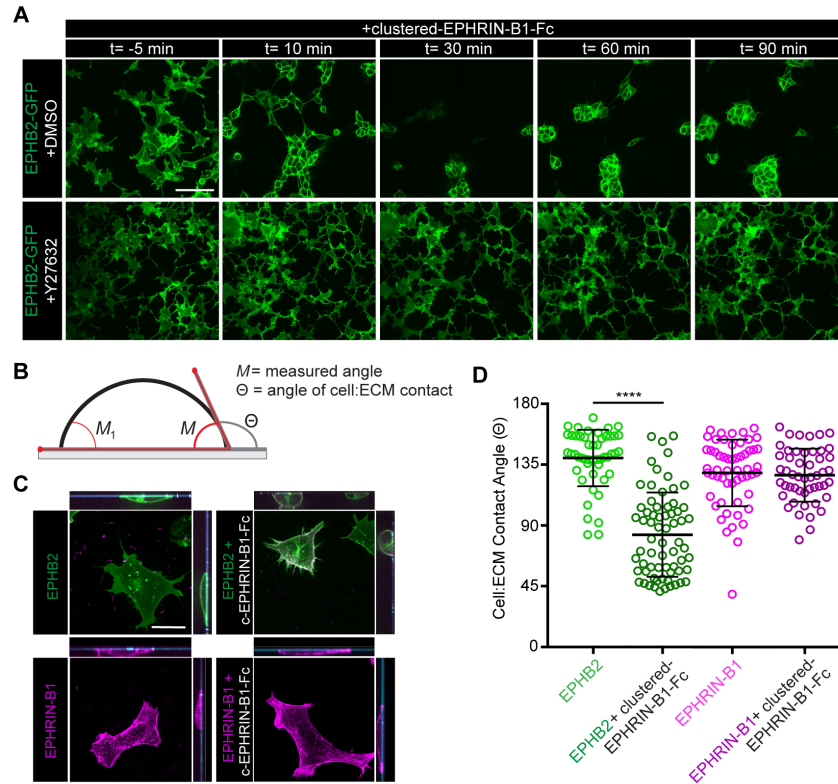


Figure A1.1. Cellular collapse upon addition of EPHRIN-B1-Fc. (A) Upon addition of clustered-EPHRIN-B1-Fc EPHB2-GFP cells dramatically collapse their processes and round up. They also cluster tightly together. Addition of Y27632 prevents this collapse behavior. Scale bar, 100 μ m. (B) Schematic for cell:ECM contact angle measurements. (C) Representative images of EPHB2 cells and EPHRIN-B1 cells with and without the addition of clustered-EPHRIN-B1-Fc. Both top down and z-view. Scale bar, 20 μ m. (D) Quantification of cell:ECM contact. Contact with ECM is dramatically reduced in EPHB2 cells upon the addition of clustered-EPHRIN-B1-Fc.

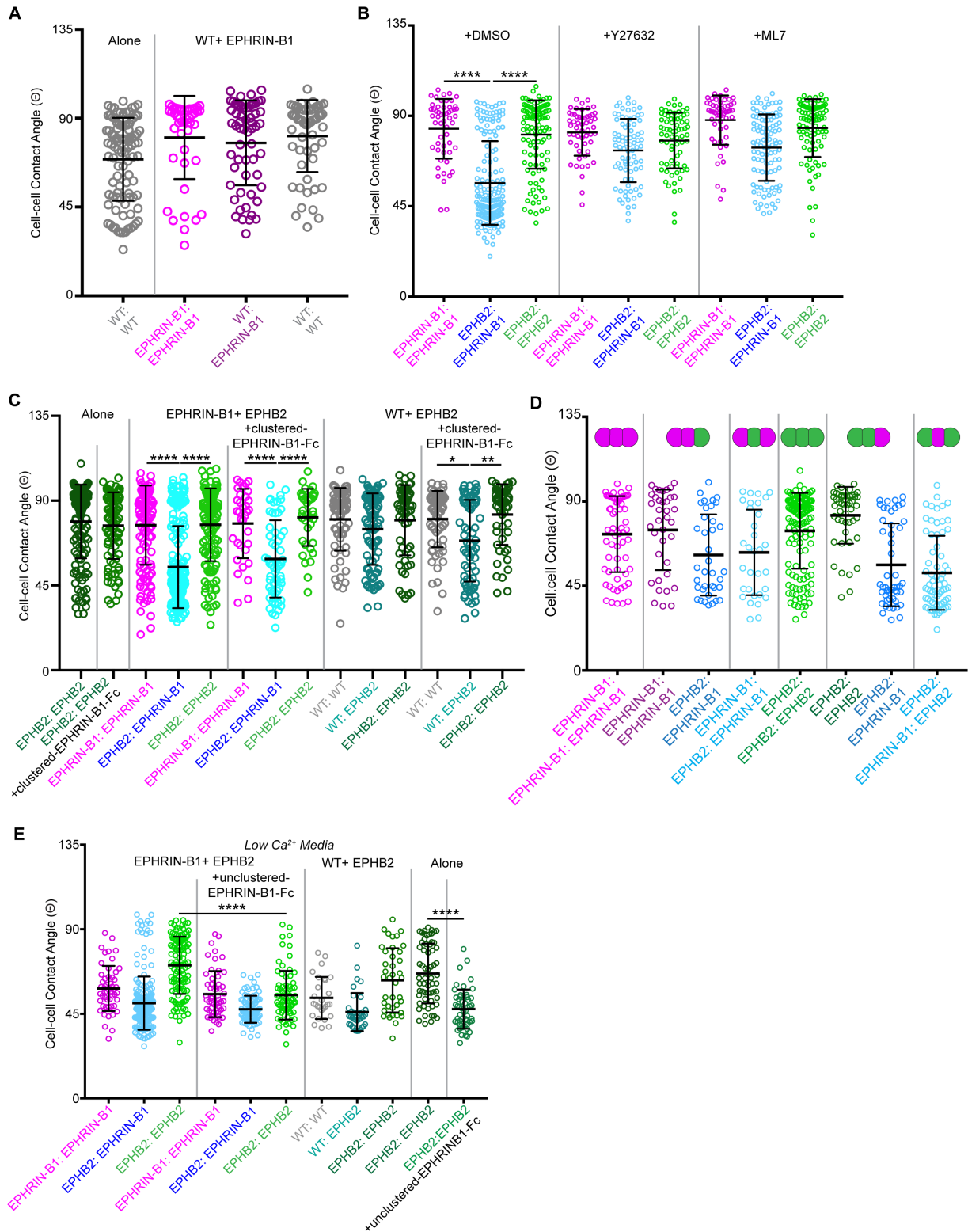
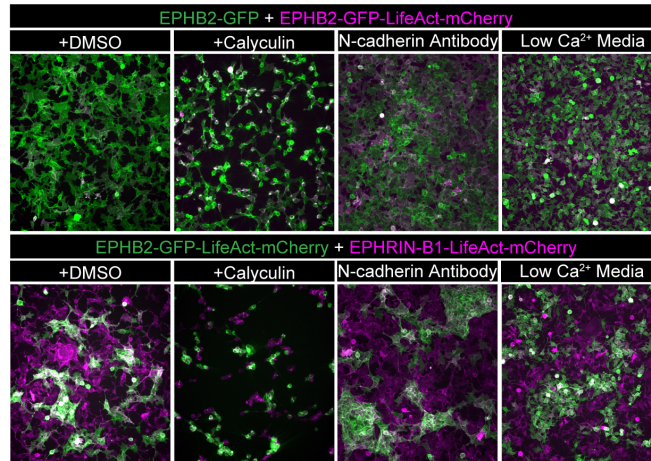


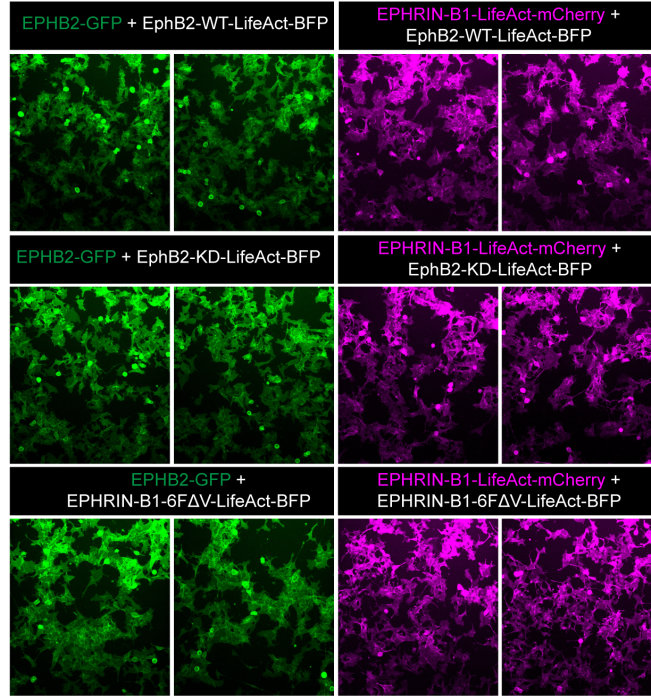
Figure A1.2. Additional cell:cell contact angle conditions. (A) Quantification of cell:cell contact angles in WT cells plates alone, and in WT and EPHRIN-B1 cells mixed wells. All cell pairs have similar interfacial tension. **(B)** Quantification of cell:cell contact angles. Quantification of cell:cell contact angles 4 hours after plating. In HEK293 media with DMSO EPHB2:EPHRIN-

B1 cell pairs show a decreased contact angle compared with EPHRIN-B1:EPHRIN-B1 homotypic cell pairs or EPHB2:EPHB2 homotypic cell pairs ****, $P < 0.0001$. (ANOVA followed by Dunnett's multiple comparison test). Upon the addition of Y27632 or ML7 EPHB2:EPHRIN-B1 cell pairs no longer show diminished contact compared with EPHB2:EPHRIN-B1 cell pairs in media with DMSO control. **(C)** Quantification of cell: cell contact angles with the addition of clustered-EPHRIN-B1-Fc. Clustered-EPHRIN-B1-Fc does not have an effect of EPHB2 cells alone or EPHRIN-B1 and EPHB2 mixed wells. Clustered-EPHRIN-B1-Fc slightly reduces contact between WT:EPHB2 heterotypic cell pairs. **(D)** Quantification of cell:cell contact angles in 3-cell-wells. There are no statistically significant changes in contact angle due to contact with a third cell. **(E)** Quantification of cell:cell contact angle in low Ca^{2+} free media. Cell:cell contacts diminish in the absence of calcium, however EPHB2:EPHB2 homotypic contacts are somewhat retained. In low Ca^{2+} media with the addition of unclustered-EPHRIN-B1-Fc EPHB2:EPHB2 contacts are diminished. EPHB2:EPHB2 cell pairs retain close contact in WT and EPHB2 mixed wells and in EPHB2 cells alone in low Ca^{2+} media. Unclustered-EPHRIN-B1-Fc diminished this contact in EPHB2 cells alone.

A



B



C

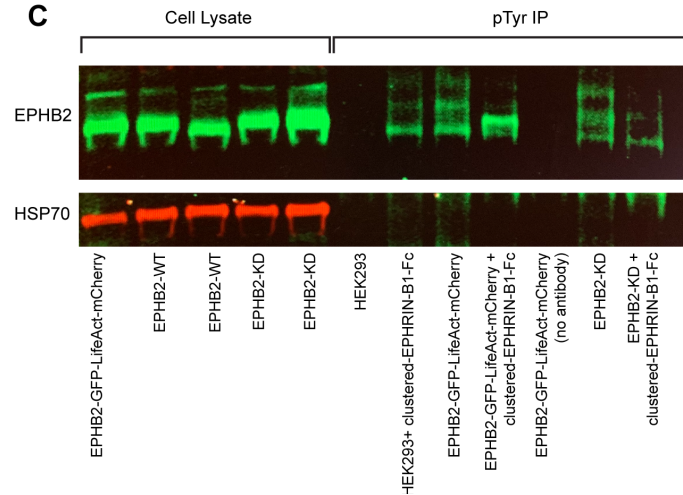


Figure A1.3. Additional cell segregation assay conditions. (A) Cell segregation in mixed populations of HEK293 cells. In the top panels EPHB2-GFP (green) cells were mixed with EPHB2-GFP-LifeAct-mCherry (magenta) cells. In bottom panels EPHB2-GFP-LifeAct-mCherry (green) cells were mixed with EPHRIN-B1-mCherry (magenta) cells. Cells were treated with vehicle (DMSO), calyculin, N-cadherin antibody, or cultured in Low Ca^{2+} media. Calyculin resulted in dramatic cell rounding, lifting off the plate, and cell death. While cells in low Ca^{2+} media still segregate they do not appear to be in tight contact with neighboring cells. Cells in regular HEK293 media with N-cadherin Antibody are indistinguishable from HEK293 media with no inhibitors. **(B)** Cell segregation in mixed populations of HEK293 cells. In the top row are EPHB2-GFP (green) cells or EPHRIN-B1-LifeAct-mCherry (magenta) cells mixed with EPHB2-WT-LifeAct-BFP (unlabeled). Segregation is observed when EPHB2-WT-LifeAct-BFP are mixed with EPHRIN-B1-LifeAct-mCherry cells (right). In the middle row are EPHB2-GFP (green) cells or EPHRIN-B1-LifeAct-mCherry (magenta) cells mixed with EPHB2-KD-LifeAct-BFP (unlabeled). EPHB2-KD-LifeAct-BFP should be kinase dead and thus prevent kinase dependant forward signaling, however these cells still segregate when mixed with EPHRIN-B1-LifeAct-mCherry cells. In the lower row are EPHB2-GFP (green) cells or EPHRIN-B1-LifeAct-mCherry (magenta) cells mixed with EPHRIN-B1-6F Δ V-LifeAct-BFP (unlabeled). EPHRIN-B1-6F Δ V-LifeAct-BFP cells should lack reverse signaling however they still segregate with EPHB2 cells. **(C)** Western blot for EPHB2 in whole cell lysate or following a pTyr IP. Although EPHB2-KD cells should eliminate kinase dependent forward signaling, phosphorylated EPHB2 is still seen in these cells indicating that they are not kinase dead.

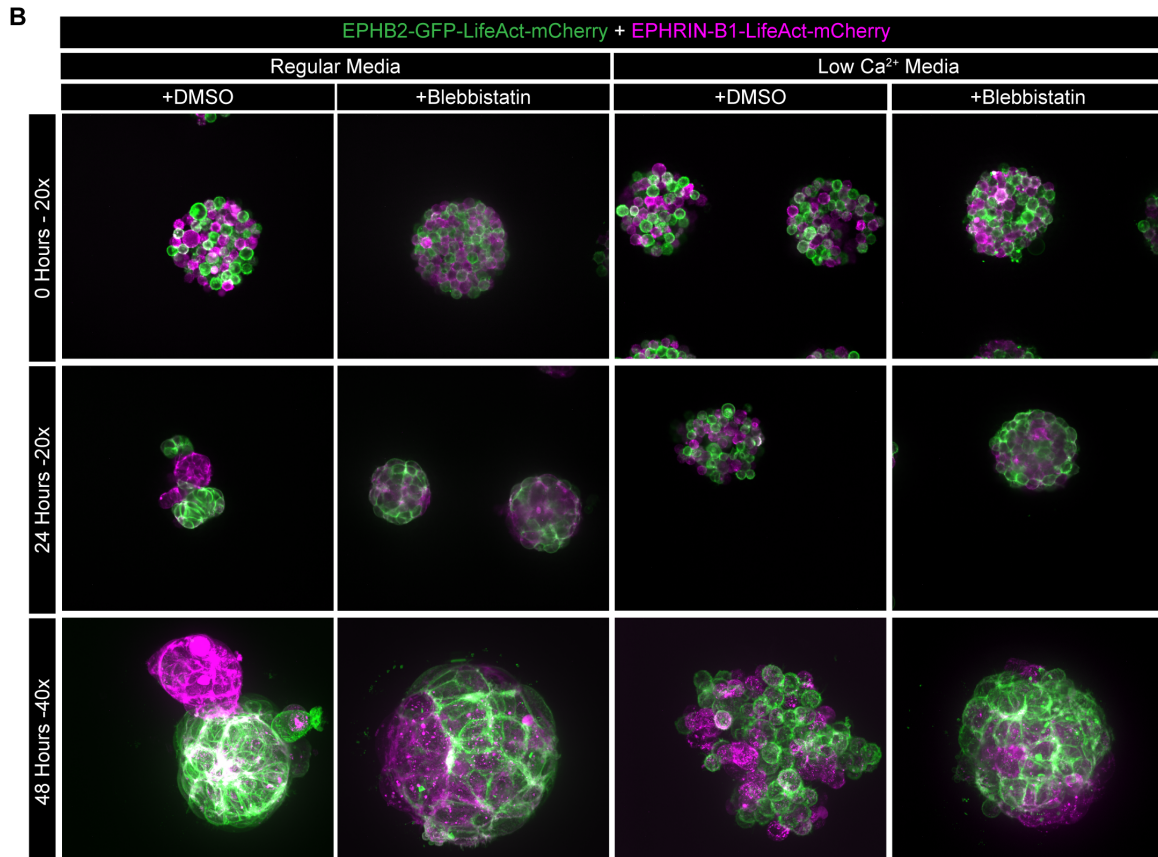
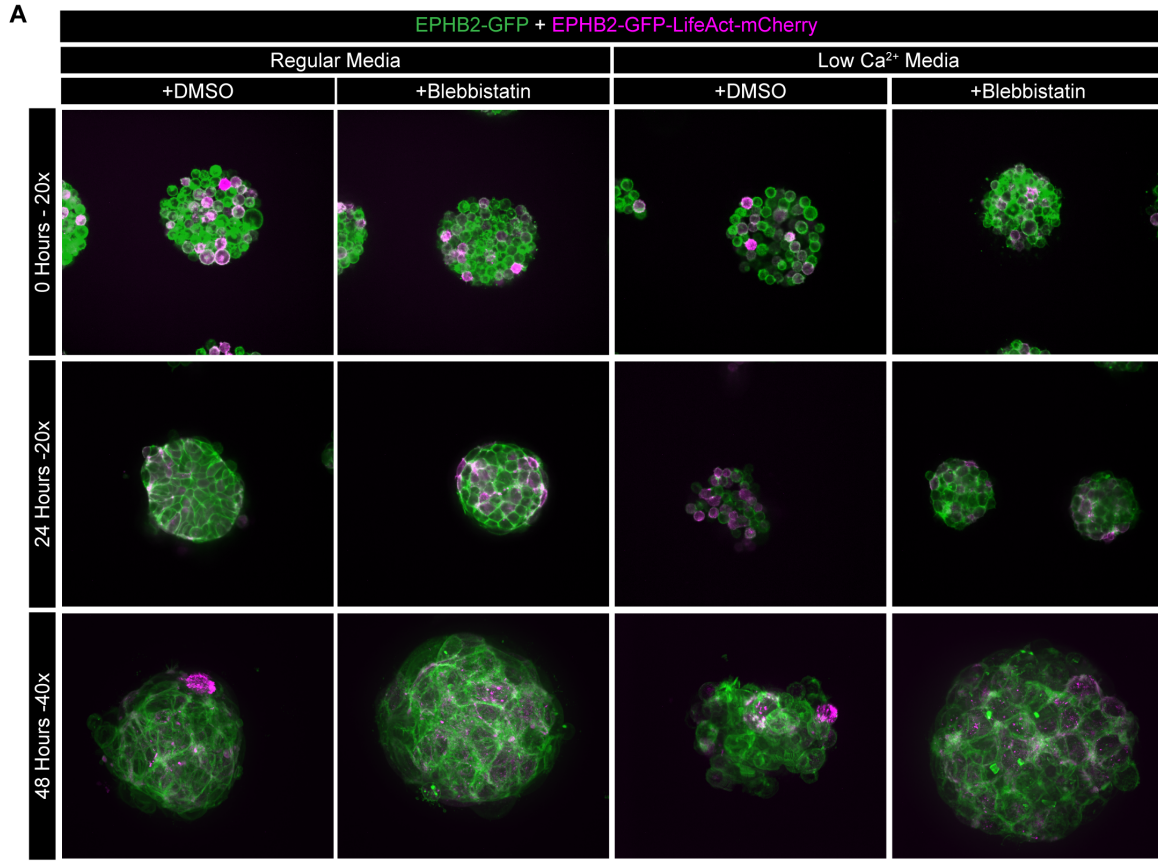


Figure A1.4. Segregation hierarchy in microwells in low Ca²⁺ media. (A) HEK293 3D cell aggregates in circular agarose microwells (180 μm). EPHB2-GFP (green) cells mixed with EPHB2-GFP-LifeAct-mCherry cells in regular or low Ca²⁺ media with or without blebbistatin. In regular media all aggregates are fairly spherical. In low Ca²⁺ media alone the cells do not aggregate as well, however upon the addition of blebbistatin in low Ca²⁺ conditions adherent spherical aggregates form. **(B)** HEK293 3D cell aggregates in circular agarose microwells (180 μm). EPHB2-GFP-LifeAct-mCherry (green) cells mixed with EPHRIN-B1-LifeAct-mCherry cells in regular or low Ca²⁺ media with or without blebbistatin. In regular media cells segregate and minimize contact between populations, however with the addition of blebbistatin the aggregates become quite spherical. In low Ca²⁺ media alone the cells do not aggregate as well, however upon the addition of blebbistatin in low Ca²⁺ conditions adherent spherical aggregates form.

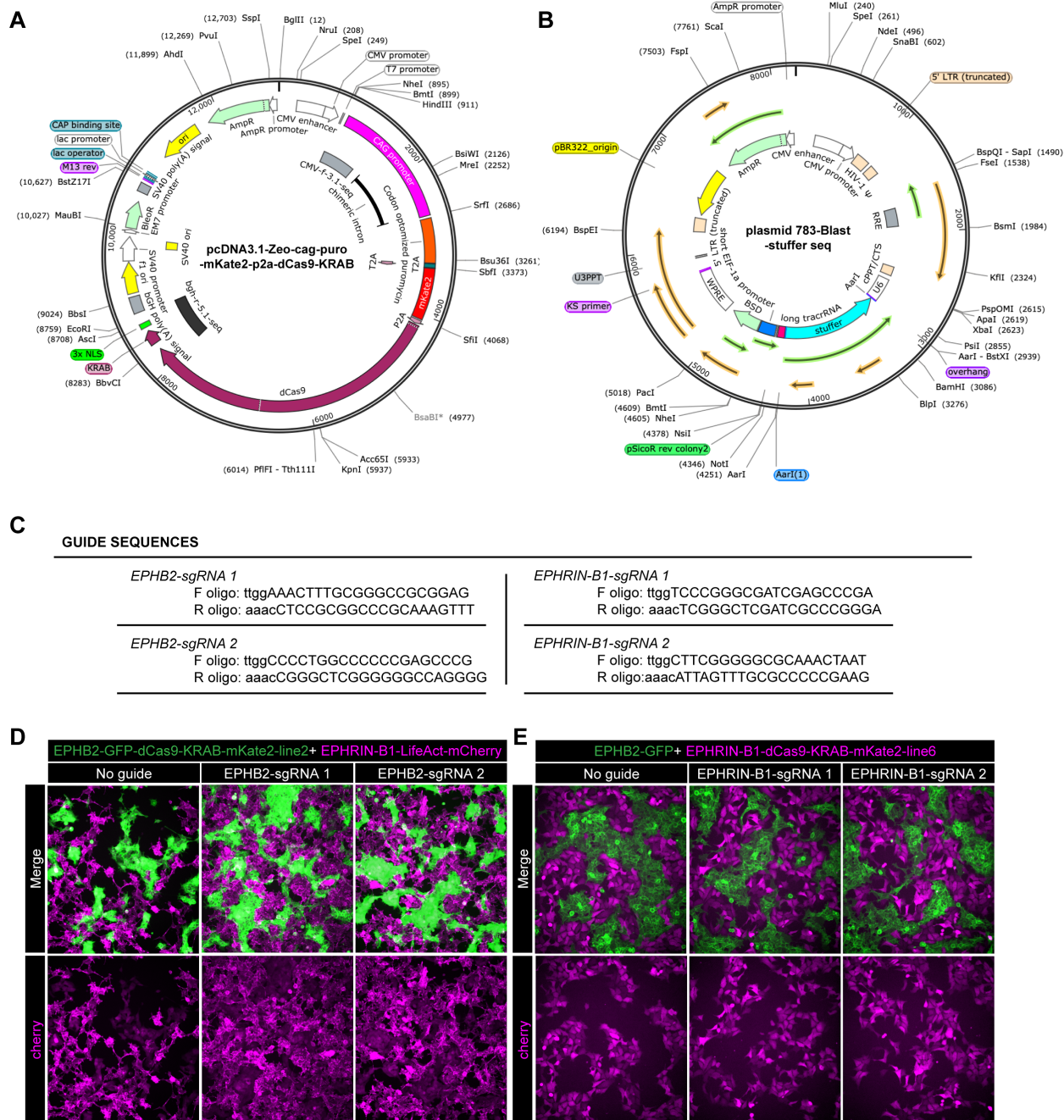


Figure A1.5. CRISPRi in HEK293 cells. (A) Plasmid map of plasmid used to generate dCas9-KRAB cell lines. **(B)** Plasmid map of plasmid used to introduce sgRNAs into dCas9-KRAB cell lines. **(C)** sgRNA sequences for EPHB2 and EPHRIN-B1 knock down. **(D)** Cell segregation in mixed populations of HEK293 cells. In the left panels EPHB2-GFP-dCas9-KRAB-mKate2-line2 (green) cells were mixed with EPHRIN-B1-LifeAct-mCherry (magenta) cells. While EPHB2-GFP-dCas9-KRAB-mKate2-line2 cells express the dCas9-KRAB construct, seen by mKate expression (bottom row), these cells still undergo segregation, even with the addition of EPHB2-sgRNAs 1 and 2. **(E)** Cell segregation in mixed populations of HEK293 cells. In the left panels EPHB2-GFP (green) cells were mixed with EPHRIN-B1-dCas9-KRAB-mKate2-line2 (magenta) cells. While EPHRIN-B1-dCas9-KRAB-mKate2-line2 cells express the dCas9-KRAB construct, seen by

mKate expression, these cells still undergo segregation, even with the addition of EPHRIN-B1-sgRNAs 1 and 2.

A DESIGN AND ORDER SGRNAs
 Design 20nt spacer sequences (for example using an online tool such as Church lab algorithm or the Doetch lab algorithm or use our libraries). Add overhangs that are compatible with the AarI digest, F oligo add TTGG, R oligo add AAAC.
 As example for the overhangs:
 sgRNA: gcactctgagcaagatgag.
 Forward sequence to order: TTGGcactctgagcaagatgag
 Reverse sequence to order: AAACtctctgactcagatgac
 Order the oligos from IDT.

PREPARE THE MP783 PLASMID

Transform the plasmid.

- ≈25 ul of bacteria (competent Stellar cells, in O3 in -80) – take out from freezer and put on ice
 - 100ul in one tube tube, aliquot and freeze down on dry ice and put back in freezer asap if not use all)
- 20 ng plasmid (or take 1 ul from vector DB)
- Add plasmid to bacteria and incubate on ice for 30 min
- Preheat SOC solution or LB in 37°C and take out AMP-plates from fridge
- Transfer the bacteria-plasmid mix to a 15ml miniprep tube
- Heat shock 45 sec at 42°C water bath
- Back on ice quickly (2 min) to cool down → 37°C
- Add 250ul preheated SOC solution
- Put in shaker/incubator for 30 min to 1 hour
- Dilute bacteria-plasmid mix 1:25 – Add 10 ul to 250ul 1XLB or put everything on the plates. Mix in eppendorf tube and put in 15ml miniprep tube. (The rest of the bacteria mix can be added to 1xLB + Amp and put in shaker over night as backup.)
- Put out on agar plates with beads
- Place in incubator over night (15-08)

Pick single colonies the following day and start minipreps, purify plasmid DNA from the bacteria using QIAprep Spin Miniprep Kit according to protocol.

DIGEST WITH AarI

Digest plasmids with AarI over night.

For 1 µg of DNA:

- 1 µg of DNA
- 2 µl of 10× AarI buffer
- 0.4 µl of 50× oligonucleotide
- 1 µl of AarI enzyme
- H₂O up to 20 µl
- Incubation at 37°C overnight

Run digested vector on 0.5% agarose gel, the expected result is a ~9kb backbone band and a 1.3kb stuffer sequence. Gel extract the backbone from the gel using Macherey-Nagel Nucleo-Spin gel extraction kit, discard the stuffer sequence.

ANNEAL SGRNAs

Add H₂O to make oligos 100nM. Dilute to 10 uM and then to 1uM. Add 5ul of each oligo to 90ul with 1X annealing buffer (100 mM Tris pH7.5, 1 M NaCl, 10 mM EDTA).

Incubate 95° for 5 min, and then cool down gradually to 4°C using a PCR cyclor.
 Put on ice.

LIGATION

- 50 ng of plasmid backbone (AarI digested plasmid)
- 3 µl of double stranded oligo
- 1 µl of T4 ligase
- 2 µl T4 buffer
- H₂O up to 20 µl
- Incubate at 16°C overnight
- Inactivate at 65°C for 15 min.

It's important to include a negative control where no insert/oligo is added to assess background/undigested plasmid/self-annealing.

TRANSFORM

Transform your ligated product as above. Put the entire reaction on LB-Amp-plates over night and pick colonies for miniprep the following day. Prep about 5 colonies/sgRNA cloning. Send for sequencing to confirm correct insertions (using Quintara).

Figure A1.6. sgRNA cloning protocol. (A) Protocol obtained from the McManus lab for cloning sgRNAs into plasmid-783 for CRISPRi.

Table A1.1. Guide Sequences.

<p><i>EPHB2-sgRNA 1</i> F oligo: ttggAAACTTTGCGGGCCGCGGAG R oligo: aaacTCCGCGGCCCGCAAAGTTT</p>	<p><i>EPHRIN-B1-sgRNA 1</i> F oligo: ttggTCCCGGGCGATCGAGCCCGA R oligo: aaacTCGGGCTCGATCGCCCGGA</p>
<p><i>EPHB2-sgRNA 2</i> F oligo: ttggCCCCTGGCCCCCGAGCCCG R oligo: aaacCGGGCTCGGGGGCCAGGGG</p>	<p><i>EPHRIN-B1-sgRNA 2</i> F oligo: ttggCTTCGGGGGCGCAAATAAT R oligo: aaacATTAGTTTGCGCCCCGAAG</p>
<p><i>MYH9-sgRNA 1</i> F oligo: ttggGAGGACTTTCTCGAGCGCTC R oligo: aaacGAGCGCTCGAGAAAGTCCTC</p>	<p><i>MYH10-sgRNA 1</i> F oligo: ttggGCGCCACCATCTTCGGCTGA R oligo: aaacTCAGCCGAAGATGGTGGCGC</p>
<p><i>MYH9-sgRNA 2</i> F oligo: ttggAGGGCACGGAAGGCTAAGCA R oligo: aaacTGCTTAGCCTTCCGTGCCCT</p>	<p><i>MYH10-sgRNA 2</i> F oligo: ttggAGGCGCTGGATCTGTGGTGC R oligo: aaacCGACCACAGATCCAGCGCCT</p>
<p><i>CDH2-sgRNA 1</i> F oligo: ttggTGATGACAAATAGCGGGCCG R oligo: aaacCGGCCCGCTATTTGTCATCA</p>	<p><i>GFP-sgRNA 1</i> F oligo: ttggGACCAGGCTGGGCACCACCC R oligo: aaacGGTGCCCATCCTGGTC</p>
<p><i>CDH2-sgRNA 2</i> F oligo: ttggGGAAGCCGCGAGGGATGCAG R oligo: aaacCTGCATCCCTCGCGGCTTCC</p>	

References

- Abbruzzese, G., S.F. Becker, J. Kashef, and D. Alfandari. 2016. ADAM13 cleavage of cadherin-11 promotes CNC migration independently of the homophilic binding site. *Dev. Biol.* 415:383–390. doi:10.1016/j.ydbio.2015.07.018.
- Abercrombie, M., and J.E. Heaysman. 1953. Observations on the social behaviour of cells in tissue culture. I. Speed of movement of chick heart fibroblasts in relation to their mutual contacts. *Exp. Cell Res.* 5:111–131. doi:10.1016/0014-4827(53)90098-6.
- Abu-Issa, R., G. Smyth, I. Smoak, K. Yamamura, and E.N. Meyers. 2002. Fgf8 is required for pharyngeal arch and cardiovascular development in the mouse. *Dev. Camb. Engl.* 129:4613–4625.
- Adams, R.H., F. Diella, S. Hennig, F. Helmbacher, U. Deutsch, and R. Klein. 2001. The Cytoplasmic Domain of the Ligand EphrinB2 Is Required for Vascular Morphogenesis but Not Cranial Neural Crest Migration. *Cell.* 104:57–69. doi:10.1016/S0092-8674(01)00191-X.
- Addison, M., and D.G. Wilkinson. 2016. Segment Identity and Cell Segregation in the Vertebrate Hindbrain. *Curr. Top. Dev. Biol.* 117:581–596. doi:10.1016/bs.ctdb.2015.10.019.
- Addison, M., Q. Xu, J. Cayuso, and D.G. Wilkinson. 2018. Cell Identity Switching Regulated by Retinoic Acid Signaling Maintains Homogeneous Segments in the Hindbrain. *Dev. Cell.* 45:606-620.e3. doi:10.1016/j.devcel.2018.04.003.
- Agrawal, P., M. Wang, S. Kim, A.E. Lewis, and J.O. Bush. 2014. Embryonic expression of EphA receptor genes in mice supports their candidacy for involvement in cleft lip and palate. *Dev. Dyn. Off. Publ. Am. Assoc. Anat.* 243:1470–1476. doi:10.1002/dvdy.24170.

- Araki, I., and H. Nakamura. 1999. Engrailed defines the position of dorsal di-mesencephalic boundary by repressing diencephalic fate. *Development*. 126:5127–5135.
- Astin, J.W., J. Batson, S. Kadir, J. Charlet, R.A. Persad, D. Gillatt, J.D. Oxley, and C.D. Nobes. 2010. Competition amongst Eph receptors regulates contact inhibition of locomotion and invasiveness in prostate cancer cells. *Nat. Cell Biol.* 12:1194–1204.
doi:10.1038/ncb2122.
- Bachir, A.I., A.R. Horwitz, W.J. Nelson, and J.M. Bianchini. 2017. Actin-Based Adhesion Modules Mediate Cell Interactions with the Extracellular Matrix and Neighboring Cells. *Cold Spring Harb. Perspect. Biol.* 9. doi:10.1101/cshperspect.a023234.
- Baeyens, N., S. Nicoli, B.G. Coon, T.D. Ross, K. Van den Dries, J. Han, H.M. Lauridsen, C.O. Mejean, A. Eichmann, J.-L. Thomas, J.D. Humphrey, and M.A. Schwartz. 2015. Vascular remodeling is governed by a VEGFR3-dependent fluid shear stress set point. *eLife*. 4. doi:10.7554/eLife.04645.
- Bahm, I., E.H. Barriga, A. Frolov, E. Theveneau, P. Frankel, and R. Mayor. 2017. PDGF controls contact inhibition of locomotion by regulating N-cadherin during neural crest migration. *Dev. Camb. Engl.* 144:2456–2468. doi:10.1242/dev.147926.
- Bailles, A., C. Collinet, J.-M. Philippe, P.-F. Lenne, E. Munro, and T. Lecuit. 2019. Genetic induction and mechanochemical propagation of a morphogenetic wave. *Nature*. 1–7.
doi:10.1038/s41586-019-1492-9.
- Battle, E., J.T. Henderson, H. Beghtel, M.M.W. van den Born, E. Sancho, G. Huls, J. Meeldijk, J. Robertson, M. van de Wetering, T. Pawson, and H. Clevers. 2002. β -Catenin and TCF Mediate Cell Positioning in the Intestinal Epithelium by Controlling the Expression of EphB/EphrinB. *Cell*. 111:251–263. doi:10.1016/S0092-8674(02)01015-2.

- Battle, E., and D.G. Wilkinson. 2012. Molecular Mechanisms of Cell Segregation and Boundary Formation in Development and Tumorigenesis. *Cold Spring Harb. Perspect. Biol.* 4. doi:10.1101/cshperspect.a008227.
- Becker, N., T. Seitanidou, P. Murphy, M.G. Mattéi, P. Topilko, M.A. Nieto, D.G. Wilkinson, P. Charnay, and P. Gilardi-Hebenstreit. 1994. Several receptor tyrosine kinase genes of the Eph family are segmentally expressed in the developing hindbrain. *Mech. Dev.* 47:3–17. doi:10.1016/0925-4773(94)90091-4.
- Becker, S.F.S., R. Mayor, and J. Kashef. 2013. Cadherin-11 mediates contact inhibition of locomotion during *Xenopus* neural crest cell migration. *PLoS One.* 8:e85717. doi:10.1371/journal.pone.0085717.
- Bergemann, A.D., H.J. Cheng, R. Brambilla, R. Klein, and J.G. Flanagan. 1995. ELF-2, a new member of the Eph ligand family, is segmentally expressed in mouse embryos in the region of the hindbrain and newly forming somites. *Mol. Cell. Biol.* 15:4921–4929. doi:10.1128/MCB.15.9.4921.
- Berndt, J.D., M.R. Clay, T. Langenberg, and M.C. Halloran. 2008. Rho-kinase and myosin II affect dynamic neural crest cell behaviors during epithelial to mesenchymal transition *in vivo*. *Dev. Biol.* 324:236–244. doi:10.1016/j.ydbio.2008.09.013.
- Bhagavathula, N., A.W. Hanosh, K.C. Nerusu, H. Appelman, S. Chakrabarty, and J. Varani. 2007. Regulation of E-cadherin and β -catenin by Ca^{2+} in colon carcinoma is dependent on calcium-sensing receptor expression and function. *Int. J. Cancer.* 121:1455–1462. doi:https://doi.org/10.1002/ijc.22858.
- Bildsoe, H., D.A.F. Loebel, V.J. Jones, A.C.C. Hor, A.W. Braithwaite, Y.-T. Chen, R.R. Behringer, and P.P.L. Tam. 2013. The mesenchymal architecture of the cranial

- mesoderm of mouse embryos is disrupted by the loss of Twist1 function. *Dev. Biol.* 374:295–307. doi:10.1016/j.ydbio.2012.12.004.
- Blaue, C., J. Kashef, and C.M. Franz. 2018. Cadherin-11 promotes neural crest cell spreading by reducing intracellular tension—Mapping adhesion and mechanics in neural crest explants by atomic force microscopy. *Semin. Cell Dev. Biol.* 73:95–106. doi:10.1016/j.semcdb.2017.08.058.
- Bornhorst, D., P. Xia, H. Nakajima, C. Dingare, W. Herzog, V. Lecaudey, N. Mochizuki, C.-P. Heisenberg, D. Yelon, and S. Abdelilah-Seyfried. 2019. Biomechanical signaling within the developing zebrafish heart attunes endocardial growth to myocardial chamber dimensions. *Nat. Commun.* 10:1–10. doi:10.1038/s41467-019-12068-x.
- Brasch, J., O.J. Harrison, B. Honig, and L. Shapiro. 2012. Thinking outside the cell: how cadherins drive adhesion. *Trends Cell Biol.* 22:299–310. doi:10.1016/j.tcb.2012.03.004.
- Brodland, G.W. 2002. The Differential Interfacial Tension Hypothesis (DITH): a comprehensive theory for the self-rearrangement of embryonic cells and tissues. *J. Biomech. Eng.* 124:188–197. doi:10.1115/1.1449491.
- Bush, J.O., and P. Soriano. 2010. Ephrin-B1 forward signaling regulates craniofacial morphogenesis by controlling cell proliferation across Eph-ephrin boundaries. *Genes Dev.* 24:2068–2080. doi:10.1101/gad.1963210.
- Calzolari, S., J. Terriente, and C. Pujades. 2014. Cell segregation in the vertebrate hindbrain relies on actomyosin cables located at the interhombomeric boundaries. *EMBO J.* 33:686–701. doi:10.1002/embj.201386003.

- Campàs, O., T. Mammoto, S. Hasso, R.A. Sperling, D. O'Connell, A.G. Bischof, R. Maas, D.A. Weitz, L. Mahadevan, and D.E. Ingber. 2014. Quantifying cell-generated mechanical forces within living embryonic tissues. *Nat. Methods*. 11:183–189.
doi:10.1038/nmeth.2761.
- Canty, L., E. Zarour, L. Kashkooli, P. François, and F. Fagotto. 2017. Sorting at embryonic boundaries requires high heterotypic interfacial tension. *Nat. Commun*. 8:1–15.
doi:10.1038/s41467-017-00146-x.
- Carmona-Fontaine, C., H.K. Matthews, S. Kuriyama, M. Moreno, G.A. Dunn, M. Parsons, C.D. Stern, and R. Mayor. 2008. Contact inhibition of locomotion *in vivo* controls neural crest directional migration. *Nature*. 456:957–961. doi:10.1038/nature07441.
- Carmona-Fontaine, C., E. Theveneau, A. Tzekou, M. Tada, M. Woods, K.M. Page, M. Parsons, J.D. Lambris, and R. Mayor. 2011. Complement fragment C3a controls mutual cell attraction during collective cell migration. *Dev. Cell*. 21:1026–1037.
doi:10.1016/j.devcel.2011.10.012.
- Carvalho, J.R., I.C. Fortunato, C.G. Fonseca, A. Pezzarossa, P. Barbacena, M.A. Dominguez-Cejudo, F.F. Vasconcelos, N.C. Santos, F.A. Carvalho, and C.A. Franco. 2019. Non-canonical Wnt signaling regulates junctional mechanocoupling during angiogenic collective cell migration. *eLife*. 8. doi:10.7554/eLife.45853.
- Carver, E.A., K.F. Oram, and T. Gridley. 2002. Craniosynostosis in Twist heterozygous mice: a model for Saethre-Chotzen syndrome. *Anat. Rec*. 268:90–92. doi:10.1002/ar.10124.
- Cayuso, J., A. Dzementsei, J.C. Fischer, G. Karemore, S. Caviglia, J. Bartholdson, G.J. Wright, and E.A. Ober. 2016. EphrinB1/EphB3b Coordinate Bidirectional Epithelial-

- Mesenchymal Interactions Controlling Liver Morphogenesis and Laterality. *Dev. Cell.* 39:316–328. doi:10.1016/j.devcel.2016.10.009.
- Cayuso, J., Q. Xu, M. Addison, and D.G. Wilkinson. 2019. Actomyosin regulation by Eph receptor signaling couples boundary cell formation to border sharpness. *eLife.* 8:e49696. doi:10.7554/eLife.49696.
- Cerchiari, A.E., J.C. Garbe, N.Y. Jee, M.E. Todhunter, K.E. Broaders, D.M. Peehl, T.A. Desai, M.A. LaBarge, M. Thomson, and Z.J. Gartner. 2015. A strategy for tissue self-organization that is robust to cellular heterogeneity and plasticity. *Proc. Natl. Acad. Sci.* 112:2287–2292. doi:10.1073/pnas.1410776112.
- Chai, Y., X. Jiang, Y. Ito, P. Bringas, J. Han, D.H. Rowitch, P. Soriano, A.P. McMahon, and H.M. Sucov. 2000. Fate of the mammalian cranial neural crest during tooth and mandibular morphogenesis. *Dev. Camb. Engl.* 127:1671–1679.
- Chapman, D.L., N. Garvey, S. Hancock, M. Alexiou, S.I. Agulnik, J.J. Gibson-Brown, J. Cebra-Thomas, R.J. Bollag, L.M. Silver, and V.E. Papaioannou. 1996. Expression of the T-box family genes, Tbx1-Tbx5, during early mouse development. *Dev. Dyn. Off. Publ. Am. Assoc. Anat.* 206:379–390. doi:10.1002/(SICI)1097-0177(199608)206:4<379::AID-AJA4>3.0.CO;2-F.
- Chen, Z.F., and R.R. Behringer. 1995. twist is required in head mesenchyme for cranial neural tube morphogenesis. *Genes Dev.* 9:686–699. doi:10.1101/gad.9.6.686.
- Cheng, Y.-C., M. Amoyel, X. Qiu, Y.-J. Jiang, Q. Xu, and D.G. Wilkinson. 2004. Notch activation regulates the segregation and differentiation of rhombomere boundary cells in the zebrafish hindbrain. *Dev. Cell.* 6:539–550. doi:10.1016/s1534-5807(04)00097-8.

- Choe, C.P., A. Collazo, L.A. Trinh, L. Pan, C.B. Moens, and J.G. Crump. 2013. Wnt-dependent epithelial transitions drive pharyngeal pouch formation. *Dev. Cell.* 24:296–309. doi:10.1016/j.devcel.2012.12.003.
- Choe, C.P., and J.G. Crump. 2015. Eph-Pak2a signaling regulates branching of the pharyngeal endoderm by inhibiting late-stage epithelial dynamics. *Dev. Camb. Engl.* 142:1089–1094. doi:10.1242/dev.115774.
- Clay, M.R., and M.C. Halloran. 2013. Rho activation is apically restricted by Arhgap1 in neural crest cells and drives epithelial-to-mesenchymal transition. *Development.* 140:3198–3209. doi:10.1242/dev.095448.
- Clay, M.R., and M.C. Halloran. 2014. Cadherin 6 promotes neural crest cell detachment via F-actin regulation and influences active Rho distribution during epithelial-to-mesenchymal transition. *Dev. Camb. Engl.* 141:2506–2515. doi:10.1242/dev.105551.
- Coles, E.G., L.A. Taneyhill, and M. Bronner-Fraser. 2007. A critical role for Cadherin6B in regulating avian neural crest emigration. *Dev. Biol.* 312:533–544. doi:10.1016/j.ydbio.2007.09.056.
- Compagni, A., M. Logan, R. Klein, and R.H. Adams. 2003. Control of skeletal patterning by ephrinB1-EphB interactions. *Dev. Cell.* 5:217–230. doi:10.1016/s1534-5807(03)00198-9.
- Connelly, J.T., J.E. Gautrot, B. Trappmann, D.W.-M. Tan, G. Donati, W.T.S. Huck, and F.M. Watt. 2010. Actin and serum response factor transduce physical cues from the microenvironment to regulate epidermal stem cell fate decisions. *Nat. Cell Biol.* 12:711–718. doi:10.1038/ncb2074.

- Cooke, J., C. Moens, L. Roth, L. Durbin, K. Shiomi, C. Brennan, C. Kimmel, S. Wilson, and N. Holder. 2001. Eph signalling functions downstream of Val to regulate cell sorting and boundary formation in the caudal hindbrain. *Dev. Camb. Engl.* 128:571–580.
- Cooke, J.E., H.A. Kemp, and C.B. Moens. 2005. EphA4 is required for cell adhesion and rhombomere-boundary formation in the zebrafish. *Curr. Biol. CB.* 15:536–542. doi:10.1016/j.cub.2005.02.019.
- Cooke, J.E., and C.B. Moens. 2002. Boundary formation in the hindbrain: Eph only it were simple.. *Trends Neurosci.* 25:260–267. doi:10.1016/s0166-2236(02)02134-3.
- Cortina, C., S. Palomo-Ponce, M. Iglesias, J.L. Fernández-Masip, A. Vivancos, G. Whissell, M. Humà, N. Peiró, L. Gallego, S. Jonkheer, A. Davy, J. Lloreta, E. Sancho, and E. Batlle. 2007. EphB-ephrin-B interactions suppress colorectal cancer progression by compartmentalizing tumor cells. *Nat. Genet.* 39:1376–1383. doi:10.1038/ng.2007.11.
- Cousin, H., G. Abbruzzese, C. McCusker, and D. Alfandari. 2012. ADAM13 function is required in the 3 dimensional context of the embryo during cranial neural crest cell migration in *Xenopus laevis*. *Dev. Biol.* 368:335–344. doi:10.1016/j.ydbio.2012.05.036.
- Crump, J.G., L. Maves, N.D. Lawson, B.M. Weinstein, and C.B. Kimmel. 2004. An essential role for Fgfs in endodermal pouch formation influences later craniofacial skeletal patterning. *Development.* 131:5703–5716. doi:10.1242/dev.01444.
- Dady, A., C. Blavet, and J.-L. Duband. 2012. Timing and kinetics of E- to N-cadherin switch during neurulation in the avian embryo. *Dev. Dyn. Off. Publ. Am. Assoc. Anat.* 241:1333–1349. doi:10.1002/dvdy.23813.

- Dady, A., and J.-L. Duband. 2017. Cadherin interplay during neural crest segregation from the non-neural ectoderm and neural tube in the early chick embryo. *Dev. Dyn. Off. Publ. Am. Assoc. Anat.* 246:550–565. doi:10.1002/dvdy.24517.
- Dahmann, C., and K. Basler. 2000. Opposing transcriptional outputs of Hedgehog signaling and engrailed control compartmental cell sorting at the *Drosophila* A/P boundary. *Cell.* 100:411–422. doi:10.1016/s0092-8674(00)80677-7.
- Das, D., D. Jülich, J. Schwendinger-Schreck, E. Guillon, A.K. Lawton, N. Dray, T. Emonet, C.S. O’Hern, M.D. Shattuck, and S.A. Holley. 2019. Organization of Embryonic Morphogenesis via Mechanical Information. *Dev. Cell.* 49:829-839.e5. doi:10.1016/j.devcel.2019.05.014.
- Davis, S., N.W. Gale, T.H. Aldrich, P.C. Maisonpierre, V. Lhotak, T. Pawson, M. Goldfarb, and G.D. Yancopoulos. 1994. Ligands for EPH-related receptor tyrosine kinases that require membrane attachment or clustering for activity. *Science.* 266:816–819. doi:10.1126/science.7973638.
- Davy, A., J. Aubin, and P. Soriano. 2004. Ephrin-B1 forward and reverse signaling are required during mouse development. *Genes Dev.* 18:572–583. doi:10.1101/gad.1171704.
- Davy, A., J.O. Bush, and P. Soriano. 2006. Inhibition of gap junction communication at ectopic Eph/ephrin boundaries underlies craniofrontonasal syndrome. *PLoS Biol.* 4:e315. doi:10.1371/journal.pbio.0040315.
- Davy, A., and P. Soriano. 2007. Ephrin-B2 forward signaling regulates somite patterning and neural crest cell development. *Dev. Biol.* 304:182–193. doi:10.1016/j.ydbio.2006.12.028.

- Deckelbaum, R.A., G. Holmes, Z. Zhao, C. Tong, C. Basilico, and C.A. Loomis. 2012. Regulation of cranial morphogenesis and cell fate at the neural crest-mesoderm boundary by engrailed 1. *Development*. 139:1346–1358. doi:10.1242/dev.076729.
- Dohn, T.E., and J.S. Waxman. 2012. Distinct phases of Wnt/ β -catenin signaling direct cardiomyocyte formation in zebrafish. *Dev. Biol.* 361:364–376. doi:10.1016/j.ydbio.2011.10.032.
- Dougherty, K.J., L. Zagoraiou, D. Satoh, I. Rozani, S. Doobar, S. Arber, T.M. Jessell, and O. Kiehn. 2013. Locomotor Rhythm Generation Linked to the Output of Spinal Shox2 Excitatory Interneurons. *Neuron*. 80:920–933. doi:10.1016/j.neuron.2013.08.015.
- Duchemin, A.-L., H. Vignes, and J. Vermot. 2019. Mechanically activated piezo channels modulate outflow tract valve development through the Yap1 and Klf2-Notch signaling axis. *eLife*. 8. doi:10.7554/eLife.44706.
- Duguay, D., R.A. Foty, and M.S. Steinberg. 2003. Cadherin-mediated cell adhesion and tissue segregation: qualitative and quantitative determinants. *Dev. Biol.* 253:309–323. doi:10.1016/s0012-1606(02)00016-7.
- Dzamba, B.J., and D.W. DeSimone. 2018. Extracellular Matrix (ECM) and the Sculpting of Embryonic Tissues. *Curr. Top. Dev. Biol.* 130:245–274. doi:10.1016/bs.ctdb.2018.03.006.
- Eberhart, J.K., X. He, M.E. Swartz, Y.-L. Yan, H. Song, T.C. Boling, A.K. Kunerth, M.B. Walker, C.B. Kimmel, and J.H. Postlethwait. 2008. MicroRNA Mirn140 modulates Pdgf signaling during palatogenesis. *Nat. Genet.* 40:290–298. doi:10.1038/ng.82.

- Eickholt, B.J., S.L. Mackenzie, A. Graham, F.S. Walsh, and P. Doherty. 1999. Evidence for collapsin-1 functioning in the control of neural crest migration in both trunk and hindbrain regions. *Dev. Camb. Engl.* 126:2181–2189.
- Eisenhoffer, G.T., P.D. Loftus, M. Yoshigi, H. Otsuna, C.-B. Chien, P.A. Morcos, and J. Rosenblatt. 2012. Crowding induces live cell extrusion to maintain homeostatic cell numbers in epithelia. *Nature*. 484:546–549. doi:10.1038/nature10999.
- Elosegui-Artola, A., I. Andreu, A.E.M. Beedle, A. Lezamiz, M. Uroz, A.J. Kosmalska, R. Oria, J.Z. Kechagia, P. Rico-Lastres, A.-L. Le Roux, C.M. Shanahan, X. Trepas, D. Navajas, S. Garcia-Manyes, and P. Roca-Cusachs. 2017. Force Triggers YAP Nuclear Entry by Regulating Transport across Nuclear Pores. *Cell*. 171:1397-1410.e14. doi:10.1016/j.cell.2017.10.008.
- Escot, S., C. Blavet, E. Faure, S. Zaffran, J.-L. Duband, and C. Fournier-Thibault. 2016. Disruption of CXCR4 signaling in pharyngeal neural crest cells causes DiGeorge syndrome-like malformations. *Development*. 143:582–588. doi:10.1242/dev.126573.
- Fagotto, F. 2014. The cellular basis of tissue separation. *Development*. 141:3303–3318. doi:10.1242/dev.090332.
- Fairchild, C.L., and L.S. Gammill. 2013. Tetraspanin18 is a FoxD3-responsive antagonist of cranial neural crest epithelial-to-mesenchymal transition that maintains cadherin-6B protein. *J Cell Sci*. 126:1464–1476. doi:10.1242/jcs.120915.
- Farlie, P.G., R. Kerr, P. Thomas, T. Symes, J. Minichiello, C.J. Hearn, and D. Newgreen. 1999. A paraxial exclusion zone creates patterned cranial neural crest cell outgrowth adjacent to rhombomeres 3 and 5. *Dev. Biol.* 213:70–84. doi:10.1006/dbio.1999.9332.

- Fernandez-Gonzalez, R., S. de M. Simoes, J.-C. Röper, S. Eaton, and J.A. Zallen. 2009. Myosin II dynamics are regulated by tension in intercalating cells. *Dev. Cell.* 17:736–743. doi:10.1016/j.devcel.2009.09.003.
- Foty, R.A., and M.S. Steinberg. 2005. The differential adhesion hypothesis: a direct evaluation. *Dev. Biol.* 278:255–263. doi:10.1016/j.ydbio.2004.11.012.
- Francis, K., and B.O. Palsson. 1997. Effective intercellular communication distances are determined by the relative time constants for cyto/chemokine secretion and diffusion. *Proc. Natl. Acad. Sci. U. S. A.* 94:12258–12262.
- Franco, C.A., M.L. Jones, M.O. Bernabeu, A.-C. Vion, P. Barbacena, J. Fan, T. Mathivet, C.G. Fonseca, A. Ragab, T.P. Yamaguchi, P.V. Coveney, R.A. Lang, and H. Gerhardt. 2016. Non-canonical Wnt signalling modulates the endothelial shear stress flow sensor in vascular remodelling. *eLife.* 5:e07727. doi:10.7554/eLife.07727.
- Fraser, S., R. Keynes, and A. Lumsden. 1990. Segmentation in the chick embryo hindbrain is defined by cell lineage restrictions. *Nature.* 344:431–435. doi:10.1038/344431a0.
- Frisdal, A., and P.A. Trainor. 2014. Development and evolution of the pharyngeal apparatus. *WIREs Dev. Biol.* 3:403–418. doi:https://doi.org/10.1002/wdev.147.
- Gale, N.W., S.J. Holland, D.M. Valenzuela, A. Flenniken, L. Pan, T.E. Ryan, M. Henkemeyer, K. Strebhardt, H. Hirai, D.G. Wilkinson, T. Pawson, S. Davis, and G.D. Yancopoulos. 1996. Eph Receptors and Ligands Comprise Two Major Specificity Subclasses and Are Reciprocally Compartmentalized during Embryogenesis. *Neuron.* 17:9–19. doi:10.1016/S0896-6273(00)80276-7.

- Gammill, L.S., C. Gonzalez, and M. Bronner-Fraser. 2007. Neuropilin 2/semaphorin 3F signaling is essential for cranial neural crest migration and trigeminal ganglion condensation. *Dev. Neurobiol.* 67:47–56. doi:10.1002/dneu.20326.
- Ganzler, S.I., and C. Redies. 1995. R-cadherin expression during nucleus formation in chicken forebrain neuromeres. *J. Neurosci.* 15:4157–4172. doi:10.1523/JNEUROSCI.15-06-04157.1995.
- Garg, V., C. Yamagishi, T. Hu, I.S. Kathiriya, H. Yamagishi, and D. Srivastava. 2001. Tbx1, a DiGeorge syndrome candidate gene, is regulated by sonic hedgehog during pharyngeal arch development. *Dev. Biol.* 235:62–73. doi:10.1006/dbio.2001.0283.
- Gassmann, M., F. Casagrande, D. Orioli, H. Simon, C. Lai, R. Klein, and G. Lemke. 1995. Aberrant neural and cardiac development in mice lacking the ErbB4 neuregulin receptor. *Nature.* 378:390–394. doi:10.1038/378390a0.
- Genuth, M.A., C.D.C. Allen, T. Mikawa, and O.D. Weiner. 2018. Chick cranial neural crest cells use progressive polarity refinement, not contact inhibition of locomotion, to guide their migration. *Dev. Biol.* 444 Suppl 1:S252–S261. doi:10.1016/j.ydbio.2018.02.016.
- Gerety, S.S., H.U. Wang, Z.F. Chen, and D.J. Anderson. 1999. Symmetrical mutant phenotypes of the receptor EphB4 and its specific transmembrane ligand ephrin-B2 in cardiovascular development. *Mol. Cell.* 4:403–414. doi:10.1016/s1097-2765(00)80342-1.
- Giger, R.J., J.-F. Cloutier, A. Sahay, R.K. Prinjha, D.V. Levenson, S.E. Moore, S. Pickering, D. Simmons, S. Rastan, F.S. Walsh, A.L. Kolodkin, D.D. Ginty, and M. Geppert. 2000. Neuropilin-2 Is Required *In Vivo* for Selective Axon Guidance Responses to Secreted Semaphorins. *Neuron.* 25:29–41. doi:10.1016/S0896-6273(00)80869-7.

- Giudicelli, F., E. Taillebourg, P. Charnay, and P. Gilardi-Hebenstreit. 2001. Krox-20 patterns the hindbrain through both cell-autonomous and non cell-autonomous mechanisms. *Genes Dev.* 15:567–580. doi:10.1101/gad.189801.
- Golding, J.P., M. Dixon, and M. Gassmann. 2002. Cues from neuroepithelium and surface ectoderm maintain neural crest-free regions within cranial mesenchyme of the developing chick. *Dev. Camb. Engl.* 129:1095–1105.
- Golding, J.P., D. Sobieszczuk, M. Dixon, E. Coles, J. Christiansen, D. Wilkinson, and M. Gassmann. 2004. Roles of erbB4, rhombomere-specific, and rhombomere-independent cues in maintaining neural crest-free zones in the embryonic head. *Dev. Biol.* 266:361–372. doi:10.1016/j.ydbio.2003.11.003.
- Golding, J.P., P. Trainor, R. Krumlauf, and M. Gassmann. 2000. Defects in pathfinding by cranial neural crest cells in mice lacking the neuregulin receptor ErbB4. *Nat. Cell Biol.* 2:103–109. doi:10.1038/35000058.
- Gong, J., R. Körner, L. Gaitanos, and R. Klein. 2016. Exosomes mediate cell contact-independent ephrin-Eph signaling during axon guidance. *J. Cell Biol.* 214:35–44. doi:10.1083/jcb.201601085.
- Gonzalez-Quevedo, R., Y. Lee, K.D. Poss, and D.G. Wilkinson. 2010. Neuronal regulation of the spatial patterning of neurogenesis. *Dev. Cell.* 18:136. doi:10.1016/j.devcel.2009.11.010.
- Graham, A., I. Heyman, and A. Lumsden. 1993. Even-numbered rhombomeres control the apoptotic elimination of neural crest cells from odd-numbered rhombomeres in the chick hindbrain. *Dev. Camb. Engl.* 119:233–245.

- Groenendijk, B.C.W., B.P. Hierck, A.C. Gittenberger-De Groot, and R.E. Poelmann. 2004. Development-related changes in the expression of shear stress responsive genes KLF-2, ET-1, and NOS-3 in the developing cardiovascular system of chicken embryos. *Dev. Dyn. Off. Publ. Am. Assoc. Anat.* 230:57–68. doi:10.1002/dvdy.20029.
- Guthrie, S., and A. Lumsden. 1991. Formation and regeneration of rhombomere boundaries in the developing chick hindbrain. *Dev. Camb. Engl.* 112:221–229.
- Guthrie, S., V. Prince, and A. Lumsden. 1993. Selective dispersal of avian rhombomere cells in orthotopic and heterotopic grafts. *Development.* 118:527–538.
- Hadjantonakis, A.-K., M. Gertsenstein, M. Ikawa, M. Okabe, and A. Nagy. 1998. Non-invasive sexing of preimplantation stage mammalian embryos. *Nat. Genet.* 19:220–222. doi:10.1038/893.
- Handly, L.N., A. Pilko, and R. Wollman. Paracrine communication maximizes cellular response fidelity in wound signaling. *eLife.* 4. doi:10.7554/eLife.09652.
- Harris, A.K. 1976. Is cell sorting caused by differences in the work of intercellular adhesion? A critique of the steinberg hypothesis. *J. Theor. Biol.* 61:267–285. doi:10.1016/0022-5193(76)90019-9.
- Harris, T.J.C., and U. Tepass. 2010. Adherens junctions: from molecules to morphogenesis. *Nat. Rev. Mol. Cell Biol.* 11:502–514. doi:10.1038/nrm2927.
- Hashimoto, H., F.B. Robin, K.M. Sherrard, and E.M. Munro. 2015. Sequential contraction and exchange of apical junctions drives zippering and neural tube closure in a simple chordate. *Dev. Cell.* 32:241–255. doi:10.1016/j.devcel.2014.12.017.

- He, F., and P. Soriano. 2013. A Critical Role for PDGFR α Signaling in Medial Nasal Process Development. *PLoS Genet.* 9:e1003851. doi:10.1371/journal.pgen.1003851.
- He, L., G. Si, J. Huang, A.D.T. Samuel, and N. Perrimon. 2018. Mechanical regulation of stem-cell differentiation by the stretch-activated Piezo channel. *Nature.* 555:103–106. doi:10.1038/nature25744.
- Heisenberg, C.-P., and Y. Bellaïche. 2013. Forces in Tissue Morphogenesis and Patterning. *Cell.* 153:948–962. doi:10.1016/j.cell.2013.05.008.
- Heissler, S.M., and J.R. Sellers. 2016. Kinetic Adaptations of Myosins for Their Diverse Cellular Functions. *Traffic Cph. Den.* 17:839–859. doi:10.1111/tra.12388.
- Henkemeyer, M., L.E. Marengere, J. McGlade, J.P. Olivier, R.A. Conlon, D.P. Holmyard, K. Letwin, and T. Pawson. 1994. Immunolocalization of the Nuk receptor tyrosine kinase suggests roles in segmental patterning of the brain and axonogenesis. *Oncogene.* 9:1001–1014.
- Heyman, I., A. Faissner, and A. Lumsden. 1995. Cell and matrix specialisations of rhombomere boundaries. *Dev. Dyn.* 204:301–315. doi:10.1002/aja.1002040308.
- Himanen, J.P., L. Yermekbayeva, P.W. Janes, J.R. Walker, K. Xu, L. Atapattu, K.R. Rajashankar, A. Mensinga, M. Lackmann, D.B. Nikolov, and S. Dhe-Paganon. 2010. Architecture of Eph receptor clusters. *Proc. Natl. Acad. Sci.* 107:10860–10865. doi:10.1073/pnas.1004148107.
- Hirai, H., Y. Maru, K. Hagiwara, J. Nishida, and F. Takaku. 1987. A novel putative tyrosine kinase receptor encoded by the eph gene. *Science.* 238:1717–1720. doi:10.1126/science.2825356.

- Ho, W.K.W., L. Freem, D. Zhao, K.J. Painter, T.E. Woolley, E.A. Gaffney, M.J. McGrew, A. Tzika, M.C. Milinkovitch, P. Schneider, A. Drusko, F. Matthäus, J.D. Glover, K.L. Wells, J.A. Johansson, M.G. Davey, H.M. Sang, M. Clinton, and D.J. Headon. 2019. Feather arrays are patterned by interacting signalling and cell density waves. *PLoS Biol.* 17:e3000132. doi:10.1371/journal.pbio.3000132.
- Huang, C., M.-C. Kratzer, D. Wedlich, and J. Kashef. 2016. E-cadherin is required for cranial neural crest migration in *Xenopus laevis*. *Dev. Biol.* 411:159–171. doi:10.1016/j.ydbio.2016.02.007.
- Hubaud, A., and O. Pourquié. 2014. Signalling dynamics in vertebrate segmentation. *Nat. Rev. Mol. Cell Biol.* 15:709–721. doi:10.1038/nrm3891.
- Hubaud, A., I. Regev, L. Mahadevan, and O. Pourquié. 2017. Excitable Dynamics and Yap-Dependent Mechanical Cues Drive the Segmentation Clock. *Cell.* 171:668-682.e11. doi:10.1016/j.cell.2017.08.043.
- Huelsken, J., R. Vogel, B. Erdmann, G. Cotsarelis, and W. Birchmeier. 2001. beta-Catenin controls hair follicle morphogenesis and stem cell differentiation in the skin. *Cell.* 105:533–545. doi:10.1016/s0092-8674(01)00336-1.
- Inada, M., G. Izawa, W. Kobayashi, and M. Ozawa. 2016. 293 cells express both epithelial as well as mesenchymal cell adhesion molecules. *Int. J. Mol. Med.* 37:1521–1527. doi:10.3892/ijmm.2016.2568.
- Inoue, T., O. Chisaka, H. Matsunami, and M. Takeichi. 1997. Cadherin-6 Expression Transiently Delineates Specific Rhombomeres, Other Neural Tube Subdivisions, and Neural Crest Subpopulations in Mouse Embryos. *Dev. Biol.* 183:183–194. doi:10.1006/dbio.1996.8501.

- Ishii, M., J. Sun, M.-C. Ting, and R.E. Maxson. 2015. Chapter Six - The Development of the Calvarial Bones and Sutures and the Pathophysiology of Craniosynostosis. *In Current Topics in Developmental Biology*. Y. Chai, editor. Academic Press. 131–156.
- Jackson, A., S. Kasah, S.L. Mansour, B. Morrow, and M.A. Basson. 2014. Endoderm-specific deletion of *Tbx1* reveals an FGF-independent role for *Tbx1* in pharyngeal apparatus morphogenesis. *Dev. Dyn. Off. Publ. Am. Assoc. Anat.* 243:1143–1151.
doi:10.1002/dvdy.24147.
- Jacobelli, J., R.S. Friedman, M.A. Conti, A.-M. Lennon-Dumenil, M. Piel, C.M. Sorensen, R.S. Adelstein, and M.F. Krummel. 2010. Confinement-optimized three-dimensional T cell amoeboid motility is modulated via myosin IIA-regulated adhesions. *Nat. Immunol.* 11:953–961. doi:10.1038/ni.1936.
- Janes, P.W., B. Griesshaber, L. Atapattu, E. Nievergall, L.L. Hii, A. Mensinga, C. Chheang, B.W. Day, A.W. Boyd, P.I. Bastiaens, C. Jørgensen, T. Pawson, and M. Lackmann. 2011. Eph receptor function is modulated by heterooligomerization of A and B type Eph receptors. *J. Cell Biol.* 195:1033–1045. doi:10.1083/jcb.201104037.
- Jiang, X., S. Iseki, R.E. Maxson, H.M. Sucov, and G.M. Morriss-Kay. 2002. Tissue origins and interactions in the mammalian skull vault. *Dev. Biol.* 241:106–116.
doi:10.1006/dbio.2001.0487.
- Jimenez-Guri, E., F. Udina, J.-F. Colas, J. Sharpe, L. Padrón-Barthe, M. Torres, and C. Pujades. 2010. Clonal Analysis in Mice Underlines the Importance of Rhombomeric Boundaries in Cell Movement Restriction during Hindbrain Segmentation. *PLOS ONE*. 5:e10112. doi:10.1371/journal.pone.0010112.

- Jørgensen, C., A. Sherman, G.I. Chen, A. Pasculescu, A. Poliakov, M. Hsiung, B. Larsen, D.G. Wilkinson, R. Linding, and T. Pawson. 2009. Cell-Specific Information Processing in Segregating Populations of Eph Receptor Ephrin-Expressing Cells. *Science*. 326:1502–1509. doi:10.1126/science.1176615.
- Jung, H.S., P.H. Francis-West, R.B. Widelitz, T.X. Jiang, S. Ting-Berreth, C. Tickle, L. Wolpert, and C.M. Chuong. 1998. Local inhibitory action of BMPs and their relationships with activators in feather formation: implications for periodic patterning. *Dev. Biol.* 196:11–23. doi:10.1006/dbio.1998.8850.
- Kadir, S., J.W. Astin, L. Tahtamouni, P. Martin, and C.D. Nobes. 2011. Microtubule remodelling is required for the front-rear polarity switch during contact inhibition of locomotion. *J. Cell Sci.* 124:2642–2653. doi:10.1242/jcs.087965.
- Kague, E., M. Gallagher, S. Burke, M. Parsons, T. Franz-Odenaal, and S. Fisher. 2012. Skeletogenic fate of zebrafish cranial and trunk neural crest. *PLoS One*. 7:e47394. doi:10.1371/journal.pone.0047394.
- Kale, G.R., X. Yang, J.-M. Philippe, M. Mani, P.-F. Lenne, and T. Lecuit. 2018. Distinct contributions of tensile and shear stress on E-cadherin levels during morphogenesis. *Nat. Commun.* 9:1–16. doi:10.1038/s41467-018-07448-8.
- Karaman, R., and G. Halder. 2018. Cell Junctions in Hippo Signaling. *Cold Spring Harb. Perspect. Biol.* 10:a028753. doi:10.1101/cshperspect.a028753.
- Kashef, J., A. Köhler, S. Kuriyama, D. Alfandari, R. Mayor, and D. Wedlich. 2009. Cadherin-11 regulates protrusive activity in *Xenopus* cranial neural crest cells upstream of Trio and the small GTPases. *Genes Dev.* 23:1393–1398. doi:10.1101/gad.519409.

- Kemp, H.A., J.E. Cooke, and C.B. Moens. 2009. EphA4 and EfnB2a maintain rhombomere coherence by independently regulating intercalation of progenitor cells in the zebrafish neural keel. *Dev. Biol.* 327:313–326. doi:10.1016/j.ydbio.2008.12.010.
- Kim, N.-G., and B.M. Gumbiner. 2015. Adhesion to fibronectin regulates Hippo signaling via the FAK-Src-PI3K pathway. *J. Cell Biol.* 210:503–515. doi:10.1083/jcb.201501025.
- Kindberg, A.A., and J.O. Bush. 2019. Cellular organization and boundary formation in craniofacial development. *genesis*. 57:e23271. doi:10.1002/dvg.23271.
- Kintner, C. 1992. Regulation of embryonic cell adhesion by the cadherin cytoplasmic domain. *Cell*. 69:225–236. doi:10.1016/0092-8674(92)90404-z.
- Krieg, M., Y. Arboleda-Estudillo, P.-H. Puech, J. Käfer, F. Graner, D.J. Müller, and C.-P. Heisenberg. 2008. Tensile forces govern germ-layer organization in zebrafish. *Nat. Cell Biol.* 10:429–436. doi:10.1038/ncb1705.
- Kulesa, P.M., and S.E. Fraser. 1998. Neural crest cell dynamics revealed by time-lapse video microscopy of whole embryo chick explant cultures. *Dev. Biol.* 204:327–344. doi:10.1006/dbio.1998.9082.
- Kullander, K., and R. Klein. 2002. Mechanisms and functions of Eph and ephrin signalling. *Nat. Rev. Mol. Cell Biol.* 3:475–486. doi:10.1038/nrm856.
- Ladoux, B., W.J. Nelson, J. Yan, and R.M. Mège. 2015. The mechanotransduction machinery at work at adherens junctions. *Integr. Biol.* 7:1109–1119. doi:10.1039/c5ib00070j.
- Lane, M.C., M.A. Koehl, F. Wilt, and R. Keller. 1993. A role for regulated secretion of apical extracellular matrix during epithelial invagination in the sea urchin. *Dev. Camb. Engl.* 117:1049–1060.

- Lawton, A.K., A. Nandi, M.J. Stulberg, N. Dray, M.W. Sneddon, W. Pontius, T. Emonet, and S.A. Holley. 2013. Regulated tissue fluidity steers zebrafish body elongation. *Development*. 140:573–582. doi:10.1242/dev.090381.
- Lecuit, T., and P.-F. Lenne. 2007. Cell surface mechanics and the control of cell shape, tissue patterns and morphogenesis. *Nat. Rev. Mol. Cell Biol.* 8:633–644. doi:10.1038/nrm2222.
- Lecuit, T., and A.S. Yap. 2015. E-cadherin junctions as active mechanical integrators in tissue dynamics. *Nat. Cell Biol.* 17:533–539. doi:10.1038/ncb3136.
- Lee, C.H., and B.M. Gumbiner. 1995. Disruption of gastrulation movements in *Xenopus* by a dominant-negative mutant for C-cadherin. *Dev. Biol.* 171:363–373. doi:10.1006/dbio.1995.1288.
- Lee, J.S., Q. Yu, J.T. Shin, E. Sebzda, C. Bertozzi, M. Chen, P. Mericko, M. Stadtfeld, D. Zhou, L. Cheng, T. Graf, C.A. MacRae, J.J. Lepore, C.W. Lo, and M.L. Kahn. 2006. Klf2 is an essential regulator of vascular hemodynamic forces *in vivo*. *Dev. Cell.* 11:845–857. doi:10.1016/j.devcel.2006.09.006.
- Lee, Y., L.V. McIntire, and K. Zygorakis. 1994. Analysis of endothelial cell locomotion: Differential effects of motility and contact inhibition. *Biotechnol. Bioeng.* 43:622–634. doi:10.1002/bit.260430712.
- Levine, E., C.H. Lee, C. Kintner, and B.M. Gumbiner. 1994. Selective disruption of E-cadherin function in early *Xenopus* embryos by a dominant negative mutant. *Development*. 120:901–909.
- Lewandoski, M., and G.R. Martin. 1997. Cre-mediated chromosome loss in mice. *Nat. Genet.* 17:223–225. doi:10.1038/ng1097-223.

- Lewis, A.E., J. Hwa, R. Wang, P. Soriano, and J.O. Bush. 2015. Neural crest defects in ephrin-B2 mutant mice are non-autonomous and originate from defects in the vasculature. *Dev. Biol.* 406:186–195. doi:10.1016/j.ydbio.2015.08.021.
- Lin, Y.-C., M. Boone, L. Meuris, I. Lemmens, N. Van Roy, A. Soete, J. Reumers, M. Moisse, S. Plaisance, R. Drmanac, J. Chen, F. Speleman, D. Lambrechts, Y. Van de Peer, J. Tavernier, and N. Callewaert. 2014. Genome dynamics of the human embryonic kidney 293 lineage in response to cell biology manipulations. *Nat. Commun.* 5:4767. doi:10.1038/ncomms5767.
- Lowell, S., P. Jones, I. Le Roux, J. Dunne, and F.M. Watt. 2000. Stimulation of human epidermal differentiation by Delta–Notch signalling at the boundaries of stem-cell clusters. *Curr. Biol.* 10:491–500. doi:10.1016/S0960-9822(00)00451-6.
- Lumsden, A., and R. Krumlauf. 1996. Patterning the vertebrate neuraxis. *Science.* 274:1109–1115. doi:10.1126/science.274.5290.1109.
- Lumsden, A., N. Sprawson, and A. Graham. 1991. Segmental origin and migration of neural crest cells in the hindbrain region of the chick embryo. *Dev. Camb. Engl.* 113:1281–1291.
- Lye, C.M., G.B. Blanchard, H.W. Naylor, L. Muresan, J. Huisken, R.J. Adams, and B. Sanson. 2015. Mechanical Coupling between Endoderm Invagination and Axis Extension in *Drosophila*. *PLOS Biol.* 13:e1002292. doi:10.1371/journal.pbio.1002292.
- Ma, X., K. Takeda, A. Singh, Z.-X. Yu, P. Zervas, A. Blount, C. Liu, J.A. Towbin, M.D. Schneider, R.S. Adelstein, and Q. Wei. 2009. Conditional ablation of nonmuscle myosin II-B delineates heart defects in adult mice. *Circ. Res.* 105:1102–1109. doi:10.1161/CIRCRESAHA.109.200303.

- Maître, J.-L., H. Berthoumieux, S.F.G. Krens, G. Salbreux, F. Jülicher, E. Paluch, and C.-P. Heisenberg. 2012. Adhesion functions in cell sorting by mechanically coupling the cortices of adhering cells. *Science*. 338:253–256. doi:10.1126/science.1225399.
- Maître, J.-L., and C.-P. Heisenberg. 2013. Three functions of cadherins in cell adhesion. *Curr. Biol. CB*. 23:R626-633. doi:10.1016/j.cub.2013.06.019.
- Martz, E., and M.S. Steinberg. 1973. Contact inhibition of what? An analytical review. *J. Cell. Physiol.* 81:25–37. doi:10.1002/jcp.1040810104.
- Mathavan, K., V. Khedgikar, V. Bartolo, and D. Alfandari. 2017. The ectodomain of cadherin-11 binds to erbB2 and stimulates Akt phosphorylation to promote cranial neural crest cell migration. *PLOS ONE*. 12:e0188963. doi:10.1371/journal.pone.0188963.
- Matis, M., D.A. Russler-Germain, Q. Hu, C.J. Tomlin, and J.D. Axelrod. 2014. Microtubules provide directional information for core PCP function. *eLife*. 3:e02893. doi:10.7554/eLife.02893.
- Matsunami, H., and M. Takeichi. 1995. Fetal brain subdivisions defined by R- and E-cadherin expressions: evidence for the role of cadherin activity in region-specific, cell-cell adhesion. *Dev. Biol.* 172:466–478. doi:10.1006/dbio.1995.8029.
- Matsuoka, T., P.E. Ahlberg, N. Kessar, P. Iannarelli, U. Dennehy, W.D. Richardson, A.P. McMahon, and G. Koentges. 2005. Neural Crest Origins of the Neck and Shoulder. *Nature*. 436:347–355. doi:10.1038/nature03837.
- Matthews, H.K., L. Marchant, C. Carmona-Fontaine, S. Kuriyama, J. Larraín, M.R. Holt, M. Parsons, and R. Mayor. 2008. Directional migration of neural crest cells *in vivo* is

- regulated by Syndecan-4/Rac1 and non-canonical Wnt signaling/RhoA. *Development*. 135:1771–1780. doi:10.1242/dev.017350.
- Maves, L., W. Jackman, and C.B. Kimmel. 2002. FGF3 and FGF8 mediate a rhombomere 4 signaling activity in the zebrafish hindbrain. *Development*. 129:3825–3837.
- Meléndez-Herrera, E., and A. Varela-Echavarría. 2006. Expression of secreted semaphorins and their receptors in specific neuromeres, boundaries, and neuronal groups in the developing mouse and chick brain. *Brain Res*. 1067:126–137. doi:10.1016/j.brainres.2005.10.028.
- Mellitzer, G., Q. Xu, and D.G. Wilkinson. 1999. Eph receptors and ephrins restrict cell intermingling and communication. *Nature*. 400:77–81. doi:10.1038/21907.
- Merrill, A.E., E.G. Bochukova, S.M. Brugger, M. Ishii, D.T. Pilz, S.A. Wall, K.M. Lyons, A.O.M. Wilkie, and R.E. Maxson. 2006. Cell mixing at a neural crest-mesoderm boundary and deficient ephrin-Eph signaling in the pathogenesis of craniosynostosis. *Hum. Mol. Genet*. 15:1319–1328. doi:10.1093/hmg/ddl052.
- Minoux, M., and F.M. Rijli. 2010. Molecular mechanisms of cranial neural crest cell migration and patterning in craniofacial development. *Development*. 137:2605–2621. doi:10.1242/dev.040048.
- Mitrossilis, D., J.-C. Röper, D. Le Roy, B. Driquez, A. Michel, C. Ménager, G. Shaw, S. Le Denmat, L. Ranno, F. Dumas-Bouchiat, N.M. Dempsey, and E. Farge. 2017. Mechanotransductive cascade of Myo-II-dependent mesoderm and endoderm invaginations in embryo gastrulation. *Nat. Commun*. 8:13883. doi:10.1038/ncomms13883.

Mochizuki, A., N. Wada, H. Ide, and Y. Iwasa. 1998. Cell-cell adhesion in limb-formation, estimated from photographs of cell sorting experiments based on a spatial stochastic model. *Dev. Dyn.* 211:204–214. doi:10.1002/(SICI)1097-0177(199803)211:3<204::AID-AJA2>3.0.CO;2-L.

Mongera, A., P. Rowghanian, H.J. Gustafson, E. Shelton, D.A. Kealhofer, E.K. Carn, F. Serwane, A.A. Lucio, J. Giammona, and O. Campàs. 2018. A fluid-to-solid jamming transition underlies vertebrate body axis elongation. *Nature.* 561:401–405. doi:10.1038/s41586-018-0479-2.

Moraes, F., A. Nóvoa, L.A. Jerome-Majewska, V.E. Papaioannou, and M. Mallo. 2005. Tbx1 is required for proper neural crest migration and to stabilize spatial patterns during middle and inner ear development. *Mech. Dev.* 122:199–212. doi:10.1016/j.mod.2004.10.004.

Muncie, J.M., and V.M. Weaver. 2018. The Physical and Biochemical Properties of the Extracellular Matrix Regulate Cell Fate. *Curr. Top. Dev. Biol.* 130:1–37. doi:10.1016/bs.ctdb.2018.02.002.

Nakada, M., J.A. Niska, H. Miyamori, W.S. McDonough, J. Wu, H. Sato, and M.E. Berens. 2004. The Phosphorylation of EphB2 Receptor Regulates Migration and Invasion of Human Glioma Cells. *Cancer Res.* 64:3179–3185. doi:10.1158/0008-5472.CAN-03-3667.

Nakagawa, S., and M. Takeichi. 1995. Neural crest cell-cell adhesion controlled by sequential and subpopulation-specific expression of novel cadherins. *Dev. Camb. Engl.* 121:1321–1332.

Nakagawa, S., and M. Takeichi. 1998. Neural crest emigration from the neural tube depends on regulated cadherin expression. *Dev. Camb. Engl.* 125:2963–2971.

Niethamer, T.K., and J.O. Bush. 2019. Getting direction(s): The Eph/ephrin signaling system in cell positioning. *Dev. Biol.* 447:42–57. doi:10.1016/j.ydbio.2018.01.012.

Niethamer, T.K., A.R. Larson, A.K. O'Neill, M. Bershteyn, E.C. Hsiao, O.D. Klein, J.H. Pomerantz, and J.O. Bush. 2017. EPHRIN-B1 Mosaicism Drives Cell Segregation in Craniofrontonasal Syndrome hiPSC-Derived Neuroepithelial Cells. *Stem Cell Rep.* 8:529–537. doi:10.1016/j.stemcr.2017.01.017.

Niethamer, T.K., T. Teng, M. Franco, Y.X. Du, C.J. Percival, and J.O. Bush. 2020. Aberrant cell segregation in the craniofacial primordium and the emergence of facial dysmorphology in craniofrontonasal syndrome. *PLoS Genet.* 16:e1008300. doi:10.1371/journal.pgen.1008300.

Olesnicky Killian, E.C., D.A. Birkholz, and K.B. Artinger. 2009. A role for chemokine signaling in neural crest cell migration and craniofacial development. *Dev. Biol.* 333:161–172. doi:10.1016/j.ydbio.2009.06.031.

O'Neill, A.K., A.A. Kindberg, T.K. Niethamer, A.R. Larson, H.-Y.H. Ho, M.E. Greenberg, and J.O. Bush. 2016. Unidirectional Eph/ephrin signaling creates a cortical actomyosin differential to drive cell segregation. *J. Cell Biol.* 215:217–229. doi:10.1083/jcb.201604097.

Osborne, N.J., J. Begbie, J.K. Chilton, H. Schmidt, and B.J. Eickholt. 2005. Semaphorin/neuropilin signaling influences the positioning of migratory neural crest cells within the hindbrain region of the chick. *Dev. Dyn.* 232:939–949. doi:https://doi.org/10.1002/dvdy.20258.

- Osumi-Yamashita, N., Y. Ninomiya, H. Doi, and K. Eto. 1996. Rhombomere formation and hind-brain crest cell migration from prorrhombomeric origins in mouse embryos. *Dev. Growth Differ.* 38:107–118. doi:<https://doi.org/10.1046/j.1440-169X.1996.00013.x>.
- Padmanabhan, R., and L.A. Taneyhill. 2015. Cadherin-6B undergoes macropinocytosis and clathrin-mediated endocytosis during cranial neural crest cell EMT. *J Cell Sci.* 128:1773–1786. doi:10.1242/jcs.164426.
- Pasquale, E.B. 2010. Eph receptors and ephrins in cancer: bidirectional signalling and beyond. *Nat. Rev. Cancer.* 10:165–180. doi:10.1038/nrc2806.
- Pathak, M.M., J.L. Nourse, T. Tran, J. Hwe, J. Arulmoli, D.T.T. Le, E. Bernardis, L.A. Flanagan, and F. Tombola. 2014. Stretch-activated ion channel Piezo1 directs lineage choice in human neural stem cells. *Proc. Natl. Acad. Sci. U. S. A.* 111:16148–16153. doi:10.1073/pnas.1409802111.
- Peretz, Y., N. Eren, A. Kohl, G. Hen, K. Yaniv, K. Weisinger, Y. Cinnamon, and D. Sela-Donenfeld. 2016. A new role of hindbrain boundaries as pools of neural stem/progenitor cells regulated by Sox2. *BMC Biol.* 14:57. doi:10.1186/s12915-016-0277-y.
- Pestel, J., R. Ramadass, S. Gauvrit, C. Helker, W. Herzog, and D.Y.R. Stainier. 2016. Real-time 3D visualization of cellular rearrangements during cardiac valve formation. *Dev. Camb. Engl.* 143:2217–2227. doi:10.1242/dev.133272.
- Piekarski, N., J.B. Gross, and J. Hanken. 2014. Evolutionary innovation and conservation in the embryonic derivation of the vertebrate skull. *Nat. Commun.* 5:5661. doi:10.1038/ncomms6661.

- Poliakov, A., M.L. Cotrina, A. Pasini, and D.G. Wilkinson. 2008. Regulation of EphB2 activation and cell repulsion by feedback control of the MAPK pathway. *J. Cell Biol.* 183:933–947. doi:10.1083/jcb.200807151.
- Porazinski, S., J. de Navascués, Y. Yako, W. Hill, M.R. Jones, R. Maddison, Y. Fujita, and C. Hogan. 2016. EphA2 Drives the Segregation of Ras-Transformed Epithelial Cells from Normal Neighbors. *Curr. Biol. CB.* 26:3220–3229. doi:10.1016/j.cub.2016.09.037.
- Prospéri, M.-T., P. Lépine, F. Dingli, P. Paul-Gilloteaux, R. Martin, D. Loew, H.-J. Knölker, and E. Coudrier. 2015. Myosin 1b functions as an effector of EphB signaling to control cell repulsion. *J. Cell Biol.* 210:347–361. doi:10.1083/jcb.201501018.
- Pryor, S.E., V. Massa, D. Savery, P. Andre, Y. Yang, N.D.E. Greene, and A.J. Copp. 2014. Vangl-dependent planar cell polarity signalling is not required for neural crest migration in mammals. *Dev. Camb. Engl.* 141:3153–3158. doi:10.1242/dev.111427.
- Redies, C., and M. Takeichi. 1996. Cadherins in the developing central nervous system: an adhesive code for segmental and functional subdivisions. *Dev. Biol.* 180:413–423. doi:10.1006/dbio.1996.0315.
- del Rio, A., R. Perez-Jimenez, R. Liu, P. Roca-Cusachs, J.M. Fernandez, and M.P. Sheetz. 2009. Stretching single talin rod molecules activates vinculin binding. *Science.* 323:638–641. doi:10.1126/science.1162912.
- Risley, M., D. Garrod, M. Henkemeyer, and W. McLean. 2009. EphB2 and EphB3 forward signalling are required for palate development. *Mech. Dev.* 126:230–239. doi:10.1016/j.mod.2008.10.009.

Rodríguez-Franco, P., A. Brugués, A. Marín-Llauradó, V. Conte, G. Solanas, E. Batlle, J.J.

Fredberg, P. Roca-Cusachs, R. Sunyer, and X. Trepap. 2017. Long-lived force patterns and deformation waves at repulsive epithelial boundaries. *Nat. Mater.* 16:1029–1037.

doi:10.1038/nmat4972.

Rohani, N., L. Canty, O. Luu, F. Fagotto, and R. Winklbauer. 2011. EphrinB/EphB Signaling

Controls Embryonic Germ Layer Separation by Contact-Induced Cell Detachment. *PLOS*

Biol. 9:e1000597. doi:10.1371/journal.pbio.1000597.

Sadaghiani, B., and C.H. Thiébaud. 1987. Neural crest development in the *Xenopus laevis*

embryo, studied by interspecific transplantation and scanning electron microscopy. *Dev.*

Biol. 124:91–110. doi:10.1016/0012-1606(87)90463-5.

Salvucci, O., and G. Tosato. 2012. Essential roles of EphB receptors and EphrinB ligands in

endothelial cell function and angiogenesis. *Adv. Cancer Res.* 114:21–57.

doi:10.1016/B978-0-12-386503-8.00002-8.

Scarpa, E., A. Szabó, A. Bibonne, E. Theveneau, M. Parsons, and R. Mayor. 2015. Cadherin

Switch during EMT in Neural Crest Cells Leads to Contact Inhibition of Locomotion via

Repolarization of Forces. *Dev. Cell.* 34:421–434. doi:10.1016/j.devcel.2015.06.012.

Schaupp, A., O. Sabet, I. Dudanova, M. Ponsérre, P. Bastiaens, and R. Klein. 2014. The

composition of EphB2 clusters determines the strength in the cellular repulsion

response. *J. Cell Biol.* 204:409–422. doi:10.1083/jcb.201305037.

Schiffmacher, A.T., R. Padmanabhan, S. Jhingory, and L.A. Taneyhill. 2014. Cadherin-6B is

proteolytically processed during epithelial-to-mesenchymal transitions of the cranial

neural crest. *Mol. Biol. Cell.* 25:41–54. doi:10.1091/mbc.E13-08-0459.

- Schiffmacher, A.T., V. Xie, and L.A. Taneyhill. 2016. Cadherin-6B proteolysis promotes the neural crest cell epithelial-to-mesenchymal transition through transcriptional regulation. *J. Cell Biol.* 215:735–747. doi:10.1083/jcb.201604006.
- Sechrist, J., G.N. Serbedzija, T. Scherson, S.E. Fraser, and M. Bronner-Fraser. 1993. Segmental migration of the hindbrain neural crest does not arise from its segmental generation. *Dev. Camb. Engl.* 118:691–703.
- Seiradake, E., K. Harlos, G. Sutton, A.R. Aricescu, and E.Y. Jones. 2010. An extracellular steric seeding mechanism for Eph-ephrin signaling platform assembly. *Nat. Struct. Mol. Biol.* 17:398–402. doi:10.1038/nsmb.1782.
- Shimozono, S., T. Imura, T. Kitaguchi, S.-I. Higashijima, and A. Miyawaki. 2013. Visualization of an endogenous retinoic acid gradient across embryonic development. *Nature.* 496:363–366. doi:10.1038/nature12037.
- Shoval, I., A. Ludwig, and C. Kalcheim. 2007. Antagonistic roles of full-length N-cadherin and its soluble BMP cleavage product in neural crest delamination. *Development.* 134:491–501. doi:10.1242/dev.02742.
- Shyer, A.E., T.R. Huycke, C. Lee, L. Mahadevan, and C.J. Tabin. 2015. Bending gradients: How the intestinal stem cell gets its home. *Cell.* 161:569–580. doi:10.1016/j.cell.2015.03.041.
- Shyer, A.E., A.R. Rodrigues, G.G. Schroeder, E. Kassianidou, S. Kumar, and R.M. Harland. 2017. Emergent cellular self-organization and mechanosensation initiate follicle pattern in the avian skin. *Science.* 357:811–815. doi:10.1126/science.aai7868.
- Simões-Costa, M., and M.E. Bronner. 2015. Establishing neural crest identity: a gene regulatory recipe. *Development.* 142:242–257. doi:10.1242/dev.105445.

- Singh, A., T. Saha, I. Begemann, A. Ricker, H. Nüsse, O. Thorn-Seshold, J. Klingauf, M. Galic, and M. Matis. 2018. Polarized microtubule dynamics directs cell mechanics and coordinates forces during epithelial morphogenesis. *Nat. Cell Biol.* 20:1126–1133. doi:10.1038/s41556-018-0193-1.
- Slováková, J., M. Sikora, S. Caballero-Mancebo, S.F.G. Krens, W.A. Kaufmann, K. Huljev, and C.-P. Heisenberg. 2020. Tension-dependent stabilization of E-cadherin limits cell-cell contact expansion. *bioRxiv*. 2020.11.20.391284. doi:10.1101/2020.11.20.391284.
- Smith, A., V. Robinson, K. Patel, and D.G. Wilkinson. 1997. The EphA4 and EphB1 receptor tyrosine kinases and ephrin-B2 ligand regulate targeted migration of branchial neural crest cells. *Curr. Biol.* 7:561–570. doi:10.1016/S0960-9822(06)00255-7.
- Solanas, G., C. Cortina, M. Sevillano, and E. Batlle. 2011. Cleavage of E-cadherin by ADAM10 mediates epithelial cell sorting downstream of EphB signalling. *Nat. Cell Biol.* 13:1100–1107. doi:10.1038/ncb2298.
- Soo, K., M.P. O'Rourke, P.-L. Khoo, K.A. Steiner, N. Wong, R.R. Behringer, and P.P.L. Tam. 2002. Twist function is required for the morphogenesis of the cephalic neural tube and the differentiation of the cranial neural crest cells in the mouse embryo. *Dev. Biol.* 247:251–270. doi:10.1006/dbio.2002.0699.
- Steed, E., N. Faggianelli, S. Roth, C. Ramspacher, J.-P. Concordet, and J. Vermot. 2016. klf2a couples mechanotransduction and zebrafish valve morphogenesis through fibronectin synthesis. *Nat. Commun.* 7:11646. doi:10.1038/ncomms11646.
- Steinberg, M.S. 1963. Reconstruction of Tissues by Dissociated Cells. *Science*. 141:401–408. doi:10.1126/science.141.3579.401.

- Steinberg, M.S., and M. Takeichi. 1994. Experimental specification of cell sorting, tissue spreading, and specific spatial patterning by quantitative differences in cadherin expression. *Proc. Natl. Acad. Sci. U. S. A.* 91:206–209. doi:10.1073/pnas.91.1.206.
- Stirbat, T.V., A. Mgharbel, S. Bodenec, K. Ferri, H.C. Mertani, J.-P. Rieu, and H. Delanoë-Ayari. 2013. Fine Tuning of Tissues' Viscosity and Surface Tension through Contractility Suggests a New Role for α -Catenin. *PLOS ONE*. 8:e52554. doi:10.1371/journal.pone.0052554.
- Stramer, B., and R. Mayor. 2017. Mechanisms and *in vivo* functions of contact inhibition of locomotion. *Nat. Rev. Mol. Cell Biol.* 18:43–55. doi:10.1038/nrm.2016.118.
- Strobl-Mazzulla, P.H., and M.E. Bronner. 2012. A PHD12–Snail2 repressive complex epigenetically mediates neural crest epithelial-to-mesenchymal transition. *J. Cell Biol.* 198:999–1010. doi:10.1083/jcb.201203098.
- Tabler, J.M., C.P. Rice, K.J. Liu, and J.B. Wallingford. 2016. A novel ciliopathic skull defect arising from excess neural crest. *Dev. Biol.* 417:4–10. doi:10.1016/j.ydbio.2016.07.001.
- Takeda, M., M.M. Sami, and Y.-C. Wang. 2018. A homeostatic apical microtubule network shortens cells for epithelial folding via a basal polarity shift. *Nat. Cell Biol.* 20:36–45. doi:10.1038/s41556-017-0001-3.
- Tallquist, M.D., and P. Soriano. 2003. Cell autonomous requirement for PDGFR α in populations of cranial and cardiac neural crest cells. *Development*. 130:507–518. doi:10.1242/dev.00241.

- Taneyhill, L.A., E.G. Coles, and M. Bronner-Fraser. 2007. Snail2 directly represses cadherin6B during epithelial-to-mesenchymal transitions of the neural crest. *Dev. Camb. Engl.* 134:1481–1490. doi:10.1242/dev.02834.
- Tao, H., M. Zhu, K. Lau, O.K.W. Whitley, M. Samani, X. Xiao, X.X. Chen, N.A. Hahn, W. Liu, M. Valencia, M. Wu, X. Wang, K.D. Fenelon, C.C. Pasilio, D. Hu, J. Wu, S. Spring, J. Ferguson, E.P. Karuna, R.M. Henkelman, A. Dunn, H. Huang, H.-Y.H. Ho, R. Atit, S. Goyal, Y. Sun, and S. Hopyan. 2019. Oscillatory cortical forces promote three dimensional cell intercalations that shape the murine mandibular arch. *Nat. Commun.* 10:1703. doi:10.1038/s41467-019-09540-z.
- Taylor, H.B., A. Khuong, Z. Wu, Q. Xu, R. Morley, L. Gregory, A. Poliakov, W.R. Taylor, and D.G. Wilkinson. 2017. Cell segregation and border sharpening by Eph receptor-ephrin-mediated heterotypic repulsion. *J. R. Soc. Interface.* 14. doi:10.1098/rsif.2017.0338.
- Teddy, J.M., and P.M. Kulesa. 2004. *In vivo* evidence for short- and long-range cell communication in cranial neural crest cells. *Development.* 131:6141–6151. doi:10.1242/dev.01534.
- Teng, C.S., M. Ting, D.T. Farmer, M. Brockop, R.E. Maxson, and J.G. Crump. 2018. Altered bone growth dynamics prefigure craniosynostosis in a zebrafish model of Saethre-Chotzen syndrome. *eLife.* 7:e37024. doi:10.7554/eLife.37024.
- Terriente, J., S.S. Gerety, T. Watanabe-Asaka, R. Gonzalez-Quevedo, and D.G. Wilkinson. 2012. Signalling from hindbrain boundaries regulates neuronal clustering that patterns neurogenesis. *Development.* 139:2978–2987. doi:10.1242/dev.080135.

- Theil, T., M. Frain, P. Gilardi-Hebenstreit, A. Flenniken, P. Charnay, and D.G. Wilkinson. 1998. Segmental expression of the EphA4 (Sek-1) receptor tyrosine kinase in the hindbrain is under direct transcriptional control of Krox-20. *Dev. Camb. Engl.* 125:443–452.
- Theveneau, E., L. Marchant, S. Kuriyama, M. Gull, B. Moepps, M. Parsons, and R. Mayor. 2010. Collective chemotaxis requires contact-dependent cell polarity. *Dev. Cell.* 19:39–53. doi:10.1016/j.devcel.2010.06.012.
- Theveneau, E., B. Steventon, E. Scarpa, S. Garcia, X. Trepap, A. Streit, and R. Mayor. 2013. Chase-and-run between adjacent cell populations promotes directional collective migration. *Nat. Cell Biol.* 15:763–772. doi:10.1038/ncb2772.
- Tian, H., B. Biehs, S. Warming, K.G. Leong, L. Rangell, O.D. Klein, and F.J. de Sauvage. 2011. A reserve stem cell population in small intestine renders Lgr5-positive cells dispensable. *Nature.* 478:255–259. doi:10.1038/nature10408.
- Ting, M.-C., N.L. Wu, P.G. Roybal, J. Sun, L. Liu, Y. Yen, and R.E. Maxson. 2009. EphA4 as an effector of Twist1 in the guidance of osteogenic precursor cells during calvarial bone growth and in craniosynostosis. *Development.* 136:855–864. doi:10.1242/dev.028605.
- Totaro, A., M. Castellan, G. Battilana, F. Zanconato, L. Azzolin, S. Giulitti, M. Cordenonsi, and S. Piccolo. 2017. YAP/TAZ link cell mechanics to Notch signalling to control epidermal stem cell fate. *Nat. Commun.* 8:15206. doi:10.1038/ncomms15206.
- Townes, P.L., and J. Holtfreter. 1955. Directed movements and selective adhesion of embryonic amphibian cells. *J. Exp. Zool.* 128:53–120. doi:https://doi.org/10.1002/jez.1401280105.
- Trainor, P., and R. Krumlauf. 2000. Plasticity in mouse neural crest cells reveals a new patterning role for cranial mesoderm. *Nat. Cell Biol.* 2:96–102. doi:10.1038/35000051.

- Tran, T.S., A.L. Kolodkin, and R. Bharadwaj. 2007. Semaphorin Regulation of Cellular Morphology. *Annu. Rev. Cell Dev. Biol.* 23:263–292.
doi:10.1146/annurev.cellbio.22.010605.093554.
- Trappmann, B., J.E. Gautrot, J.T. Connelly, D.G.T. Strange, Y. Li, M.L. Oyen, M.A. Cohen Stuart, H. Boehm, B. Li, V. Vogel, J.P. Spatz, F.M. Watt, and W.T.S. Huck. 2012. Extracellular-matrix tethering regulates stem-cell fate. *Nat. Mater.* 11:642–649.
doi:10.1038/nmat3339.
- Tümpel, S., L.M. Wiedemann, and R. Krumlauf. 2009. Hox genes and segmentation of the vertebrate hindbrain. *Curr. Top. Dev. Biol.* 88:103–137. doi:10.1016/S0070-2153(09)88004-6.
- Turing, A.M. 1952. The chemical basis of morphogenesis. *Philos. Trans. R. Soc. Lond. B. Biol. Sci.* 237:37–72. doi:10.1098/rstb.1952.0012.
- Twigg, S.R.F., C. Babbs, M.E.P. van den Elzen, A. Goriely, S. Taylor, S.J. McGowan, E. Giannoulatou, L. Lonie, J. Ragoussis, E. Sadighi Akha, S.J.L. Knight, R.M. Zechi-Ceide, J.A.M. Hoogeboom, B.R. Pober, H.V. Toriello, S.A. Wall, M. Rita Passos-Bueno, H.G. Brunner, I.M.J. Mathijssen, and A.O.M. Wilkie. 2013. Cellular interference in craniofrontonasal syndrome: males mosaic for mutations in the X-linked EFNB1 gene are more severely affected than true hemizygotes. *Hum. Mol. Genet.* 22:1654–1662.
doi:10.1093/hmg/ddt015.
- Twigg, S.R.F., R. Kan, C. Babbs, E.G. Bochukova, S.P. Robertson, S.A. Wall, G.M. Morriss-Kay, and A.O.M. Wilkie. 2004. Mutations of ephrin-B1 (EFNB1), a marker of tissue boundary formation, cause craniofrontonasal syndrome. *Proc. Natl. Acad. Sci. U. S. A.* 101:8652–8657. doi:10.1073/pnas.0402819101.

- Ulmer, B., C. Hagenlocher, S. Schmalholz, S. Kurz, A. Schweickert, A. Kohl, L. Roth, D. Sela-Donenfeld, and M. Blum. 2013. Calponin 2 acts as an effector of noncanonical Wnt-mediated cell polarization during neural crest cell migration. *Cell Rep.* 3:615–621. doi:10.1016/j.celrep.2013.02.015.
- Vicente-Manzanares, M., X. Ma, R.S. Adelstein, and A.R. Horwitz. 2009. Non-muscle myosin II takes centre stage in cell adhesion and migration. *Nat. Rev. Mol. Cell Biol.* 10:778–790. doi:10.1038/nrm2786.
- Villar-Cerviño, V., M. Molano-Mazón, T. Catchpole, M. Valdeolmillos, M. Henkemeyer, L.M. Martínez, V. Borrell, and O. Marín. 2013. Contact repulsion controls the dispersion and final distribution of Cajal-Retzius cells. *Neuron.* 77:457–471. doi:10.1016/j.neuron.2012.11.023.
- Vitelli, F., M. Morishima, I. Taddei, E.A. Lindsay, and A. Baldini. 2002. Tbx1 mutation causes multiple cardiovascular defects and disrupts neural crest and cranial nerve migratory pathways. *Hum. Mol. Genet.* 11:915–922. doi:10.1093/hmg/11.8.915.
- Voiculescu, O., E. Taillebourg, C. Pujades, C. Kress, S. Buart, P. Charnay, and S. Schneider-Maunoury. 2001. Hindbrain patterning: Krox20 couples segmentation and specification of regional identity. *Dev. Camb. Engl.* 128:4967–4978.
- Voltes, A., C.F. Hevia, C. Engel-Pizcueta, C. Dingare, S. Calzolari, J. Terriente, C. Norden, V. Lecaudey, and C. Pujades. 2019. Yap/Taz-TEAD activity links mechanical cues to progenitor cell behavior during zebrafish hindbrain segmentation. *Dev. Camb. Engl.* 146. doi:10.1242/dev.176735.
- Wahl, S., H. Barth, T. Ciossek, K. Aktories, and B.K. Mueller. 2000. Ephrin-A5 Induces Collapse of Growth Cones by Activating Rho and Rho Kinase. *J. Cell Biol.* 149:263–270.

- Watanabe, T., Y. Sato, D. Saito, R. Tadokoro, and Y. Takahashi. 2009. EphrinB2 coordinates the formation of a morphological boundary and cell epithelialization during somite segmentation. *Proc. Natl. Acad. Sci.* 106:7467–7472. doi:10.1073/pnas.0902859106.
- Wayne Brodland, G., and H.H. Chen. 2000. The mechanics of cell sorting and envelopment. *J. Biomech.* 33:845–851. doi:10.1016/S0021-9290(00)00011-7.
- White, R.J., Q. Nie, A.D. Lander, and T.F. Schilling. 2007. Complex Regulation of *cyp26a1* Creates a Robust Retinoic Acid Gradient in the Zebrafish Embryo. *PLOS Biol.* 5:e304. doi:10.1371/journal.pbio.0050304.
- Wieland, I., S. Jakubiczka, P. Muschke, M. Cohen, H. Thiele, K.L. Gerlach, R.H. Adams, and P. Wieacker. 2004. Mutations of the Ephrin-B1 Gene Cause Craniofrontonasal Syndrome. *Am. J. Hum. Genet.* 74:1209–1215.
- Wilkinson, D.G. 2001. Multiple roles of EPH receptors and ephrins in neural development. *Nat. Rev. Neurosci.* 2:155–164. doi:10.1038/35058515.
- Winklbauer, R. 2015. Cell adhesion strength from cortical tension – an integration of concepts. *J. Cell Sci.* 128:3687–3693. doi:10.1242/jcs.174623.
- Wizenmann, A., and A. Lumsden. 1997. Segregation of rhombomeres by differential chemoaffinity. *Mol. Cell. Neurosci.* 9:448–459. doi:10.1006/mcne.1997.0642.
- Woods, M.L., C. Carmona-Fontaine, C.P. Barnes, I.D. Couzin, R. Mayor, and K.M. Page. 2014. Directional collective cell migration emerges as a property of cell interactions. *PloS One.* 9:e104969. doi:10.1371/journal.pone.0104969.

- Wu, Z., T.G. Ashlin, Q. Xu, and D.G. Wilkinson. 2019. Role of forward and reverse signaling in Eph receptor and ephrin mediated cell segregation. *Exp. Cell Res.* 381:57–65. doi:10.1016/j.yexcr.2019.04.040.
- Xu, Q., G. Alldus, N. Holder, and D.G. Wilkinson. 1995. Expression of truncated Sek-1 receptor tyrosine kinase disrupts the segmental restriction of gene expression in the *Xenopus* and zebrafish hindbrain. *Development.* 121:4005–4016.
- Xu, Q., G. Mellitzer, V. Robinson, and D.G. Wilkinson. 1999. *In vivo* cell sorting in complementary segmental domains mediated by Eph receptors and ephrins. *Nature.* 399:267–271. doi:10.1038/20452.
- Yang, J., S.A. Mani, J.L. Donaher, S. Ramaswamy, R.A. Itzykson, C. Come, P. Savagner, I. Gitelman, A. Richardson, and R.A. Weinberg. 2004. Twist, a Master Regulator of Morphogenesis, Plays an Essential Role in Tumor Metastasis. *Cell.* 117:927–939. doi:10.1016/j.cell.2004.06.006.
- Yen, H.-Y., M.-C. Ting, and R.E. Maxson. 2010. Jagged1 functions downstream of Twist1 in the specification of the coronal suture and the formation of a boundary between osteogenic and non-osteogenic cells. *Dev. Biol.* 347:258–270. doi:10.1016/j.ydbio.2010.08.010.
- Yi, C., S. Troutman, D. Fera, A. Stemmer-Rachamimov, J.L. Avila, N. Christian, N.L. Persson, A. Shimono, D.W. Speicher, R. Marmorstein, L. Holmgren, and J.L. Kissil. 2011. A Tight Junction-Associated Merlin-Angiomotin Complex Mediates Merlin's Regulation of Mitogenic Signaling and Tumor Suppressive Functions. *Cancer Cell.* 19:527–540. doi:10.1016/j.ccr.2011.02.017.

- York, J.R., T. Yuan, O. Lakiza, and D.W. McCauley. 2018. An ancestral role for Semaphorin3F-Neuropilin signaling in patterning neural crest within the new vertebrate head. *Development*. 145. doi:10.1242/dev.164780.
- Yoshida, T., P. Vivatbutstiri, G. Morriss-Kay, Y. Saga, and S. Iseki. 2008. Cell lineage in mammalian craniofacial mesenchyme. *Mech. Dev.* 125:797–808. doi:10.1016/j.mod.2008.06.007.
- Yu, H.-H., and C.B. Moens. 2005. Semaphorin signaling guides cranial neural crest cell migration in zebrafish. *Dev. Biol.* 280:373–385. doi:10.1016/j.ydbio.2005.01.029.
- Zhao, H., J. Feng, T.-V. Ho, W. Grimes, M. Urata, and Y. Chai. 2015. The suture provides a niche for mesenchymal stem cells of craniofacial bones. *Nat. Cell Biol.* 17:386–396. doi:10.1038/ncb3139.
- Zhu, M., H. Tao, M. Samani, M. Luo, X. Wang, S. Hopyan, and Y. Sun. 2020. Spatial mapping of tissue properties *in vivo* reveals a 3D stiffness gradient in the mouse limb bud. *Proc. Natl. Acad. Sci.* doi:10.1073/pnas.1912656117.

Publishing Agreement

It is the policy of the University to encourage open access and broad distribution of all theses, dissertations, and manuscripts. The Graduate Division will facilitate the distribution of UCSF theses, dissertations, and manuscripts to the UCSF Library for open access and distribution. UCSF will make such theses, dissertations, and manuscripts accessible to the public and will take reasonable steps to preserve these works in perpetuity.

I hereby grant the non-exclusive, perpetual right to The Regents of the University of California to reproduce, publicly display, distribute, preserve, and publish copies of my thesis, dissertation, or manuscript in any form or media, now existing or later derived, including access online for teaching, research, and public service purposes.

DocuSigned by:

Abigail Kindberg

91B9401F3208439...

Author Signature

3/22/2021

Date